UNIVERSITÀ DEGLI STUDI DI TRIESTE
e
UNIVERSITÀ CA' FOSCARI DI VENEZIA

XXXII CICLO DEL DOTTORATO DI RICERCA IN

CHIMICA

SYNTHESIS AND CHARACTERIZATION OF BIOPOLYMERS AND TRANSITION METAL COMPLEXES FOR THE VALORIZATION OF BIOMASSES

Settore scientifico-disciplinare: **CHIM/04**

DOTTORANDO
ROBERTO SOLE

COORDINATORE
PROF. BARBARA MILANI

SUPERVISORE DI TESI
PROF. VALENTINA BEGHETTO

ANNO ACCADEMICO 2018/2019

ABSTRACT

The valorisation of animal and vegetable biomass is a core topic of bioeconomy and is presently supported by several international reports. Its relevance significantly increased in the last decades due to the environmental issues related to the massive use of oil for the production of fuels, fuel additives, fine chemicals and polymers, which are a threaten for modern society. Thus, the replacement of petrochemicals by biomass derived compounds is seen as an attractive and eco-friendly solution to preserve the environmental equilibrium.

The PhD thesis here presented describes new solutions for the valorisation of biomass and biomass derived platform chemicals.

For instance, animal proteins recovered as a waste byproduct from leather industry have been identified as a biomass to be exploited. Starting from this feedstock, the work here presented provides a novel protocol for the production of biobased retanning agents for leather production aiming to replace commonly used petrochemical derived retanning agent. The method developed takes advantage of glycerol, a biomass derived compound.

However, the most abundant biomass feedstock directly provided by Nature is lignocellulosic biomass. This work focuses on the conversion, *via* catalytic hydrogenation, of platform chemicals obtained by cellulosic fraction, such as furfural, levulinic acid, 5-hydroxymethylfurfural (5-HMF).
The reduction of these platform chemicals to the corresponding high-value alcohols makes use of novel organometallic species. We designed a series of *click* based ligands and studied their coordination behaviour with transition metal complexes.

In particular, a small library of mononuclear and dimeric palladium complexes bearing chiral triazolyl-oxazoline (TryOx) ligands have been synthetized and fully characterized by means of NMR and FTIIR spectroscopies, ESI-MS spectrometry, DFT calculations and X-rays. Moreover, preliminary test on the hydrogenation of biomass derived furfural have been carried out.

In parallel, ruthenium complexes bearing pyridilaminotriazole NNN *click* based ligands were synthetized and characterized. Furthermore, a deep investigation on the catalytic activity of these complexes has been performed. A broad range of carbonyl compounds have been reduced with excellent selectivity observed in some depicted cases. *Inter alia,* biomass derived furfural and 5-

hydroxymethylfurfural have been selectively hydrogenated to furfuryl alcohol and 2,5-bis(hydroxymethillfurfural) respectively in high yields.

Finally, hydrogenation of carbonyl compounds, included biomass derived chemicals, in aqueous media has been described. A water soluble triazole-thioether ligand has been successfully used for the *in situ* hydrogenation of biomass derived carbonyls compounds. Experimental results showed interesting recyclability of the active catalyst.

SOMMARIO

La valorizzazione delle biomasse, siano esse di origini naturale o vegetale, è una tematica che negli ultimi anni ricopre un ruolo centrale nel campo della bioeconomia ed è fortemente sostenuta da numerosi report internazionali.

Oggigiorno, infatti, la società richiede il preservamento dell'equilibrio ambientale mediante la riduzione dell'uso dei combustibili fossili per la produzione di carburanti, additivi per carburanti, prodotti chimici e polimeri.

Pertanto, la sostituzione dei prodotti petrolchimici con composti derivati da biomasse è vista come un'attraente soluzione eco-sostenibile.

Tenendo conto di queste osservazioni, la tesi di dottorato qui presentata descrive delle nuove tecnologie sviluppate per la valorizzazione delle biomasse e dei prodotti chimici da esse derivate.

In primo luogo, è stata affrontata la tematica del recupero di biomasse animali da importanti processi industriali e il loro utilizzo per la produzione di prodotti chimici per l'industria. Nella fattispecie, le proteine animali recuperate da scarti dell'industria conciaria sono state identificate come potenziale biomassa ad oggi non pienamente sfruttata. In questo lavoro viene descritto un nuovo protocollo per la produzione di agenti riconcianti per la produzione di pellami sintetizzati a partire da proteine animali. Lo scopo principale è quello di sostituire gli agenti riconcianti utilizzati comunemente e derivati per la maggior parte da combustibili fossili. Il protocollo utilizzato sfrutta inoltre il glicerolo, un altro composto derivato dalla biomassa.

Tuttavia, la materia prima più abbondante fornita direttamente dalla Natura è la biomassa lignocellulosica. Parte di questo lavoro si concentra sulla conversione di *platform chemicals* ottenuti dalla frazione cellulosica, e.g. furfurale, acido levulinico, 5-idrossimetilfurfurale (5-HMF), acido itaconico. Tali prodotti sono stati oggetto di studio attraverso reazioni di idrogenazione mediante l'uso di complessi organometallici a base di metalli di transizione.

Diversi leganti azotati, sintetizzati mediante reazioni di *click chemistry*, sono stati sintetizzati e la loro chimica di coordinazione a determinati metalli di transizione è stata ampiamente investigata.

In prima istanza ci si è concentrati sulla sintesi di una piccola libreria di complessi di palladio coordinati a ligandi chirali triazolil-ossazolinici (TryOx). La particolare chimica di coordinazione di questi nuovi

leganti è stata investigata mediante spettroscopia NMR e FTIIR, spettrometria ESI-MS, calcoli DFT e raggi X. Con i complessi caratterizzati in mano, sono stati effettuati test preliminari sull'idrogenazione del furfurale derivato da biomassa che hanno determinato la potenziale attività catalitica dei complessi sintetizzati.

Parallelamente, sono stati sintetizzati e caratterizzati complessi di rutenio contenenti ligandi che presentano la funzionalità amino triazoliche. Con tali complessi è stata condotta un'indagine approfondita sulla loro attività catalitica in reazioni di idrogenazione. Una vasta gamma di composti carbonilici è stata ridotta con, in alcuni casi, eccellenti selettività. Tra gli altri, il furfurale 5-idrossimetilfurfurale, derivati da biomasse, sono stati selettivamente idrogenati in alcool furfurilico e 2,5-diidrossimetilfurfurale in rese elevate.

Infine, è stata descritta l'idrogenazione dei composti carbonilici, inclusi i prodotti chimici derivati dalla biomassa, in solvente acquoso. Un legante triazolo-tioetere solubile in acqua, sintetizzato mediante la combinazione di due approcci *click*, come la CuAAC e la thiol-ene, ha dato buoni risultati nell'idrogenazione di composti carbonilici. I risultati sperimentali, inoltre, hanno mostrato un'interessante riciclabilità della specie catalitica attiva.

LIST OF ABBREVIATIONS

5-HMF	5-Hydroxymethylfurfural
BHMF	2,5-bis(hydroxymethyl)furan
CA	Cinnamyl Alochol
CIN	Cinnamaldehyde
CuAAC	Copper Azide-Alkyne Cycloaddition
DFT	Density Functional Theory
DPA	Dipyridylamine
DPPB	1,4-bis(diphneylphosphine)butane
EA	Elemental Analysis
ESI-MS	Electrospray Ionization Mass Spectrometry
EWG	Electron Withdrawing Group
FA	Furfuryl Alcohol
FT-IR	Fourier Transformed InfraRed
FUR	Furfural
GLY	Glycerol
GC	Gas Cromatography
GC-MS	Gass Cromatography Mass Spetrometry
GPC	Gel Permeation Chromatography
GVL	γ-ValeroLactone
ICP-MS	Inductively Coupled Plasma Mass Spectrometry
LA	Levulinic Acid
MA	Maleic Anhydride
MW	Molecular Weight
NMR	Nuclear Magnetic Resonance
PA	3-Phenylpropionaldehyde
PP	3-Phenylpropanol
TON	Turn Over Number
TOF	Turn Over Frequency

TPPTS	3,3′,3″-Phosphanetriyltris(benzenesulfonic acid) Trisodium Salt

INDEX

1. INTRODUCTION

1.1 BIOMASS VALORISATION

In the last decades, an increasing concern regarding the extensive use of fossil fuel reserves and related drawbacks prompted the scientific community to search for sustainable and eco-friendly alternatives. Beside this alerting status, the majority of chemicals which are routinely used in common industrial and house holding activities are still consisting of petrochemical derived polymers, additives, fuels, solvents, pharmaceuticals, pesticides, detergents etc.[1] Energy market, accounting for 1.5 trillion dollars, is as well dominated by fossil fuels approximately 80% of primary energy consumption is provided by oil, coal or gas.[2] *Inter alia*, plastic is expected to account 20% of the world's total oil consumption by 2050.[3] Albeit reservoirs of crude oil are dwindling and are likely to be exhausted in 40 years, a number of advantages such as extraction costs, availability and versatility made oil over the time the undisputed source for energy and materials.[4–6] Moreover, a major concern derived from the burning of fossil fuels regards the over-emission of greenhouse gas (GHG), which are causing global warming.[7,8]

Several international reports such as the *Kyoto protocol* [9] or, very recently, the *United Nations Climate Change Secretariat*,[10] emphasize the necessity to adopt environmental-friendly policies in order to prevent the massive pollution of the environment from oil derived long-term degradable material.[3,11–14] In this context, *reduce-reuse-recycle* (Figure 1.1) is a virtuous example of waste management for cities and a practical application of circular economy, an economic concept which aims to minimize wastes, pollution and emissions.[15]

As a matter of fact, the topic of biomass valorization has considerably risen in the last years as a natural response to the hinted environmental issues which are threatening modern society.[16] Biomass represents the most abundant, available, cheap and renewable feedstock directly provided by Nature. It has been successfully exploited for the production of energy, accounting more than 60% of total energy collected by renewable resources.[17] However, it is still undeveloped the use of biomass for the production of fine chemicals and biopolymers thus leading to the conclusion that new synthetic routes must be found to properly replace petrochemicals with biomass derived renewable and sustainable chemicals.

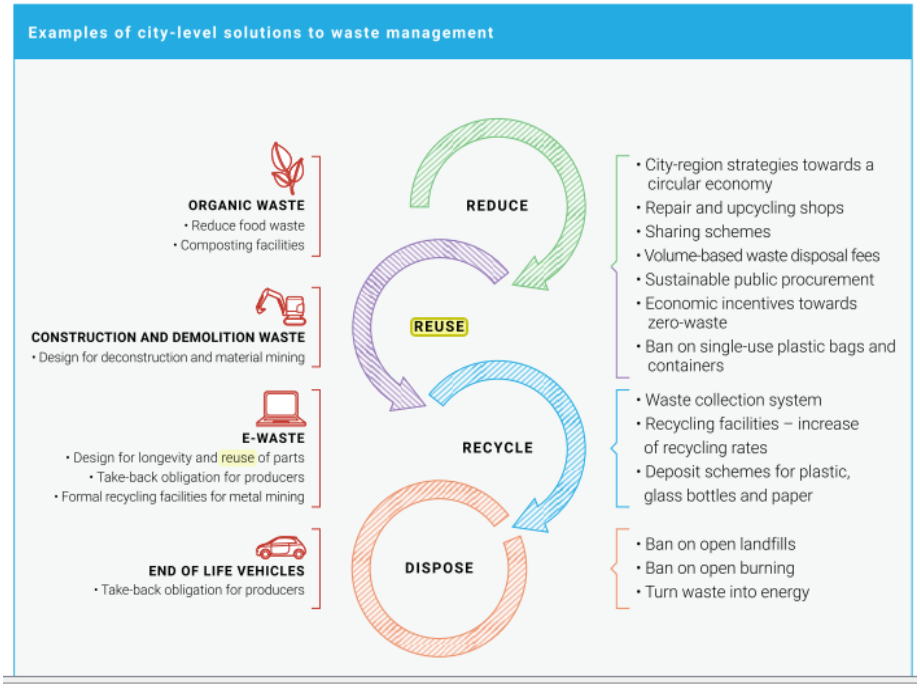

Figure 1.1. City-level solutions to waste management[13]

According to the International Union of Pure and Applied Chemistry (IUPAC), biomass is identified as any *material produced by the growth of microorganisms, plants or animals*. The main source of biomass is derived from agriculture residues and forestry rests. According to the EU report on b*iomass production, supply, uses and flows in the European Union,*[18] it is estimated that over 75% of vegetal biomass derived from agriculture is used as animal feed and food. Similarly, 52% of woody biomass is used as material for constructions. A considerable part of biomass recovered from vegetable materials not suitable for animal feed production is considered to be waste and, because of this, is burned to generate heat.

Classification of biomass also include organic materials derived from animal sources. As a consequence, collagen waste obtained by fundamental industrial processes such as food and leather industries rather than raw hides and skins collected from slaughterhouses, must find a proper collocation in terms of valorization. Food manufacturing sector is producing yearly 90 million tons of food waste,[19] most of it containing animal derived organic material.

All this in mind, it is mandatory to gather new solutions in order to find a better collocation for these waste streams.

1.1.1 Valorization of vegetal biomass

Generally, the term vegetable or plant biomass is referred to lignocellulosic biomass containing three major components: lignin, cellulose and hemicellulose.[17]

Much research has been focused on developing new chemical approaches for the valorization of the various components which render vegetable biomass an attractive feedstock.[20]

Lignin is an amorphous, natural and highly cross-linked polymer made of substituted phenols and filled by highly crystalline cellulose and hemicellulose, an amorphous carbohydrate polymer consisting of C5 and C6 sugars.[17,21,22] All together, these three components give strength and robustness to the plant structure (**Figure 1.2**).

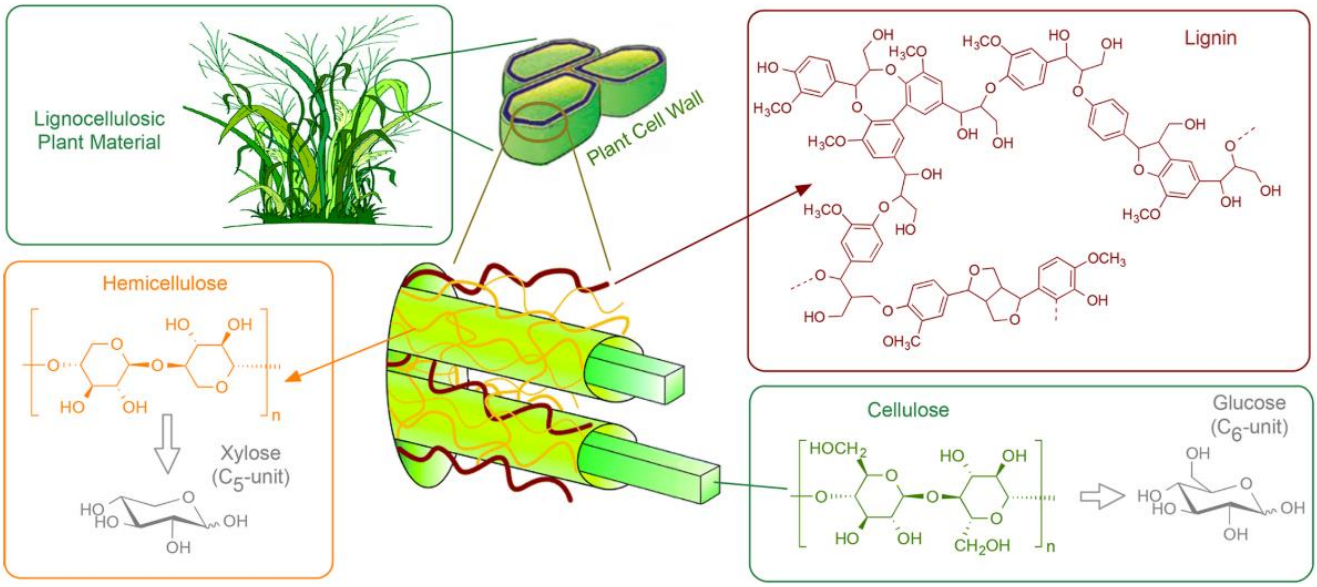

Figure 1.2. Main constituents of lignocellulosic biomass[23]

Obtaining fine chemicals from lignin by selective depolymerization of its polymeric structure is no easy matter. Several linkage types β-O-4, β-5, β-β, 5-5', 4-O-5, β-1' (**Figure 1.3**) of different nature (single, double, fourfold bonds) makes it impossible to achieve simple aromatics such as unsubstituted phenol on industrial scale.[24]

The biosynthesis route of lignin proceeds through the conversion of phenilaniline and tyrosine into the three main building blocks of lignin: *p*-coumaryl, coniferyl and sinapyl alcohols (**Figure 1.4**).[25] The oxidative coupling of these compounds, also named monolignols, forms the complex structure of lignin.

The heterogenous and chaotic network of lignin is derived by the different amount of methoxy group surrounding the phenolic nucleus of phenylpropanoid monolignols, which are conventionally identified as H (*p*-hydroxyphenyl), G (guaiacyl) and S (syringyl). Percentages of each structure strongly depends from the plant type. In many cases, even the same plant can present different lignin compositions. In an ideal scenario, a biorefinery should include as first step specific pre-treatment processes in order to reduce complexity and heterogenous nature of lignin.

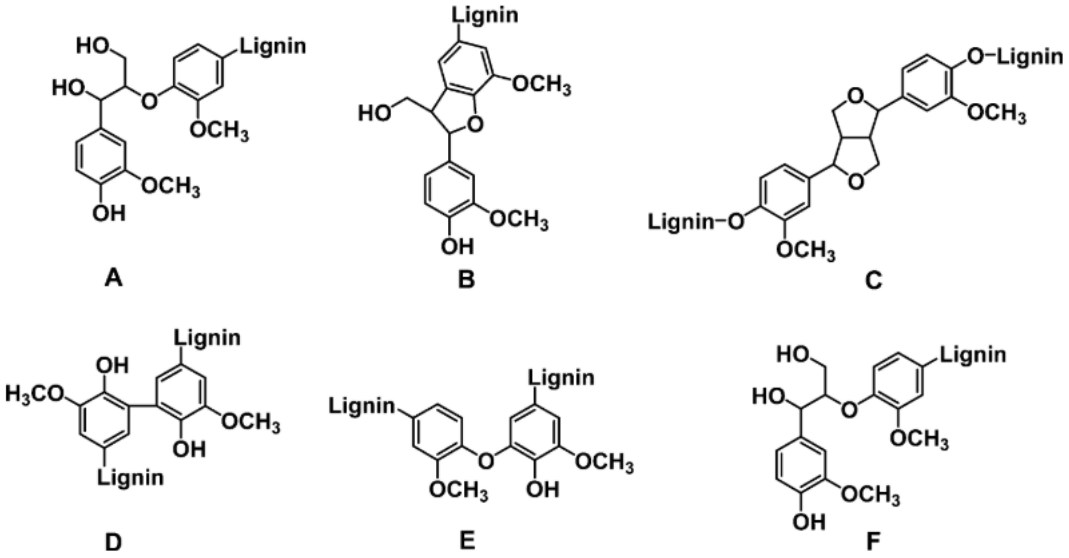

Figure 1.3. Common linkages type in lignin. β-O-4 (**A**), β-5 (**B**), β-β′ (**C**), 5-5′ (**D**), 4-O-5 (**E**), β-1′ (**F**)[26]

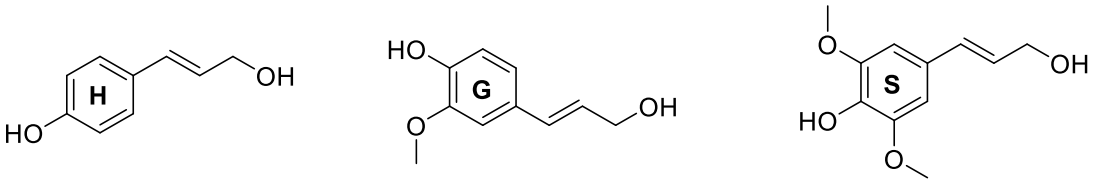

p-cumaryl alcohol coniferyl alcohol sinapyl alcohol

Figure 1.4. Monolignols

Nevertheless, an extensive literature is available highlighting the plethora of high-value adducts may be recovered from lignin valorization. In 2010 Zakzesky *et al.* [17] published a remarkable review

summarizing typical structures tracked in lignin resembling linkage types. A broad amount of substructures and reactions can be derived for each linkage type. For instance, β-O-4 bond containing models can be fragmented to repristinate lignin building blocks (*p*-coumaryl, coniferyl and sinapyl alcohols) and further processed to form arenes, quinones, vanillin.[17]Otherwise, β-O-4 may stay intact and hydroxyl groups can be oxidized to corresponding aldehydes. Cleavage of carbon-carbon linkages (5-5', β-1'), which is one of the most stable bonds in lignocellulosic biomass thus very hard to break selectively, is generally present in the form of dimeric arenes differently substituted with methoxy or hydroxyl groups. Oxidation, reduction, fragmentation and repolymerization are catalytic strategies developed to exploit this lignin fraction. β-5 linkage is usually ascribable to five member rings linking two aromatics which can be converted to valuable monomers such vanillin or vanillic acid. Using benzofuran and dihydrobenzofuran as model substrates for β-5 linkage even allowed to produce simple hydrocarbons including ethylbenzene or phenol.[27]

Finally, 4-O-5 linkages can be found in the form of oligomers. Promising results have been obtained for the conversion of model compounds reporting 4-O-5 bonds into phenolic or benzene containing compounds.

A detailed description regarding the valorization of this attractive component goes beyond the scope of this work. A number of recent reviews are reported in the references chapter which deeply investigate the topic. [1,17,21,22,25,26,28–33]

While hemicellulose is an heterogeneous matrix staffed with C5 (xylose, arabinose) and C6 sugars (galactose, glucose, mannose), cellulose is a linear polymer consisting up to 10.000 units of D-glucopyranose connected by ether bonds. Beside the huge amount of biomass derived carbohydrates which are yearly provided by Nature, just 3-4% is accounted to be used by humans.

In this frame, sugarcane and sugar beet molasses, brown viscous and syrupy materials recovered as by-products from the refining of sugar process, are mainly composed by disaccharides (sucrose) and monosaccharides (glucose and fructose). Over 40 million tons are yearly generated and used as animal feed and for the production of bioethanol.[34,35]

As aforesaid, revenue streams can be provided for this feedstock. Data hinted should stimulate the chemical community to develop practical tools for the valorization of cellulose derived carbohydrates.

Several so-called platform chemicals can be obtained from sugars. A biomass derived platform chemical is an intermediate molecule, which is produced from biomass at a competitive cost and can be transformed into a number of valuable intermediates, preferably in a large scale process.

In 2004 the United States department of Energy (DOE) listed a group of 15 compounds (**Figure 1.5**) which could be produced from biorefinery carbohydrates.[36] This report, subsequently revised and updated in further versions[37], rapidly became a milestone among scientists working on the field of green chemistry, showing the importance to invest on conversion of carbohydrates in initial platform chemicals.

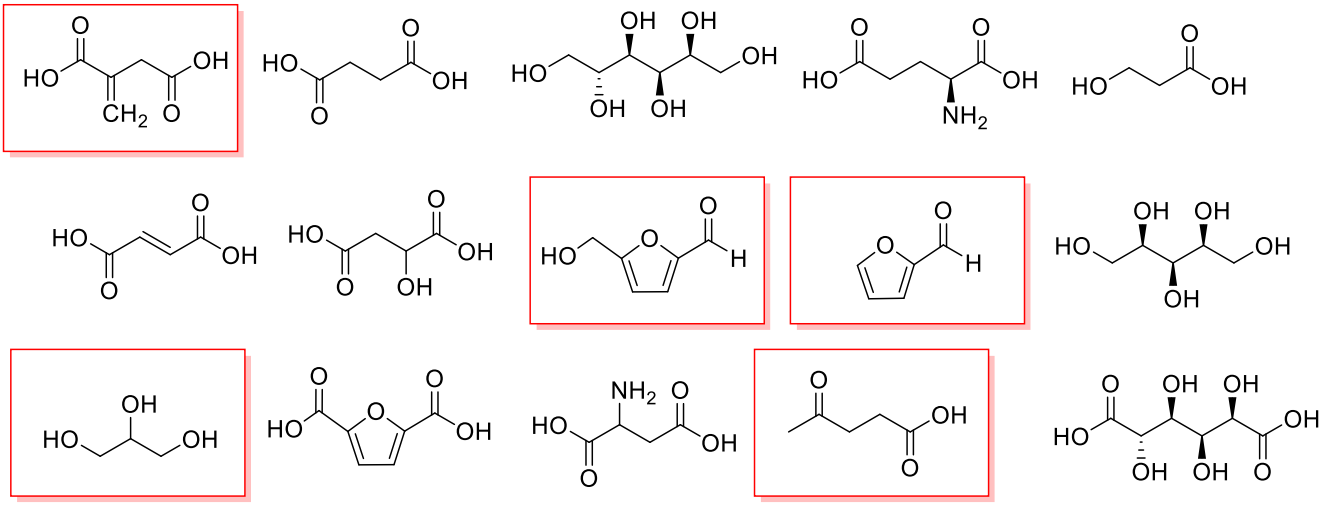

Figure 1.5. Sugar derived platform chemicals. In red are depicted compounds studied in this work

Valorization of sugar derived chemicals depicted in red on **Figure 1.5** have been extensively studied for different applications over this thesis. Hence, a brief description of these compounds is provided below.

1.1.1.1 Glycerol (GLY)

The market demand for the production of GLY (1,2,3-propanetriol) has nowadays reached the record-level of 2 million tones yearly [38] for a global turnover of $2.1 billion by 2018.[39]

GLY has been historically recovered as by-product from soap manufacturing either produced from propylene oxide and it was mainly used to produce nitroglycerin and dynamite.

Nonetheless, since the exploit of biodiesel and oleochemicals manufacturing has emerged in the last decades, an exponential growth in the production of GLY, recovered as by-product from these processes, led to the availability of huge amounts of this feedstock. Biodiesel is generally produced by transesterification between triglycerides from vegetable oils and methanol, in the presence of a base (NaOH, KOH) or an acid (H_2SO_4) catalyst (Scheme 1.1).[40] GLY can also be produced by fermentation of sugars directly or as by-product in the biosynthesis of ethanol.

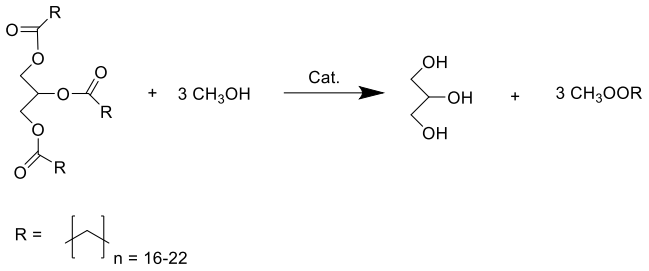

Scheme 1.1. GLY production from the biodiesel synthesis process

Recovering of material from the biodiesel manufacturing affords a 50% purity of GLY along with methanol, water, inorganic salts, unreacted mono- di- and triglycerides. To overcome these drawbacks, several types of treatments have been developed on industrial scale, allowing to yield a purity grade of GLY around 80-95%. Purity of 99.8% grade is reachable by distillation or ion exchange processes.

GLY has been used for a wide range of applications, ranging from the production of biofuels and fuels additives,[40] hydrogen and syngas,[41] high value fine chemicals,[42–47] polymers,[31,48,49] pharmaceuticals.[50] Over 20% of the GLY produced is accounted to be used for plastic and resins manufacturing.[51]

Due to the presence of three hydroxyl groups, this C3 platform molecule can undergo several chemical transformations to get access to high value fine chemicals (Scheme 1.2).

Selective oxidation of GLY can lead to the synthesis of chemicals with high industrial interest such as dihydroxyacetone, used as building block for new biodegradable polymers, glyceric acid, glyceraldehyde, hydroxy-pyruvic acid, mesoxalic acid, tartronic acid. Selective hydrogenolysis is an attractive route which can allows to get access to very important high value diols such as 1,2- propanediol, 1,3-propanediol or ethylene glycol. These C3 diols cover important roles in several industrial processes for the synthesis of cosmetics, pharmaceuticals, fragrances, detergents and are usually produced from propylene oxide. GLY

can also undergo dehydration in order to get acrolein, a major chemical since it is used for the synthesis of acrylic acid esters. Prominent GLY derived chemicals are the corresponding esters: GLY monoesters, obtained by esterification with carboxylic acids rather than transesterification with their methyl esters, cover a considerable fragment of food and cosmetic industry as they are used as emulsifier or detergent.[52] Finally, carbonylation of GLY is a fascinating tool emerging in the last years which can afford glycerol carbonates, a recent hot topic since they can be converted to epichloridin (Epicerol).[53] GLY carbonates can be used as Volatile Organic Compounds (VOC) solvents instead of petrochemical derived solvents or for polymer production.[54]

An interesting application relies on the use of glycerol based biodegradable and water soluble polymers. *Inter* alia, even if not much explored, biopolymers can be apply for the leather and textile industry. [55–57]

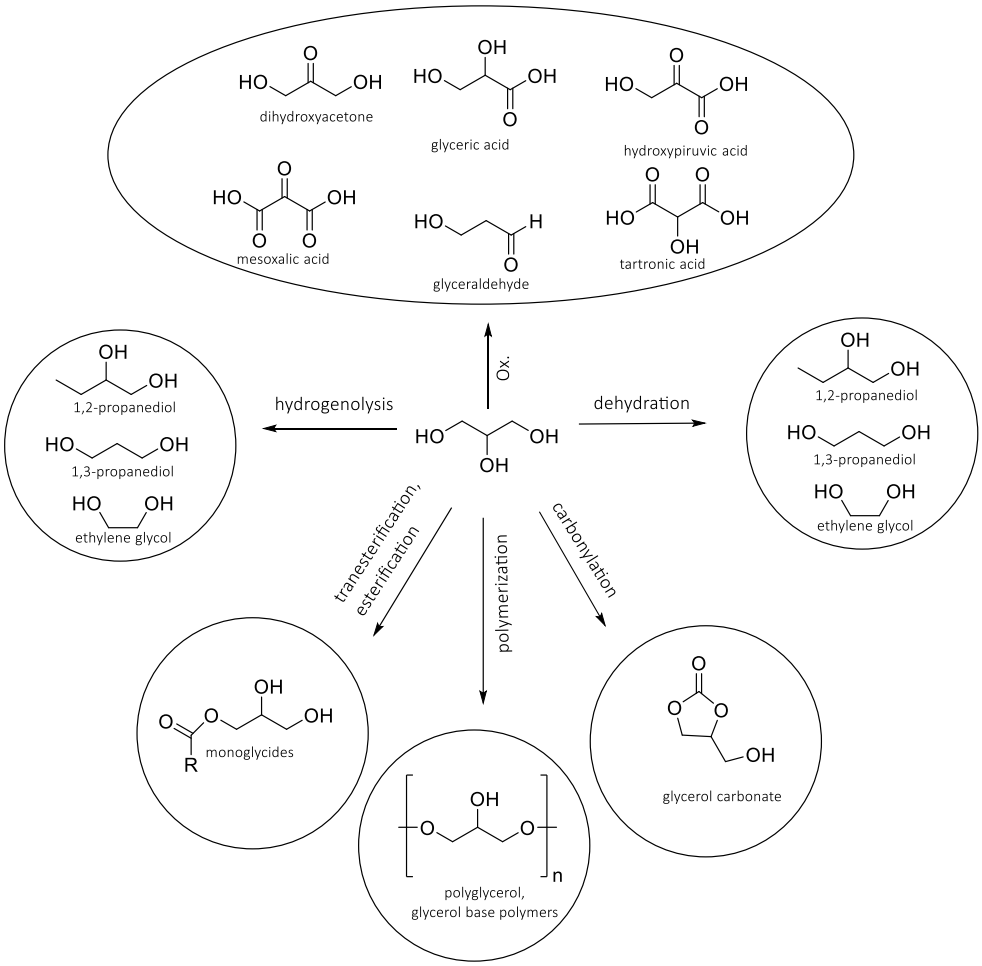

Scheme 1.2. GLY derived compounds

1.1.1.2 Furfural (FUR)

In 1831 Johann Wolfgang Döbereiner. G. Fownes reported for the first time the synthesis of an almond odorant liquid which was lately named, in 1845, furfural (FUR). Nowadays, FUR has become a well-known building block synthetized by acid catalyzed conversion of vegetable biomass derived pentosanes. Notably, FUR is one of the few compounds for whose production the biomass transformation is economically advantageous in respect to the petrochemical process.[58] China is the main producer, accounting around 200kT/year. Together with the Republic of South Africa and Dominican Republic 90% of the global production is covered.[59] Golden expectations derive from FUR according to the prevision on its production, which is expected to duplicate by 2022. [60]

Presently FUR is industrially produced by homogenous hydrolysis and dehydration of xylan/xylose carried out by acid catalysts such HCCOH, CH_3COOH, HCl, H_2SO_4, HNO_3 or HPO_3. First industrial process was developed back in 1921 by Quaker Oats, which used dilute sulfuric acid affording ~50% yield of FUR.[61] Similar procedures are still used today.[58] A detailed mechanism for the dehydration of pentoses to furfural is still object of deep investigations. Nevertheless, it has been proved that the rate limiting step is the dehydration of the pentose monomers into furfural, as the hydrolysis of pentosans into pentoses in the presence of H_2SO_4 is faster. Thus, kinetic studies are generally focused on the dehydration of pentoses (Scheme 1.3).[62]

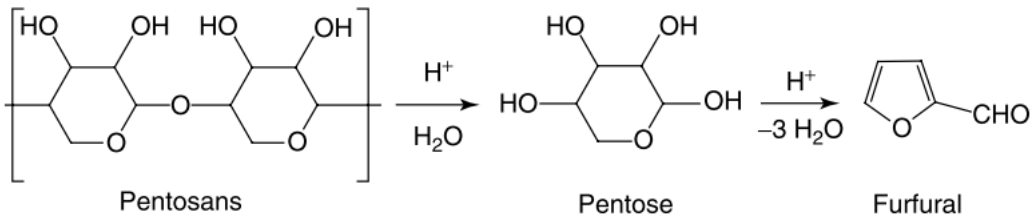

Scheme 1.3. Net reaction pathway for the production of furfural from pentoses[62]

It is generally accepted that the conversion of xylose to furfural involves a series of elementary steps, albeit the pathway is not completely acquired. The most widely accepted mechanism, proposed by Zeitsch *et al.* (Scheme 1.4)*,*[62] involves two eliminations in the positions 1,2 and one elimination involving position 1,4, leading to the formation of the aromatic ring.

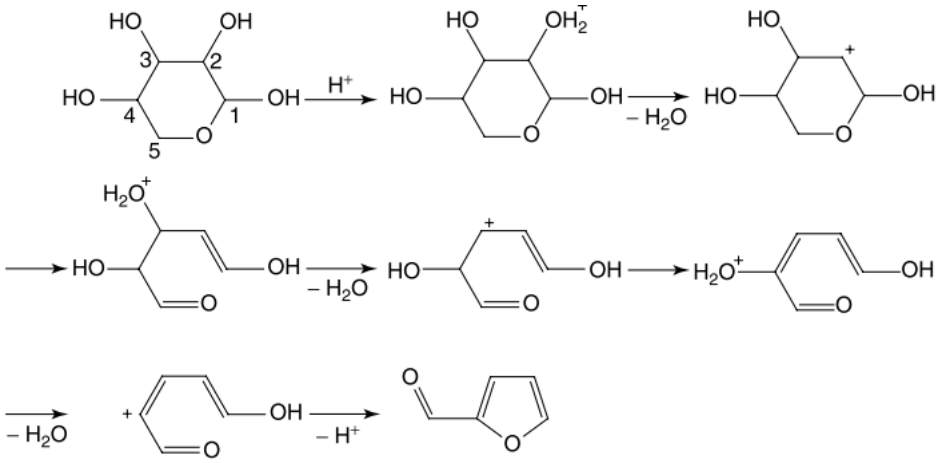

Scheme 1.4. Mechanism proposed by Zeitsch[62]

A detailed scenario of mechanism investigations relying on furfural formation from carbohydrate feedstock is reported on references. [62–67]

The possibility to convert a renewable and cheap feedstock to fuels, additives and fine chemicals prompted scientists to increase interest on this C5-platform molecule. It is worth to mention that over 80 chemicals have been directly or indirectly derived from FUR (Scheme 1.5).[68] For instance, it is considered a promising platform chemical for the production of lignocellulosic biofuels [69,70] as demonstrated by the recent results achieved by 2-methylfuran (2-MF), which has been applied for a road trial of 90.000 Km in a gasoline blend.[71] On the other side, the possibility to get access to a library of C4 and C5 high value chemicals by a number of chemical approaches such as selective hydrogenation, hydrogenolysis, oxidation or decarboxylation, made FUR a prominent building block platform. In particular, C5 chemicals are generally produced through consecutive steps of selective hydrogenation and/or hydrogenolysis, while the C4 chemicals are mainly synthesized with selective oxidation as the first step. The largest part of FUR produced, around 65%, is converted to furfuryl alcohol (FA),[72] an important chemical used mainly as monomer for the synthesis of furan resins.

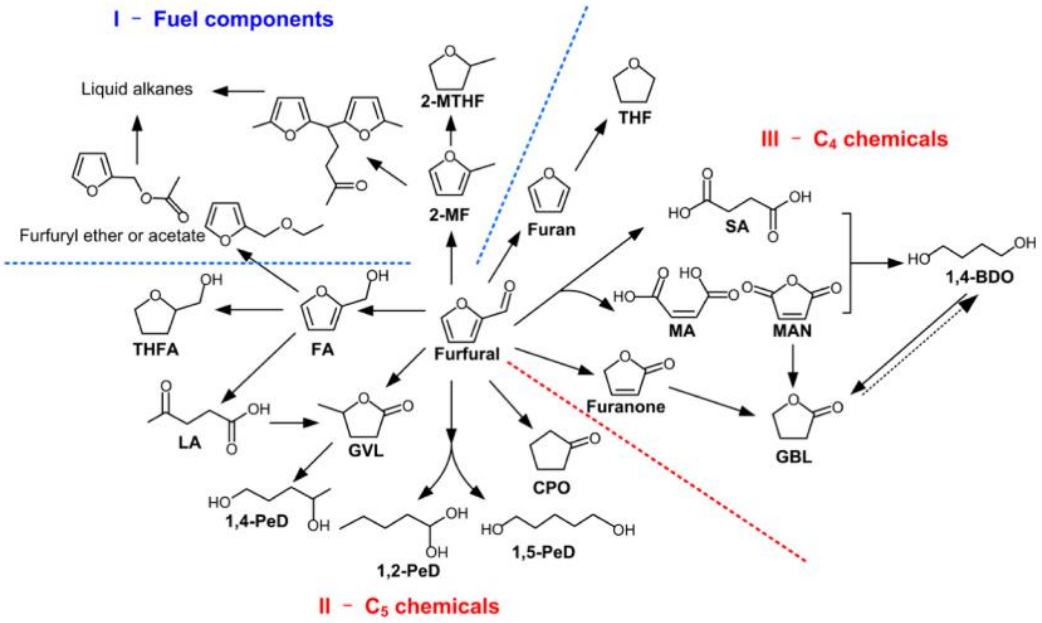

Scheme 1.5. Chemicals derived from FUR[58]

Levulinic acid (LA) is an important platform chemical that can be produced from C5 sugar via FUR or from C6 sugars via 5-HMF (see following chapter). The conversion of FUR to LA proceeds through selective hydrogenation of FUR to FA and subsequent hydrolysis of FA to LA. According to Scheme 1.6, three hydration steps and two dehydration steps are required in order to achieve LA from FA.

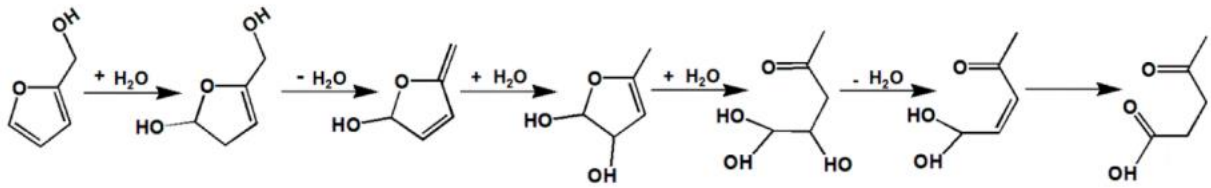

Scheme 1.6. Production of LA from FA

1.1.1.3 Levulinic Acid (LA)

Since 1950s levulinic acid (LA) was recognized to have a great potential as precursor of a portfolio of biomass derived chemicals having numerous market applications (Scheme 1.7).[73,74] Levulinate esters, such as methyl levulinate, are currently used for application in cosmetic, solvent production, polycarbonates, herbicides and biofuels.[75] MeTHF is used as eco-friendly alternative to THF as solvent,

taking advantage of an higher boiling point.[76] 1,4-Pentandiol is a suitable building block for the synthesis of biobased polymers.[77] The green approach leading to the synthesis of γ-valerolactone (GVL) from the reduction of 5-hydroxymethylfurfural (HMF) is worth mentioning; this fascinating route affords LA along to formic acid which acts as hydrogen source to form GVL. This platform chemical has found several applications in the scenario of bioeconomy thanks to the plethora of fine chemicals which can be obtained from it.[78] *Inter alia,* it can be converted to adipic acid, the precursor for Nylon, opening up a sustainable route for a major chemical.[79,80]

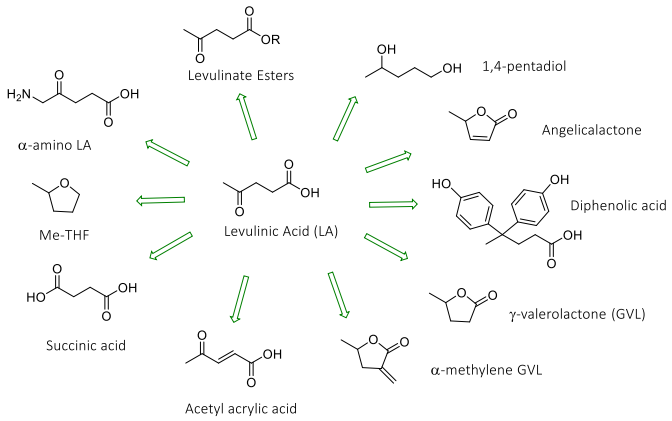

Scheme 1.7. Products derived from LA[81]

Originally, large part of LA production was produced from maleic anhydride and other petrochemicals. However, production costs were still too high to compete as precursor for the direct synthesis of chemicals from fossil fuels. Nowadays, LA is mainly produced from biomass by the well-known Biofine process,[82] which reduced the production price to 0.09-0.22 $/Kg.[83]

The Biofine process consists of a two-stage acid hydrolysis catalyzed by H_2SO_4 carried out at high temperatures. The main advantage of this pioneering process relies on the possibility to recover LA and furfural as final products instead of monomeric sugars. First, acid hydrolysis of cellulose allows to recover monosaccharide sugars which are then converted to HMF. This step has been widely investigated in the past and a clear mechanistic explanation is still not present in the literature (see Chapter **1.1.1.4**). HMF is then converted in the mixed flow reactor of the second stage to furfural, LA, formic acid, and other products (**Scheme 1.8**).[82,84] This procedure provides 50% yield of LA based on cellulose feedstock with 98% purity, while H_2SO_4 catalyst can be recovered and reused. However, other companies, such as

DSM,[85] Segetis[86] and GFBiochemicals[87], more recently developed new technologies for the synthesis of LA from biomass.

Several mechanisms have been proposed for the formation of LA from 5-HMF, but no definitive proof is present in the literature.[88–90] The mechanism proposed by Šunjić describes the production of LA from 5-HMF with a rehydration process consisting on the addition of a water molecule to the C2-C3 furanic double bond followed by a dehydration/hydration sequence to form unstable tricarbonyl intermediate TI, which decomposes to give LA and formic acid in equimolar amounts (Scheme 1.8).

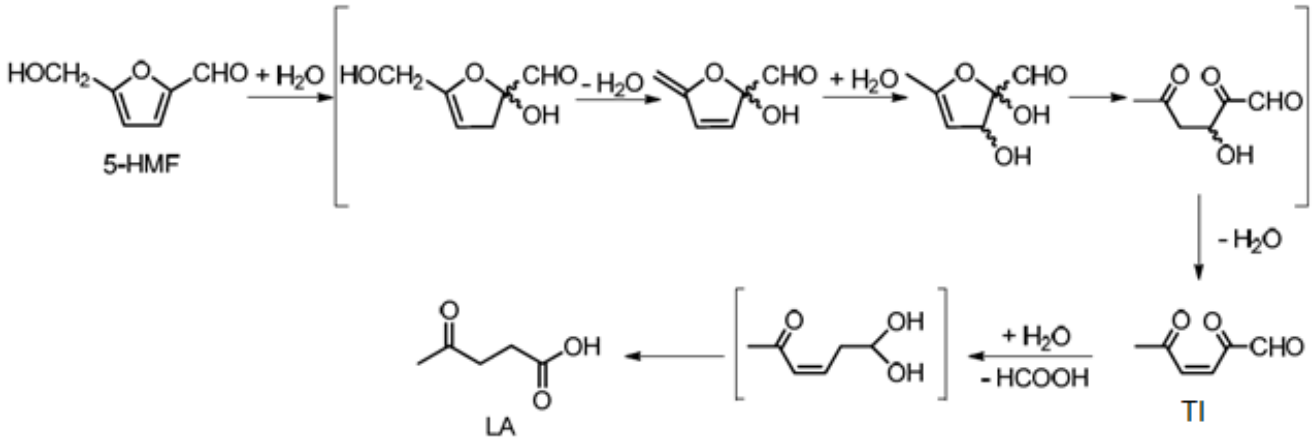

Scheme 1.8. Proposed mechanism for the formation of LA from HMF

Flannely et al. reported an LA yield of 71% using fructose as a starting material by applying 2 wt% H_2SO_4 in water at 150 °C for 2 h. Doherty and co-workers performed research on the degradation of glucose with 0.1 M H_2SO_4 at 200 °C.[64] The highest LA yield of 45% was obtained after 30 minutes.

1.1.1.4 5-Hydroxymethylfurfural (5-HMF)

First report on 5-HMF date back to 19th century, when Dull *et al.* obtained by heating inulin with oxalic acid solution under pressure. In the subsequent years, several other attempts to obtain HMF in different ways were published. In the 20th century, studies concerning the mechanism of dehydration of hexoses to HMF occupied a large part of the literature dealing with HMF, recovered as product of sequential dehydration steps (see later on this chapter).

Recently, with the advent of green chemistry and biomass valorization, it has been regarded as one of the most interesting biomass derived platform chemicals, being inserted in the "Top 10 + 4" DOE

list, the updated version of the biomass derived chemicals described by the US Department of Energy. [36,37,91,92] As a consequence, number of publications related to HMF increased over the last few years (Figure 1.6).

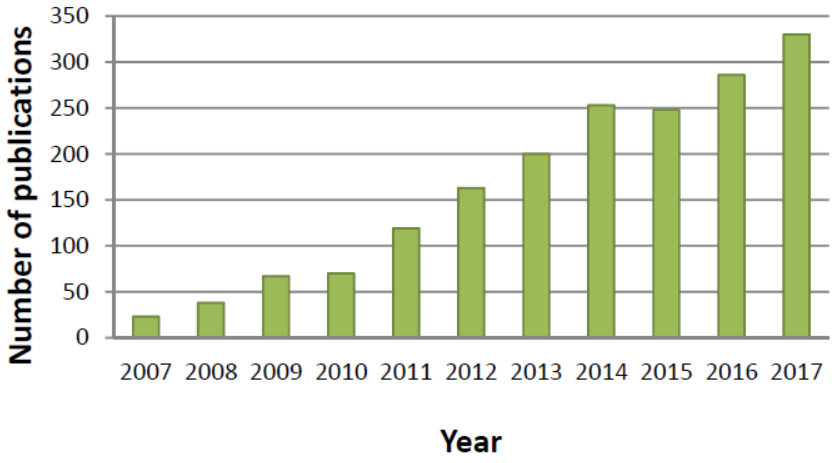

Figure 1.6. Number of publications on HMF in the period 2007 – 2017. Source: Web of Science (Keyword: 5-hydroxymethylfurfural).

As a matter of fact, 5-HMF can be selectively synthetized from sugars, in particular fructose, and acts as a precursor of a portfolio of fine chemicals (Scheme 1.9).

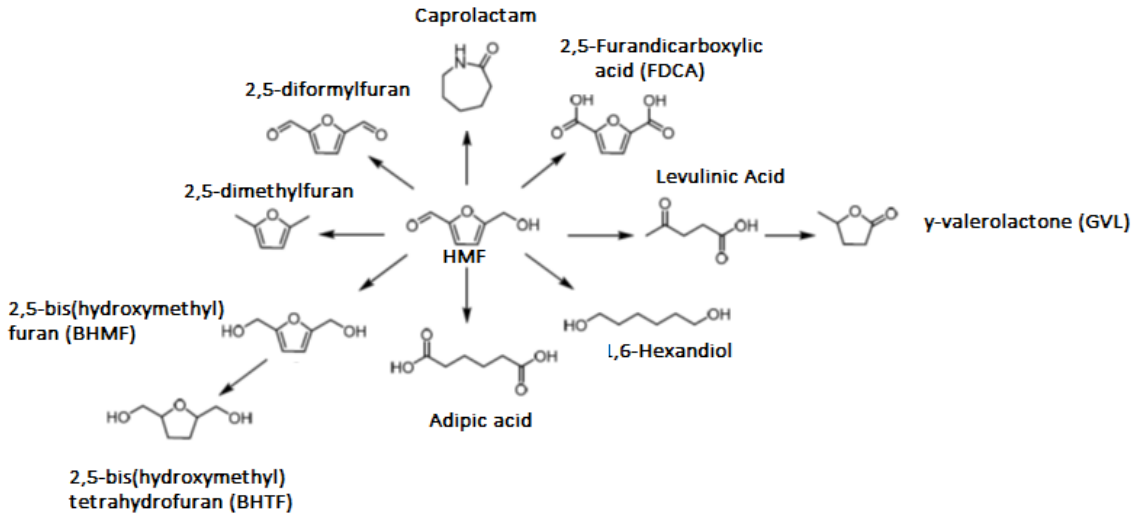

Scheme 1.9. High value chemicals from 5-HMF

Albeit three different routes have been described for its synthesis, the most widely accepted route for HMF formation concerns the direct dehydration of a hexose, even if this approach has still not found a definitive mechanistic proof.[93]

The most widely accepted mechanism regards the production of 5-HMF *via* an acid-catalyzed dehydration, in which three molecules of water are removed from the corresponding sugar molecules (Scheme 1.10).

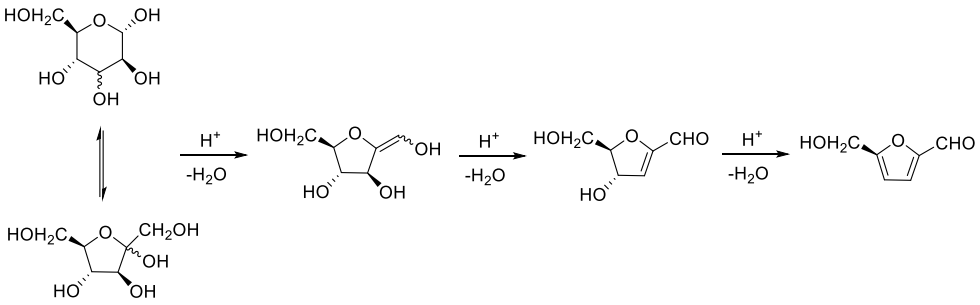

Scheme 1.10. Formation of HMF from fructose via cyclic mechanism

Additional insights in the mechanism of HMF formation can be found in the different reactivity of fructose compared to that of glucose. In general, fructose is much more reactive and selective toward HMF than glucose.

There are two other possible routes to achieve HMF from hexoses which will be not described in detail on this work. The first one is possible by the time hexoses undergo Maillard reactions in the presence of amines and amino-acids via Amadori compound. Finally, HMF can be produced by aldol condensation of C3 smaller molecules.

1.1.2 Animal derived biomass

Due to the high demand of biomass which is expected to be required by biorefineries in the near future to supply an heterogenous spectrum of bio-based building block, it is imperative to search for alterative feedstocks in addition to lignocellulosic biomass. In this context, biomass containing high amounts of animal derived proteins and collagen may assume a primary role.

Many industrial sectors routinely produce high volumes of waste containing proteins. As a matter of fact, European Union produces approximately 90 million tonnes of food waste yearly, 38% of which directly derive by the food manufacturing sector.[19]

Similarly, leather industry is highly environmental demanding and produces huge quantities of solid wastes containing protein. In fact, processing of one metric ton of raw hides produces approximately 200 kg of tanned leather along with 200–250 kg of tanned leather waste, 190–350 kg of non-tanned waste. This latter example assume even more importance in Italy, considering that 1.415 tanneries are operating in this country producing around the 60% of the EU production.[94]

All these examples are representative to indicate the significant quantity of proteins that can be recovered from industrial processes, showing the order of magnitude of organic material containing protein which is daily produced or recovered from industrial wastes and mostly converted into animal feed rather than fertilizers.

Ideally, essential amino acids (**Figure 1.7**) derived by these proteins should be employed in animal diet, as they are considered a major factor in the growth of animals,[95] while non-essential amino acids could be used as feedstock to produce chemicals, since they are not privileged compounds in animal diet.

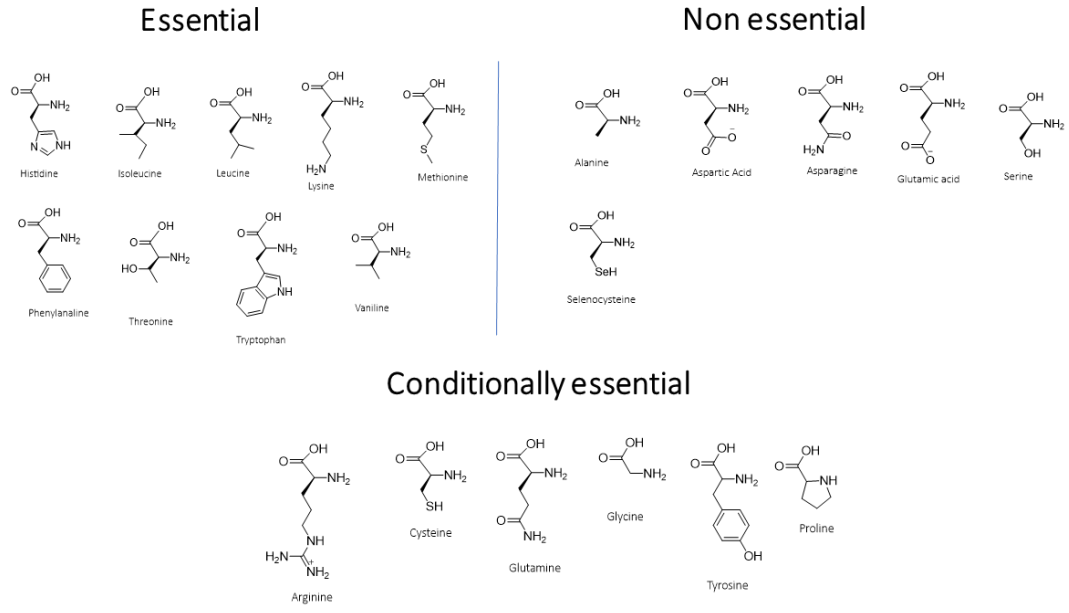

Figure 1.7. Essential, non-essential and conditionally essential amino acids.

However, suitable pretreatment processes are required to take advantage of this useful feedstock. Proteins need to be isolated and hydrolyzed in order to recover the amino acids. Afterwards, it is possible to separate this mixture into single amino acids and finally the development of chemical approaches for the conversion to fine chemicals is possible.

Hydrolytic methods aim to recover single amino acids from protein mixtures. Time, temperature, additives and hydrolysis agent are factors that affect the quality of the process, which is generally determined by a parameter named degree of hydrolysis (DH) and calculated as the ratio between the number of cleaved peptide bonds and the total number of peptide bonds.[96] Several methods have been investigated over the time. [97] Acidic (HCl, methanesulfonic acid), alkaline (NaOH, KOH), microwave assisted and enzymatic hydrolysis are the most widely used methods.

Enzymatic hydrolysis of proteins allows to produce short chain peptides and polypeptides while preserving the chirality of amino acids amine and carboxylic terminal groups. Importantly, this method provides chromium free post- tanned peptides, giving new life to a contaminated product otherwise difficult to reuse. [98]

The most abundant, non-essential amino acid derived from proteins is glutamic acid, which can be converted to *N*-methyl pyrrolidone or *N*-vinylpyrrolidone.[99] L -lysine, which on contrary lies in the list of essential amino acids, has been used for the synthesis of commodity chemicals such as 1,5-diaminopentane, caprolactam and 5-amino valeric acid.[100]

Arginine has been used to produce, *via* enzymatic hydrolysis, urea and ornithine, which can be then decarboxylated to form 1,4-butanediamine. Serine has also been valorized trough conversion to ethanolamine *via* decarboxylation.[101]

Collagen proteins can also be employed for the preparation of biodegradable polymers with a broad range of applications. [102,103]

1.2 HOMOGENEOUS CATALYSIS

1.2.1 Homogenous catalysis

It is widely accepted that the true inventor of homogenous catalysis has to be identified in Otto Roelen, which in 1938, during his investigations on the Fischer-Tropsch process at Ruhrchemie (now

Oxea), surprisingly discovered that $HCo(CO)_4$ complex was highly active in the so called oxo-synthesis, lately named hydroformylation.[104] Excellent regioselectivities reached by rhodium and cobalt catalysts made over the time hydroformylation one of the few industrial processes employing homogenous catalysts.[105]

Although the advantages in industrial applications provided by older heterogenous catalysts are well-know, as confirmed by the primary role they acquired over the time for the most important mineral oil transformations, homogenous catalysis presents many potential benefits (Table 1.1).

De facto, homogenous catalysis offers the great benefit to allow detailed understanding of reaction mechanism (catalytic cycles). As a consequence, it is possible to tune activity of the catalyst by modulating electronic and steric properties of these molecular defined complexes.

Recycle and costs of the complexes are among the main disadvantages rendering homogenous catalysis hard to be applied for high-volume industrial processes. Drawbacks which are instead circumnavigated by heterogenous catalysts, since they can offer low production costs and, if necessary, easily recycling of the catalysts.

A challenging task is rising from several research groups in order to develop a route which can join advantages of the two opposite philosophies to build up a bridge connecting these two technologies.

Table 1.1. Advantages and disadvantages of homogenous catalysis vs heterogenous catalysis[104]

	Homogeneous catalysis	**Heterogeneous catalysis**
Activity (relative to metal content)	High	Variable
Selectivity	High	Variable
Reaction conditions	Mild	Harsh
Service life of catalysts	Variable	Long
Sensitivity toward catalyst poisons	Low	High
Diffusion problems	None	May be important
Catalyst recycling	Expensive	Not necessary
Variability of steric and electronic properties of catalysts	Possible	Not possible
Mechanistic understanding	Plausible under random conditions	More or less impossible

The field of organometallic surface science, elaborated by Basset and coworkers since 90s,[106,107] showed that well-defined molecular architectures can be reacted in a defined way with functional groups of inorganic materials building up an established chemical environment.

More recently, a very interesting route has been developed by immobilizing well-defined transition metal complexes to an inorganic support (*via* solvothermal synthesis as a practical example). Paralyzing this system provide highly active, selective nanoparticles which can recycled and reused.[108]

A further promising route involve the use of multiphase systems, whereas the homogenous catalyst is confined into a solvent immiscible to the phase where products are recovered. This procedure allows to separate the catalyst phase by simple liquid/liquid extraction opening up to the possibility of recovery and recycling.[109,110]

Homogenous catalysis is a unique tool and plays a key role in enabling the valorization of biomass into fuels and chemicals to create more sustainable processes. Nowadays, the attention to chemicals based on renewable resources is rapidly increasing throughout the entire chemical industry giving new outputs for homogenous catalysis. [111]

1.2.1. Selective homogenous hydrogenation of carbonyl compounds to alcohols

Among the never-ending library of reactions catalyzed by homogenous catalysts, this thesis will treat one in particular, which is among the most extensively studied reaction still appealing the chemical community, *id est* homogeneous hydrogenation. The industrial relevance of homogeneous catalysts in hydrogenation reactions lies mainly in their very high chemo-, regio-, and enantio- selectivity. [112]

Usually hydrogenation is performed under molecular hydrogen atmosphere, while the hydrogenation of unsaturated or polar groups *via* transfer hydrogenation is referred to the use of hydrogen donor molecules, such as alcohols.

While a plethora of functional groups can be selectively hydrogenated, for the sake of simplicity the selective reduction of carbonyl compounds will be discussed. In this frame, the majority of biomass-derived platform chemicals own a C=O group.[113] The reduction of aldehydes, ketones, esters, acids, and anhydrides to alcohols is one of the most fundamental and widely employed reactions in synthetic chemistry. [114]

At laboratory scale, the easiest method to hydrogenate carbonyl compounds is by using stochiometric reducing agents like sodium borohydride and lithium aluminum hydride. However, the use of these reagents at industrial scale suffers of many drawbacks due the expensive clean-up of boron and aluminum wastes after reaction. Therefore, methodologies taking advantage of cleaner procedures are required by industries.

All this in mind, homogenous hydrogenation by using clean molecular hydrogen own the characteristics to be applied for industrial purposes. [115]

First tentative of carbonyl hydrogenation by using organometallic soluble complexes was reported by Coffey and coworker in the 60s using $[Ir(H)_3(PPh_3)_3]$ as catalyst precursor.[116]

Graziani *et al.* reported notable chemoselective hydrogenation of C=O over C=C using iridium complexes bearing phosphine ligands, although conversion and turnovers were not maximized.[117–119]Several other iridium complexes were proposed since these early studies, although selectivity has hardly been reached by iridium catalysts, often requiring large excesses of bulky phosphine ligands, which strongly increase the overall process cost.[120]

Surprisingly, the renowned Wilkinson's catalysts $[RhCl(PPh_3)_3]$ used for the efficient hydrogenation of olefin was found to be inactive for carbonyl hydrogenation as a result of the competing decarbonylation reaction. Although several other rhodium complexes have been proposed, they were less active and selective than ruthenium complexes, while maintaining higher costs.

In contrast, ruthenium is considered the most widely used metal source for the hydrogenation of carbonyls. Moreover, it considerably cheaper than other precious transition metals used for catalytic homogenous hydrogenation. To date, price of ruthenium is accounted for 8.79 €/g, while iridium costs 47.81 €/g and rhodium reach 171.40 €/g. [121]

$[RuCl_2(PPh_3)_3]$ catalyst have been tested by Tsuji and Suzuki in 1977 and it was capable to hydrogenate a range of aromatic and aliphatic aldehydes at 10 bar H_2.[122] Complete conversion were observed at 80 °C while even at room temperature the catalyst was moderately active. Besides excellent activity, this simple catalyst was not chemoselective towards C=O hydrogenation in the presence of C=C bonds.

The real landmark for chemoselective carbonyl hydrogenations is represented by the outstanding work produced by Noyori with the discovery of BINAP ligand in 1980 [123] and later of BINAP-diamine ligands (**Figure 1.8**).[124]

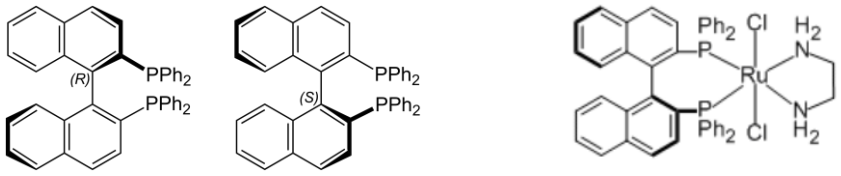

Figure 1.8. BINAP ligands and a Ru BINAP-diamine complex

The latter opened-up a breakthrough in metal-ligand cooperation (MLC) theory. MLC theory supports the critical role of ligands of both the metal and the ligand, which are directly involved in bond activation processes, by contrast to "classical" transition metal catalysis where the ligand acts as a spectator, while all key transformations occur at the metal center. [125] Although Noyori-type catalysts were developed for asymmetric hydrogenation, meaning they may be too expensive for not enantioselective hydrogenations, they inspired the design of many cheaper ligands which could be used for hydrogenation reactions. Selectivity is a crucial issue. In particular, chemoselective hydrogenation of α,β-unsaturated aldehydes and ketones, which allows to recover allyl-alcohols, is a peculiar tool which measures versality of an homogenous catalyst. As emphasized by Dupau, allyl alcohols are products of relevant importance for both the pharmaceutical as well as flavor and fragrance industries.[115]

The hydrogenation of C=C double bound is thermodynamically favored by approximately 35 kJ mol^{-1} in respect to C=O moiety.[126] According to classical hydrogenation mechanism, the coordinating fashion is different, since double bond coordinates *via* η^2 fashion, whereas carbonyl bond to the metal *via* the end-on oxygen atom (**Scheme 1.11**). All this in mind, the logical conclusion is that a system with peculiar steric properties has to be design in order to achieve selectivity towards allyl alcohols.

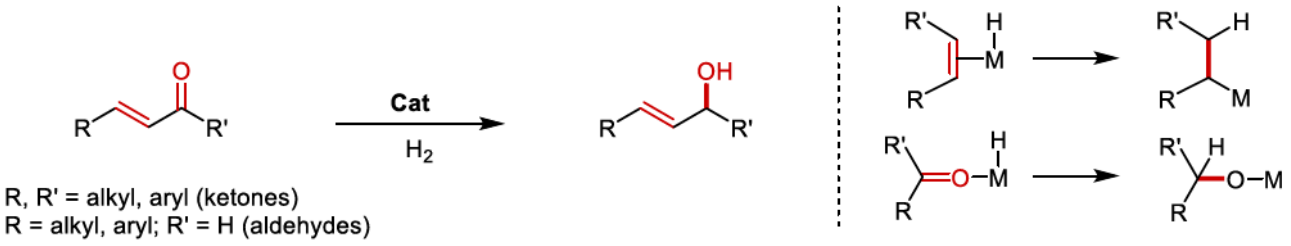

Scheme 1.11. Selective hydrogenation of α,β-unsaturated ketones and aldehydes

Albeit a number of heterogenous catalysts have been used for this purpose, they hardly reach over 90% selectivity to the corresponding allylic alcohol.[127] On the other hand, not many homogenous catalysts were used. Very recently, Puylaert *et al.* [128] extended the scope to a portfolio of ketones and aldehydes using cheap ruthenium NNN catalyst. Water soluble complexes have been also used for carbonyl hydrogenation, often employing 3,3′,3″-Phosphanetriyltris(benzenesulfonic acid) trisodium salt (TPPTS) as ligand.[129–131]

1.2.2 Mechanisms of carbonyl hydrogenation

Catalytic homogenous hydrogenations of polar bonds such as ketones and aldehydes are known to proceed either *via* an inner-sphere (Schrock-Osborn) or an outer-sphere mechanism (**Scheme 1.12**).The inner-sphere mechanism involves the coordination of the substrate to a free site of the metal centre (B) made vacant by displacement of a ligand **(I)**. Insertion of the C=O bond into the metal hydride **(II)** leads to the alkoxide complex (C). Oxidative addition of H_2 **(III)** forms the hydrogen complex (D-E) from which the alcohol is released to reform the active catalyst A **(V) [ref]**.

In contrast, Ikariya, Noyori and co-workers greatly improved activities and selectivities by using Ru-diphosphine-diamine type. [132–134]

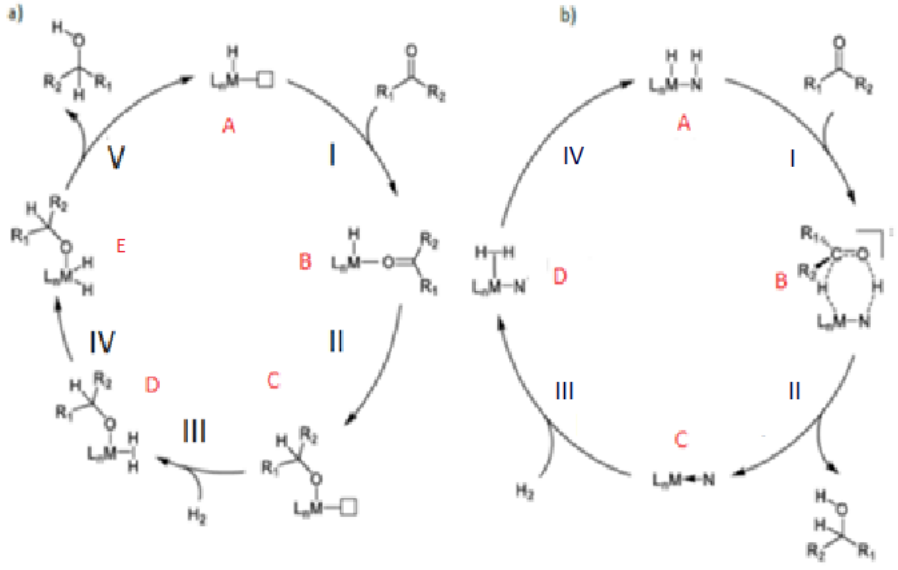

Scheme 1.12. Inner-sphere **(a)** vs outer-sphere **(b)** mechanism.

Rationalizing these findings, it was proposed that the diamine ligand does not just only provides steric and electronic properties, but rather that the N-H functionality in the diamine ligand combined with the Ru-H adds a proton and a hydride to a polarized double bond, such as a carbonyl group. In particular, coordination of the substrate **(I)** leads to the formation of complex B. Concerted migration of hydride and proton to the substrate releases the product **(II)** forming the coordinative unsaturated amido complex C. Coordination of dihydrogen **(III)** and successive heterosplitting **(IV)** regenerate dihydride A (**Scheme 1.12b**). Importantly, the oxidation state of the metal remains the same throughout the catalytic cycle.

1.2.3 Homogenous hydrogenation of biomass derived platform chemicals

The use of homogenous catalysts for the conversion of biomass derived platform chemicals has been extensively investigated in the last years. As aforementioned, the possibility to obtain high-value products with yields and selectivity arduous to reach by heterogenous catalysts, is pushing the design and development of new routes based on homogenous catalysts.

Several reviews summarized the recent advances in biomass valorization through homogenous catalysis.[21,111,113,135,136] Valorization of levulinic acid, furfural and HMF will be highlighted.

1.2.3.1 Complexes for homogenous hydrogenation of LA to GVL

On of the most important compounds derived from LA reduction is γ-valerolactone (GVL) (**Scheme 1.13**). Beside the use of heterogenous catalysts,[137,138] has proved to be an useful tool, several transition metal complexes have showed remarkable activities for this transformation.

The use of ruthenium catalysts, summarized in **Table 1.2**, date back in 1984, when Ikariya and co-workers used $RuCl_2(PPh_3)_3$ (**Figure1.9**, **1**) to achieve GVL with 86% yield, in toluene (Entry 1).[139] Later, it was found that combination of $Ru(acac)_3$ (**2**) with PBu_3 (**L1**),[140] TPPTS (**L2**) or P(*n*-Oct)$_3$ (**L3**) [141] successfully lead to excellent yields of GVL (Entries 2-4). $Ru(acac)_3$ and $RuCl_3$ were tested along with a series of water-soluble ligands by Kühn and co-workers for the hydrogenation of LA in aqueous solutions.

TPPTS resulted to be the best ligand.[142] Similarly, Tukacs *et al.* tested a range of different sulfonated phosphine to investigate the role of the ligand in the *in situ* hydrogenation of LA to GVL using $Ru(acac)_3$ as metal precursor in a solvent- and additive-free system.[143] It was established that electron-donating phosphine, such as *n*Bu-DPPDS (**L4**), are more active than the Ru/TPPTS system with a maximum TON of 6370 (Entry 5). Ten equivalents of phopshine ligand were used for each hydrogenation experiment. Later, the same authors developed an *in situ* ruthenium 1,4-bis(diphneylphosphine)butane (DPPB, **L5**) system improving the TON up to 12740 (Entry 6).[144] The catalyst was recycled up to 10 cycles. In the same year, Beller and coworkers used instead a triphos ligand (TPP, **L6**) to achieve a remarkable TON of 75.855 (Entry 7).[145] However, it is important to point out that TPPTS ligands, generally utilized for a plethora of homogenous reactions in water phase, are quite expensive ligands, as they are sold for 250 €/g by Sigma-Aldrich.[146]

Iridium complexes as well have been used for this reaction leading and generally provides better performances in terms of TON and TOF. In 2012 Zhou and co-workers reported a catalytic system formed by $Ir[COE]_2Cl_2$ (**3**) and a pyridine-based PNP pincer ligand (**L7**), requiring stochiometric amount of base to be activated, which allowed to obtain GVL in high yield at a maximum TON of 71.000 (Entry 8).[147]

Deng and co-workers changed successfully used several types of half-sandwich iridium complexes (**4**) under mild reaction conditions (Entry 9).[148] These kind of iridium complexes revealed high activities, as demonstrated as well by Fischmeister using a molecular defined [Cp*Ir(dpa)(OSO_3)] (**5**) complex (dpa=dipyridylamine), as reported in Entry 10.

Recently, approaches using non-noble metals such are emerging, as reported by Song and co-workers showing the potential of an Iron complex (**6**) bearing a 2,6-diaminopyridine (PNP) scaffold as ligand.[149]

Table 1.2. Most significant complexes used for the hydrogenation of LA to GVL under H_2.

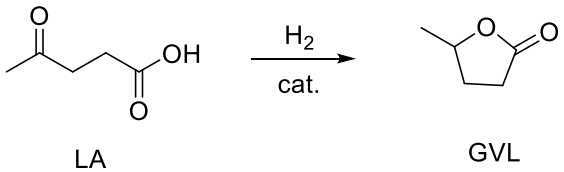

Entry	Cat.	Solvent	Conditions	Conv. %(Yield)	Ref.
1	$RuCl_2(PPh_3)_3$	Toluene	180°C, 12 bar, 24h	99 (86)	[139]

2	$Ru(acac)_3/PBu_3$	NH_4PF_6	135 °C, 100 bar, 8h	99	[140]
3	$Ru(acac)_3$/TPPTS	H_2O	140 °C, 70 bar, 12h	99	[140]
4	$Ru(acac)_3/P(n\text{-}Oct)_3$	NH_4PF_6	160 °C, 100 bar, 18h	99	[141]
5	$Ru(acac)_3$/Bu-DPPDS	H_2O	140°C, 10 bar, 4.5h	(99)	[143]
6	$Ru(acac)_3$/DPPB	/	160°C, 100 bar, 0.6h	(99)	[144]
7	$Ru(acac)_3$/TPP	/	140°C, 80 bar, 168h	(99)	[145]
8	$Ir[COE]_2Cl_2$/PNP ligand	EtOH	100 °C, 50 bar, 15h	(96)	[147]
9	$[(Cp^*IrCl_2]_2$/ 4,4-dimethoxy-2,2-bipyridine	H_2O	120°C, 100 bar, 4h	(98)	[148]
10	$[Cp^*Ir(dpa)(OSO_3)]$	H_2O	110°C, 5 bar, 16h	(99)	[150]
11	[FeH (PNP)COBr]	MeOH	100°C, 50 bar, 2h	97(95)	[149]

a)

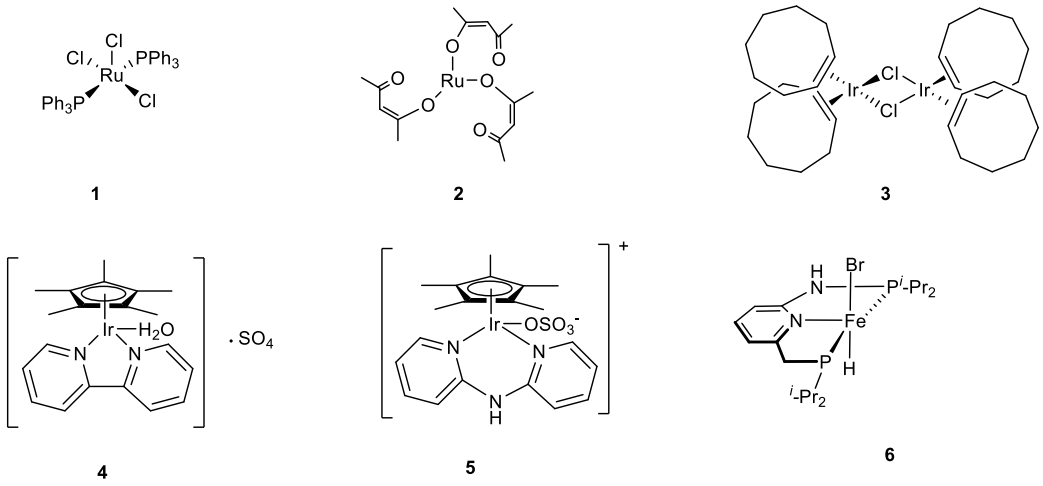

b)

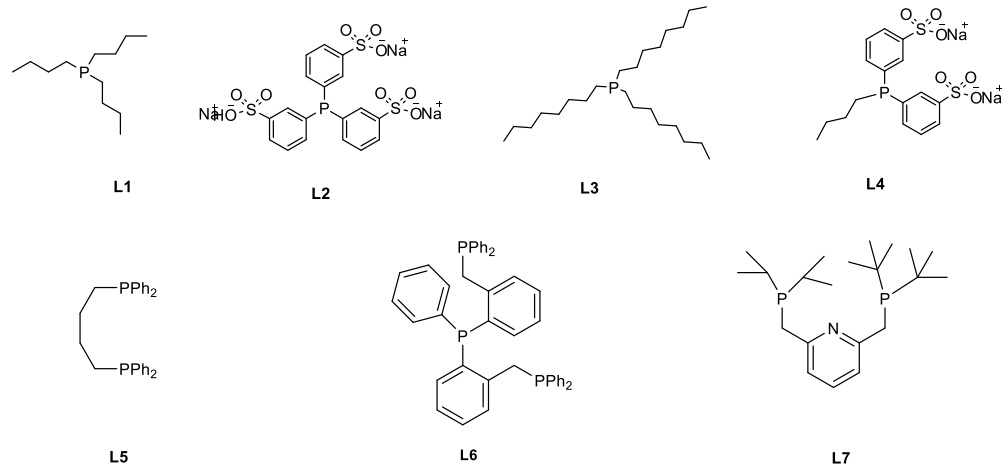

Figure 1.9. a) Examples of complexes active for hydrogenation of LA to GVL b) Ligands added *in situ*

1.2.3.2 Complexes for homogenous hydrogenation of HMF to BHMF

Reduction of 5-HMF leads to the synthesis of the corresponding diol 2,5-bis(hydroxymethy)lfuran (BHMF) which is an highly desiderable product for the production of polymers,[151] additives,[152]bioactive compounds,[153] fuels.[154] While several and efficient reports have been reported using heterogenous catalysts,[155] studies conducted by homogenous catalysts are rare and reported in **Table 1.3**.

Pasini *et al.* reported the use of Shvo's catalyst $[Ph_4(\eta^5\text{-}C_4CO)_2H(CO)_4Ru_2]$- (μ-H) (**7**)working at 90 °C and 10 bar of hydrogen pressure for 1 hour in toluene affording quantitative yield of BHMF (Entry 1). [156] In this paper a tentative of catalyst recycle has been proposed. Cooling down the autoclave after reaction favors DHMF precipitation and filtration with high yields, without loss of catalyst activity, which is confined in the organic phase so being reused. However, maximum scale up of this procedure have been reported up to 5 mmol of HMF.

Similarly, de Vries and co-workers[128] reported 93% isolated yield of BHMF by using ruthenium pincer complexes (**8**)bearing 2-(ethylthio)-N-[(pyridin-2-yl)methyl]ethan-1-amine) as ligand (NNS) (Entry2). The reaction is run in isopropanol at 80 °C and 30 bar for 1 h (catalyst loading 0.5 mol %). A non-precious catalyst has been also used by Beller and co-worker, which reported a 64% isolated yield of HMF by using a manganese PNP pincer complex (**9**, Entry 3).[157] To the best of our knowledge, these are the only available approaches for the selective hydrogenation of 5-HMF to BHMF by homogenous catalysis.

Table 1.3 Most significant complexes used for the hydrogenation of 5-HMF to BHMF under H_2.

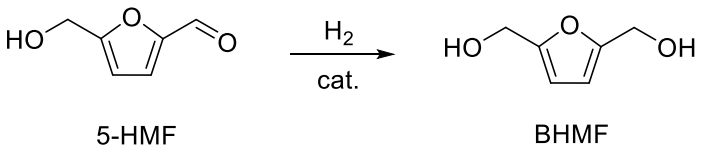

5-HMF BHMF

Entry	Cat.	Solvent	Conditions	Conv. %(Yield)	Ref.
1	$[Ph_4(\eta^5\text{-}C_4CO)_2H(CO)_4Ru_2]$-(μ-H)	Toluene	90°C, 10 bar, 1h	(99)	[156]
2	$[RuCl_2(NNS)PPh_3]$	*i*-Prop	80°C, 30 bar, 1h	99 (93)	[128]

3	[$MnCO_2$(PNP)Br]	Toluene	100 °C, 30 bar	90 (64)	[157]

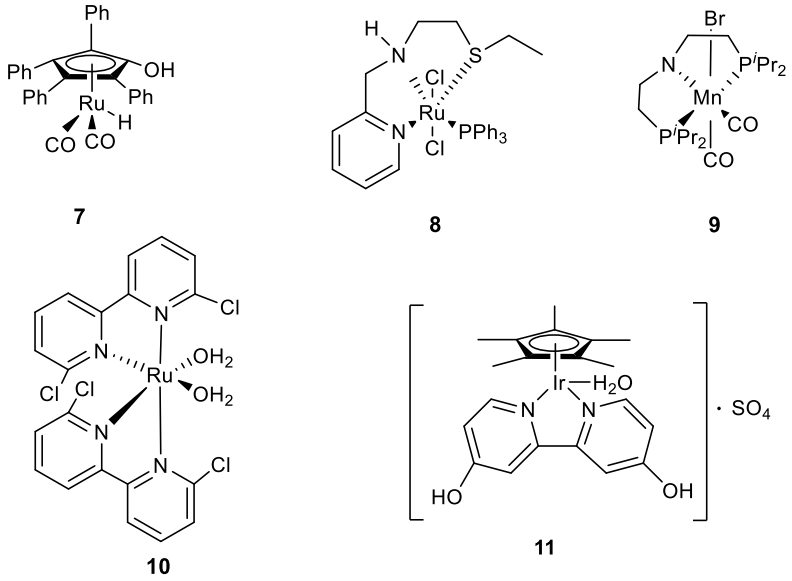

Figure 1.10. Examples of complexes active for hydrogenation of FUR to FA and of HMF to BHMF

1.2.3.3 Complexes for homogenous hydrogenation of FUR to FA

Selective homogenous hydrogenation of FUR to FA has been accomplished by few transition metal complexes reported in **Table 1.4**. In 2010 Huang *et al.* used the well-known $RuCl_2(PPh_3)_3$ (**1**)complex to yield furfural with good yields (Entry 1).[158] In this study it is showed that acetic acid accelerates the conversion of FUR probably due to the formation of $[Ru(O_2CCH_3)_2(PPh_3)_3]$ species.

In 2012 Gowda *et al.* reported the conversion of FUR to FA by using a ruthenium bis(diamine) complexs. (Entry 2).[159] Best reaction conditions were found to be 100°C, 2 hours and 50 bar oh hydrogen pressure by using **10**. 1.0 mol% of catalyst was necessary to achieve this result.

J. de Vries and co-workers used **8** achieving excellent isolated yield of FA (Entry 3).

A water soluble and recyclable semisandwich iridium complex (**11**) was reported by Wu *et al*. in 2016 (Entry 4).[160]Interestingly, pH was found to play a crucial role in the activity of the catalyst. At pH=5.0 the complex with electron-donating substituents on the bypiridine scaffold resulted the most efficient, while

stronger conditions were required with different ligands. However, studies regarding the recyclability of the catalyst were not provided.

Table 1.4 Most significant complexes used for the hydrogenation of FUR to FA under H_2.

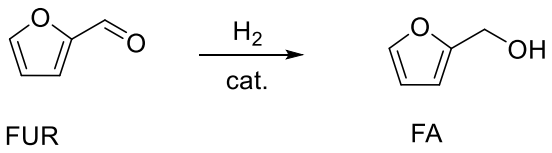

Entry	Cat.	Solvent	Conditions	Conv. %(Yield)	Ref.
1	$RuCl_2(PPh_3)_3$	/	70 °C, 20 bar, 3h	93.6%	[158]
2	*cis*-[Ru(6,6′-Cl_2bpy)$_2$(OH_2)$_2$](CF_3SO_3)$_2$	EtOH	100 °C, 50 bar, 2h	99	[159]
3	[$RuCl_2$(NNS)PPh_3]	*i*-Prop	80°C, 30 bar, 1h	99 (93)	[128]
4	[Cp*Ir(di-OH-bpy)(OH_2)][SO_4]	H_2O	120 °C, 10 bar, 1h	99	[160]

1.3 CLICK CHEMISTRY

In 2001 K. B. Sharpless and co-workers coined the term *Click Chemistry*, describing a novel concept of organic synthesis based on the use of a few simple high-yielding reactions.[161] This type of reaction must adhere a set of concepts. They must be modular, stereospecific and wide in scope, with no limitations by functional groups. Products need to be isolated in high yields by using simple, cheap and environmental-friendly purification processes such as crystallization or distillation, while chromatographic methods should be avoided. Inoffensive byproducts should be generated if any. Reactions conditions must be very mild and possibly insensitive to oxygen and water. According to these principles, the choose of a benign solvent is highly preferred, together with readily and commercially available starting materials.

It is worth to mention that click reactions have high thermodynamic driving force, usually above 20 kcal mol^{-1}, meaning that such processes proceed to completion rapidly.

All these principles fit well with the landmark concepts developed by P. T. Anastas in 1998, describing a new philosophy for chemical routes named *Green Chemistry* (**Figure 1.11**).[162]

Sharpless classified a set of extremely reliable reactions useful for the synthesis of building block libraries:[161,163,164]

- Cycloaddition reactions, in particular 1,3-dipolar and hetero-Diels-Alder reactions
- Nucleophilic ring-opening reactions, especially regarding epoxides, aziridines, cyclic sulfates, cyclic sulfamidates.
- Carbonyl chemistry of the non-aldol type (formation of oxime ethers, hydrazones, aromatic heterocylces)
- Addition to carbon-carbon multiple bonds: oxidation, epoxidation, dihydroxaylation, aziridination, nitrosyl and sulfenyl halide additions, some Michael addition.

Figure 1.11. 12 principles of green chemistry[165]

Among the portfolio of click reactions which emerged in the last years, two pioneering approaches will be highlighted:

- the copper azide-alkyne cycloaddition (CuAAC), for the formation of 1,4-disubstituted triazoles;
- the Thiol-ene addition of thiols to C=C double bonds for the formation of thioethers.

1.3.1 Cu Azide-alkyne cycloaddition (CuAAC)

In 1961 Rolf Huisgen reported the first cycloaddition between 1,3-dipolar azides and dipolarophile alkynes yielding a mixture of 1,4-1,5 disubstituted 1,2,3-1*H*-triazoles.[166–168]This approach was not catalyzed by transition metals complexes and needed to be carried out at 98 °C.

Inspired by these findings, in 2002 K.B. Shrapless and M. Meldal independently developed a new route for the regiospecific synthesis of 1,4-disubstiuted-1,2,3-triazoles by copper(I) catalysts (**Scheme 1.13**), which was named copper azide-alkyne cycloaddition (CuAAC). [164,169]

Later, the same research group devised a ruthenium catalyzed route for the synthesis of 1,5-disubstiuted-1,2,3-triazoles.[170,171]

CuAAC is conventionally considered the first click reaction developed for organic synthesis, as it owns all the criteria required by click chemistry. It proceeds at mild reaction conditions, generally room temperature, in a mixture of benign solvents such as water and *t*-ButOH. Commercially available starting materials, such as NaN_3 and alkynes are required for the formation of the triazole ring. The use of cheap copper salts as copper sulfate or copper acetate, $CuSO_4{\cdot}5H_2O$, $Cu(CH_3COO)_2$ has shown to be efficient as sources of copper(I) active catalysts, while sugar derived sodium ascorbate is generally used as reducing agent. Pure products are generally afforded by simple liquid-liquid extraction thus avoiding long and expensive purification processes such as flash chromatography.

Due to their facile accessibility, click-based triazole compounds have been extensively investigated for a wide range of applications, ranging from pharma,[172–174] polymers,[175–177] coordination chemistry,[178,179] drug delivery,[163,180] materials.[173]

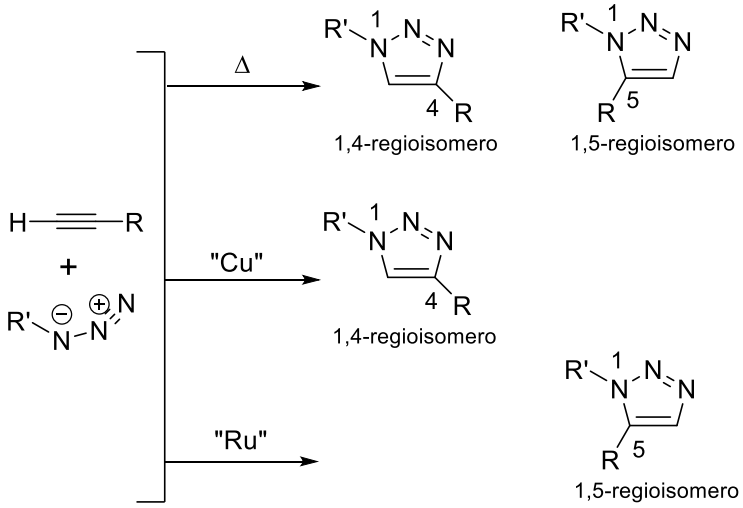

Scheme 1.13. Different approaches for the syntheis of 1,2,3 triazoles

In their seminal work on CuAAC, Sharpless and Fokin proposed an early mechanism involving mononuclear Cu(I) species as active catalysts. [164]

As reported in **Scheme 1.14**, coordination of alkyne to *in situ* generated Cu(I) active catalysts was expected to afford a copper acetylide complex (**A**). Further coordination of azide was thought to give azide-acetylide Cu(I) complex (**B**) which then undergoes ring closure through the six-member ring (**C**). Finally, the product is released and Cu(I) is regenerated. However, this early mechanism has been further implemented by the same authors which provided extensive DFT calculations. They demonstrated that the formation of a six-membered copper(III) metallacycle is 14.9 kcal mol^{-1} compared to a barrier of 25.7 kcal mol^{-1} for the uncatalyzed cycloaddition, providing then an explanation for the enormous rate acceleration by using copper(I) as catalyst.[181] Cu(I)-acetylides interacting with organoazides were finally isolated by Straub.[182]

In 2013, Fokin and colleagues published an elegant mechanistic study in which they show the ineffective role of monomeric copper-acetylide complexes towards organic azides unless an exogenous copper catalyst is added.[183]

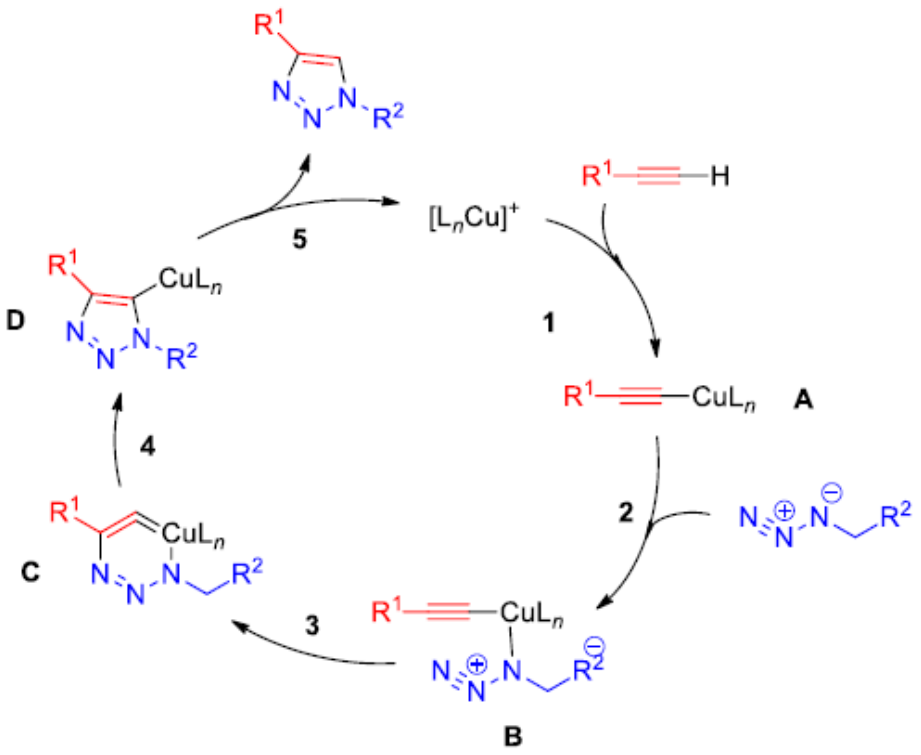

Scheme 1.14. Early CuAAC mechanism with mononuclear copper species[164]

This experimental evidence leads to the conclusion that dinuclear species are the active catalysts involved into the CuAAC, according to the new mechanism reported in Scheme 1.15.

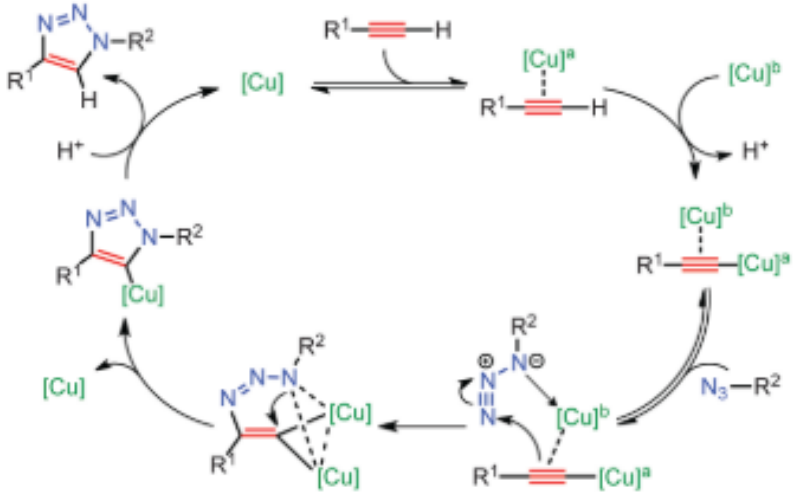

Scheme 1.15. CuAAC mechanism with dinuclear copper species[183]

Such a postulated π,σ-bis(copper) acetylide intermediate type and a new bis(metallated) triazole complex, viewed as one of the resting states of the catalytic cycle, were isolated and X-ray structurally characterized by Bertrand, by using the strong properties σ-donating and π-accepting properties of cyclic (alkyl)(amino) carbenes for the isolation of copper metal ions.[184] The mechanism reported in Scheme 1.18 is, to date, the most updated version for the CuAAC click reaction.

1.3.2 Thiol-Ene click reaction

Based on the considerations established by *Click Chemistry*, a new click reaction powerfully emerged few years later and it was named thiol-ene, as it focuses on the weak sulfur-hydrogen bonds of thiols which results in a crowd of high yielding chemical reactions. The addition of thiols to activated carbon-carbon double bonds was early reported since the beginning of 20th century, when T. Posner described the interaction among thiophenol and a range of either aliphatic and aromatic olefins to give corresponding thioethers. [185]

Due to the extremely reactive nature of thiols, reaction times necessary to achieve quantitative conversion of the substrates have been estimated to be less than 1-10 seconds. From a chemical point of view, thiols (traditionally referred in the literature as mercaptans) are considered as soft nucleophiles due the combination of d-orbitals and the inherent electron density associated with sulfur, thus high reactivity with substrates prone to reaction with strong nucleophiles is associated to thiols.

One more attracting advantage represented by thiol-ene is the possibility to trigger the reaction by the use of light or photoinitiators systems. This capability could offer an intriguing alternative to the use of catalysts or synthetic radical initiators, thus increasing the applicability of the reaction to biological systems and biomaterials. On the other side, the main disadvantage is identified in the notoriously malodourous of thiol, which make derived compounds hard to be used in a large scale.

As schematized by Hoyle and Bowman (Scheme 1.16),[186] two different reaction pathways have been proposed for the thiol-ene reaction: a) thiol-ene free radical addition to electron-rich/electron poor C=C: b) catalyzed thiol Michael addition to electron-deficient C=C.

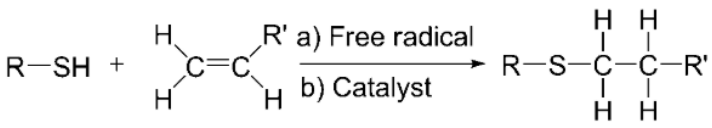

Scheme 1.16. Thiol-Ene net reaction

Thiols can be classified as a) aromatic thiols b) thiolacetate (i.e. thiol glycolate) c) thiolpropionate thiols thiols and alkyl thiols. It is important to recognize which type of substrate is used in order to evaluate the mechanism which fits finer. In this frame, a comprehensive knowledge of corresponding thiolates and thiyl radicals is also required. As reported in Scheme 1.17 sulfur-hydrogen bond of alkyl thiols is easily cleaved *via* homolysis, while suffering low pKa.

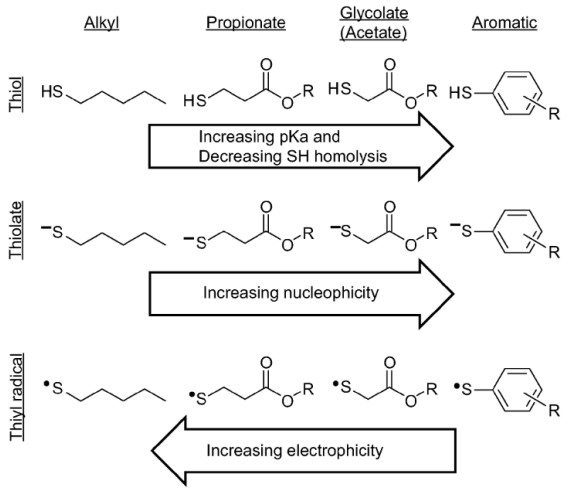

Scheme 1.17. Classes of thiols and corresponding thiolates and thiyl radicals, ordered by pKa, nucleophicity and electrophicity[187]

The broad portfolio of commercially available thiols is reflected into the wide range of chemical reactions which own the characteristics to proceed *via* thiol-ene reaction (Scheme 1.18).

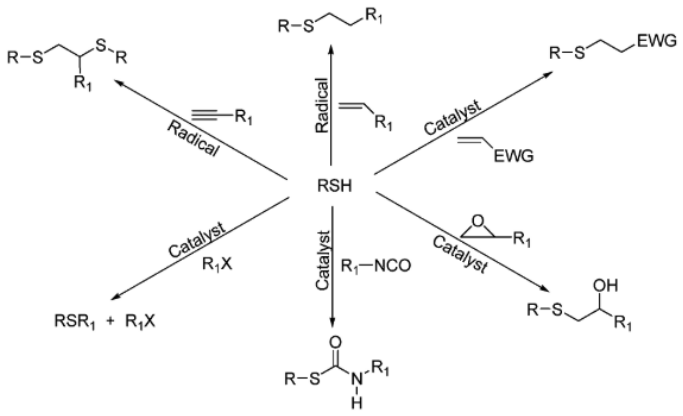

Scheme 1.18. Reactivity of thiols[187]

The radical reaction mechanism involves a series of subsequent steps. The first step, named initiation, consists in the generation of thiyl radical, which can occur photochemically, by heating or *via* redox. Generally, photochemical initiation is preferable since it allows milder reaction conditions and doesn't need radical initiators. However, also methodologies that provide for a thermal or redox initiation are commonly used. The clickable nature of the reaction is mainly derived from the second step, which alternates a chain transfer process with a propagation process (Scheme 1.19). The radical formed during the initiation step, adds to the double bond to form a radical intermediate centered on the atom carbon in position 2; subsequently a hydrogen atom is is provided from the thiol to afford the final product and, at the same time, a new reactive radical is formed.

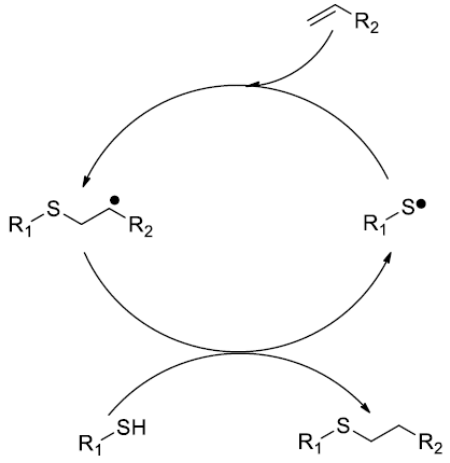

Scheme 1.19. Thiol-ene radical mechanism

Thiol-ene reactions can also proceed *via* Michael addition thus catalyzed by a base, some of which can also act as nucleophiles. An electronic poor double bond C = C, activated by a vicinal electron withdrawing group, is required. The generally accepted mechanism for this type of reaction is outlined in Scheme 1.20. A base, B, deprotonates the thiol generating a thiolate anion, RS^-, and its acid Conjoined BH^+. The thiolate anion thus generated attacks the electrophilic carbon atom in β position of the C=C bond, generating an anionic intermediate with the negative charge on the central carbon, acting itself as a strong base which deprotonates H+, providing the final thioether and regenerating the catalyst base.

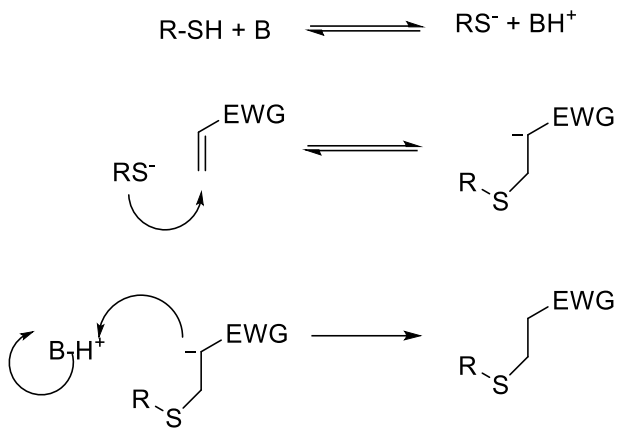

Scheme 1.20. Mechanism of Michael addition type thiol-ene click reaction

1.4 REFERENCES

[1] T. I. J. Dugmore, J. H. Clark, J. Bustamante, J. A. Houghton, A. S. Matharu, *Top. Curr. Chem.* 2017, *375*, 1–49.

[2] J. Jose´goldemberg, *Energy Policy* 2006, *34*, 2185–2190.

[3] Claudia Giacovelli, *UNEP (2018). Single-Use Platics: A Roadmap for Sustainability*, 2018.

[4] E. Cséfalvay, I. T. Horváth, *ACS Sustain. Chem. Eng.* 2018, *6*, 8868–8874.

[5] S. Shafiee, E. Topal, *Energy Policy* 2009, *37*, 181–189.

[6] I. Capellán-Pérez, M. Mediavilla, C. de Castro, Ó. Carpintero, L. J. Miguel, *Energy* 2014, *77*, 641–666.

[7] W. P. Nel, C. J. Cooper, *Energy Policy* 2009, *37*, 166–180.

[8] L. Chiari, A. Zecca, *Energy Policy* 2011, *39*, 5026–5034.

[9] *Kyoto Protocol to the United Nations Framework Convention on Climate Change United Nations*, 1998.

[10] UNCCS, *United Nations Clim. Chang. Secr.* 2019.

[11] Eurostat, *Sustainable Development in the European Union 2015*, 2015.

[12] European Commission, 2014, 1–54.

[13] UNEP, 2017, 1–29.

[14] OECD, *OECD Publ.* 2004, *Biomass an*, 1–21.

[15] M. Geissdoerfer, P. Savaget, N. M. P. Bocken, E. J. Hultink, *J. Clean. Prod.* 2017, *143*, 757–768.

[16] D. M. Alonso, S. H. Hakim, S. Zhou, W. Won, O. Hosseinaei, J. Tao, V. Garcia-Negron, A. H. Motagamwala, M. A. Mellmer, K. Huang, et al., *Sci. Adv.* 2017, *3*, 1–7.

[17] J. Zakzeski, P. C. A. Bruijnincx, A. L. Jongerius, B. M. Weckhuysen, *Chem. Rev.* 2010, *110*, 3552–3599.

[18] A. Camia, N. Rober, R. Jonsson, R. Pilli, S. Garcia-Condado, R. Lopez-Lozano, M. van der Velde, T. Ronzon, P. Gurria, R. M'Barek, et al., *Biomass Production, Supply, Uses and Flows in the European Union. First Results from an Integrated Assessment*, 2018.

[19] European Commission, *Preparatory Study on Food Waste across EU 27*, 2010.

[20] J. H. Clark, R. Luque, A. S. Matharu, *Annu. Rev. Chem. Biomol. Eng.* 2012, *3*, 183–207.

[21] J. G. de Vries, *Chem. Rec.* 2016, *16*, 2783–2796.

[22] A. Corma Canos, S. Iborra, A. Velty, *Chem. Rev.* 2007, *107*, 2411–2502.

[23] L. László, L. Mika, † Edit Cséfalvaycséfalvay, A.́ Ron, N. Németh, *Chem. Rev.* 2017, *118*, 505–613.

[24] C. O. Tuck, E. Pérez, I. T. Horváth, R. A. Sheldon, M. Poliakoff, *Science* 2012, *337*, 695–699.

[25] W. Schutyser, T. Renders, S. Van Den Bosch, S. F. Koelewijn, G. T. Beckham, B. F. Sels, *Chem. Soc. Rev.* 2018, *47*, 852–908.

[26] Z. Zhang, J. Song, B. Han, *Chem. Rev.* 2017, *117*, 6834–6880.

[27] G. S. Macala, T. D. Matson, C. L. Johnson, R. S. Lewis, A. V. Iretskii, P. C. Ford, *ChemSusChem* 2009, *2*, 215–217.

[28] P. Gallezot, *Chem. Soc. Rev.* 2012, *41*, 1538–1558.

[29] C. H. Zhou, X. Xia, C. X. Lin, D. S. Tong, J. Beltramini, *Chem. Soc. Rev.* 2011, *40*, 5588–5617.

[30] V. K. Ponnusamy, D. D. Nguyen, J. Dharmaraja, S. Shobana, J. R. Banu, R. G. Saratale, S. W. Chang, G. Kumar, *Bioresour. Technol.* 2019, *271*, 462–472.

[31] F. H. Isikgor, C. R. Becer, *Polym. Chem.* 2015, *6*, 4497–4559.

[32] R. A. Sheldon, *Green Chem.* 2014, *16*, 950–963.

[33] Q. Meng, M. Hou, H. Liu, J. Song, B. Han, *Nat. Commun.* 2017, *8*, 1–8.

[34] J. Howard, D. W. Rackemann, J. P. Bartley, C. Samori, W. O. S. Doherty, *ACS Sustain. Chem. Eng.* 2018, *6*, 4531–4538.

[35] C. Samorí, C. Torri, D. Fabbri, G. Falini, C. Faraloni, P. Galletti, S. Spera, E. Tagliavini, G. Torzillo, *ChemSusChem* 2012, *5*, 1501–1512.

[36] B. Program, T. Werpy, G. Petersen, *Top Value Added Chemicals from Biomass Volume I-Results of Screening for Potential Candidates from Sugars and Synthesis Gas Produced by the Staff at Pacific Northwest National Laboratory (PNNL) National Renewable Energy Laboratory (NREL) Office of Biomass*, n.d.

[37] J. J. Bozell, G. R. Petersen, *Green Chem.* 2010, *12*, 539–554.

[38] R. Ciriminna, C. Della Pina, M. Rossi, M. Pagliaro, *Eur. J. Lipid Sci. Technol.* 2014, *116*, 1432–1439.

[39] "Glycerol Market - Global Industry Analysis, Size, Growth and Forecast 2012-2018," can be found under https://www.transparencymarketresearch.com/glycerol-market.html, n.d.

[40] U. I. Nda-Umar, I. Ramli, Y. H. Taufiq-Yap, E. N. Muhamad, *Catalysts* 2019, *9*, 15.

[41] C. A. Schwengber, H. J. Alves, R. A. Schaffner, F. A. Da Silva, R. Sequinel, V. R. Bach, R. J. Ferracin, *Renew. Sustain. Energy Rev.* 2016, *58*, 259–266.

[42] A. Brandner, K. Lehnert, A. Bienholz, M. Lucas, P. Claus, *Top. Catal.* 2009, *52*, 278–287.

[43] C. H. Zhou, J. N. Beltramini, Y. X. Fan, G. Q. Lu, *Chem. Soc. Rev.* 2008, *37*, 527–549.

[44] P. S. Kong, M. K. Aroua, W. M. A. W. Daud, *Renew. Sustain. Energy Rev.* 2016, *63*, 533–555.

[45] S. Ren, X. P. Ye, *Fuel Process. Technol.* 2015, *140*, 148–155.

[46] L. Prati, P. Spontoni, A. Gaiassi, *Top. Catal.* 2009, *52*, 288–296.

[47] A. Behr, J. Eilting, K. Irawadi, J. Leschinski, F. Lindner, *Green Chem.* 2008, *10*, 13–30.

[48] O. Valerio, J. M. Pin, M. Misra, A. K. Mohanty, *ACS Omega* 2016, *1*, 1284–1295.

[49] J. R. Dontulwar, D. K. Borikar, B. B. Gogte, *Carbohydr. Polym.* 2006, *65*, 207–210.

[50] M. Calderón, M. A. Quadir, S. K. Sharma, R. Haag, *Adv. Mater.* 2010, *22*, 190–218.

[51] R. Christoph, B. Schmidt, U. Steinberner, W. Dilla, R. Karinen, in *Ullmann's Encycl. Ind. Chem.*, Wiley-VCH Verlag GmbH & Co. KGaA, Weinheim, Germany, 2006.

[52] F. Jérôme, G. Kharchafi, I. Adam, J. Barrault, *Green Chem.* 2004, *6*, 72–74.

[53] "DGF Conference Hamburg," can be found under http://www.dgfett.de/meetings/archiv/hamburg/, n.d.

[54] M. O. Sonnati, S. Amigoni, E. P. Taffin De Givenchy, T. Darmanin, O. Choulet, F. Guittard, *Green Chem.* 2013, *15*, 283–306.

[55] Z. Wang, J. Zhuge, H. Fang, B. A. Prior, *Biotechnol. Adv.* 2001, *19*, 201–223.

[56] G. P. da Silva, M. Mack, J. Contiero, *Biotechnol. Adv.* 2009, *27*, 30–39.

[57] C. K. Liu, *J. Appl. Polym. Sci.* 2002, *87*, 1221–1231.

[58] X. Li, P. Jia, T. Wang, *ACS Catal.* 2016, *6*, 7621–7640.

[59] A. S. Mamman, J. M. Lee, Y. C. Kim, I. T. Hwang, N. J. Park, Y. K. Hwang, J. S. Chang, J. S. Hwang, *Biofuels, Bioprod. Biorefining* 2008, *2*, 438–454.

[60] "MarketWatch: Stock Market News - Financial News," can be found under https://www.marketwatch.com/, n.d.

[61] H. J. Brownlee, E. S. Carl Miner, *Ind. Eng. Chem.* 2019, *40*, 201–204.

[62] K. J. Zeitsch, *The Chemistry and Technology of Furfural and Its Many By-Products*, Elsevier, The Netherlands, 2000.

[63] B. Pignataro, *Ideas in Chemistry and Molecular Sciences*, Wiley-VCH Verlag GmbH & Co. KGaA, Weinheim, Germany, 2010.

[64] M. J. Antal, T. Leesomboon, W. S. Mok, G. N. Richards, *Carbohydr. Res.* 1991, *217*, 71–85.

[65] B. Danon, G. Marcotullio, W. De Jong, *Green Chem.* 2014, *16*, 39–54.

[66] P. J. Deuss, K. Barta, J. G. De Vries, *Catal. Sci. Technol.* 2014, *4*, 1174–1196.

[67] Y. Luo, Z. Li, X. Li, X. Liu, J. Fan, J. H. Clark, C. Hu, *Catal. Today* 2019, *319*, 14–24.

[68] W. De Jong, G. Marcotullio, *Int. J. Chem. React. Eng.* 2010, *8*.

[69] A. Demirbas, *Energy Convers. Manag.* 2008, *50*, 14–34.

[70] J. C. Serrano-Ruiz, J. A. Dumesic, *Energy Environ. Sci.* 2011, *4*, 83–99.

[71] J. P. Lange, E. Van Der Heide, J. Van Buijtenen, R. Price, *ChemSusChem* 2012, *5*, 150–166.

[72] N. S. Iegemund, H. Aktiengesellschaft, F. Republic, F. R. E. D. B. Ehr, M. Mining, M. Company, S. Paul, *Ullmann's Encyclopedia of Industrial Chemistry: Fluorine Compounds, Organic*, Wiley, 2000.

[73] R. H. Leonard, *Ind. Eng. Chem.* 1956, *48*, 1331–1341.

[74] F. D. Pileidis, M. M. Titirici, *ChemSusChem* 2016, *9*, 562–582.

[75] "Products & applications - Avantium," can be found under https://www.avantium.com/yxy/products-applications/, n.d.

[76] D. F. Aycock, *Org. Process Res. Dev.* 2007, *11*, 156–159.

[77] F. van der Klis, R. J. I. Knoop, J. H. Bitter, L. A. M. van den Broek, *J. Polym. Sci. Part A Polym. Chem.* 2018, *56*, 1903–1906.

[78] Z. Zhang, *ChemSusChem* 2016, *9*, 156–171.

[79] S. Raoufmoghaddam, M. T. M. Rood, F. K. W. Buijze, E. Drent, E. Bouwman, *ChemSusChem* 2014, *7*, 1984–1990.

[80] A. Marckwordt, F. El Ouahabi, H. Amani, S. Tin, N. V. Kalevaru, P. C. J. Kamer, S. Wohlrab, J. G. de Vries, *Angew. Chemie - Int. Ed.* 2019, *58*, 3486–3490.

[81] A. Caretto, A. Perosa, *ACS Sustain. Chem. Eng.* 2013, *1*, 989–994.

[82] F. S. Hayess, D. Ross; Hayess MHB, *The Biofine Process e Production of Levulinic Acid, Furfural and Formic Acid from Lignocellulosic Feedstock. In: Kamm B, Gruber P, Kamm M, Editors. Biorefineries e Industrial Processes and Products*, Wiley-VCH Verlag, Weinheim, Germany, 2006.

[83] J. J. Bozell, L. Moens, D. C. Elliott, Y. Wang, G. G. Neuenscwander, S. W. Fitzpatrick, R. J. Bilski, J. L. Jarnefeld, in *Resour. Conserv. Recycl.*, Elsevier Science Publishers B.V., 2000, pp. 227–239.

[84] A. Mukherjee, M. J. Dumont, V. Raghavan, *Biomass and Bioenergy* 2015, *72*, 143–183.

[85] *Process for the Production of a Biomass Hydrosylate*, 2012, WO 2014/087016 Al.

[86] "United States Patent: 9073841," can be found under http://patft.uspto.gov/netacgi/nph-Parser?d=PALL&p=1&u=%2Fnetahtml%2FPTO%2Fsrchnum.htm&r=1&f=G&l=50&s1=9073841.PN.&OS=PN/9073841&RS=PN/9073841, n.d.

[87] "GFBiochemicals," can be found under http://www.gfbiochemicals.com/company/, n.d.

[88] G. Yang, E. A. Pidko, E. J. M. Hensen, *J. Catal.* 2012, *295*, 122–132.

[89] J. Horvat, B. Klaić, B. Metelko, V. Šunjić, *Tetrahedron Lett.* 1985, *26*, 2111–2114.

[90] J. Zhang, E. Weitz, *ACS Catal.* 2012, *2*, 1211–1218.

[91] A. A. Rosatella, S. P. Simeonov, R. F. M. Frade, C. A. M. Afonso, *Green Chem.* 2011, *13*, 754–793.

[92] L. Hu, J. Xu, S. Zhou, A. He, X. Tang, L. Lin, J. Xu, Y. Zhao, *ACS Catal.* 2018, *8*, 2959–2980.

[93] R. J. Van Putten, J. C. Van Der Waal, E. De Jong, C. B. Rasrendra, H. J. Heeres, J. G. De Vries, *Chem. Rev.* 2013, *113*, 1499–1597.

[94] B. Michael, C. Michele, R. Stefan, B. M. Scalet, R. Serge, D. S. Luis, *Best Available Techniques (BAT) Reference Document for the Tanning of Hides and Skins (Integrated Pollution Prevention and Control)*, Publicatio Office Of The European Union, Luxembourg, 2013.

[95] A. M. Teekens, M. E. Bruins, J. M. van Kasteren, W. H. Hendriks, J. P. Sanders, *J. Sci. Food Agric.* 2016, *96*, 2603–2612.

[96] L. Cavani, A. Margon, L. Sciubba, C. Ciavatta, C. Marzadori, *AIMS Agric. Food* 2017, *2*, 221–232.

[97] M. Fountoulakis, H. W. Lahm, *J. Chromatogr. A* 1998, *826*, 109–134.

[98] H. Jiang, J. Liu, W. Han, *Waste Manag. Res.* 2016, *34*, 399–408.

[99] T. M. Lammens, D. De Biase, M. C. R. Franssen, E. L. Scott, J. P. M. Sanders, *Green Chem.* 2009, *11*,

1562–1567.

[100] A. V. Pukin, C. G. Boeriu, E. L. Scott, J. P. M. Sanders, M. C. R. Franssen, *J. Mol. Catal. B Enzym.* 2010, *65*, 58–62.

[101] J. Sanders, E. Scott, R. Weusthuis, H. Mooibroek, *Macromol. Biosci.* 2007, *7*, 105–117.

[102] S. N. Mukhopadhyay, P. Saha, N. Saha, L. Saha, K. Kolomaznik, *J. Am. leather Chem. Assoc.* 2004, *99*, 449–456.

[103] M. Catalina, J. Cot, A. M. Balu, J. C. Serrano-Ruiz, R. Luque, *Green Chem.* 2012, *14*, 308–312.

[104] B. Cornils, W. A. Herrmann, M. Beller, R. Paciello, Eds. , *Applied Homogeneous Catalysis with Organometallic Compounds*, Wiley-VCH Verlag GmbH & Co. KGaA, Weinheim, Germany, 2017.

[105] R. Franke, D. Selent, A. Börner, *Chem. Rev.* 2012, *112*, 5675–5732.

[106] J.-M. Basset, R. Psaro, D. Roberto, R. Ugo, Eds. , *Modern Surface Organometallic Chemistry*, Wiley-VCH Verlag GmbH & Co. KGaA, Weinheim, Germany, 2009.

[107] C. Lecuyer, F. Quignard, A. Choplin, D. Olivier, J.-M. Basset, *Angew. Chemie Int. Ed. English* 1991, *30*, 1660–1661.

[108] K. Murugesan, M. Beller, R. V. Jagadeesh, *Angew. Chemie - Int. Ed.* 2019, *58*, 5064–5068.

[109] B. Cornils, W. A. Herrmann, *Aqueous-Phase Organometallic Catalysis Edited By*, Wiley-VCH Verlag, Weinheim, Germany, 2004.

[110] B. Cornils, W. A. Herrmann, J. Horvat, W. Leitner, S. Mecking, H. Olivier-Bourbigou, D. Vogt, Eds. , *Multiphase Homogenous Catalysis*, Wiley-VCH Verlag GmbH & Co. KGaA, Weinheim, Germany, 2005.

[111] P. J. Deuss, K. Barta, J. G. De Vries, *Catal. Sci. Technol.* 2014, *4*, 1174–1196.

[112] S. Bhaduri, D. Mukesh, Eds. , *Homogeneous Catalysis Mechanisms and Industrial Applications*, Wiley-VCH Verlag GmbH & Co. KGaA, Weinheim, Germany, n.d.

[113] A. Y. Li, A. Moores, *ACS Sustain. Chem. Eng.* 2019, *7*, 10182–10197.

[114] J. G. de Vries, C. J. Elsevier, Eds. , *The Handbook of Homogeneous Hydrogenation*, Wiley-VCH Verlag GmbH & Co. KGaA, Weinheim, Germany, 2006.

[115] P. Dupau, *Top. Organomet. Chem., Vol.42: Organometallics as Catalysts in the Fine Chemical Industry*, Springer International Publishing, Berlin, Heidelberg, 2011.

[116] R. S. Coffey, *Chem. Commun.* 1967, 923–924.

[117] R. Spogliarich, E. Farnetti, J. Kašpar, M. Graziani, E. Cesarotti, *J. Mol. Catal.* 1989, *50*, 19–29.

[118] E. Farnetti, M. Pesce, J. Kašpar, R. Spogliarich, M. Graziani, *J. Chem. Soc. Chem. Commun.* 1986, 746–747.

[119] E. Farnetti, G. Nardin, M. Graziani, *J. Organomet. Chem.* 1991, *417*, 163–172.

[120] R. X. Li, X. J. Li, N. B. Wong, K. C. Tin, Z. Y. Zhou, T. C. W. Mak, *J. Mol. Catal. A Chem.* 2002, *178*, 181–190.

[121] "Quotazione metalli - Legor," can be found under http://www.legor.com/it/quotazione-metalli, n.d.

[122] J. Tsuji, H. Suzuki, *Chem. Lett.* 1977, *6*, 1085–1086.

[123] A. Miyashita, A. Yasuda, H. Takaya, K. Toriumi, T. Ito, T. Souchi, R. Noyori, *J. Am. Chem. Soc.* 1980, *102*, 7932–7934.

[124] T. Ohkuma, H. Ooka, S. Hashiguchi, T. Ikariya, R. Noyori, *J. Am. Chem. Soc.* 1995, *117*, 2675–2676.

[125] J. R. Khusnutdinova, D. Milstein, *Angew. Chemie - Int. Ed.* 2015, *54*, 12236–12273.

[126] C. J. Kliewer, M. Bieri, G. A. Somorjai, *J. Am. Chem. Soc.* 2009, *131*, 9958–9966.

[127] A. Stolle, T. Gallert, C. Schmöger, B. Ondruschka, 2013, *3*, 2112.

[128] P. Puylaert, R. van Heck, Y. Fan, A. Spannenberg, W. Baumann, M. Beller, J. Medlock, W. Bonrath, L. Lefort, S. Hinze, et al., *Chem. - A Eur. J.* 2017, *23*, 8473–8481.

[129] M. Hernandez, P. Kalck, *J. Mol. Catal. A Chem.* 1997, *116*, 131–146.

[130] B. Cornils, *J. Mol. Catal. A Chem.* 1999, *143*, 1–10.

[131] J. M. Grosselin, C. Mercier, G. Allmang, F. Grass Rhone-Poulenc Recherches, S.-F. Cedex, *Organometallics* 1991, *10*, 370.

[132] H. Doucet, T. Ohkuma, K. Murata, T. Yokozawa, M. Kozawa, E. Katayama, A. F. England, T. Ikariya, R. Noyori, *Angew. Chemie - Int. Ed.* 1998, *8552*, 1703–1707.

[133] K. Abdur-Rashid, A. J. Lough, R. H. Morris, *Organometallics* 2000, *19*, 2655–2657.

[134] K. Abdur-Rashid, M. Faatz, A. J. Lough, R. H. Morris, *J. Am. Chem. Soc.* 2001, *123*, 7473–7474.

[135] T. A. Bender, J. A. Dabrowski, M. R. Gagné, *Nat. Rev. Chem.* 2018, *2*, 35–46.

[136] M. Besson, P. Gallezot, C. Pinel, *Chem. Rev.* 2014, *114*, 1827–1870.

[137] S. De, B. Saha, R. Luque, *Bioresour. Technol.* 2015, *178*, 108–118.

[138] K. Yan, Y. Yang, J. Chai, Y. Lu, *Appl. Catal. B Environ.* 2015, *179*, 292–304.

[139] K. Osakada, T. Ikariya, S. Yoshikawa, *J. Organomet. Chem.* 1982, *231*, 79–90.

[140] H. Mehdi, V. Fábos, R. Tuba, A. Bodor, L. T. Mika, I. T. Horváth, in *Top. Catal.*, 2008, pp. 49–54.

[141] F. M. A. Geilen, B. Engendahl, A. Harwardt, W. Marquardt, J. Klankermayer, W. Leitner, *Angew. Chemie - Int. Ed.* 2010, *49*, 5510–5514.

[142] C. Delhomme, L. A. Schaper, M. Zhang-Preße, G. Raudaschl-Sieber, D. Weuster-Botz, F. E. Kühn, *J. Organomet. Chem.* 2013, *724*, 297–299.

[143] J. M. Tukacs, D. Király, A. Strádi, G. Novodarszki, Z. Eke, G. Dibó, T. Kégl, L. T. Mika, *Green Chem.* 2012, *14*, 2057–2065.

[144] J. M. Tukacs, M. Novák, G. Dibó, L. T. Mika, *Catal. Sci. Technol.* 2014, *4*, 2908–2912.

[145] A. Dutta Chowdhury, R. Jackstell, M. Beller, *ChemCatChem* 2014, *6*, 3360–3365.

[146] "Triphenylphosphine-3,3′,3′′-trisulfonic acid trisodium salt ≥95.0% | Sigma-Aldrich," can be found under https://www.sigmaaldrich.com/catalog/product/aldrich/744034?lang=it&region=IT, n.d.

[147] W. Li, J. H. Xie, H. Lin, Q. L. Zhou, *Green Chem.* 2012, *14*, 2388–2390.

[148] J. Deng, Y. Wang, T. Pan, Q. Xu, Q. X. Guo, Y. Fu, *ChemSusChem* 2013, *6*, 1163–1167.

[149] Y. Yi, H. Liu, L. P. Xiao, B. Wang, G. Song, *ChemSusChem* 2018, *11*, 1474–1478.

[150] S. Wang, H. Huang, V. Dorcet, T. Roisnel, C. Bruneau, C. Fischmeister, *Organometallics* 2017, *36*, 3152–3162.

[151] C. Zeng, H. Seino, J. Ren, K. Hatanaka, N. Yoshie, *Macromolecules* 2013, *46*, 1794–1802.

[152] E. R. Sacia, M. Balakrishnan, A. T. Bell, *J. Catal.* 2014, *313*, 70–79.

[153] Joel M. Harris, A. Mark D. Keranen, G. A. O'Doherty, *J. Org. Chem.* 1999, *64*, 2982–2983.

[154] Y. Román-Leshkov, C. J. Barrett, Z. Y. Liu, J. A. Dumesic, *Nature* 2007, *447*, 982–985.

[155] L. Hu, J. Xu, S. Zhou, A. He, X. Tang, L. Lin, J. Xu, Y. Zhao, *ACS Catal.* 2018, *8*, 2959–2980.

[156] T. Pasini, G. Solinas, V. Zanotti, S. Albonetti, F. Cavani, A. Vaccari, A. Mazzanti, S. Ranieri, R. Mazzoni, *Dalt. Trans.* 2014, *43*, 10224–10234.

[157] S. Elangovan, C. Topf, S. Fischer, H. Jiao, A. Spannenberg, W. Baumann, R. Ludwig, K. Junge, M. Beller, *J. Am. Chem. Soc.* 2016, *138*, 8809–8814.

[158] F. Huang, W. Li, Q. Lu, X. Zhu, *Chem. Eng. Technol.* 2010, *33*, 2082–2088.

[159] A. S. Gowda, S. Parkin, F. T. Ladipo, *Appl. Organomet. Chem.* 2012, *26*, 86–93.

[160] W. P. Wu, Y. J. Xu, S. W. Chang, J. Deng, Y. Fu, *ChemCatChem* 2016, *8*, 3375–3380.

[161] H. C. Kolb, M. G. Finn, K. B. Sharpless, *Angew. Chemie - Int. Ed.* 2001, *40*, 2004–2021.

[162] P. T. Anastas, J. C. Warner, Eds. , *Green Chemistry: Theory and Practice*, Oxford Univ Pr, 1998.

[163] H. C. Kolb, K. B. Sharpless, *Drug Discov. Today* 2003, *8*, 1128–1137.

[164] V. V. Rostovtsev, L. G. Green, V. V. Fokin, K. B. Sharpless, *Angew. Chemie - Int. Ed.* 2002, *41*, 2596–2599.

[165] "12 Principles of Green Chemistry - American Chemical Society," can be found under https://www.acs.org/content/acs/en/greenchemistry/principles/12-principles-of-green-chemistry.html, n.d.

[166] R. Huisgen, *Proc. Chem. Soc.* 1961, 101.

[167] R. Huisgen, *Angew. Chemie - Int. Ed.* 1963, *2*, 565–632.

[168] R. Huisgen, *J. Org. Chem.* 1976, *41*, 403–419.

[169] C. W. Tornøe, C. Christensen, M. Meldal, *J. Org. Chem.* 2002, *67*, 3057–3064.

[170] L. Zhang, X. Chen, P. Xue, H. H. Y. Sun, I. D. Williams, K. B. Sharpless, V. V Fokin, G. Jia, *J. Am. Chem. Soc.* 2005, *127*, 15998–15999.

[171] L. Kyhn Rasmussen, B. C. Boren, V. V Fokin, *Org. Lett.* 2007, *9*, 5337–5339.

[172] S. G. Agalave, S. R. Maujan, V. S. Pore, *Chem. - An Asian J.* 2011, *6*, 2696–2718.

[173] J. Huo, H. Hu, M. Zhang, X. Hu, M. Chen, D. Chen, J. Liu, G. Xiao, Y. Wang, Z. Wen, *J. Enzyme Inhib. Med. Chem.* 2017, *26*, 1–21.

[174] R. Kharb, P. Chander, S. & Mohammed, S. Yar, *J. Enzyme Inhib. Med. Chem.* 2011, *26*, 1–21.

[175] M. Meldal, *Macromol. Rapid Commun.* 2008, *29*, 1016–1051.

[176] A. R. Katritzky, N. K. Meher, S. Hanci, R. Gyanda, S. R. Tala, S. Mathai, R. S. Duran, S. Bernard, F. Sabri, S. K. Singh, et al., *J. Polym. Sci. Part A Polym. Chem.* 2008, *46*, 238–256.

[177] P. Leophairatana, C. C. De Silva, J. T. Koberstein, *J. Polym. Sci. Part A Polym. Chem.* 2018, *56*, 75–84.

[178] D. Schweinfurth, L. Hettmanczyk, L. Suntrup, B. Sarkar, *Zeitschrift fur Anorg. und Allg. Chemie* 2017, *643*, 554–584.

[179] Q. V. C. Van Hilst, N. R. Lagesse, D. Preston, J. D. Crowley, *Dalt. Trans.* 2018, *47*, 997–1002.

[180] P. Thirumurugan, D. Matosiuk, K. Jozwiak, *Chem. Rev* 2013, *113*, 4905–4979.

[181] F. Himo, T. Lovell, R. Hilgraf, V. V Rostovtsev, L. Noodleman, † K Barry Sharpless, V. V Fokin, *J. Am. Chem. Soc.* 2005, *127*, 210–216.

[182] C. Nolte, P. Mayer, B. F. Straub, *Angew. Chemie - Int. Ed.* 2007, *46*, 2101–2103.

[183] B. T. Worrell, J. A. Malik, V. V. Fokin, *Science* 2013, *340*, 457–460.

[184] L. Jin, D. R. Tolentino, M. Melaimi, G. Bertrand, *Sci. Adv.* 2015, *1*, e1500304.

[185] T. Posner, *Berichte der Dtsch. Chem. Gesellschaft* 1905, *38*, 646–657.

[186] C. E. Hoyle, C. N. Bowman, *Angew. Chemie - Int. Ed.* 2010, *49*, 1540–1573.

[187] C. E. Hoyle, A. B. Lowe, C. N. Bowman, *Chem. Soc. Rev.* 2010, *39*, 1355–1387.

2 AIM AND STRUCTURE OF THE THESIS

This thesis aims to provide new technologies for the valorization of biomass and it is structured as described below.

At first, Chapter 3 presents the valorization of animal biomass which were used for the synthesis of biopolymers with retanning activity to produce eco-friendly leather. The characterization of the starting materials, intermediates and final biopolymer has been deeply discussed. The influence of the enzymatic hydrolytic process, which allowed to recover hydrolyzed proteins has been described as well. Finally, retanning tests on leather with the new biopolymers allowed to evaluate their activity during the leather process.

Subsequently, Chapter 4 offers a description of novel palladium complexes bearing novel click based TryOX ligands. The peculiar coordination fashion of these ligands is described and initial tests of their catalytic activity for the reduction of biomass derived furfural showed promising data.

Chapter 5 takes into account the synthesis and characterization of novel ruthenium complexes bearing click based NNN ligands which revealed to be highly active in the reduction of carbonyl compounds. Biomass compounds such as furfural and 5-hydroxymethylfurfural has been selected as biomass derived platform chemicals to be valorized.

In conclusion, chapter 6 shows results achieved by the *in situ* hydrogenation of biomass derived carbonyl compounds through the catalyst system formed by $[Ir(\eta^4\text{-COD})Cl]_2$ and a novel water soluble ligand prepared by means of CuAAC and thiol-ene *click* reactions.

3. BIOMASS DERIVED BIOPOLYMERS FOR ECOFRIENDLY LEATHER

3.1 INTRODUCTION

Tanning of hides and skins is one of mankind's oldest trades. The EU leather industry contributes considerably to the social and economic scenario, counting nearly 24.000 companies and 400.000 employees, with a turnover of more than 31 billion Euros. [1,2]

Currently, the tanning of hides involves a set of sequential steps (Scheme 3.1). Tanning, retanning, and fat-liquoring are the most relevant transformations in the process and may require the use of polymeric materials.

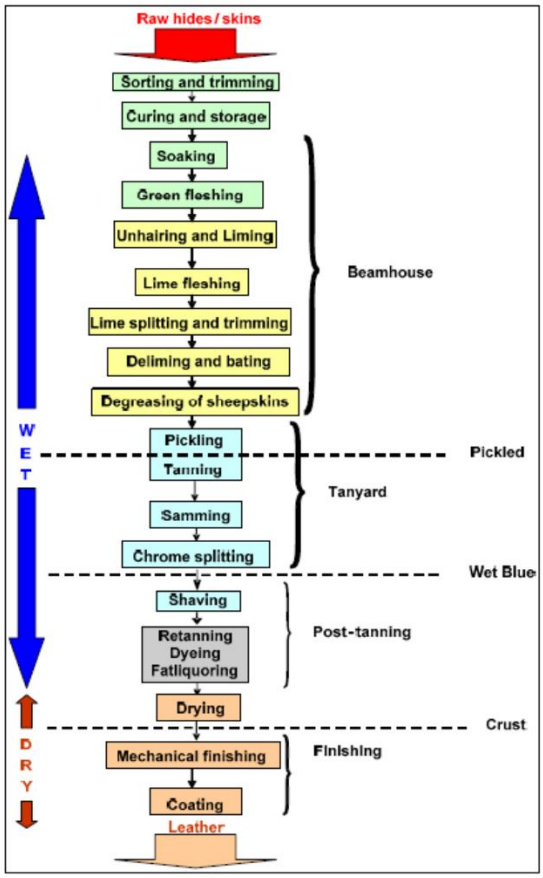

Scheme 3.1. Steps of the industrial process for leather making [1]

Several environmental concerns arise from the tanning industry. As a matter of fact, today over 85% of the hides processed worldwide are tanned with basic chromium sulphate due to its very high efficiency, low cost and good quality of the leather obtained. Nevertheless, harmless Cr(III) present in the slurries may be oxidized to toxic and harmful Cr(VI) species.[3–5]

Further drawbacks derive from the production of salts, mainly chlorides and sulphates, which contribute to high values of salt concentrations in the discharged wastewater.[6,7] Besides the use of chromium, on the blacklist of chemicals commonly used in the leather industry petrochemical based reagents occupy some of the top positions.

Among the broad spectrum of chemicals used in leather industry, retanning agents cover a very important phase as they are used to provide specific physical and mechanical properties to the final product.

Retanning agents can be classified as i) inorganic mineral compounds: chrome, aluminium, zirconium salts ii) organic substances: syntans (condensation products of aromatic compounds like phenol, naphthalene sulphonic acid with formaldehyde or urea) synthetic tannins, resins and aldehydes. Organic retanning agents are used daily during tanning and retanning processes because of their low cost and high quality of the leather obtained. Nevertheless, these chemicals are generally derived from fossil fuels feedstock. For these reasons, a sustainable alternative to replace these chemicals is required by leather industry.

In this frame, industry in general is nowadays transitioning towards greener production to address environmental issues, as the demand for ecological alternatives increases, prompted by European directives in favour of the circular economy.[1,8,9] Thus, raw hides and skins, by-products of slaughterhouses, must be correctly characterized in terms of environmental footprint, to grant them an allocation in accordance with their impact.

Having in mind the circular economy principles we identified the possibility to recover and reuse metal-containing tanned leather scraps to produce biopolymers to be employed as retanning agents, capable to replace petrochemical derived reagents, an interesting environmental challenge. In the last decade the recovery, recycle and reuse of industrial wastes as renewable feedstocks has been one of the main challenges of green chemistry and the circular economy.[10]

As far as animal-derived biomass is concerned, a high amount of collagen-containing by-products are produced yearly as post-tanning waste, which represent a precious source of protein and, when an hydrolytic process is performed, amino acids. Although the high content of nitrogen makes hydrolysed proteins an excellent additive for animal feed, a growing number of virtuous examples taking advantage of this feedstock are present in the literature.[11,12] As recently reviewed by Sànchez and coworkers, higher value polymeric products for cosmetic applications are normally obtained starting from untanned collagen scraps or trimmings.[13]

Chrome tanned leather scraps and shavings are instead commonly converted into fertilizers by thermal or enzymatic transformation.[14–16] This hydrolysed collagen may also be employed for the production of low-cost surfactants, high chrome fixation auxiliaries, fillers for paper, etc.[17–19] Biodegradability is often associated to the use of hydrolysates for the manufacture of polymers. For example, Kolomaznik *et al.* used hydrolysates for the production of biodegradable antiskid agents in polyvinyl chloride (PVC) and rubber compounds.[20] Kresalkova *et al.* obtained biodegradable polyvinyl alcohol (PVA) based films modified to be applied in agricultural applications.[21] Few higher value applications have been developed for the use of chrome tanned hydrolytes in combination with oxazolidines or acrylates as retanning agents.[22]

Noteworthy, in 2012 Luque and coworkers[23] synthetized tanning waste derived renewable biopolymers with different shapes. They recovered collagen from two types of leather waste: *splits* from pickled hides and *whet white* hides from a chromium-free process. The biopolymers synthetized could be modified with crosslinking agents to improve material properties in order to be used in the field of cosmetics, medicine or veterinary. Due to biocompatibility of collagen, an interesting application lies in the preparation of wound-healing materials. [24]

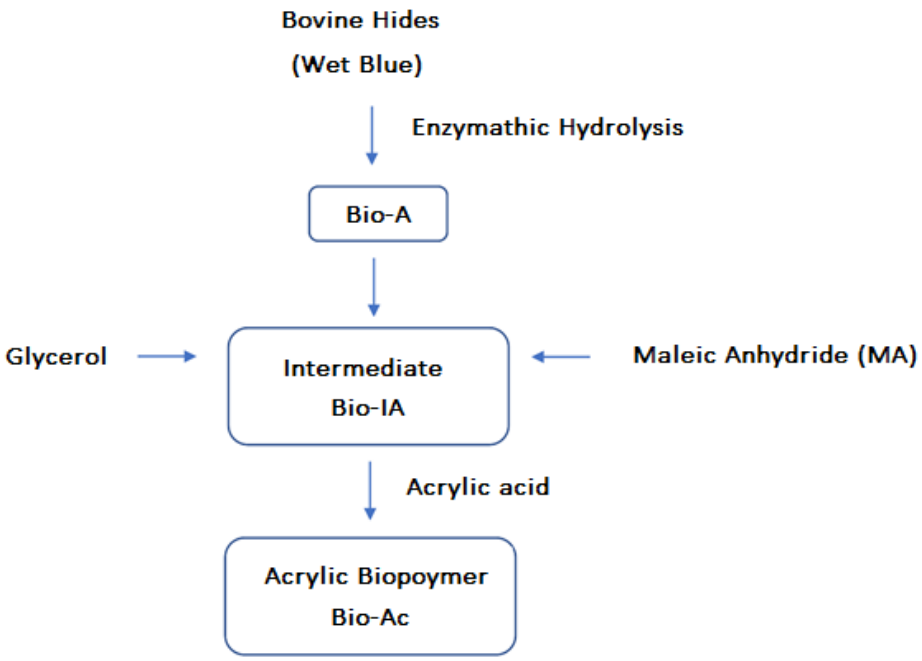

Scheme 3.2 Synthetic process for the synthesis of Bio-Ac

With all this in mind, in this work we wish to report a combined enzymatic and chemical protocol which employs tannery by-products as feedstock to produce high value biopolymers. In particular, the action of different enzymes on chrome tanned bovine leather scraps to produce hydrolysed biomass was tested. The low molecular weight water-soluble hydrolysates have then been employed as building blocks to produce high value biopolymers for retanning. To the best of our knowledge this is the first example of a combined chemo-enzymatic transformation of animal biomass waste to produce biopolymers for the leather industry. The novelty of the work here reported relies in the use of enzymatically hydrolysed chrome tanned collagen waste as a building block for the production of biopolymers for the leather industry. The overall industrial process to generate a biobased acrylic polymer (Bio-Ac) is reported in Scheme 3.2. According to this strategy, hydrolysed proteins derived from leather bovine scraps (Bio-A) are first reacted with glycerol and MA. Afterwards, a radical copolymerization is achieved in aqueous media in the presence of acrylic acid until complete conversion to Bio-Ac is observed.

3.2 RESULTS AND DISCUSSION

The work here reported foresees three different steps for the processing of animal biomass which will be described separately in the sections below.

3.2.1 Enzymatic Hydrolysis

Chrome shavings recovered at the end of the tanning process were obtained and used as raw material to provide hydrolysed water soluble collagen (Bio-A). Biomass was selected according to availability of the feedstock, standardization of the biomass and analytical issues. This biomass is widely available and does not present standardization problems. For these reasons, it represents an ideal substrate to process via enzymatic hydrolysis. Fully Controlled Enzymatic Hydrolysis (FCEH®) is an alternative to chemical hydrolysis which can be applied to raw materials of animal or plant origin, allowing the recovery of peptides and polypeptides in good yields, while preserving the chirality of the amino acids. Enzymatic digestion is an interesting technology to recover animal hydrolysates. Since the 1980s this technique has been commercially exploited. The first example reported was applied to produce instant whipping

agents for pastry.[25] In the present work, a FCEH® process was conducted to produce Bio-A. Following standard literature protocols,[26] bovine leather scraps were dispersed in water inside a stirred bioreactor equipped with temperature, weight and pH control. The selected enzymatic pool, made up of specific proteolytic enzymes, was introduced in the reactor. The mixture was kept under stirring at 50-60 °C for up to 12 hours, depending on the type of enzyme and characteristics of the desired finished product. Then, the liquid suspension was subjected to centrifugation, clarification and filtration. The liquid fraction thus obtained was finally introduced in a falling film vacuum evaporation plant until the desired concentration was achieved to obtain a hydrosoluble powder. Data obtained after the hydrolysis for Bio-A are listed in Table 3.1. Hydrolysed biomass analysis was subjected to elemental analysis with titration to determine free amino acid content (Table 3.2) and microbiological tests for bacterial contaminants.

Table 3.1 Elemental analysis of Bio-A.

Analysed Parameter	Bio-A
Organic nitrogen (N) %	15.4 ± 0.3
Total carbon (C) %	42.6 ± 1.0
Dry matter %	94.2 ± 2.0
Ashes %	6.6 ± 0.5
pH	5.7 ± 0.5
Total aminoacids %	96.8 ± 3.0
Free aminoacids %	1.8 ± 0.4
Hydrolysis degree	9.2 ± 1.1
Cr (III) (mg/Kg)	40 ± 2
Cr (VI) (mg/Kg)	<0.5[(a)]
Salmonella spp	ABSENT
Coliforms (UFC/g)	<10

(a) Quantification limit of the instrument.

Table 3.2 Analysis of the aminoacid composition of Bio-A.

Aminoacids [a]	Total (%)	Free (%)[b]	Aminoacids [a]	Total (%)	Free (%)[b]
Hydroxyproline	11.0	<lq	Cysteine	<lq	<lq
Aspartic acid	4.9	<lq	Tyrosine	1.0	<lq
Serine + asparagine	3.4	0.1	Hydroxylisine	1.2	<lq
Glutamic acid	9.2	0.2	Valine	2.3	<lq
Glycine	22.2	0.2	Metionine	0.9	<lq
Hystidine + glutamine	0.9	<lq	Ornitine	0.5	<lq
Arginine	8.2	0.1	Lysine	3.4	<lq
Threonine	1.1	1.0	Isoleucine	1.4	<lq
Alanine	7.9	0.1	Leucine	2.9	<lq
Proline	12.5	0.1	Phenilalanine	1.9	<lq
γ - Aminobutyric acid	<lq	<lq	Tryptophan	<lq	<lq
α - Aminobutyric acid	<lq	<lq	Total	96.8	1.8

[a] Aminoacids were determined by electron spray technique (ESI-MAS) using analytical method IDL 1.2.23. [b] lq: quantification limit: 0.1 %.

3.2.2 Characterization of Bio-A, Bio-IA and Bio-Ac

3.2.2.1 Elemental Analysis

Enzymatic hydrolysis on Bio-A proceeded with a hydrolysis degree (HD) of 9.2%, in accordance to similar hydrolytic processes reported in literature.[27] HD indicates the intensity of the hydrolysis process and it's calculated as the ratio between number of cleaved peptide bonds and the total number of peptide bonds. This kind of hydrolysis allows to recover almost free-chromium proteins, since Cr (III) level was detected at very low concentrations (40 mg/Kg). Harmful Cr (VI) was not detected. Proof of microbiological stability is given by the absence of *Salmonella* and coliforms.

3.2.2.2 NMR studies

Collagen is a protein made up of α- and β-amino acids linked by peptide bonds. Some of the amino acids present in the collagen structure, such as for example glutamic acid, arginine and lysine have more than one carboxylic or amino functional group, so unreacted pendant COOH

and NH_2 functionalities are present. ^{1}H-NMR signals of the hydrolysate protein Bio-A prevalently derive from glycine moieties linked to other amino acids, mainly proline (Pro) and hydroxyproline (Hyp).[28] As expected for complex molecules, the ^{1}H-NMR spectrum of the hydrolysed protein Bio-A shows numerous unresolved signals, as reported by Vatansever et al.[29]

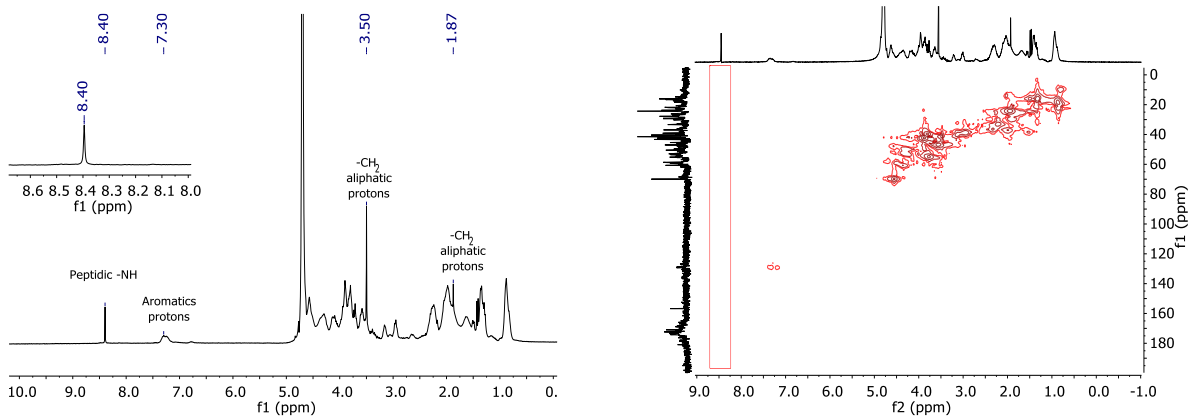

Figure 3.1 ^{1}H- and ^{1}H-^{13}C HMQC spectra of hydrolysed collagen protein in D_2O.

The signals between 0.7 and 4.7 ppm may be attributed to different CH_2 moieties due to the various amino acids present in the biopolymer. A relevant signal is the singlet at 8.4 ppm, which is zoomed in the upper left corner of **Figure 3.1** and is assumed to correspond to the -NH amide protons of the protein from animal biomass. A ^{1}H ^{13}C HMQC NMR experiment carried out on Bio-A further highlighted that no coupling between the proton at 8.4 ppm and a carbon atom is present, so the signal may be attributed to NH amide protons. A weak unresolved multiplet between 7.1 and 7.4 ppm is characteristic of the aromatic part of amino acids present in Bio-A (phenylaniline, tyrosine).

According to the synthetic strategy reported in **Scheme 3.3**, Bio-A is then reacted with glycerol and MA to give intermediate Bio-IA. Different experiments were carried out in the presence of variable amounts in *wt*% of glycerol, MA and Bio-A. The first experiments carried out with ratios of glycerol/MA between 10/90 and 45/55 *wt/wt*%, gave very viscous mixtures which could not be easily recovered from the reaction vessel. Thus, for all further tests a glycerol/MA ratio ≥50/50 *wt/wt*% was employed.

It is important to note that glycerol is known to stabilize the triple-helical structure of solubilized collagen due to the formation of hydrogen bonds and other low energy interactions

modifying the solvation shell of the protein.[30] In fact, glycerol is a common plasticizer for polymers and specifically its effect is supposed to inhibit the self-association of collagen, increasing the stability of the protein; nevertheless, no reaction should occur between the protein and glycerol. To verify this hypothesis, equal amounts of Bio-A and glycerol where mixed together at room temperature and the ^{1}H-NMR spectrum of the sample recovered corresponds to a mixture of the unreacted starting materials, confirming that no reaction takes place.

From the comparison of the ^{1}H-NMR spectra of three Bio-IA samples prepared with different *wt*% of Bio-A/glycerol/MA **Figure 3.2**) it appears that a set of doublet of doublets due to the olefinic protons of the maleate ester in the region between 6.00 and 6.55 ppm becomes more and more intense as the amount of glycerol and maleic anhydride increase. In accordance with the literature,[31] an acid catalysed reaction between MA and glycerol proceeds to form the corresponding maleate ester I1 (**Scheme 3.3**).

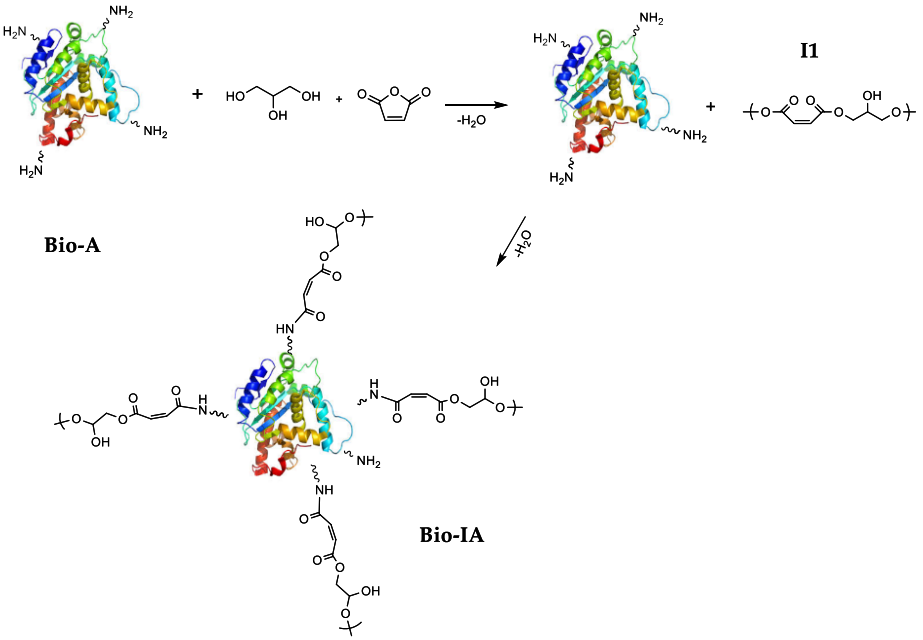

Scheme 3.3 Supposed reaction mechanism between glycerol, maleic anhydride and Bio-A.

These data moreover substantiate the hypothesis that the condensation between glycerol and MA proceeds faster than the reaction between MA and Bio-A. The maleate ester I1, can

then react with free amine groups present in Bio-A to give a Bio-A-maleate (Bio-IA) building block (**Scheme 3.3**). ^{1}H-NMR of Bio-IA is reported in **Figure 3.2**.

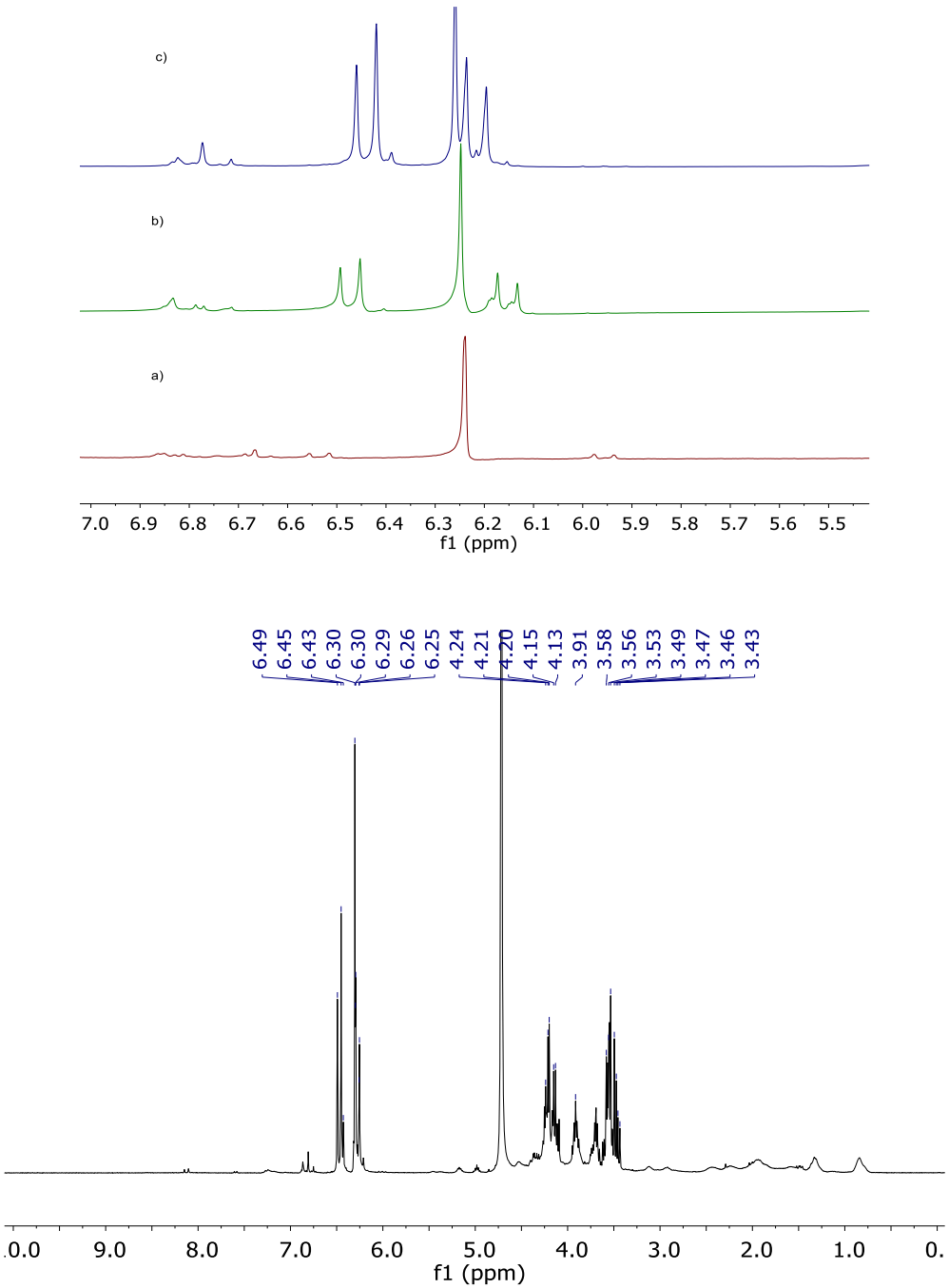

Figure 3.2. Above are depicted part of the ^{1}H-NMR spectra of Bio-IA samples prepared with a) Bio-A/glycerol/MA = 70/15/15 *wt*%, b) Bio-A/glycerol/MA = 50/25/25 *wt*%, c) Bio-A/glycerol/MA = 30/35/35 *wt*%.Below, the full spectrum of Bio-IA.

When a higher amount of MA was used, crystallization of unreacted maleic anhydride was observed, leading to gradual decomposition of Bio-IA. For this reason, all further tests were

carried out with a ratio Bio-A/glycerol/MA = 30/35/35 *wt*%. Bio-Ac is achieved via copolymerization of Bio-IA with acrylic acid (10 *wt*%), in the presence of a radical initiator (hydrogen peroxide), according to standard procedure.[32] The ^{1}H-NMR spectrum of Bio-Ac (**Figure 3.3**) shows characteristic polyacrylate signals between 1.25 and 2.5 ppm.[33] It is possible to assume that Bio-IA is fully converted to the polymerized product, since maleate olefinic signals between 6.00 and 6.55 ppm, are no longer observed.

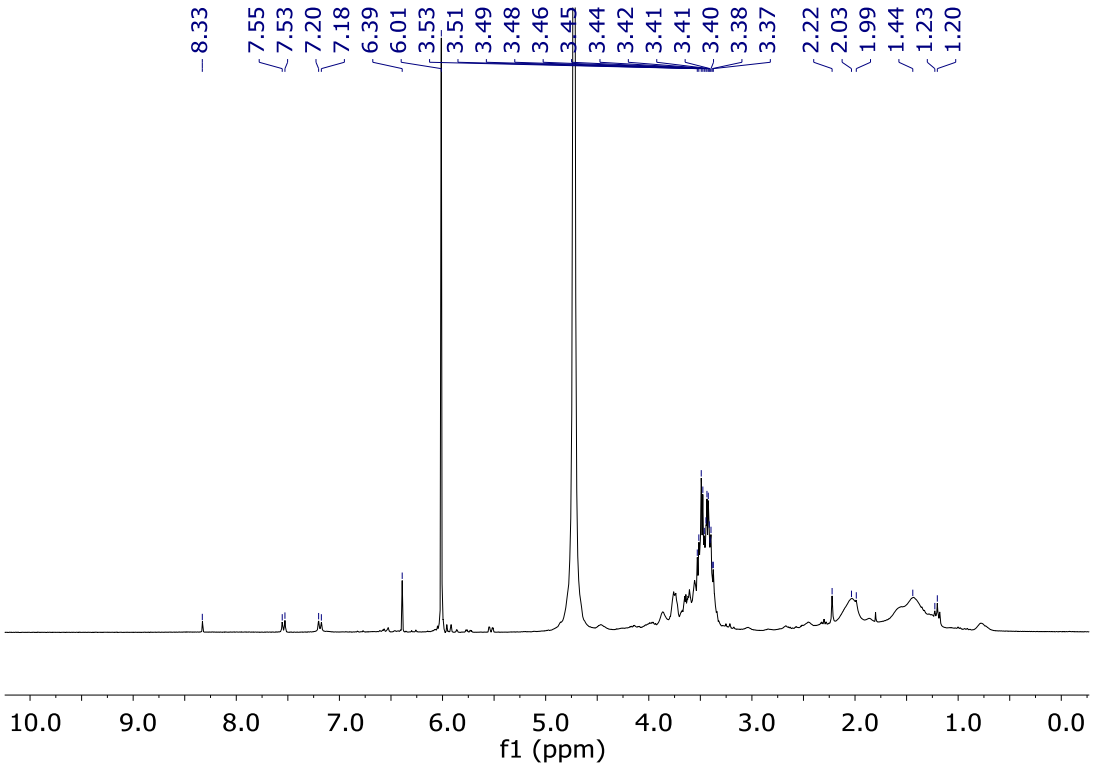

Figure 3.3 ^{1}H-NMR of Bio-Ac.

3.2.2.3 FTIR Analysis

In accordance to literature,[34–37] the FTIR spectrum of Bio-A (blue spectrum, **Figure 3.4**) is mainly characterized by C=O stretching (1700–1640 cm^{-1}) and N-H bending (1570–1550 cm^{-1}) absorbances. Bio-IA (red spectrum, **Figure 3.4**) shows a broad signal between 3100 and 2800 cm^{-1}, characteristic of COOH functional groups together with C=O stretching adsorptions at 1718 cm^{-1} and 1214 cm^{-1}, confirming the presence of maleate ester.[38] FTIR adsorptions of the amide groups of the protein are only slightly affected, in agreement with NMR data. In accordance to literature,[39] absorptions due to C-O stretching (1200–900 cm^{-1}) and C-O-C stretching (1200–1100 cm^{-1}) were assigned to the glycerol moiety.

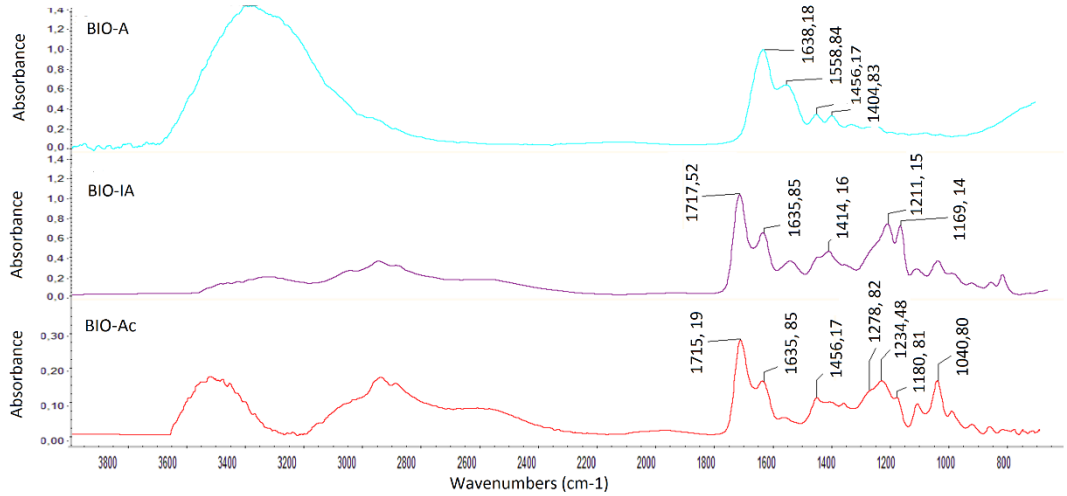

Figure 3.4 FTIR spectra in ATR mode of Bio-A, Bio-IA, Bio-Ac.

3.2.2.4 GPC studies

GPC analysis were performed on hydrolysed proteins (Bio-A), intermediate (Bio-IA) and the final biopolymer (Bio-Ac), as reported in **Table 3.3**. The average molecular weight (Mw) of Bio-A is 5.149 Da, a value which is close to data reported in the literature for hydrolysed proteins derived from bovine hides.[40] Functionalization of Bio-A with glycerol and MA allows to increase Mw to 7.722. This means that, according to the reaction mechanism supposed in **Scheme 3.3**, I1 reaches a molecular weight around 2.5 KDa. Finally, racial co-polymerization of Bio-IA leads to the formation of Bio-Ac, having a Mw of approximately 42.000 Da.

Table 3.3 MW data acquired for biomass intermediates and biopolymers.

Sample	Mw (Da)
Bio-A	5.149
Bio-IA	7.722
Bio-Ac	42.400

3.2.3. Characterization of Bio-Ac Retanned Leather

3.2.3.1. Application Tests: Leather Retanning

Bio-Ac was tested on conventionally chrome tanned bovine leather as a retanning agent. The haptic and physical characteristics of the crust Bio-Ac leather were compared to crust

leather achieved using conventional retanning products such as syntans and acrylic resins (Table 3.4). All the post-tanning steps involve the fixation of a solute in solution onto a solid (collagen hide). We may assume that the diffusion and penetration of Bio-Ac into the collagen may be described, in accordance to literature,[28] as a two-step process defined as follows: i) transfer of the reagent from the solution to the substrate (collagen hide); ii) formation of different interactions or bonds (hydrophobic, electrostatic, covalent) between the reagent and the solid collagen. The diffusion and penetration of the retanning agent will be influenced by the chemical nature of the solute, by the pH at which the treatment is carried out and by the tanning agent employed. In a pH range between 5.0 and 7.0 Bio-Ac may be assumed to work in a similar manner to an anionic retanning agent having good filling power and grain fixation.[41,42]

Preliminary physical mechanical tests, reported in Table 3.4 and Table 3.5, were selected in order to verify the quality of Bio-Ac crust for automotive application. Presently the automotive compartment is one of the most appealing markets for green and sustainable tanning systems.

Data obtained show that Bio-Ac retanned leather has very good light fastness, probably due to a low concentration of reactive functional groups on the absorbed biopolymer such as for example carbon-carbon double bonds, which are responsible for color changes over time.[40] Refractometric fogging is very similar to both acrylic and phenolic leather products, while gravimetric fogging is moderately lower. Organoleptic characteristics of Bio-Ac crust reveal a higher grain tightness and fullness but an overall lower softness. These phenomena may be explained, in accordance to literature,[43] assuming that the absorption of Bio-Ac influences the thickness of the collagen fiber, reducing their mobility hence, increasing tightness and fullness while reducing softness. The dyeing is somewhat more intense compared to references.

Table 3.4. Physical Tests for Crust Leather.

Recipe [a]	Retanning	Light Fastness [b]	Fogging Refractometric [c]	Fogging Gravimetric [d]
Acrylic Biopolymer	Bio-Ac (6%)	5	99	0.8
Standard	Acrylic resin (6%)	4	96	2.3
Standard	Phenolic Syntan (6%)	4	94	3.5

[a] Wetting back: ethoxylated surfactant (0.3%); fatliquoring: sulphited oil (3%), dyeing: acid brown 425 (4%); % based on wet blue weight; [b] Light fastness 72 h/BST 50 °C (blue wool scale) measured according to UNI EN IOS 105-B02; [c] Fogging refractometric 6 h/75 °C (%) measured according to ISO 17071 A; [d] Fogging gravimetric 6 h/100 °C (mg) measured according to ISO 17071 B.

Table 3.5. Mechanical Tests for Crust Leather.

Recipe [a]	Retanning	Grain Distension [b]		Grain Strength [b]		Tear Strength [c]
		Elongation (nm)	Load (Kg)	Elongation (nm)	Load (Kg)	
Acrylic Biopolymer	Bio-Ac (6%)	8.36	18	12.55	40	0.8
Standard	Acrylic resin (6%)	8.73	19	11.65	30	2.3
Standard	Phenolic Syntan (6%)	6.39	16	10.67	48	3.5

[a] Wetting back: ethoxylated surfactant (0.3%); fat-liquoring: sulphited oil (3%), dyeing: acid brown 425 (4%); % based on wet blue weight; [b] Grain distension and grain strength measured according to EN IOS 3379; [c] Horizontal and vertical tear strength measured according to EN ISO 3377-2 ; all values are the result of measurements on three different samples.

Although mechanistic studies are beyond the scope of this work, it may be inferred that the retanning action of Bio-Ac is favoured by the acrylic moiety present in the polymer which favours the fixation of Bio-Ac to the amine functional groups available in the hides after chrome tanning.[42] This hypothesis seems to be in good agreement with the physical mechanical tests reported in Table 3.5 and with SEM images (see below), which show a similar behaviour of Bio-Ac to retanning acrylic resins more than to phenolic syntans. These results confirm that the biopolymer may be suitable for producing leather for automotive use, which requires low emission levels to ensure a healthy vehicle cabin environment.[44]

3.2.3.2 SEM analysis

Crust leather samples prepared by standard chrome tanning and Bio-Ac retanning, exhibit a clean grain surface, and in general, SEM observations are in good agreement with analogous

data reported in literature.[45–48] At low magnification (**Figure 3.5**, picture a) it is possible to observe the grain at the top of the image. Fibre structure appears to be in good conditions, well opened without looseness visible. SEM images (**Figure 3.5**, pictures b,c) show tightly packed, smoothly oriented fibres and well aggregated collagen fibers (increasing the grain leather strength) which agree with the overall considerations reported above regarding tightness and fullness.

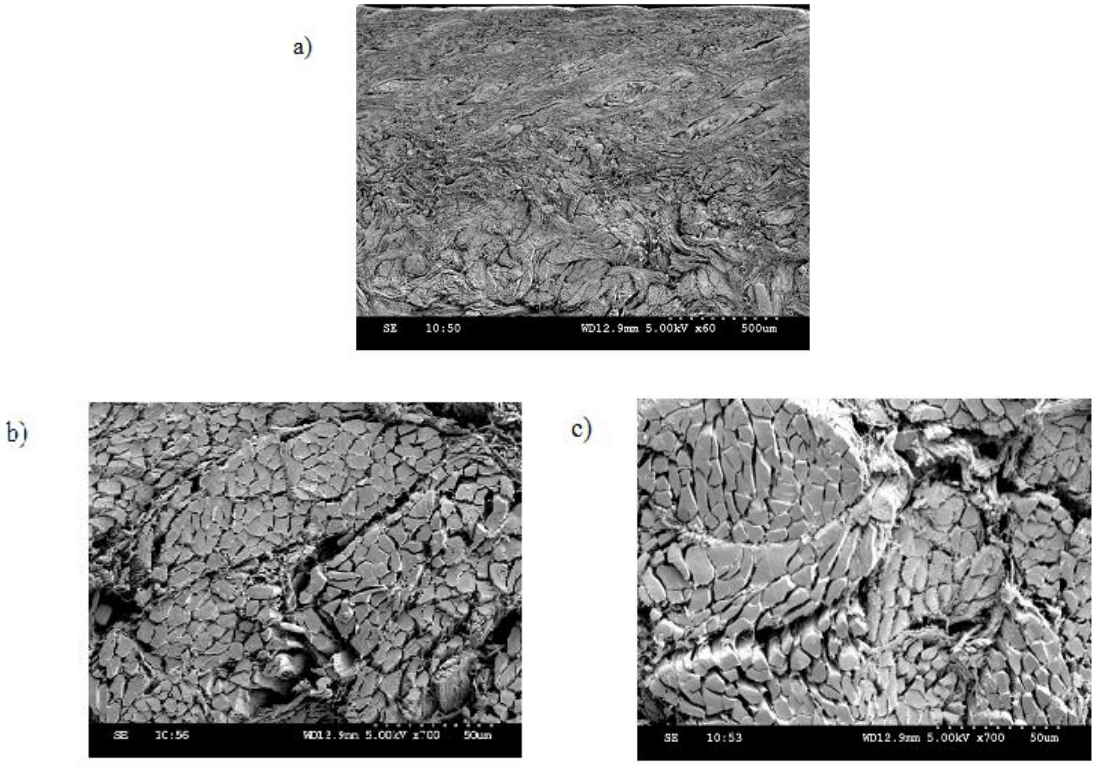

Figure 3.5. Leather sample cross sections at low magnification (**a**, ×60) and higher magnification (**b–c**, ×700).

3.3 EXPERIMENTAL

3.3.1 Materials

All reagents were purchased from Sigma-Aldrich (St. Louis, MO, USA)) and used without any purification. Chrome tanned collagen scraps were obtained from treated bovine hides (wet blue scraps) and furnished by Codyeco S.p.A. (S. Croce sull'Arno, PI, Italy). ILSA S.p.a. (**A**rzignano, VI, Italy) provided hydrolysed Bio-A. Bio-IA and Bio-Ac were synthetized by Codyeco S.p.A.

3.3.2 Methods

Elemental analysis was performed for hydrolysed Bio-A proteins. Ashes were determined by weight loss at 105 °C and at 550 °C respectively (Reg.CE 152/2009 IO-CEN); organic matter (OM) by loss in ignition (OM = dry matter–ash); pH in water (3/50, *w/v*); total carbon (TC) by wet oxidation method with potassium dichromate (MI 1.2.9-Ed.2 Rev.2:2017); total nitrogen (TKN, MI 1.2.9–Ed.2 Rev.2:2017) via the Kjeldhal method; ammonium nitrogen (NH_4^+ -N) by extraction with diluted HCl and steam distillation with magnesium oxide (UNI EN 15475:2009); total organic nitrogen (TON) by difference (TON = TKN–NH_4^+ -N). Hydrolysis degree has been calculated following known method (G.U. 26/01/01 n°21, DM 21/12/00). Microbiological stability of the hydrolysed product was evaluated through salmonella (DM 1337 27/01/2014 GU 42 29/02/2014) and coliforms (ISO 4832:2006) content. Total metals were determined by acid digestion with ultrapure nitric acid and hydrogen peroxide (Merck, Darmstadt, Germany) in Teflon bombs in the microwave oven (Milestone, Sorisole, BG, Italy) and determination by Microwave Plasma Atomic Emission Spectrometry (MP_AES, Agilent, Santa Clara, CA, USA). Post-retanned leather samples were examined using a scanning electron microscope (SEM; S-3000 N, Hitachi, Chiyoda, Tokio, Japan) operating at 5 kV.

3.3.3 Enzymatic Hydrolysis

Bio-A supplied by ILSA S.p.A. was produced through an advanced fully controlled enzymatic hydrolysis process (FCEH ®) using a combination of proteolytic enzymes (endo- and exo-proteases) derived from non-genetically modified organisms. Extraction is followed by a concentration phase and spray-drying in order to obtain a hydrosoluble powder. Stability of the product is ensured both by the origin of the byproducts and by the specific plant process.

3.3.4 Structural Characterization

FTIR spectra were recorded by using a Thermo Nicolet Protegè 460 spectrometer (Thermo Fisher Scientific, Waltham, MA, USA), in a range frequency between 4000–400 cm^{-1}. All the spectra have been collected in ATR mode. Elemental analysis was performed using the official analytical protein methods according to the corresponding Italian regulation (D.Lgs. 75/2010) and European Regulation (CE 2003/2003). Gel Permeation chromatography (GPC) was performed for Bio-A, Bio-IA and Bio-Ac with a Yarra sec 2000 column (300 × 7.8 mm, Phenomenex, Bologna, BO, Italy). Calibration curves were btaned using a Gel Filtration

Molecular Weight Marker Kit for Molecular Weights 6.500–66.000 Da (Catalogue Number MWGF60, Sigma Aldrich). ^{1}H- and HMQC ^{13}C-NMR spectra were recorded on an AVANCE 300 spectrometer (Bruker, Billerica, MA, USA). The chemical shift values of the spectra are reported in units with reference to the residual solvent signal. The proton assignments were performed by standard chemical shift correlations.

3.3.5 Retanning Tests

General procedure for the retanning tests: soaked chrome tanned bovine leather (wet blue) has been retanned according to conventional method, employing Bio-Ac, acrylic or phenol retanning agents and natural fat liquoring agents to produce crust upper leather. These leather samples were employed for physical-mechanical tests. Light fastness of retanned leather was rated (from 1 to 5) by visual assessment of experienced tanners

3.4 CONCLUSIONS

Enzymatically hydrolysed proteins derived from industrial waste biomass are used in this study as starting material for the synthesis of a new acrylic biopolymer (Bio-Ac). Enzymatic hydrolysis allowed to recover water soluble lower molecular weight proteins which have been firstly reacted with glycerol and maleic anhydride. Afterwards, copolymerization with acrylic acid leads to the final biopolymer. Each synthetic step has been optimised by varying reaction parameters and the products fully characterised by NMR and FTIR spectroscopy. Molecular weights were calculated by means of GPC chromatography, showing a final Mw of 42.400 Da. Application of Bio-Ac as retanning agent has been successfully implemented. SEM analysis and physical tests on leather retanned with Bio-Ac show similar quality and performances of leather treated with commonly used fossil fuel derived chemicals. Based on these results, we believe that Bio-Ac represents the first example of a biomass derived biopolymer used as retanning agent for a more sustainable tannery process in agreement to the principles of circular economy. Further different biomass sources, such as molasses, will be evaluated in order to provide an improved protocol for the synthesis of biomass derived biopolymers as retanning agents together with LCA data.

3.5 REFERENCES

[1] B. Michael, C. Michele, R. Stefan, B. M. Scalet, R. Serge, D. S. Luis, *Best Available Techniques (BAT) Reference Document for the Tanning of Hides and Skins (Integrated Pollution Prevention and Control)*, Publicatio Office Of The European Union, Luxembourg, 2013.

[2] "The leather sector in figures: global trade in 2016," can be found under https://conseilnationalducuir.org/en/press/releases/2018-01-24, n.d.

[3] P. Kush, K. Deori, A. Kumar, S. Deka, *J. Mater. Chem. A* 2015, *3*, 8098–8106.

[4] M. T. Uddin, M. A. Islam, S. Mahmud, M. Rukanuzzaman, *J. Hazard. Mater.* 2009, *164*, 53–60.

[5] P. K. Boruah, P. Borthakur, G. Darabdhara, C. K. Kamaja, I. Karbhal, M. V. Shelke, P. Phukan, D. Saikia, M. R. Das, *RSC Adv.* 2016, *6*, 11049–11063.

[6] V. Beghetto, L. Agostinis, V. Gatto, R. Samiolo, A. Scrivanti, *J. Clean. Prod.* 2019, *220*, 864–872.

[7] I. Ilou, S. Souabi, K. Digua, *Int. J. Sci. Res.* 2014, *3*, 1706–1715.

[8] European Commission, *Com* 2015, *614 final*, 21.

[9] European Commission, *Publ. Off. Eur. Union* 2010, 20.

[10] L. A. Pfaltzgraff, M. De Bruyn, E. C. Cooper, V. Budarin, J. H. Clark, *Green Chem.* 2013, *15*, 307–314.

[11] V. J. Sundar, J. Raghavarao, C. Muralidharan, A. B. Mandal, *Crit. Rev. Environ. Sci. Technol.* 2011, *41*, 2048–2075.

[12] V. John Sundar, A. Gnanamani, C. Muralidharan, N. K. Chandrababu, A. B. Mandal, *Rev. Environ. Sci. Bio/Technology* 2011, *10*, 151–163.

[13] M. I. Avila Rodríguez, L. G. Rodríguez Barroso, M. L. Sánchez, *J. Cosmet. Dermatol.* 2018, *17*, 20–26.

[14] L. F. Cabeza, M. M. Taylor, G. L. Dimaio, E. M. Brown, W. N. Marmer, R. Carrió, P. J.

Celma, J. Cot, *Waste Manag.* 1998, *18*, 211–218.

[15] X. Dang, M. Yang, B. Zhang, H. Chen, Y. Wang, *Environ. Sci. Pollut. Res.* 2019, *26*, 7277–7283.

[16] I. F. Pahlawan, S. Sutyasmi, G. Griyanitasari, *IOP Conf. Ser. Earth Envinron. Sci* 2019, *230*, 012083.

[17] B. Zehra, H. R. Nawaz, B. A. Solangi, U. Nadeem, M. Zeeshan, *Proc. Pakistan Acad. Sci.* 2014, *51*, 337–343.

[18] L. M. Santos, M. Gutterres, *J. Clean. Prod.* 2007, *15*, 12–16.

[19] O. Yilmaz, I. Cem Kantarli, M. Yuksel, M. Saglam, J. Yanik, *Resour. Conserv. Recycl.* 2007, *49*, 436–448.

[20] K. Kolomazník, M. Mládek, F. Langmaier, D. Janácová, M. M. Taylor, *J. Am. Leather Chem. Assoc.* 1999, *95*, 55–63.

[21] M. Kresalkova, L. Hnanickova, J. Kupec, K. Kolomaznick, P. . Alexy, *J. Am. leather Chem. Assoc.* 2002, *97*, 143–149.

[22] A. Afşar, G. Gülümser, A. Aslan, B. Ocak, *Tekst. ve Konfeksiyon* 2010, *20*, 37–40.

[23] M. Catalina, J. Cot, A. M. Balu, J. C. Serrano-Ruiz, R. Luque, *Green Chem.* 2012, *14*, 308–312.

[24] M. Catalina, J. Cot, M. Borras, J. de Lapuente, J. González, M. A. Balu, R. Luque, *Materials (Basel).* 2013, *6*, 1599–1607.

[25] R. C. Gunther, *J. Am. Oil Chem. Soc.* 1979, *56*, 345–349.

[26] J. Kanagaraj, K. C. Velappan, N. K. Chandra Babu, S. Sadulla, *J. Sci. Ind. Res. (India).* 2006, *65*, 541–548.

[27] L. Cavani, A. Margon, L. Sciubba, C. Ciavatta, C. Marzadori, *AIMS Agric. Food* 2017, *2*, 221–232.

[28] A. D. Covington, T. Covington, *Tanning Chemistry: The Science of Leather*, The Royal Society Of Chemistry, Cambridge, UK, 2009.

[29] B. Vatansever, B. Binici, *J. Chem. Metrol.* 2015, *1*, 1–15.

[30] R. Penkova, I. Goshev, S. Gorinstein, P. Nedkov, *Food Chem.* 1999, *66*, 483–487.

[31] O. Valerio, J. M. Pin, M. Misra, A. K. Mohanty, *ACS Omega* 2016, *1*, 1284–1295.

[32] I. Ristic, A. Miletic, N. Sad, O. Govedarica, *Phys. Chem. 2016* 2016, 685–688.

[33] R. Melinda Molnar, M. Bodnar, J. F. Hartmann, J. Borbely, *Colloid Polym. Sci.* 2009, *287*, 739–744.

[34] B. B. Doyle, E. G. Bendit, E. R. Blout, *Biopolymers* 1975, *14*, 937–957.

[35] N. P. Camacho, P. West, P. A. Torzilli, R. Mendelsohn, *Biopolym. - Biospectroscopy Sect.* 2001, *62*, 1–8.

[36] T. Riaz, R. Zeeshan, F. Zarif, K. Ilyas, N. Muhammad, S. Z. Safi, A. Rahim, S. A. A. Rizvi, I. U. Rehman, *Appl. Spectrosc. Rev.* 2018, *53*, 703–746.

[37] B. De Campos Vidal, M. L. S. Mello, *Micron* 2011, *42*, 283–289.

[38] J. Lisperguer, C. Nuñez, P. Perez-Guerrero, *J. Chil. Chem. Soc.* 2013, *58*, 1937–1940.

[39] S. Salehpour, M. A. Dubé, *Macromol. React. Eng.* 2012, *6*, 85–92.

[40] D. Castiello, E. Chiellini, P. Cinelli, S. D'Antone, P. Monica, M. Salvadori, M. Seggiani, *J. Appl. Polym. Sci.* 2009, *114*, 3827–3834.

[41] Y. Zhang, L. Wang, *Polym. - Plast. Technol. Eng.* 2009, *48*, 285–291.

[42] L. Jin, Y. Wei, Y. Wang, Y. Li, *J. Soc. Leather Technol. Chem.* 2014, *98*, 222–228.

[43] R. Bianli, F. Qi, C. Yuye, L. Yunjun, Z. Xianglong, *J. Soc. Leather Technol. Chem.* 2018, *102*, 289–292.

[44] Underwriters Laboratories UL LLC, *Vehicle Interior Air Quality: Addressing Chemical Exposure in Automobiles*, 2015.

[45] G. Krishnamoorthy, S. Sadulla, P. K. Sehgal, A. B. Mandal, *J. Clean. Prod.* 2013, *42*, 277–286.

[46] E. H. A. Nashy, A. I. Hussein, M. M. Essa, *J. Am. Leather Chem. Assoc.* 2011, *106*, 241–

248.

[47] S. Sivasubramanian, B. Murali Manohar, A. Rajaram, R. Puvanakrishnan, *Chemosphere* 2008, *70*, 1015–1024.

[48] W. Xu, J. Zhou, Y. Wang, B. Shi, *Int. J. Polym. Sci.* 2016, 1–7.

4. SYNTHESIS, CHARACERIZATION AND CATALITYC ACTIVITY OF NEW TRIAZOLYL-OXAZOLINE CHIRAL LIGANDS COORDINATED TO Pd(II) METAL CENTERS

4.1 INTRODUCTION

Design and development of novel and efficient ligands is a core activity in transition-metal catalysis because organic ligands properties ultimately affect the steric and electronic characteristics of metal centres allowing to improve and tune activity, regioselectivity and (when appropriate) enantioselectivity of the metal-catalyzed reactions. Expected benefits include milder reaction conditions, improved chemo-, regio- and stereo-selectivity eventually leading to more sustainable chemical processes. After more than 40 years, pyridine-oxazolines (PyOx, Scheme 4.1), a class of chiral N,N-bidentate ligands originally conceived by H. Brunner in 1980',[1,2] continue to attract chemists interest as confirmed by the recent reviews appeared in the literature.[3–5]

Likewise, in the last two decades nitrogen ligands containing triazole rings drew increasing attention not only in relation with their coordination characteristics but also because their structures can be easily modified taking advantage of the modular nature of the copper catalyzed [2+3] alkyne-azide cycloaddition.[6,7] Inspired by the chemical structure of PyOx ligands, we devised the synthesis of a novel type of chiral N,N-bidentate ligand in which a chiral oxazoline ring bears as the substituent a triazolyl moiety (Scheme 4.1). We are confident this novel class of ligands will find applications in different fields of coordination chemistry and asymmetric catalysis. In this connection, it is to remark that owing to the modular nature of triazole synthesis it will be possible to prepare libraries of these ligands allowing for a fine tuning of their characteristics.

Furthermore, it should be noted that beyond the plain structural similarity with PyOx ligands, TryOxs could display some unprecedented coordination chemistry. As a matter of fact, it is generally assumed that while the σ-donor strengths of the triazole and pyridine are not very different, pyridines are considered to be a better π acceptors than 1,2,3- triazoles.[8] These characteristics can be exploited in other fields; for instance in a preliminary account on the synthesis of a TryOx prototype [9] we have already shown that TryOxs can be successfully employed in combination with some lanthanides to give photoluminescent species. We wish to report herein an improved protocol for the synthesis of chiral TryOx ligands and preliminary studies on their coordination to Pd(II) metal centers. Inspection of the literature reveals that achiral TryOx ligands (i.e. species as depicted in

Scheme 1 in which R=H) have been previously synthesized by Cook [10] and by Maas.[11] In particular, it is worth to mention that Maas showed by X-ray diffraction analysis that the achiral TryOx having R1=benzyl and R=H behaves towards Cu(II) as a monodentate ligand, coordination occurring through the N atom of the oxazoline.

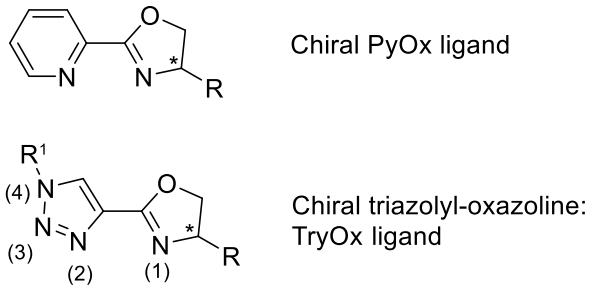

Scheme 4.1. Chemicals structures of PyOx and TryOx ligands

After having extensively studied the coordination fashion of TryOx ligands, preliminary tests on the catalytic activity of the complexes have been carried out. In agreement with the scope of this thesis, hydrogenation of biomass derived furfural is currently under investigation.

4.2 RESULTS AND DISCUSSION

4.2.1 Ligand synthesis

The approach developed to synthesize the new triazolyl-oxazoline ligands **4a-c** is outlined in Scheme 4.2.

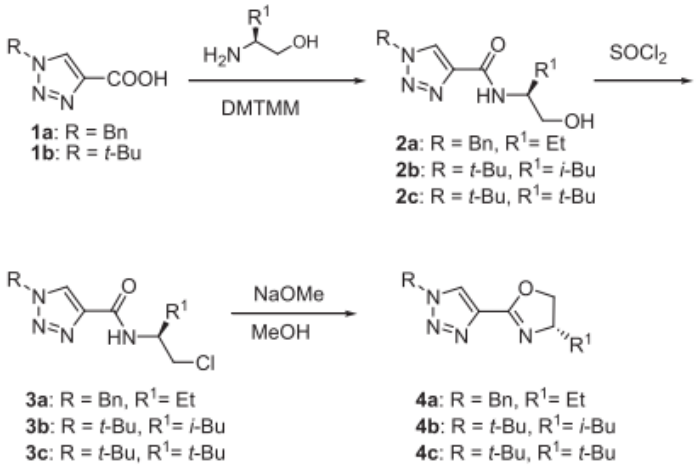

Scheme 4.2. Synthetic approach for the synthesis of TryOx ligands **4a-c**

Cu(I) catalyzed coupling of benzyl azide or *t*-butyl azide with either propiolic acid or methyl propiolate (followed by alkaline hydrolysis) is a prompt entry to prepare in high yield 1-benzyl or 1-*t*-butyl-1*H*-1,2,3- triazole-4-carboxylic acids **1a** and **1b**, respectively. Then, reaction of **1a,b** with chiral amino alcohols affords amides **2a-c**. Some different protocols were tested in order to improve the yield of this reaction. Best results were achieved using 4-(4,6-dimethoxy[1,3,5]triazin-2-yl)-4- methyl-morpholinium chloride (DMTMM) a stereoselective amine-carboxylic acid coupling agent.[12,13]

Almost quantitative yields are achieved working at room conditions in acetonitrile, purification is simply performed by rotoevaporation of the reaction mixture followed by extraction of the residues of the coupling agent with an aqueous base.

While direct cyclization of **2a-c** to **4a-c** affords the target compounds in low yields (about 20% after chromatographic purification), the two step sequence developed by Stoltz for the synthesis of chiral PyOxs [4] turned out to be very efficient. Specifically, Stoltz's synthetic approach entails: i) chlorination of the amide-alcohol with $SOCl_2$, and, ii) ring closure in the presence of a base. Key features are: i) the chlorination step occurs quantitatively and does not requires any purification procedure; and, ii) the ring closure proceeds with complete retention of the configuration at the chiral center, best yields being obtained in methanol using strong bases (e.g. 25% NaOMe). No particular problem arose in applying Stoltz's protocol to TryOxs synthesis; in fact, treatment of amide-alcohols **2a-c** with $SOCl_2$ gave chlorides **3a-c** quantitatively, then, treatment of **3a-c** with 10% NaOMe in methanol followed by a minimum workup allowed to obtain the sought ligands **4a-c** in 75–85% yields. Ligands **4a-c** were characterized by elemental analysis, IR, GC–MS, ^{1}H and ^{13}C NMR spectroscopies. In particular, in the ^{1}H NMR spectra the triazole proton appears as a low field singlet in the 7.89–8.09 range, while the protons of the oxazoline furnish three separate signals in the 4.5–3.8 ppm range.

4.2.2 Palladium(II) complexes synthesis

4.2.2.1 Synthesis of Pd(II)-allyl complexes

For a first preliminary evaluation of the coordination capability of ligands **4a-c**, we choose to study the reactivity of the new ligands to- wards $[Pd(\eta^3\text{-}C_3H_5)Cl]_2$ in the endeavour of synthesize the corresponding Pd(II)-allyl complexes (see **Scheme 4.3**). As a matter of fact, nowadays palladium based catalytic processes have gained an exceptional importance in chemical synthesis and particularly in cross-coupling reactions. Among the almost infinite number of species which can be used as the catalyst or the precatalysts in palladium-catalyzed cross-coupling reactions, palladium-allyl complexes of the type $[PdX(\eta^3\text{-allyl})(L)]$ (X: anion) have a privileged position because of their stability,

well established structure, and certainty of composition.[14] Moreover, the peculiar nature of the π-allyl moiety allows to use it as coordination reporter, for instance enabling to establish through space correlations by 2D NMR techniques. The palladium-allyl complexes **Pd1a-c** are promptly obtained by treating $[Pd(\eta^3\text{-}C_3H_5)Cl]_2$ with a silver salt (AgX: $X^- = BF_4^-$, ClO_4^-,PF_6^-) in dichloromethane; filtration of precipitated AgCl followed by addition of the ligand (**Scheme 4.3**) leads to pale yellow solutions from which the sought allyl complexes are recovered by precipitation with diethyl ether. Elemental analyses agree with the proposed formulation; in the ESI-MS spectra the most important peaks correspond to the cations $[[Pd(\eta^3\text{-}C_3H_5)$**(4a-c)**$]^+$, the isotope patterns being in good agreement with the calculated ones. The Λ_M of 10^{-3} M solutions of these species in acetone are in the 120–150 Ω^{-1} cm^2 mol^{-1} range confirming that these species are 1:1 electrolytes.[15] In the ^1H and ^{13}C NMR spectra of complexes **Pd1a-c** there are present two distinct sets of resonances which are promptly attributed to the coordinated ligand and the allyl moiety, respectively.

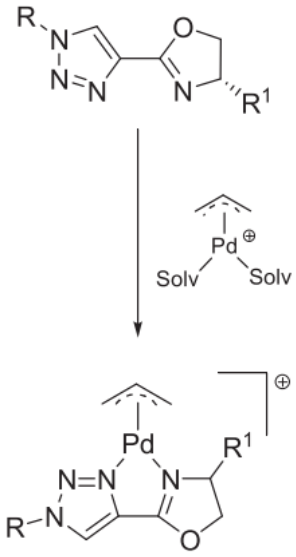

Scheme 4.3. Synthesis of palladium-allyl-*TryOx* complexes **Pd1a-C**

Comparison of the NMR chemical shifts of free and coordinated **4a-c** resonances indicates that they behave as N,N-chelating ligands. Coordination of the triazolyl moiety is demonstrated by a downfield shift of 0.4–0.8 ppm of the resonance due to the triazole ring proton, and coordination of the oxazoline ring is proved by a downfield shift of about 0.5 ppm of all the oxazoline protons.

Upon coordination to palladium, the ^{13}C NMR the signal due to the C-H of triazole is shifted downfield of about 1.3–1.8 ppm, this effect is accompanied by an upfield shift of the triazole

quaternary carbon re- sonance which is of only about 0.5 ppm for **Pd1b**,c but as large as 2.0 ppm for **Pd1a.**

In the ^{1}H NMR spectra, the signals relevant to the allyl moiety are displaced to lower fields and become broad indicating dynamic behaviour. In all cases, the syn protons give a single broad resonance, while the resonances relevant to anti protons appear as two broad distinct signals.

Although some different counterions (BF_4^-, ClO_4^-, PF_6^-) were employed, we did not succeed in obtaining single crystals suitable for X- rays analysis; thus, DFT calculations were performed in order to get some deeper insights on the structural features of the allyl-complexes. The DFT-optimized structures of **Pd1a** and **Pd1c** are depicted in **Figure 4.1**, while a selection of computed bond lengths and angles is reported in the caption. The introduction of different substituents on the heterocycles causes negligible variations of the Pd-C_{allyl} bond lengths. The Pd-N(2)(triazole) (see **Scheme 4.1** for atom numbering) distance is roughly the same in the two compounds, while the Pd-N(oxazoline) bond length is slightly longer in **Pd1c**, probably because of the higher steric bulk of the *t*-butyl substituent with respect to the ethyl one. As expected, no stationary points were found trying to optimize the geometry of isomers where the ligands are coordinated by the oxazoline nitrogen and the triazole N(3).

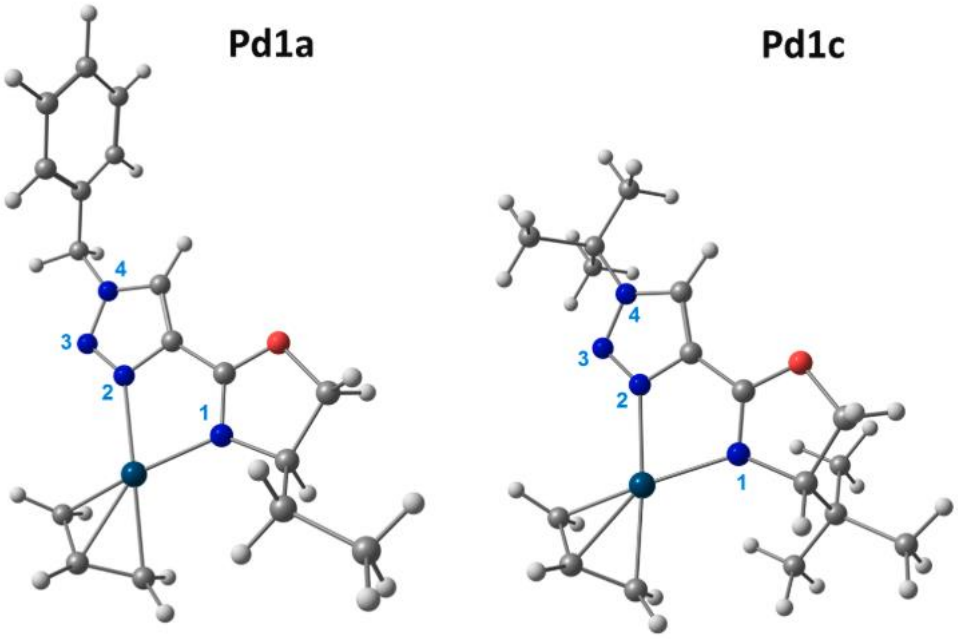

Figure 4.1. DFT-optimized structures of **Pd1a** and **Pd1c** (C-PCM/ωB97X calculations, acetonitrile as continuous medium). Color map: hydrogen, white; carbon, grey; nitrogen, blue; oxygen, red; palladium, green. Selected computed bond lengths for **Pd1a** (Å): Pd-C_{allyl}(trans-oxazoline) 2.110; Pd-

C_{allyl}(trans-triazole) 2.105; Pd-C_{allyl}(central) 2.127; Pd-N(oxazoline) 2.157; Pd-N(2)(triazole) 2.161. Selected computed angles for **Pd1a** (°): C_{allyl}(terminal)-Pd-C_{allyl}(terminal) 69.6; N(2)(triazole)-Pd-N(oxazoline) 77.3; N(2)(triazole)- Pd-C_{allyl}(trans-triazole) 173.2; N(oxazoline)-Pd- C_{allyl}(trans-oxazoline) 173.0. Selected computed bond lengths for **Pd1c** (Å): Pd-C_{allyl}(trans-oxazoline) 2.106; Pd-C_{allyl}(trans-triazole) 2.108; Pd-C_{allyl}(central) 2.124; Pd-N(oxazoline) 2.182; Pd-N(2)(triazole) 2.157. Selected computed angles for **Pd1a** (°): C_{allyl}(terminal)-Pd-C_{allyl}(terminal) 69.4; N(2)(triazole)- Pd-N(oxazoline) 77.4; N(2)(triazole)-Pd-C_{allyl}(trans- triazole) 174.8; N(oxazoline)-Pd-C_{allyl}(trans-oxazoline) 176.0.

*4.2.2.2 Synthesis of [PdCl(μCl)(L)]2 (**Pd2a-b**)*

The picture which comes to light when TryOxs are allowed to react with species of the type $[PdCl_2L_2]$ (L=labile ligand such as CH_3CN, BnCN or even $S(CH_3)_2$) is more intriguing; for the sake of clarity the results of our investigations are gathered in **Scheme 4.4**. Due to the easy synthetic preparation, we choose as model precursor complex $[PdCl_2(CH_3CN)_2]$.

Treatment of $[PdCl_2(CH_3CN)_2]$ with 1:1 equimolecular amounts of TryOxs **4a-c** in dichloromethane at room temperature affords compounds having elemental analyses in agreement with the formulation $[PdCl_2$(**4a-c**)]. The compounds are soluble in organic solvent such as dichloromethane, chloroform, tetrahydrofuran and they are non-conducting in acetone or chloroform.

In contrast with that found in the case of the cationic allyl complexes, ^{1}H NMR spectroscopy indicates that in these species TryOxs behaves as monodentate ligands coordinating to palladium through the N atom of the oxazoline. Taking complex **Pd2a** as a representative example, we found that the chemical shift of the resonance due to the proton on the triazole ring is almost unaffected with respect to that of the free ligand ($\delta(CH)_{comp}$ = 7.83 vs $\delta(CH)_{free}$ = 7.88); on the contrary, all the resonances due to the oxazoline ring were found to give multiplets centred at 5.10, 4.60 and 4.39 δ that are significantly downfield shifted with respect the corresponding resonances of the free ligand centred at 4.44, 4.12 and 3.92 δ, respectively; the ^{1}H NMR spectra of **Pd2b** and **Pd2c** present the analogous features. The higher σ-donor ability of the oxazoline ring with respect to triazole was confirmed by the charge distribution of the ligands. DFT calculations shows that the partial charge of oxazoline N in **4a** is −0.205 a.u., while that of triazole N(2) is −0.152 a.u. In the case of **4c** the corresponding values are −0.198 and −0.155 a.u. The Hirshfeld population analyses supported this conclusion, the oxazoline N and triazole N(2) partial charges being −0.233 and −0.162 a.u. in **4a** and −0.220 and −0.166 a.u. in **4c**.

The key indication on the nature of **Pd2a-c** in solution came from their ESI-MS. As a matter of fact, the unique clusters of signals observable in these spectra correspond to cations of formulation $[(TryOx)_2Pd_2Cl_3]^+$ suggesting that **Pd2a-c** are dimeric species (see **Scheme 4.4**) with two chlorine atoms bridging two (TryOx)PdCl units. The dimeric nature of **Pd2a-b** was definitely confirmed by determining their molecular masses in solution by Vapour Phase Osmometry. Accordingly, we were intrigued to isolate crystalline samples of **Pd2a-c** suitable for X-ray diffraction analysis.

Eventually our efforts succeeded and slow evaporation of dichloromethane solutions of **Pd2a** allowed to obtain orange needles, designated as **Pd2d** in **Scheme 4.4**, that were found suitable for X-ray structural studies.

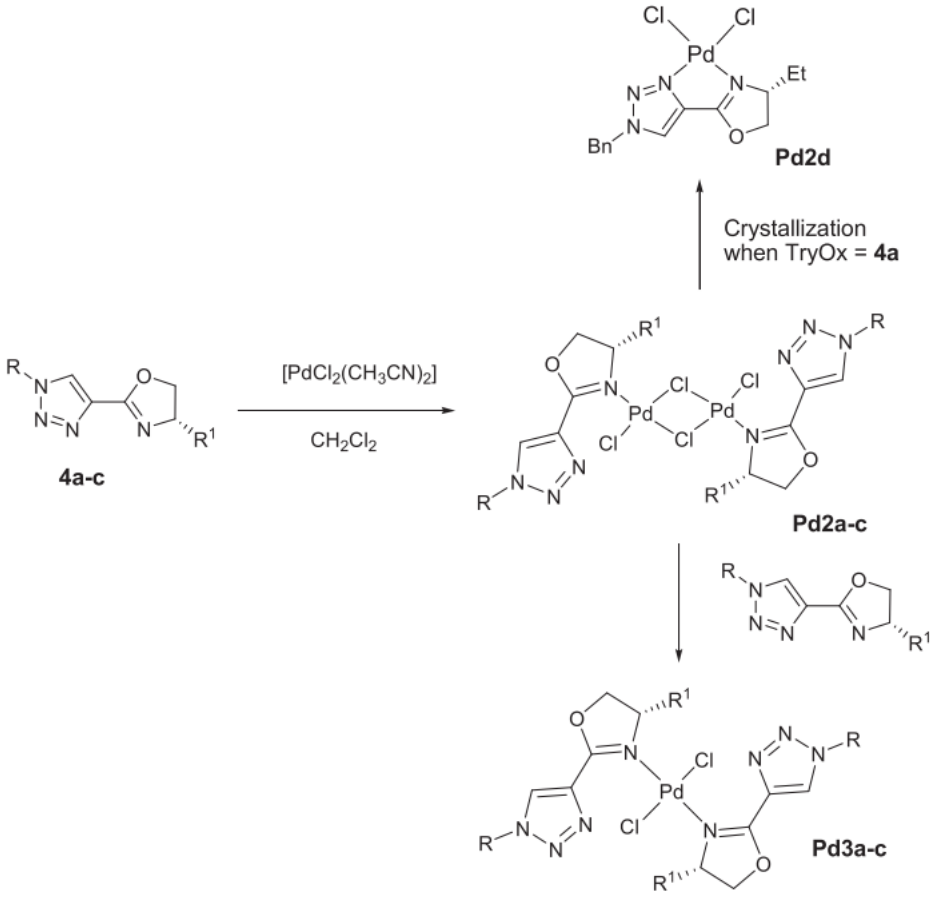

Scheme 4.4. Synthesis of palladium(II)-TryOx-chloro complexes.

*4.2.2.3 X-ray crystal structures of [($PdCl_2$(**4a**)] (**Pd2d**)*

Summaries of crystal and structure refinement data for **Pd2d** are listed in **Table 4.1**; some selected structural parameters are reported in **Table 4.2**. In the latter, data for complex **Pd2d** must be regarded as preliminary.

Table 4.1. Crystallographic data for the complexes **Pd3c** and **Pd2d**

	Pd3c	**Pd2d**
Empirical formula	$C_{26}H_{44}Cl_2N_8O_2Pd$	$C_{14}H_{16}N_4OCl_2Pd$
Formula weight	677.99	433.61
Temperature/K	300(1)	297.4(6)
Crystal system	Tetragonal	triclinic
Space group	*P* 4_1 2_1 2	*P*-1
a / Å	9.0141(13)	7.1612(14)
b / Å	9.0141(13)	8.8314(15)
c / Å	39.596(8)	13.744(3)
α / °	90	97.653(17)
β / °	90	104.208(19)
γ / °	90	90.541(14)
Volume /Å^3	3217.3(11**)**	834.3(3)
Z	4	2
ρ_{calc} Mg / m^3	1.400	1.726
μ / mm^{-1}	0.779	11.972
F(000)	1408.0	432.0
Crystal size/mm^3	0.26 × 0.21 × 0.16	0.50 × 0.09 × 0.08
Reflections collected	75000	3402
Independent reflections / R_{int}	5751 / 0.0786	2093 / 0.0817
Data/restraints/parameters	5751/51/197	2093/102/208
Goodness-of-fit [a] on F^2	1.071	1.343
Final *R* indexes [$I > 2\sigma(I)$]	R_1 [b] = 0.0371, wR_2 [c] = 0.0673	R_1 [b] = 0.1216, wR_2 [c] = 0.3268
Largest diff. peak / hole / e Å^{-3}	0.38 / -0.73	2.63 / -1.07
Flack parameter	0.001(14)	

[a] Goodness–of–fit = $[\Sigma (w (F_o^2 - F_c^2)^2] / (N_{obsvns} - N_{params})]^{1/2}$, based on all data;

[b] $R_1 = \Sigma (|Fo| - |Fc|) / \Sigma |Fo|$;

[c] $wR_2 = [\Sigma[w (F_o^2 - F_c^2)^2] / \Sigma[w (F_o^2)^2]]^{1/2}$.

Table 4.2. Some selected bond lengths () and angles () for complexes **Pd3c** and **Pd2d**

Pd3c		**Pd2d***	
Pd–Cl(1)	2.3329(12)	Pd–Cl(1)	2.288(6)
Pd–Cl(2)	2.2913(12)	Pd–Cl(2)	2.270(5)
Pd–N(1)	2.033(2)	Pd–N(1)	2.033(16)
Pd–N(1A)[a]	2.033(2)	Pd–N(2)	2.006(17)
N(1)–C(1)	1.287(3)	N(1)–C(1)	1.32(3)
N(1)–C(3)	1.502(4)		
C(1)–C(8)	1.452(5)	C(1)–C(7)	1.39(3)
C(1)–O(1)	1.346(4)		
O(1)–C(2)	1.441(5)		
C(2)–C(3)	1.516(5)		
C(8)–N(2)	1.364(4)	C(7)–N(2)	1.38(3)
N(2)–N(3)	1.310(5)	N(2)–N(3)	1.28(3)
N(3)–N(4)	1.342(4)		
N(4)–C(9)	1.343(4)		
C(9)–C(8)	1.356(5)		
Cl(2)–Pd–Cl(1)	180.00(15)	Cl(2)–Pd–Cl(1)	90.3(2)
N(1)–Pd–Cl(1)	93.38(7)	N(1)–Pd–Cl(1)	174.0(5)
N(1)–Pd–Cl(2)	86.62(7)	N(1)–Pd–N(2)	80.2(6)
N(1)–Pd–N(1A)[a]	173.24(15)	N(2)–Pd–Cl(2)	175.2(5)
N(1)–C(1)–O(1)	116.1(3)	N(1)–C(1)–C(7)	121.2(17)
C(1)–O(1)–C(2)	106.6(3)		
O(1)–C(2)–C(3)	105.6(3)		
C(3)–N(1)–C(1)	108.2(3)		
C(8)–N(2)–N(3)	107.6(3)	C(7)–N(2)–N(3)	107.5(18)
N(2)–N(3)–N(4)	108.6(3)		
N(3)–N(4)–C(9)	109.6(3)		
C(9)–C(8)–N(2)	108.6(3)		

*Data for complex **Pd2d** only preliminary; [a] at *+y*, *+x*. *1–z*.

Figure 4.2 shows the ORTEP [16] representation of **Pd2b**, with the chosen numbering scheme, with highlighted alternate positions for disordered atoms.

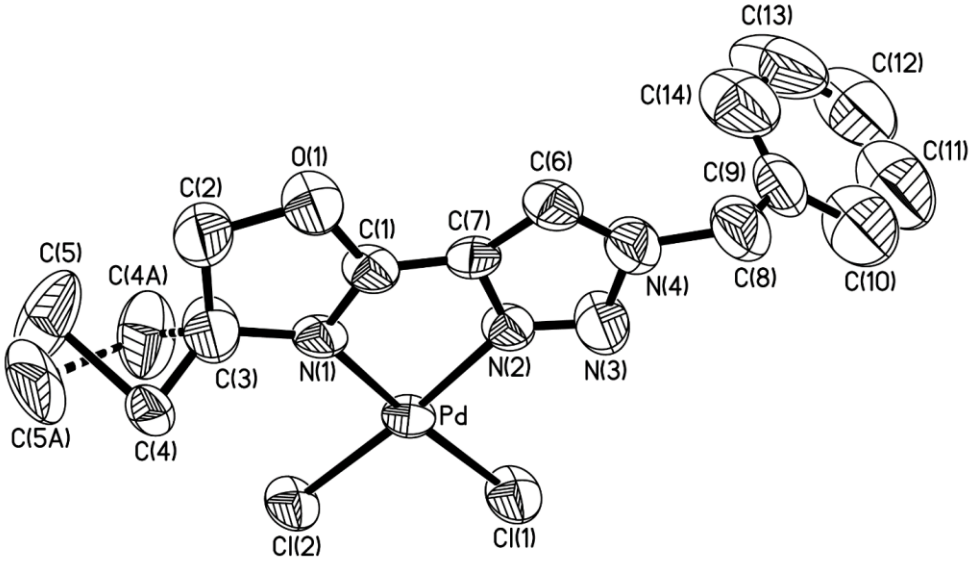

Figure 4.2. ORTEP drawing of **Pd2d**, showing also the numbering scheme. Thermal ellipsoids are at the 40% probability level. Hydrogen atoms are omitted for clarity; alternate positions of disordered atoms are drawn with dashed bonds.

The refinement procedure for [$PdCl_2$(**4a**)] was terminated when the final *R* index was still above 12%. In our opinion, this value is too high to allow a discussion of the structural parameters of the molecule; hence, such discussion will not be carried over at this stage. This also apply to the disorder of the ethyl residue branching at the chiral C(3), which could hint to the possible presence of both enantiomers of the ligand. Attempts of refining the structure in the P1 space group (two molecules in cell) failed in the very early stages of the refinement, with coordinates of corresponding atoms in two independent molecules showing strong correlations, thus compelling us to perform refinement in the P-1 space group. Available data hence do not allow to confirm or reject the presence in the solid state of only one ligand enantiomer, yet are sufficient to confirm the chemical identity of the crystallized compound and the basic arrangement of the molecule, which is briefly outlined hereafter. Complex **Pd2d** is mononuclear and neutral when in the solid state. The Pd atom is bound by two chlorides and two nitrogen atoms of the chelating ligand, in a square planar environment. Upon coordination, the triazolyloxazoline ligand makes with Pd a five-membered metallacycle (N(1), C(1), C(7), N(2), Pd), with all atoms nearly coplanar. The oxazoline and triazolyl rings of the ligand also appear nearly planar. The triazolyl ring shows a slight deviation towards an envelope arrangement

(with N(2) at the flap). A similar arrangement might also be expected for the partially saturated oxazoline ring, but it did not emerge at the present stage of the refinement. The mean planes encompassing the oxazoline and triazolyl rings do not perfectly coincide with the mean plane of the metallacycle, so that the molecule is slightly puckered overall (with the mean planes of oxazoline and of the triazolyl moieties bent towards each other and making a dihedral angle of about 5°). As for the benzyl residue branching at N(4), the mean plane of the phenyl ring and the mean plane of the metallacycle make with each other a dihedral angle of about 75°.

An inspection of the CCDC repository (Cambridge Structural Database, Version 5.40 of November 2018+3 updates)[17] for compounds having similar triazolyl-oxazoline ligands returned only five entries described in two papers.[11,18] Of these, one is a copper(II) compound,[11] containing two 2-(1-benzyl-1H-1,2,3-triazol-4-yl)-4,5- dihydrooxazole ligands, very similar to **Pd3c** discussed below, and three are iridium complexes of a modified benzooxazoline ligand.[18] Hence, to the best of our knowledge, this is the first report of a Pd(II) triazolyloxazoline complex.

According to the contrasting molar masses data in solution and the X-ray structure, we must conclude that while in solution **Pd2a** is a dimeric species in which the TryOx behaves as a monodentate ligand employing the N atom of the oxazoline, in the solid state, upon crystallization, it converts into **Pd2d** a mononuclear species in which the TryOx behaves as a N,N bidentate chelating ligand.

*4.2.2.4 Synthesis of $[PdCl_2L_2]$ (**Pd3a-b**)*

Taking into account the ease with which the chlorine bridge in dimeric **Pd2a** breaks, we were prompted to investigate the reactivity of complexes **Pd2a-c** towards the addition of a second equivalent of ligand. As a matter of fact, we were intrigued to find out if a second molecule of ligand could cleave the chlorine bridges and the co- ordination mode adopted by the ligands in the final product.

Identical compounds of formulation $[PdCl_2(TryOx)_2]$ (**Pd3a-c**, see **Scheme 4**) were obtained either adding an equivalent of ligand to **Pd2a-c** or directly allowing to react $[PdCl_2(CH_3CN)_2]$ with two equivalents of ligand. Analytical data and ESI-MS are in keeping with the proposed formulation and conductivity measurements showed that complexes **Pd3a-c** are neutral compounds in chloroform or in acetone. A single set of signals is present in both the ^{1}H and ^{13}C NMR spectra of **Pd3a-c**, indicating that both TryOx ligands are equivalent and hence that they are coordinated to palladium in the same fashion. In the ^{1}H NMR spectra a remarkable feature is that not only the oxazoline protons, but also

the triazolyl proton resonate at significantly lower fields with respect to the free ligands. Specifically, the chemical shifts of oxazoline protons are similar to these found in complexes **Pd2a-c** pointing at coordination of N atom of the oxazoline, while the triazolyl protons are found to resonate at very low fields in the 9.85–9.51 δ range, which is even lower than that found for the cationic complexes **Pd1a-c.** Rationalization of this puzzling spectral feature came from X-ray structural studies (see below) which demonstrate that there is a close non-bonding contact between the H atoms of triazoles and the Cl atoms of the complex.

*4.2.2.5 X-ray crystal structure of (**Pd3c**)*

Slow diffusion of diethyl ether into a dichloromethane solution of **Pd3c** allowed to obtain crystalline samples (orange prisms) suitable for X-ray studies. Summaries of crystal and structure refinement data for complex **Pd3c** are listed in **Table 4.1** and some selected structural para- meters are reported in **Table 4.2**.

At the end of the refinement process the final R index (below 4%) is much better than in [$PdCl_2$(**4a**)], leaving no unresolved peaks, especially around the chiral C(3) atom. **Figure 4.3** shows the ORTEP representation of the compound, with the chosen numbering scheme, with highlighted alternate positions for disordered atoms.

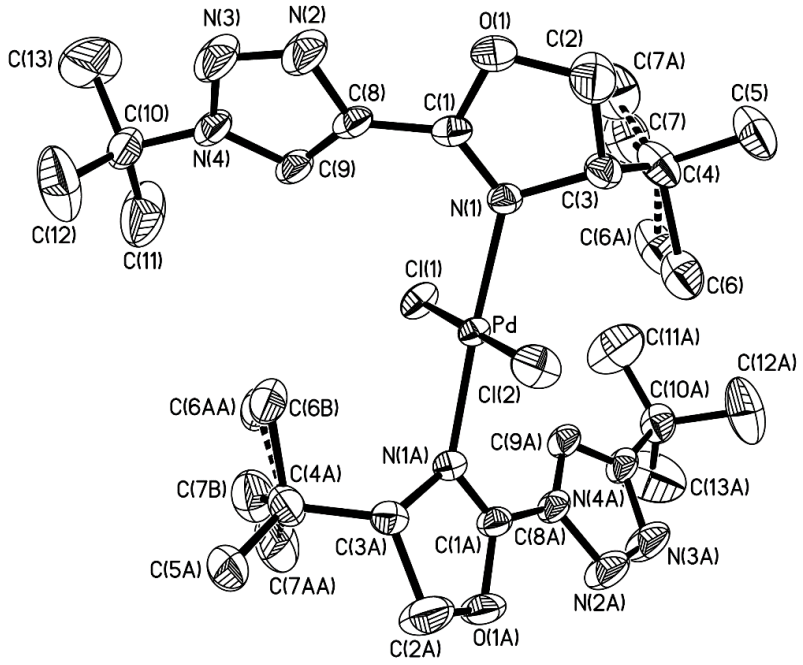

Figure 4.3. ORTEP drawing of Pd3c, showing also the numbering scheme. Thermal ellipsoids are at the 40% probability level. Hydrogen atoms are omitted for clarity; alternate positions of disordered atoms are drawn with dashed bonds

Complex **Pd3c** is mononuclear and neutral. However, opposite to what found for **Pd2d**, the triazolyl-oxazoline ligand does not chelate Pd. Instead, two ligand units act as monodentate donors (through the N(1) atom) and the coordination environment of Pd is completed by two chloride ions. In Pd3c, the asymmetric unit consists of half a molecule, so the atoms belonging to the coordination plane are strictly coplanar by symmetry and the Pd coordination environment has regular square planar geometry. In the ligand, the atoms of the triazolyl ring are co-planar within 0.01 Å, while the oxazoline ring is slightly bent towards an envelope arrangement, with the C(2) atom at the flap by 0.08 Å. The position of the tert-butyl residue branching at the chiral C(3) atom is clearly defined, so it is ascertained that in the crystal structure of $[PdCl_2(\mathbf{4c})_2]$ only one enantiomer of the ligand is present. The correct attribution of the absolute structure is supported, as indicated in the 4.3.6, by the value close to zero (0.001(14)) of the Flack parameter, calculated from 1576 selected quotients (Parsons' method).[19]

Opposite to what was found in **Pd2d**, the mean planes encompassing the triazolyl and oxazoline rings make with the coordination plane dihedral angles of 71.6 and 65.7°, respectively, and they also make a dihedral angle of 15.8° with each other. The reciprocal arrangement of the mean planes of the triazolyl and oxazoline moieties in reported compounds is mostly similar to that found in **Pd3c** (dihedral angles ranging from 5.4[11] to 10.6°.[18] Among reported com- pounds, the entity most resembling complex Pd3c is the compound described in,[11] also showing the metal bound by two monodentate ligands and two chloride ions.

With respect to bond distances in the coordination sphere, a CCDC search for mononuclear Pd(II) complexes having a PdN_2Cl_2 square planar environment (480 entries) indicates an average Pd-N, Pd-Cl distances of 2.020 Å and 2.300 Å, respectively. The values found for **Pd3c** (Pd-N bond of 2.033(2) Å, Pd-Cl lengths of 2.2913(12) and 2.3329(12) Å) look in agreement with available data. The difference between the two Pd-Cl bonds (0.042 Å) is a feature that does not appear in the pretty similar copper(II) complex [11] and points to a rather efficient intramolecular non-covalent interaction (H⋯Cl distance of 2.491 Å, about 0.5 Å shorter than the sum of van der Waals radii involving Cl(1) at one end and H(9) (and its symmetry equivalent at +y, +x, 1 − z) at the other. As for the triazolyl-oxazoline ligand, the values found in **Pd3c** of bond distances within the rings also look in reasonable agreement with the corresponding averages for reported compounds. In the triazolyl residue, the deviation between our data and mean values for corresponding bond lengths is never larger than 0.03 Å. In the oxazoline moiety there is a greater difference (largest deviation of 0.11 Å), however, most of reported

complexes are in fact benzoxazoline derivatives. When looking at the closely related complex,[11] the largest deviation reduces to 0.038 Å. The comparison between complex **Pd3c** and available data indicate substantial aromatic behavior in the triazolyl moiety and no involvement in the conjugation of the C(1)eN(1) bond of the oxazoline moiety. The latter retains instead typical double bond character (1.287(3) Å, almost identical to the average of 1.289 Å for reported compounds).

Besides to the above mentioned intramolecular contact between Cl(1) and H(9), there are virtually no intermolecular contacts worth of mention. The two 'shortest' nonbonding approaches (both only 0.05 Å shorter than the sum of the pertinent van der Waals radii loosely involve the triazolyl N(2) and N(3) atoms, which respectively engage the H(12C) and the H(5B) atoms of a nearby moiety at 1.5 − y, ½ + x, ¼ + z. These contacts create an helical motif that propagates along with the crystallographic *b* axis.

The triazole-H—Cl interaction was also detected in the DFT-optimized structures of **Pd3a** and **Pd3c** by means of Atoms-in-Molecules (AIM) analysis. The (3,−1) bond critical points (b.c.p.) of interest are depicted in **Figure 4.4** together with the paths connecting the (3,−1) and (3,−3) points and the interbasin surface. Selected properties at b.c.p. are reported in the Figure. In particular, the positive values of the Laplacian of electron density $\nabla^2 \rho$ are in agreement with electron-unshared interactions, despite the fact that the very low negative energy density (E) values could suggest a slightly covalent nature.[20]

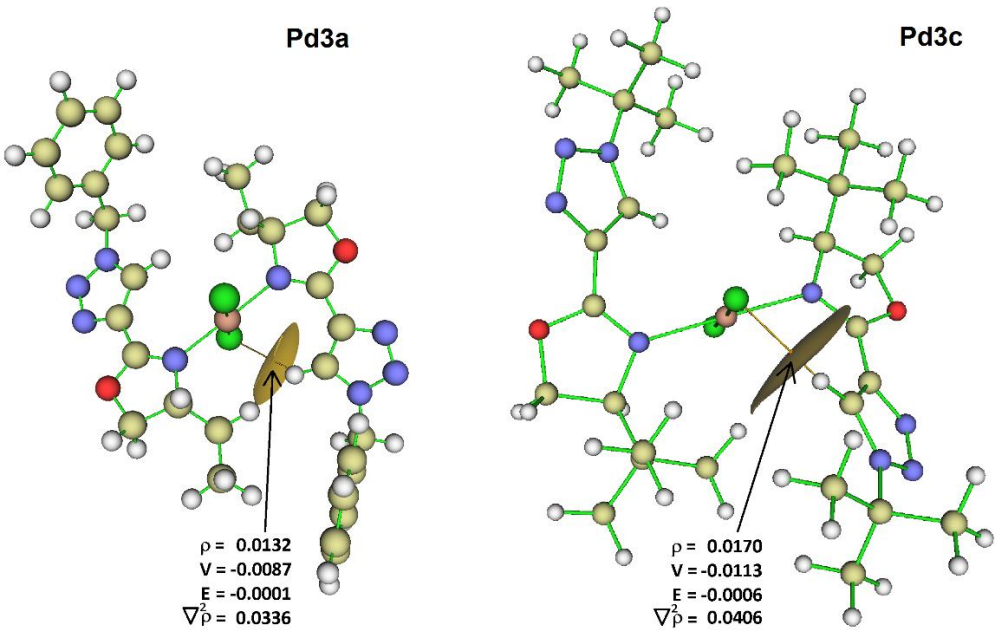

Figure 4.4. DFT-optimized structures of **Pd3a** and **Pd3c** (C-PCM/ωB97X calculations, acetonitrile as continuous medium), with H—Cl (3,−1) b.c.p. and related inter- basin surface. ρ=electron density,

V=potential energy density, E=electron density, 2ρ=Laplacian of electron density. All quantities in a.u. Color map: hydrogen, white; carbon, dark yellow; nitrogen, blue; oxygen, red; chlorine, green; palladium, pink. Cartesian coordinates are collected in supporting (Section 8.2).

4.2.3 Catalytic hydrogenations

With complexes **Pd1a-c**, **Pd2a-c** and **Pd3a-c** in hand, we explored their catalytic activity running few preliminary tests on the hydrogenation of biomass derived FUR to FA. So far, **Pd2d** was not crystallized in enough amount thus it has not been evaluated for catalytic tests.

While a large amount of ruthenium and iridium complexes have been used for the homogenous reduction of FUR to FA, as briefly summarized in section 1.2.3.3, to the best of our knowledge palladium complexes are never been used. In contrast, there's a broad library available for Pd heterogenous catalysts used to achieve this task.[21]

A catalyst screening was run at standard reaction conditions in order to evaluate the complex with best performances. As showed in **Table 4.3**, all reactions were run in MeOH at 80°C and 40 bar with a catalyst loading of 0.1 mol%. Allyl complex **Pd1c** revealed to perform better at these conditions, reaching 89% of conversion towards the formation of FA.

Table 4.3. Optimization of the reaction conditions for the catalytic hydrogenation reactions

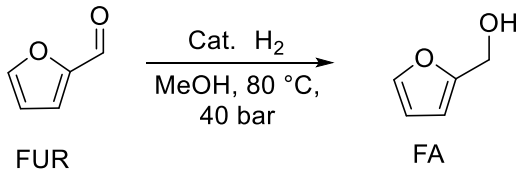

FUR FA

Entry[a]	Ligand	Yield (%)[b]
1	**Pd1a**	54
2	**Pd1b**	69
3	**Pd1c**	89
4	**Pd2a**	13
5	**Pd2b**	25
6	**Pd2c**	55
7	**Pd3a**	12
8	**Pd3b**	32
9	**Pd3c**	12

[a] Reaction conditions: Furfural = 5.3 mmol, Temp. = 80 °C, MeOH = 5.0 mL, Time = 18 hours, cat. Loading = 0.1 mol% [b] GC yields using dodecane as internal standard.

Although an extensive optimization is required in order to evaluate the catalytic properties of **Pd1a-3c**, it is possible to note that cationic Pd(II)-allyl complexes displayed better performances in contrast to the neutral $[PdCl_2L_2]$ and $[PdCl(\mu\text{-}Cl)(L)]_2$. In particular, complex **Pd3c** exhibited the best conversion probably due the significant steric hindrance provided by the *t*-butyl group. According to literature, Pd-allyl complexes have been used for different catalytic reactions,[22–25] but their use for homogenous hydrogenation is rather limited.[26]

However, further experiments are currently ongoing aiming to clarify the mechanism and the catalytic potential of the synthetized complexes.

4.3 EXPERIMENTAL

4.3.1 Materials and instrumentation

Commercial solvents (Aldrich) were purified as described in the literature.[27] (S)-(+)-2-Amino-1-butanol, (S)-(+)-2-amino-4-methyl-1-pentanol [L-leucinol, (S)-(+)-leucinol], and (S)-(+)-2-amino-3,3-dimethylbutyric acid (L-tert-leucine) were purchased from Aldrich. Benzylazide [28] and *t*-butylazide[29] were prepared according to procedures reported in the literature (caution: aliphatic azides and HN_3 are explosive and toxic). 1- Benzyl-1*H*-[1,2,3]triazole-4-carboxylic acid was prepared according to the procedure described by Gautier.[30] (S)-(+)-2-Amino-3,3-dimethylbutanol (L-tert-leucinol) was synthesized by reduction of (S)-(+)-2-amino-3,3-dimethylbutyric acid according to a literature procedure.[31] 4-(4,6- dimethoxy-1,3,5-triazin-2-yl)-4-methylmorpholinium chloride (DMTMM) was prepared as described by Kunishima.[12] $[Pd(\eta^3\text{-}C_3H_5)Cl]_2$ was prepared according to the method described by Hartley.[32] All syntheses were carried out under inert atmosphere (nitrogen) using standard Schlenk techniques. ^1H and ^{13}C {1H} NMR spectra were recorded on a Bruker AVANCE 300 spectrometer operating at 300.21 and 75.44 MHz, respectively. The chemical shift values of the spectra are reported in δ units with reference to the residual solvent signal. The proton assignments were performed by standard chemical shift correlations as well as by 1H 2D COSY experiments.

ESI-MS analyses were performed using a Finnigan LCQ-Duo ion-trap instrument, operating in positive ion mode (sheath gas N_2, source voltage 4.0 KV, capillary voltage 21 V, capillary temperature 200 °C). Sample solutions were prepared by dissolving Pd complexes (about 1 mg) in methanol (1 mL) and then further diluting with methanol (1:30). All mass spectra were recorded on freshly prepared solutions. Elemental analyses (C, H, N) were carried out at the University of Padua using a Fison EA1108 microanalyzer. IR spectra were collected in the range 4000–400 cm^{-1} using a Perkin-Elmer

Spectrum One spectrophotometer. Melting points were determined using a Büchi B-535 apparatus. Optical rotatory power values (α) were determined using a Jasco P-2000 polarimeter (Na lamp at 25 °C). Molar masses in solution were measured by Vapor Phase Osmometry (VPO) employing chloroform solutions (37 °C) on a Knaeur Dampfdruck Osmometer.

4.3.2 Ligand synthesis

*4.3.2.1 (1-t-Butyl-1H-[1,2,3]triazol-4-yl) metanoic acid (**1b**)*

In a mixture of *t*-BuOH (15 mL) and water (15 mL) were dissolved 1.50 g (15.00 mmol) of *t*-BuN_3 and 1.40 g (1.5 mL, 16.6 mmol) of methyl propiolate. Then, under nitrogen, were added in the order a solution of sodium ascorbate (0.29 g, 1.50 mmol) in water (2 mL) and finally a solution of $CuSO_4 \cdot 5H_2O$ in water (0.19 g, 0.75 mmol in 2 mL of H_2O). The mixture was kept under stirring and then after 24 h it was taken to dryness. The brown solid residue was extracted with dichloromethane, filtered and taken to small volume. The resulting oil was chromatographed on silica gel (eluent: dicholoromethane/diethylether=95/5) to give the methyl ester of **1b** as a white solid.

^{1}H NMR ($CDCl_3$, 298 K) δ: 8.16 (s, 1H), 3.94 (s, 3H), 1.70 (s, 9H).

The recovered ester was dissolved in MeOH (30 mL) and treated with 10 mL of an 10% aqueous NaOH solution. The mixture was stirred for 3 h, then the methanol was distilled off at reduced pressure. The aqueous phase was neutralized at pH = 7 by addition of 5% aq. HCl, and extracted with dichloromethane (3 × 30 mL). The reunited organic phases were dried upon anhydrous $MgSO_4$, filtered and taken to dryness in high vacuum to give **1b** as a white solid (1.86 g, 73% yield).

^{1}H NMR (acetone-d_6, 298 K) δ: 8.53 (s, 1H), 3.77 (bs, 1H, COOH),1.73 (s, 9H).

^{13}C NMR ($CDCl_3$, 298 K) δ: 164.1, 138.7, 125.7, 60.8, 30.0.

*4.3.2.2 (S)-1-Benzyl-N-(1-hydroxy-butan-2-yl)-1H-1,2,3-triazol-4- carboxyamide (**2a**)*

In a round bottomed flask, 0.48 mL (5.00 mmol) of (S)-(-)-2-amino-1-butanol and 1.03 g of **1a** (5.00 mmol) were dissolved in 50 mL of acetonitrile. Then 3.00 g (5.40 mmol) of DMTMM were added to the mixture, which was kept under stirring overnight. After removing the solvent under reduced pressure, the resulting off-white solid residue was treated with 10 wt% of aq. NaOH (10 mL). The suspension thus obtained was filtered, the recovered solid was washed with H_2O and dried under vacuum to give 0.92 g of **3a** as a white powder (70% yield).

^{1}H NMR ($CDCl_3$, 298 K) δ: 7.95 (s, 1H), 7.41–7.26 (m, 5H) 7.24 (brs, 1H), 5.54 (s, 2H), 4.12–3.90 (m, 1H), 3.81–3.59 (m, 2H), 2.70 (brs, 1H, OH), 1.76–1.52 (m, 2H), 0.99 (t, 3H, *J* =6.9 Hz).

*4.3.2.3 (S)-1-(t-Butyl)-N-(1-hydroxy-4-methylpentan-2-yl)-1H-[1,2,3]- triazol-4-carboxyamide (**2b**)*

According to the above procedure, DMTMM (1.23 g, 4.10 mmol) was added to a solution of (S)-(+)-2-amino-4-methyl-1-pentanol (0.49 g, 4.20 mmol) and 1b (0.70 g, 4.14 mmol) in acetonitrile (40 mL). Workup as for **2a** gives the sought amide as a white solid (0.79 g, 71%yield).

^{1}H NMR ($CDCl_3$, 298 K) δ: 8.14 (s, 1H), 7.21 (br d, 1H, J=8.6 Hz,NH), 4.23 (m, 1H), 3.77 (dd, 1H, J=11.1 and 3.6 Hz), 3.64 (dd, 1H, *J*=11.1 and 6.2 Hz), 2.83 (br s, 1H, OH), 1.72 (m, 1H), 1.69 (s, 9H), 1.63–1.34 (m, 2H), 0.95 (d, 6H, *J*=6.5 Hz).

*4.3.2.4 (S)-1-(t-Butyl)-N-(1-hydroxy-3,3-dimethylbutan-2-yl)-1H-[1,2,3]- triazol-4-carboxyamide (**2c**)*

According to the above procedures, DMTMM (1.94 g, 7.00 mmol)was added to a solution of (S)-(+)-2-amino-3,3-dimethylbutanol (0.82 g, 7.00 mmol) and **1b** (1.20 g, 7.00 mmol) in acetonitrile (40 mL). Workup as for **2a** allows to obtain the sought amide as a white solid (1.51 g, 81% yield).

^{1}H NMR ($CDCl_3$, 298 K) δ: 8.14 (s, 1H), 7.34 (br d, 1H, *J* = 8.6 Hz,NH), 4.09–4.00 (m, 1H), 4.00–3.88 (m, 1H), 3.66 (m, 1H), 2.71 (t, 1H, *J* = 11.0 Hz, OH), 1.68 (s, 9H), 1.02 (s, 9H).

*4.3.2.5 (S)-1-Benzyl-N-(1-chloro-butan-2-yl)-1H-[1,2,3]-triazol-4-carboxyamide (**3a**)*

A solution of $SOCl_2$ (0.9 mL, 12.1 mmol) in dichloroethane (10 mL) was drop wise added to a suspension of **2a** (1.66 g, 6.05 mmol) in dichloroethane (100 mL) under nitrogen at room temperature. The mixture was heated under stirring at 60 °C for 4 h to afford a clear pale yellow solution. Upon cooling at room temperature a white solid precipitates. The liquid phase was removed in high vacuum to give a white powder (1.70 g, 99% yield) which was characterized by ^{1}H NMR spectroscopy and used in the following step without any further purification.

^{1}H NMR ($CDCl_3$, 298 K) δ: 7.98 (s, 1H), 7.46–7.36 (m, 5H, arom.)7.28 (br d, 1H, *J* = 8.0 Hz, NH), 5.57 (s, 2H), 4.38–4.25 (m, 1H), 3.80–3.66 (m, 2H), 1.93–1.52 (m, 2H), 1.0 (t, 2H, *J* = 6.8 Hz).

*4.3.2.6 (S)-1-(t-Butyl)-N-(1-hydroxy-4-methylpentan-2-yl)-1H-[1,2,3]- triazol-4-carboxyamide (**3b**)*

The compound was prepared according to the above procedure (quantitative yield).
^{1}H NMR ($CDCl_3$, 298 K) δ: 8.13 (s, 1H), 7.18 (br d, 1H, *J* = 8.8 Hz,NH), 4.51 (m, 1H), 3.76 (dd, 1H, *J* = 11.1 and 4.4 Hz), 3.65 (dd, 1H, *J* = 11.1 and 3.9 Hz), 1.70 (s, 9H), 1.80–1.45 (m, 3H), 0.96 (d, 6H, *J* = 6.4 Hz).

*4.3.2.7 (S)-1-(t-Butyl)-N-(1-chloro-3,3-dimethylbutan-2-yl)-1H-[1,2,3]- triazol-4-carboxyamide (**3c**)*

The compound was prepared according to the above procedures (quantitative yield).

^{1}H NMR ($CDCl_3$, 298 K) δ: 8.16 (s, 1H), 7.20 (br d, 1H, *J* = 9.6 Hz,NH), 4.29 (ddd, 1H, *J* = 10.5, 9.2 and 3.4 Hz), 3.88 (dd, 1H, *J* = 11.5, and 3.4 Hz), 3.56 (dd, 1H, *J* = 11.5 and 9.2 Hz), 1.70 (s, 9H), 1.04 (s, 9H).

*4.3.2.8. 1-Benzyl-((S)-4-ethyl-4,5-dihydrooxazol-2-yl)-1H-[1,2,3]-triazole (**4a**)*

Under nitrogen, finely powdered NaOMe (1.00 g) was added to a solution of **3a** (0.58 g, 2.00 mmol) in methanol (10 mL). The resulting suspension was heated under stirring at 55 °C for 6 h, then the solution was cooled to room temperature and taken to dryness under vacuum. The solid residue was dissolved in dichloromethane (30 mL) and the suspension thus obtained was extracted with water (4 × 30 mL). The organic phase was dried over $MgSO_4$ and then filtered. The filtrate was dried under vacuum to afford 0.41 g (81% yield) of ligand **4a** as a white solid.

^{1}H NMR ($CDCl_3$, 298 K) δ: 7.89 (s, 1H), 7.40–7.25 (m, 5H), 5.55 (s, 2H). 4.49 (dd, 1H, *J* = 9.3,8.1 Hz), 4.16–4.26 (m, 1H), 4.02–4.07(m, 1H), 1.51–1.58 (m, 2H), 0.98 (t, 3H, J=7.4 Hz).

^{13}C NMR ($CDCl_3$, 298 K) δ: 157.0, 138.0, 133.92, 128.5, 129.2, 129.4, 124.9, 72.5, 68.1, 54.7, 28.6, 10.2.

M.p.: 86 °C.

Elemental analysis: $C_{14}H_{16}N_4O$ (256.30), calcd. C, 65.61; H, 6.29; N, 21.86; found: C, 65.4; H, 6.4; N, 21.8.

GC–MS: 256 [M]+, 227 [M - C_2H_5]+, 156, 106, 91.

$[\alpha]_D25$=−20.0 (c=1, CH_2Cl_2).

IR (KBr, cm^{-1}): 3070 (m), 2952 (ms), 1672 (s), 1544 (ms), 1454 (s), 1046 (s), 1004 (ms), 883 (m), 713 (s).

*4.3.2.9 1- tert-Butyl-4-((S)-1-4-isobutyl-4,5-dihydrooxazol-2-yl)-1H-1,2,3- triazole (**4b**)*

The compound was obtained as a pale yellow oil according to the above procedure (76% yield).

^{1}H NMR ($CDCl_3$, 298 K) δ: 8.04 (s, 1H), 4.47 (dd, 1H, *J* =9.3 and 8.1 Hz), 4.25 (m, 1H), 3.97 (t, 1H, *J* =8.1 Hz), 1.75 (m, 1H), 1.62 (m,1H) 1.61 (s, 9H), 1.38 (m, 1H), 0.89 (t, 6H, *J* =6.5 Hz).

^{13}C NMR ($CDCl_3$, 298 K) δ: 157.1, 136.8, 122.5, 73.2, 64.9, 60.0,45.4, 29.9 (2C), 25.4, 22.7, 22.6.
Elemental analysis: $C_{13}H_{22}N_4O$ (250.34), calcd.: C, 62.37; H, 8.86; N, 22.38; found: C, 62.2; H, 8.9; N, 22.4.

GC–MS: 250 [M]+, 193 [M – C_4H_9]+, 126, 124, 57.

$[\alpha]_D^{25}$ = −41.1 (c=1.1, CH_2Cl_2).

IR (KBr, cm^{-1}): 2959 (s), 1664 (s), 1556 (w), 1470 (w), 1372 (m), 1226 (ms), 1150 (m), 1041 (ms), 940 (w), 826 (w), 699 (w).

*4.3.2.10 2-tert-butyl-4-((S)-4-tert-butyl-4,5-dihydrooxazol-2-yl) –1H- 1,2,3-triazole (**4c**)*

The title compound was prepared according to the above procedures (85% yield).

^{1}H NMR ($CDCl_3$, 298 K) δ: 8.09 (s, 1H), 4.35 (dd, 1H, J=10.1 and 8.7 Hz), 4.22 (t, 1H, *J* =8.4 Hz), 4.02 (dd, 1H, *J* =10.1 and 8.1 Hz), 1.67 (s, 9H), 0.93 (s, 9H).

^{13}C NMR ($CDCl_3$, 298 K) δ: 157.2, 137.0, 122.5, 76.3, 68.9, 60.1, 34.0, 30.1 (3C), 26.1.

M.p.: 132 °C.

Elemental analysis: $C_{13}H_{22}N_4O$ (250.34), calcd.: C, 62.37; H, 8.86; N, 22.38; found: C, 62.2; H, 8.9; N, 22.4.

GC–MS: 250 [M]+, 193 [M – C_4H_9]+, 126, 124, 57.

$[\alpha]_D^{25}$=−46.9 (c=1, CH_2Cl_2).

IR (KBr, cm^{-1}): 3111 (w), 3067 (w), 2978 (m), 2864 (w), 1670 (s), 1550 (ms), 1461 (w), 1359 (m), 1290 (w), 1233 (s), 1156 (m), 1042 (m), 1004 (m), 953 (m), 902 (w).

4.3.3 Synthesis of Pd(II) allyl complexes

As an example, we report the details relevant to the synthesis of **Pd1a**.

*4.4.3.1. [Pd(η^3-C_3H_5)(4a)](ClO$_4$) (**Pd1a**)*

Under inert atmosphere, a methanol solution of $AgClO_4$ (0.16 g, 0.80 mmol in 20 mL) was drop wise added to a dichloromethane solution of [Pd(η^3-C_3H_5)Cl]$_2$ (145 mg, 0.40 mmol in 20 mL).

The precipitated AgCl was filtered off through celite, then a CH_2Cl_2 solution of ligand **4a** (0.20 g, 0.80 mmol in 20 mL) was added to the filtrate. The resulting pale yellow solution was stirred for 1 h under inert atmosphere, then the solvent was evaporated under reduced pressure. The obtained solid was dissolved in a few mL of CH_2Cl_2. Addition of Et_2O afforded **Pd1a** (0.32 g, 81% yield) as a pale yellow microcrystalline solid.

^{1}H NMR ($CDCl_3$, 298 K) δ: 8.83 (s, 1H), 7.42–7.36 (m, 5H, arom.),5.68 (s, 2H, CH2), 5.66 (quintet, 1H, *J* = 11.7 Hz, allyl central), 4.91–4.85 (t, 1H, CH_2 oxaz), 4.61–4.47 (overlapping broad m, 3H, allyl-syn and CH oxazoline), 3.38–3.16 (br m, 2H, allyl-anti), 1.82–1.64 (m,2H), 0.93 (t, *J* =7.0 Hz, 3H).

^{13}C NMR ($CDCl_3$, 298 K) δ: 163.2 (1C), 136.4 (1C), 133.4 (1C), 129.4 (2C), 129.2 (2C), 128.4 (1C), 126.7 (1C), 116.1 (1C, HC-allyl), 75.9 (1C), 65.5 (1C), 62.5 (1C, H2C-allyl), 60.5 (1C, H2C-allyl), 55.5 (1C), 27.6 (1C), 8.5 (1C).

M.p.: 99 °C (dec.).

Elemental analysis: $C_{17}H_{21}ClN_4O_5Pd$ (502.02), calcd. C, 40.57; H, 4.21; N, 11.13; found: C, 40.1; H, 3.96; N, 10.9. ESI-MS (m/z): calcd. for $C_{17}H_{21}N_4OPd$ ([Pd(η^3-C_3H_5)(4a)]+):403.075, found: 403.070.

Λ (1×10^{-3} M in acetone): 122 (Ω^{-1} cm^2 mol^{-1}).

IR (KBr, cm^{-1}): 3080 (s), 3029 (w), 2975 (w), 2940 (w), 2870 (w), 1753 (vw), 1657 (s), 1570 (s), 1499 (w), 1467 (m), 1458 (m), 1435 (s), 1296 (w), 1258 (m), 1137 (w), 1077 (m), 940 (w), 883 (vw), 718 (s), 690 (m), 553 (w).

*4.4.3.2 [Pd(η^3-C_3H_5)(4b)](PF$_6$) (**Pd1b**)*

^{1}H NMR ($CDCl_3$, 298 K) δ: 8.35 (s, 1H), 5.66 (quintet, 1H, *J* = 6.5 Hz, allyl central), 4.92 (t, 1H, *J* =9.0 Hz), 4.44 (t, 1H, *J* =7.2 Hz), 4.40–4.25 (br overlapping m, 3H, allyl-syn and CH-oxaz), 3.27 (br m, 2H, allyl-anti), 1.85–1.60 (m, 2H), 1.74 (s, 9H), 1.54–1.41(m, 1H), 0.96 (dd, 6H, *J* =10.6 and 5.6 Hz).

^{13}C NMR ($CDCl_3$, 298 K) δ: 164.0 (1C), 136.3 (1C), 123.8 (1C), 115.7 (HC-allyl), 63.6 (1C), 63.3 (1C), 61.6 (br, H2C-allyl), 61.00 (br, H2C-allyl), 44.9, 29.7 (3C), 25.2 (1C), 23.4 (1C), 22.0 (1C).

M.p.: 98 °C (dec.).

Elemental analysis: $C_{16}H_{27}F_6N_4OPPd$ (542.8), calcd. C, 35.4; H, 5.01; N, 10.32; found: C, 35.2; H, 4.96; N, 10.6. ESI-MS (m/z): calcd. for $C_{16}H_{27},N_4OPd$ ([Pd(η^3-C_3H_5)(4b)]+):397.122, found: 397.140.

Λ (1×10^{-3} M in acetone)=102 Ω^{-1}cm^{2}mol^{-1}.

IR (KBr, cm^{-1}): 2970 m, 1670 s, 1469 m, 1424 m, 1377 m, 1238 m, 1190, 1071, 841 vs, 558 vs.

*4.4.3.3. [Pd(η^3-C_3H_5)(4c)](ClO$_4$) (**Pd1c**)*

^{1}H NMR ($CDCl_3$, 298 K) δ: 8.48 (s, 1H), 5.73 (br m, 1H, HC-allyl), 4.87 (t, 1H, J=9.5 Hz), 4.79 (dd, 1H, J=9.2 and 4.9 Hz), 4.47 (br s, 2H, CH2 syn), 4.20 (dd, 1H, J=9.7 and 4.9 Hz), 3.48 (br d, 1H, CH anti, J=12.0 Hz), 3.22 (br d, 1H, CH anti, J=9.8 Hz), 1.78 (s, 9H, t-bu), 1.02 (s, 9H, t-bu).

^{13}C NMR ($CDCl_3$, 298 K) δ: 164.5 (1C), 136.5 (1C), 123.9 (1C), 116.1 (1C, HC-allyl), 74.3 (1C), 73.6 (1C), 63.8 (br, 1C, H2C-allyl), 63.7 (1C), 62.3 (br, 1C, H2C-allyl), 34.9 (1C), 29.8 (3C), 25.9 (3C).

Mp.: 120 °C (dec.).

Elemental analysis: $C_{16}H_{27}ClN_4O_5Pd$ (496.07), calcd. C, 38.64; H, 5.47; N, 11.27; found: C, 38.4; H, 5.66; N, 11.5.

ESI-MS (m/z): calcd. for $C_{17}H_{27}N_4OPd$ ([Pd(η^3-C_3H_5)(4c)]+): 397.122; found 397.119.

Λ (1×10^{-3} M in acetone)=137 $\Omega^{-1}cm^2mol^{-1}$.

IR (KBr, cm^{-1}): 2964 s, 1656 s, 1478 s,1427 s, 1241, vs, 1193, 1047vs, 926, 623 vs.

4.3.4 Synthesis of $[PdCl(\mu\text{-}Cl)(L)]_2$ (Pd2a-b)

As an example we report the details relevant to the synthesis of **Pd2a**.

*4.3.4.1. $[PdCl(\mu\text{-}Cl)(4a)]_2$ (**Pd2a**)*

Ligand 4a (0.13 g, 0.50 mmol) was added portion wise to a suspension of $[PdCl_2(CH_3CN)_2]$ (0.13 g, 0.50 mmol) in dichloromethane (20 mL). The resulting solution was stirred under inert atmosphere at room temperature for 20 h. The orange solution was concentrated in high vacuum to give an orange solid, that was recrystallized from di- chloromethane with diethyl ether. **Pd2a** was recovered as a yellow microcrystalline powder (0.17 g, 80% yield).

^{1}H NMR ($CDCl_3$, 298 K) δ: 7.84 (s, 1H, CH try), 7.48–7.37 (m, 5H, arom.), 5.65 (d, 1H, *J* =15.0 Hz, HHC), 5.62 (d, 1H, *J* =15.0 Hz, HHC), 5.10 (t, 1H, *J* =9.1 Hz), 4.62 (dd, 1H, *J* =5.1 and 8.3 Hz), 4.45–4.34 (br m, 1H), 2.17–2.00 (br m, 1H), 1.97–1.80 (m, 1H), 0.92 (t, 1H, *J* =7.2 Hz).

^{13}C NMR ($CDCl_3$, 298 K) δ: 163.8, 137.1, 131.5, 130.1, 129.8, 129.5, 125.9, 71.0, 63.7, 56.80, 27.3, 26.6, 8.6.

M.p.: 258 °C (dec.).

Elemental analysis: $C_{28}H_{32}Cl_4N_8O_2Pd_2$ (867.26), calcd. C, 38.78; H, 3.72; N, 12.92; found: C, 39.07; H, 3.92; N, 13.14. MW (VPO, $CHCl_3$): 753.

ESI-MS (m/z). Calcd. for $C_{28}H_{32}Cl_3N_8O_2Pd_2$+: 830.979([M−Cl−]+); found 830.987.

IR (KBr, cm^{-1}): 3080 (s), 3029 (w), 2975 (w), 2940 (w), 2870 (w), 1753 (vw), 1657 (s), 1570 (s), 1499 (w), 1467 (m), 1458 (m), 1435 (s), 1296 (w), 1258 (m), 1137 (w), 1077 (m), 940 (w), 883 (vw), 718 (s), 690 (m), 553 (w).

*4.3.4.2. $[PdCl(\mu\text{-}Cl)(4b)]_2$ (**Pd2b**)*

Following the above procedure complex **Pd2b** was obtained as an orange microcrystalline powder in 77% yield.

^{1}H NMR ($CDCl_3$, 298 K) δ: 8.08 (s, 1H), 5.18 (t, 1H, *J* =8.8 Hz), 4.55 (t, 1H, *J* =8.4) 4.49–4.39 (m, 1H), 2.38 (t, 2H, *J* =13.0 Hz) 1.73 (s, 9H), 1.64–1.41 (m, 2H) 1.00–0.90 (m, 6H).

^{13}C NMR ($CDCl_3$, 298 K) δ: 163.9, 136.7, 123.2, 78.9, 63.9, 61.8, 43.1, 29.8 (3C), 25.6, 23.7, 21.4.

M.p.:198 °C (dec).

Elemental analysis: $C_{26}H_{44}Cl_4N_8O_2Pd_2$ (855.33), calcd. C, 36.51; H, 5.19; N, 13.10; found: C, 36.7, H, 5.4; N, 13.2.

MW (VPO; $CHCl_3$): 725.

ESI-MS (m/z): calcd. for $C_{26}H_{44}Cl_3N_8O_2Pd_2$+: 819.073 ([M−Cl−]+); found 819.087.

IR (KBr, cm^{-1}): 2959 (ms), 2864 (m), 1657 (s), 1575 (s), 1474 (m), 1429 (m), 1378 (m), 1246 (ms), 1201 (m), 1074 (m), 1034 (w), 693 (w), 560 (w).

*4.3.4.3. [PdCl(μ-Cl)(4c)]$_2$ (**Pd2c**)*

Following the above procedure complex **Pd2c** was obtained as an orange microcrystalline powder in 72% yield.

^{1}H NMR ($CDCl_3$, 298 K) δ: 9.85 (s, 1H), 4.63–4.47 (2 overlapping m, 2H), 4.34 (dd, J=9.7 and 5.8 Hz), 1.51 (s, 9H), 1.26 (s, 9H).

^{13}C NMR ($CDCl_3$, 298 K) δ: 161.9, 134.4, 128.6, 75.6, 70.3, 60.8, 53.6, 34.7, 29.9 (3C), 26.4 (3C). M.p.: 200 °C (dec.).

Elemental analysis: $C_{26}H_{44}Cl_4N_8O_2Pd_2$ (855.33) [M−Cl−]+; calcd. C, 36.51; H, 5.19; N, 13.10; found: C, 36.3, H, 5.5; N, 13.3.

MW (VPO; $CHCl_3$): 760.

ESI-MS (m/z). Calcd. for $C_{26}H_{44}Cl_3N_8O_2Pd_2$+: 819.073([M−Cl−]+); found 819.088.

IR (KBr, cm^{-1}): 2972 (br s), 1651 (s), 1563 (s), 1480 (ms), 1435 (ms), 1397 (m), 1366 (ms), 1246 (s), 1188 (ms), 1080 (s), 927 (mw), 826 (w) 738 (mw) 693 (w), 560 (w).

4.3.5 Synthesis of [$PdCl_2(L)_2$] (Pd3a-b)

As an example we report the details relevant to the synthesis of **Pd3a**.

*4.3.5.1 [PdCl2(4a)$_2$] (**Pd3a**)*

Ligand **4a** (0.26 g, 1.00 mmol) was added portion wise to a suspension of [$PdCl_2(CH_3CN)_2$] (0.13 g, 0.50 mmol) in dichloromethane (20 mL). The resulting solution was stirred under inert atmosphere at room temperature for 6 h. The orange solution was concentrated in high vacuum to give an orange solid, that was recrystallized from dichloromethane with diethyl ether. **Pd3a** was recovered as a yellow microcrystalline powder (0.27 mg, 79% yield).

^{1}H NMR ($CDCl_3$, 298 K) δ: 9.85 (s, 1H, CH try), 7.51–7.27 (m, 5H,arom.), 5.70 (s, 1H, HHC), 4.65 (t, 1H, *J* =9.1 Hz), 4.48 (dd, 1H, *J* =3.8 and 9.1 Hz), 4.27 (t, 1H, *J* =8.5 Hz), 2.87 (br m, 1H), 2.09 (m,1H), 1.14 (t, 1H, *J* =7.2 Hz).

^{13}C NMR ($CDCl_3$, 298 K) δ: 163.8, 134.6, 129.1 128.9, 128.3, 128.1, 125.3, 72.3, 67.8, 54.4, 28.0, 9.6.

M.p.: 210 °C (dec.).

Elemental analysis: $C_{28}H_{32}Cl_2N_8O_2Pd$ (689.93), calcd. C, 48.74; H, 4.67; N, 16.24; found: C, 48.42; H, 4.95; N, 16.44.

ESI-MS (m/z): calcd. for $C_{28}H_{32}ClN_8O_2Pd^+$: 653.137 ([M−Cl−]+); found: 653.128.

IR (KBr, cm^{-1}): 3118 (w), 3086 (w), 2959 (mw), 2930 (w), 2883 (vw), 1676 (s), 1664 (s); 1556 (m), 1462 (m), 1385 (w), 1233 (ms), 1207 (m), 1023 (mw), 956 (w), 718 (s), 689 (w), 541 (vw).

*4.3.5.2 [PdCl2(4b)$_2$] (**Pd3b**)*

Following the above procedure complex **Pd3b** was obtained as a dark yellow microcrystalline powder in 68% yield.

^{1}H NMR ($CDCl_3$, 298 K) δ: 9.51 (s, 1H, CH try), 4.68 (t, 1H, *J* =8.8 Hz), 4.64–4.51 (m, 1H), 4.24 (t, 1H, *J* =7.8 Hz), 3.08 (br m, 1H), 1.94 (br m, 1H), 1.74 (s, 9H), 1.12 (d, *J* =6.6 Hz, 3H).

^{13}C NMR ($CDCl_3$, 298 K) δ: 160.1, 134.1, 127.0, 73.4, 65.3, 60.8, 45.0, 30.1, 25.9, 23.9, 22.1.

M.p.: 221 °C (dec.).

Elemental analysis: $C_{26}H_{44}Cl_2N_8O_2Pd$ (678.01), calcd. C, 46.06; H, 6.54; N, 16.53; found: C, 45.92; H, 6.87; N, 16.819.

ESI-MS (m/z): calcd. for $C_{26}H_{44}ClN_8O_2Pd^+$: 641.231 ([M−Cl−]+); found: 641.228.

IR (KBr, cm^{-1}): 3144 (m), 2959 (br s), 1676 (s), 1651 (s), 1556 (ms), 1467 (m), 1416 (s), 1372 (s), 1302 (m), 1238 (s), 1194 (ms), 1175 (ms), 959 (m), 839 (w), 737 (mw), 699 (mw), 601 (w), 528 (w).

*4.3.5.3 [PdCl2(4c)$_2$] (**Pd3c**)*

Following the above procedure complex **Pd3c** was obtained as a dark yellow microcrystalline powder in 72% yield.

^{1}H NMR ($CDCl_3$, 298 K) δ: 9.81 (s, 1H, CH try), 4.65–4-55 (m, 2H), 4.35 (dd, *J* =10.3, 5.9 Hz, 1H), 4.24 (t, 1H, *J* =7.8 Hz), 1.52 (s, 9H), 1.30 (s, 9H).

^{13}C NMR ($CDCl_3$, 298 K) δ: 161.9, 134.3, 128.4, 75.5, 70.3, 60.7, 34.6, 29.8, 26.4.

M.p.: 240 °C (dec.).

Elemental analysis: $C_{26}H_{44}Cl_2N_8O_2$ Pd (678.01),calcd. C, 46.06; H, 6.54; N, 16.53; found: C, 45.8; H, 6.85; N, 16.79.

ESI-MS (m/z): calcd. for $C_{26}H_{44}ClN_8O_2Pd$+: 641.231 ([M−Cl−]+); found 641.241.

IR (KBr, cm^{-1}): 3137 (w), 2966 (m), 1639 (ms), 1544 (m), 1480 (w), 1372 (ms), 1277 (ms), 1265 (s), 1169 (w), 1042 (m), 959 (w).

4.3.6 X-ray structure determination and refinement

Crystals suitable for the X-ray experiment of **Pd3c** and **Pd2d** were obtained by slow diffusion of diethyl ether into a dichloromethane solution (**Pd3c**, orange prisms) or by slow evaporation of dichloromethane solutions (**Pd2d**, orange needles). In the case of **Pd3c**, a fragment of irregular shape was cut from a small prism. The selected specimens were fastened on the goniometer head of an Oxford Diffraction Gemini diffractometer. The instrument was equipped with a 2 K × 2 K EOS CCD area detector and sealed-tube Enhance (Mo) and (Cu) X-ray sources. Data collection were performed with the ω-scans technique at 300(1) K for **Pd3c**, and 297.4(6) K for **Pd2d**, using graphite-monochromated MoKα (A, λ=0.71073) and CuKα (B, λ=1.54184) radiation in a 1024×1024 pixel mode and 4×4 (**Pd3c**) or 2×2 (**Pd2d**) pixel binning. Intensities were corrected with respect to absorption, Lorentz and polarization effects. An empirical multi-scan absorption correction based on equivalent reflections was performed with the scaling algorithm *SCALE3 ABSPACK*. Unit cell parameters were determined by least-squares refinement of 11,690 (**Pd3c**) and 858 (**Pd2d**) reflections chosen from the whole experiment. Data collection, reduction and refinalization were performed with the CrysAlis Pro software suite [CrysAlisPro, Version 1.171.38.46 (Rigaku OD, 2015).]. The structures were solved using SHELXT [33] and refined by full- matrix least-squares methods based on Fo2 with SHELXL [34] in the framework of the OLEX2 software.[35] The structure of **Pd3c** has been solved in the non-centrosymmetric P41212 space group, by means of the heavy atom methods.

The structure of **Pd2d** was instead solved by means of intrinsic phasing in the P-1 space group. In **Pd3c**, the asymmetric unit is given by half of the molecule. The refined value of the Flack parameter [19,36,37] was 0.001(14), suggesting a correct absolute structure. Both structures are affected by a little disorder. In **Pd3c**, atoms affected are C6 and C7; in **Pd2d**, atoms involved are C4 and C5. The alternate positions of these atoms and of bounded H atoms were refined with site occupation factors constrained to sum to unity. Refined sofs for alternate positions were 0.413/0.587 in **Pd3c** and 0.253/0.747 in **Pd2d**. All non-hydrogen atoms were refined anisotropically; H atoms were refined as "riding model". Other SHELX [33] restraints (RIGU) were also applied to improve the models.

The refinement of the structure of **Pd2d** was hampered by some limitations (see section 9.2) and the final R value did not drop below ca. 12% (3.71% for **Pd3c**). However, the chemical identity of the crystallized product does not look in question. Since the main purpose of the structural determination was to identify the molecular structure of the complex, we considered the proposed solution acceptable and we terminated the refinement of **Pd2d**, at this stage. The crystallographic data for **Pd2d** and **Pd3c** have been deposited at the Cambridge Crystallographic Data Center as cif files, with CCDC numbers 1,943,819 and 1943820, respectively. The data can be obtained free of charge via www.ccdc.cam.ac.uk/data_request/cif.

4.3.7 Computational details

The geometry optimizations and energy calculations were carried out using the range-separated DFT functional ωB97X [38–40] in combination with the split-valence polarized basis set of Ahlrichs and Weigend, with Dolg's and co-workers ECP for the palladium centre.[41,42] The implicit solvation model C-PCM was added considering acetonitrile as continuous medium.[43,44] The "restricted" formalism was always applied. The stationary points were characterized by vibrational analysis, from which zero-point vibrational energies and thermal corrections (T=298.15 K) were obtained.[45] Calculations were performed with Gaussian 09,[46] running on an Intel Xeon-based x86-64 workstation. The software Multiwfn (version 3.5) was used for population analyses.[47] Cartesian coordinates of the DFT-optimized structures are collected in supporting (see section 9.2).

4.3.8 Catalytic hydrogenations

A 100 ml hastelloy autoclave with magnetic stirrer was charged with the desired amount of catalyst, furfural (5.3 mmol) and 5 ml of methanol under an argon atmosphere. The autoclave vessel was flushed with 20 bar of N2 three times, with 10 bar of H_2 two times, then filled with H_2 to a desired pressure, heated to the desired temperature and stirred for the indicated time. During the reaction time the vessel was repressurized to keep the pressure over 20 bars. The pressure vessel was cooled down to room temperature and then carefully depressurized. Then 0.1 ml of the reaction mixture was filtered through celite and rinsed with acetone (1 ml), and analyzed by gas chromatography and/or the alcohol fraction isolated.

4.4 CONCLUSIONS

A convenient protocol for the synthesis of triazolyl-substituted chiral oxazolines has been developed and its efficiency has been demonstrated preparing ligands having bulky and strongly electron donor substituents.

These ligands display the ability of behave both as bidentate and as monodentate, and that in this latter case that the preferred coordination site is the oxazoline N atom. Thus it appears that the N atom of the oxazoline is a better σ-donor than the N atoms of the triazole. Subtle effects are at play when deciding the adopted coordination fashion as found in the case of Pd2a→Pd2d transformation.

Preliminary tests regarding the catalytic activity of the characterized complexes have been carried out. Reduction of FUR to FA showed some promising outputs which will be optimized in future. Further studies on the asymmetric hydrogenation of biomass derived carbonyl compounds will be evaluated as well.

4.5 REFERENCES

[1] H. Brunner, U. Obermann, *Chem. Ber.* 1989, *122*, 499–507.

[2] H. Brunner, U. Obermann, P. Wimmer, *J. Organomet. Chem.* 1986, *316*, DOI 10.1016/0022-328X(86)82093-9.

[3] G. Yang, W. Zhang, *Chem. Soc. Rev.* 2018, *47*, 1783–1810.

[4] H. Shimizu, J. C. Holder, B. M. Stoltz, *Beilstein J. Org. Chem.* 2013, *9*, 1637–1642.

[5] Z.-M. Chen, M. J. Hilton, M. S. Sigman, *J. Am. Chem. Soc.* 2016, *138*, 11461–11464.

[6] L. Liang, D. Astruc, *Coord. Chem. Rev.* 2011, *255*, 2933–2945.

[7] Q. V. C. Van Hilst, N. R. Lagesse, D. Preston, J. D. Crowley, *Dalt. Trans.* 2018, *47*, 997–1002.

[8] L. Suntrup, S. Klenk, J. Klein, S. Sobottka, B. Sarkar, *Inorg. Chem.* 2017, *56*, 5771–5783.

[9] A. Scrivanti, M. Bortoluzzi, R. Sole, V. Beghetto, *Chem. Pap.* 2018, *72*, DOI 10.1007/s11696-017-0174-z.

[10] R. Hayashi, X. Jin, G. R. Cook, *Bioorganic Med. Chem. Lett.* 2007, *17*, 6864–6870.

[11] S. Schröder, W. Frey, G. Maas, *Zeitschrift fur Naturforsch. - Sect. B J. Chem. Sci.* 2016, *71*, 683–

696.

[12] M. Kunishima, C. Kawachi, F. Iwasaki, K. Terao, S. Tani, *Tetrahedron Lett.* 1999, *40*, 5327–5330.

[13] T. I. Al-Warhi, H. M. A. Al-Hazimi, A. El-Faham, *J. Saudi Chem. Soc.* 2012, *16*, 97–116.

[14] D. P. Hruszkewycz, L. M. Guard, D. Balcells, N. Feldman, N. Hazari, M. Tilset, *Organometallics* 2015, *34*, 10.

[15] W. J. Geary, *Coord. Chem. Rev.* 1971, *7*, 81–122.

[16] C. K. Johnson, *ORTEP Report ORNL-3793*, 1965.

[17] F. H. Allen, *Acta Crystallogr. Sect. B Struct. Sci.* 2002, *58*, 380–388.

[18] Z. Mazloomi, R. Renépretorius, O. Pà, M. Albrecht, M. Diéguez, I. Virgili, M. Domingo, T. Spain, *Inorg. Chem.* 2017, *56*, 11282–11298.

[19] S. Parsons, H. D. Flack, T. Wagner, *Acta Crystallogr. Sect. B Struct. Sci. Cryst. Eng. Mater.* 2013, *69*, 249–259.

[20] S. J. Grabowski, W. A. Sokalski, E. Dyguda, J. Leszczyn´ski, L. Leszczyn´ski, *J. Phys. Chem. B* 2006, *110*, 6444–6446.

[21] Y. Wang, D. Zhao, D. Rodríguez-Padrón, C. Len, *Catalysts* 2019, *9*, 796.

[22] T. Scattolin, L. Canovese, F. Visentin, S. Paganelli, P. Canton, N. Demitri, *Appl. Organomet. Chem.* 2018, *32*, 1–10.

[23] F. Visentin, A. Togni, *Organometallics* 2007, *26*, 3746–3754.

[24] S. J. Cazin, S. P. Nolan, S. P. Steven Nolan, C. S. J Cazin, *Chem. Commun* 2017, 7990.

[25] R. A. Fernandes, J. L. Nallasivam, *Org. Biomol. Chem.* 2019, *17*, 8647.

[26] S. N. Sluijter, S. Warsink, M. Lutz, C. J. Elsevier, *Dalt. Trans.* 2013, *42*, 7365.

[27] W. L. F. Armarego, Ed. , *Purification of Laboratory Chemicals*, Elsevier Science Publishers B.V., Amsterdam, The Netehrlands, 2017.

[28] P. L. Golas, N. V. Tsarevsky, K. Matyjaszewski, *Macromol. Rapid Commun.* 2008, *29*, 1167–1171.

[29] J. C. Bottaro, P. E. Penwell, R. J. Schmitt, *Synth. Commun.* 1997, *27*, 1465–1467.

[30] A. Maisonial, P. Serafin, M. Traïkia, E. Debiton, V. Théry, D. J. Aitken, P. Lemoine, B. Viossat, A. Gautier, *Eur. J. Inorg. Chem.* 2008, 298–305.

[31] J. V. B. Kanth, M. Periasamy, *J. Org. Chem* 1991, *56*, 5964–5965.

[32] F. R. Hartley, S. R. Jones, *J. Organomet. Chem.* 1974, *66*, 465–473.

[33] G. M. Sheldrick, *Acta Crystallogr. Sect. A Found. Crystallogr.* 2015, *71*, 3–8.

[34] G. M. Sheldrick, *Acta Crystallogr. Sect. C Struct. Chem.* 2015, *71*, 3–8.

[35] O. V. Dolomanov, L. J. Bourhis, R. J. Gildea, J. A. K. Howard, H. Puschmann, *J. Appl. Crystallogr.* 2009, *42*, 339–341.

[36] G. Bernardinelli, H. D. Flack, *Acta Crystallogr. Sect. A* 1985, *41*, 500–511.

[37] H. D. Flack, *Acta Crystallogr. Sect. A* 1983, *39*, 876–881.

[38] Y. Minenkov, Å. Singstad, G. Occhipinti, V. R. Jensen, *Dalt. Trans.* 2012, *41*, 5526–5541.

[39] J. Da Chai, M. Head-Gordon, *Phys. Chem. Chem. Phys.* 2008, *10*, 6615–6620.

[40] I. C. Gerber, J. G. Ángyán, *Chem. Phys. Lett.* 2005, *415*, 100–105.

[41] F. Weigend, R. Ahlrichs, *Phys. Chem. Chem. Phys.* 2005, *7*, 3297–3305.

[42] D. Andrae, U. Häußermann, M. Dolg, H. Stoll, H. Preuß, *Theor. Chim. Acta* 1990, *77*, 123–141.

[43] V. Barone, M. Cossi, *J. Phys. Chem. A* 1998, *102*, 1995–2001.

[44] M. Cossi, N. Rega, G. Scalmani, V. Barone, *J. Comput. Chem.* 2003, *24*, 669–681.

[45] C. J. Cramer, 2003, DOI 10.1086/519640.

[46] M. Frisch, G. Trucks, H. Schlegel, *Gaussian 09, Revision C.01, Gaussian Inc.*, Wallingford CT, USA, 2010.

[47] T. Lu, F. Chen, *J. Comput. Chem.* 2012, *33*, 580–592.

5. SYNTHESIS, CHARACTERIZATION AND CATALYTIC ACTIVITY OF NOVEL RUTHENIUM COMPLEXES BEARING NNN CLICK BASED LIGANDS

5.1 INTRODUCTION

The scope of this chapter is the synthesis of a new class of ruthenium complexes bearing click based ligands to be used for the hydrogenation of a spectrum of aldehydes and ketones.

In agreement with the aim of this thesis, furfural and 5-hydorxymethylfurfural have been selected as model substrates for the potential application of the synthetized complexes to biomass derived *platform chemicals.*

In 2001 K. B. Sharpless and co-workers coined the term Click Chemistry[1–6] describing a novel concept of organic synthesis based on the use of a few simple high-yielding reactions. [7]

Inspired by this vision, many researchers started to develop new organic approaches which elegantly circumnavigate the drawbacks of older organic procedures based on the use of harsh reaction conditions, toxic reagents, long purification processes and expensive waste treatments. The prime example of click chemistry, the copper catalysed alkyne–azide cycloaddition (CuAAC), has turned over the last decade into a routine organic process for the synthesis of 1,4-disubstituted 1,2,3-triazoles. Due to their facile accessibility, click-based triazole compounds have been extensively investigated for a wide range of applications.[3,8–13] In particular, the presence of an N-donor atom in the five-membered ring structure has recently led to an increasing number of publications aiming to study the coordination chemistry of novel transition metal complexes bearing triazole ligands.[14–17] As a matter of fact, several triazole based complexes act as effective chemotherapeutics against various cancer cell lines[18,19] or as antimicrobials.[20,21] They also show interesting electrochemical and photophysical properties.[22–24]

In the field of homogeneous catalysis, in which the variation of substituents on ligands can drastically affect the activity and the selectivity of the complexes, triazole based ligands can be attractive candidates as a new class of easily tunable, cheap and accessible ligands. Late transition metal complexes bearing 1,4-disubtituted 1,2,3-triazoles are active catalysts for the Suzuki–Miyaura cross coupling,[25,26] Heck olefin arylation[27,28] and transfer hydrogenation reactions.[29–31] Notably, Leitner and co-workers recently reported the transfer hydrogenation of ketones using a non-noble Mn(I) aminotriazole bidentate complex.[32] On the other hand, to

the best of our knowledge, the ruthenium catalysed hydrogenation of carbonyl compounds under molecular hydrogen pressure, bearing triazole based ligands was reported in only one paper.[33] The catalyst was not selective towards C=O bond reduction in the presence of an alkene group, hence the fully saturated com- pound was obtained.

The ruthenium-catalysed hydrogenation of C=O functional groups usually requires electron-donating phosphorous ligands which help to stabilise the metal centre.[34–37] Extremely good results have been obtained with a number of catalysts which use the combination of diamine ligands and cheap and readily accessible phosphorus ligands for the reduction of carbonyl compounds.[38–43] However, the use of more complex phosphine ligands can lead to higher catalyst costs. The pioneering work of Gusev and co-workers[44] has demonstrated that several phosphorus-free tridentate ligands can stabilise noble or non-noble transition metal complexes for the reduction of a number of different functional groups although even these catalysts still require the stabilisation of an additional phosphine or CO ligand.[45–47]

We believe that click based tridentate triazole ligands can represent a sustainable alternative for the ruthenium-catalysed hydrogenation of carbonyl compounds. Inspired by these considerations, we herein report the synthesis of three novel ruthenium(II) complexes $Ru(NNN)(PPh_3)Cl_2$ which are highly active in the catalytic hydrogenation of ketones and aldehydes.

5.2 RESULTS AND DISCUSSION

5.2.1 Synthesis and characterization

Ligands **L1**–**L3** were prepared as shown in **Scheme 5.1**. Literature procedures were used to prepare **L1**[48] and **L2**.[11] **L3**, was synthesized starting by reaction of 2-azidoethylamine and phenylacetylene via CuAAC to yield 4-phenyl-1*H*-1,2,3-triazol-1-amine. The condensation with 2-pyridinecarboxyaldehyde and the subsequent reduction with $NaBH_4$ led to the formation of **L3** in high yield.

The preparation of the corresponding ruthenium complexes was accomplished in a straightforward manner by reacting the corresponding NNN ligand and $Ru(PPh_3)_3Cl_2$ as the precursor (**Scheme 2**). After heating the solutions under reflux in toluene for 2 h followed by cooling them to room temperature, the complexes precipitate as orange (**1**), yellow (**2**) or red

(3) solids. Washing these precipitates with diethyl ether afforded the desired products in high purities.

Analytical and spectroscopic data (HRMS, IR, ^{1}H, ^{31}P NMR) support the structures depicted.

The complexes were stored under aerobic conditions. The spectroscopic data acquired after several weeks confirmed that no significant changes had occurred, leading to the conclusion that they are fairly stable under air.

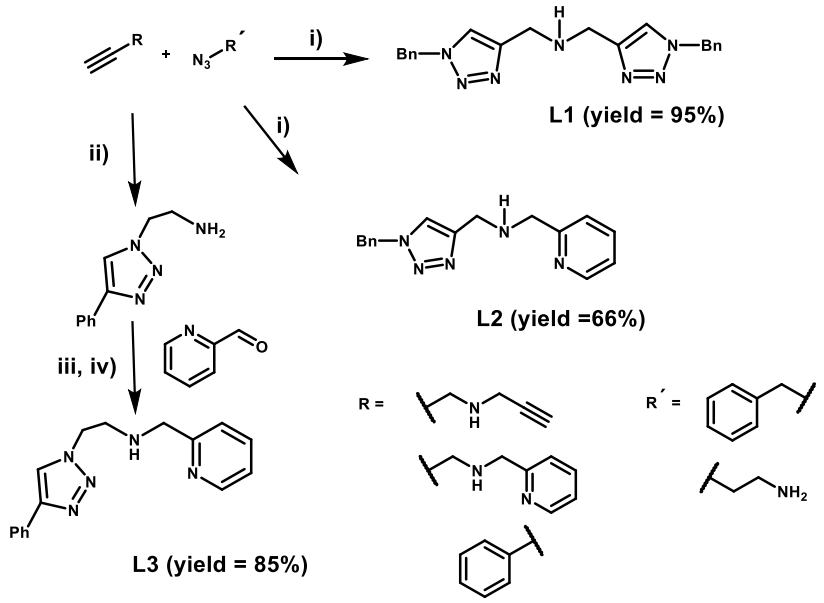

Scheme 5.1. Synthesis of triazole based ligands **L1**–**L3** (i) MeOH, H_2O, $CuSO_4 \cdot 5H_2O$ (5 mol%), sodium ascorbate (10 mol%), r.t., 18 h (ii) MeOH, H2O, $CuSO_4 \cdot 5H_2O$ (5 mol%) r.t., 18 h (iii) DCM, Na_2SO_4, r.t. 18 h (iv) MeOH, $NaBH_4$, 0°C–r.t., 18 h.

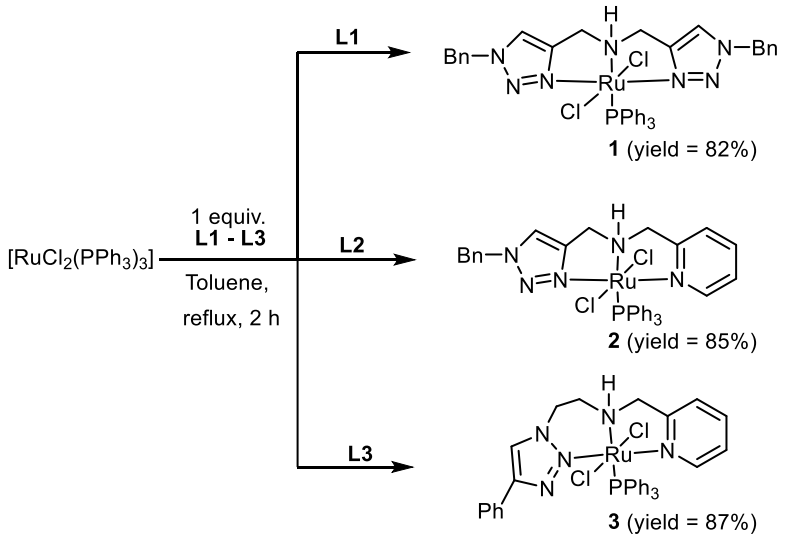

Scheme 5.2. Synthesis of $[RuCl_2(NNN)(PPh_3)]$ complexes **1**–**3**.

Layering diethyl ether over a concentrated solution of **3** in DCM afforded red crystals suitable for X-ray diffraction analysis. The solid-state structure of **3** revealed that it is the *trans*-(*mer*-NNN_{L3}) dichloride complex (**Figure 1**).

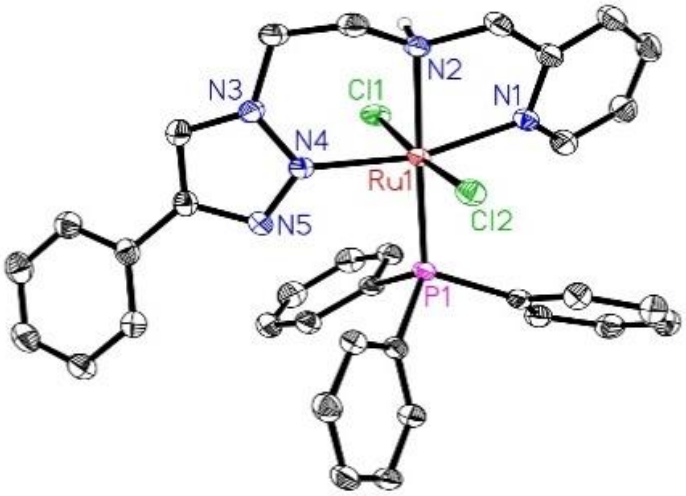

Figure 5.1. Molecular structure of **3** with displacement ellipsoids drawn at the 50% probability level. Hydrogen atoms except the N-bound are omitted for clarity.

5.2.2 Catalytic hydrogenation

With the complexes in hands, their catalytic activity towards the hydrogenation of ketones and aldehydes was evaluated, taking acetophenone as the model substrate. Hydrogenation reactions were initially performed by using 1 mmol of the substrate and 2 mL of the selected solvent, in the presence of 0.25 mol% of the metal complex and 2.5 mol% of KO^tBu as base, which is required to activate the pre-catalyst.

Metal-ligand-cooperation (MLC) is known to promote the formation of the active dihydride species in Noyori-type pincer complexes bearing NH moieties.[49,50] Complexes **2** and **3**, bearing pyridine functionalities, can also be activated by the aromatisation/ dearomatisation process of the pyridine ring, promoted by deprotonation of the benzylic protons.[51]

Hydrogenations were initially run for 18 hours, at 80 °C and 40 bar of hydrogen pressure resulting in good activities by all three catalysts, although 1 could not achieve full conversion (**Table 5.1**, entry 1).

Table 5.1. Optimization of the reaction conditions for the catalytic hydrogenation reactions

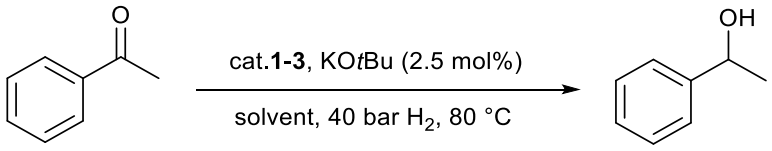

Entry[a]	Cat.	Solvent	Cat. loading (mol%)	Time (h)	Yield (%)[b]
1	1	Toluene	0.25	18	95
2	2	Toluene	0.25	1	> 99
3	3	Toluene	0.25	1	> 99
4	2	THF	0.25	1	84
5	2	*i*-PrOH	0.25	1	53
6	3	THF	0.25	1	89
7	3	*i*-PrOH	0.25	1	54
8[c]	2	Toluene	0.05	1	> 99
9[c]	3	Toluene	0.05	1	> 99
10[d]	2	Toluene	0.05	1	97
11[d]	3	Toluene	0.05	1	98
12[e]	3	Toluene	0.05	1	42
13[f]	3	Toluene	0.05	1	0
14[d]	/	Toluene	/	1	0

[a] Reaction conditions: Acetophenone (1 mmol), solvent (2 mL), 40 bar of H2, 80 °C, cat. **1–3** (0.25 mol%), KO^{t}Bu (2.5 mol%), when catalyst loading was decreased to 0.05 mol%, KO^{t}Bu was also decreased to 1.25 mol%. [b] GC yields using dodecane as internal standard. [c] H_2 =10 bar. [d] Temp. = 60 °C. e Temp. = 40 °C. [f] No base.

Encouraged by these results, we reduced the reaction time to 1 hour, maintaining the same loadings both for the catalysts and the base (**Table 5.1**, entries 2 and 3) and still achieving quantitative conversions of the substrate to the corresponding alcohol.

With the same reaction conditions, different solvents were screened for the most active catalysts **2** and **3** (**Table 5.1**, entries 4–7). Toluene appeared to be the best solvent. Looking for the activity limits of the catalysts, both catalyst and base loading were decreased to 0.05 mol% and 1.25 mol% respectively and the hydrogen pressure was reduced to 10 bar (**Table 5.1**, entries 8 and 9). Under these conditions the ketone was fully converted to the alcohol. At the same hydrogen pressure, almost full conversions were reached even at 60 °C (**Table 5.1**, entries 10 and 11). The activity has drastically decreased at 40 °C and 10 bar of hydrogen (**Table 5.1**, entry 12).

Finally, to confirm the crucial role of the base in the activation of the complexes, a base-free reaction was run but no conversion at all was observed (**Table 5.1**, entry 13). After optimisation of the reaction conditions, catalyst **3** emerged as the complex with slightly better performances. Similarly, Singh *et al*. observed that N2 coordinating triazoles were more efficient than ligands coordinating via their N3 site in the ruthenium catalysed transfer hydrogenation of ketones.[30]

The scope of catalyst **3** was evaluated and thus a range of ketones and aldehydes was hydrogenated to the corresponding alcohols (**Table 5.2**).

Table 5.2. Hydrogenation of aldehydes and ketones with catalyst **3**

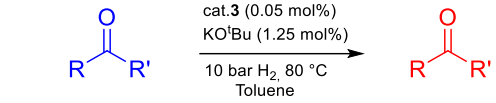

R = Alkyl, Aryl
R' = CH_3, H

Entry	1	2	3	4	5	6	7
Substrate	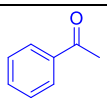	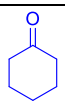	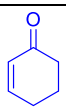	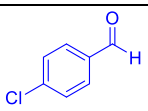	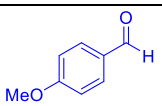	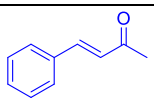	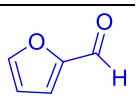
Product			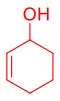	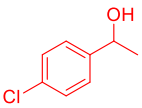	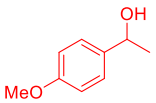	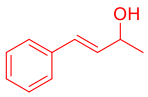	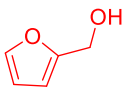
Yield	99%	99%	99%	98%	89%	Traces	97%
Entry	8	9	10	11	12	13	14
Substrate	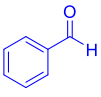	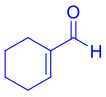	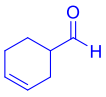	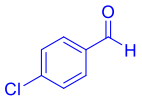	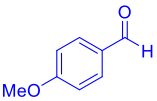	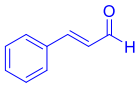	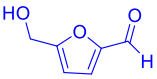
Product		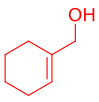	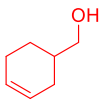	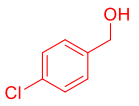	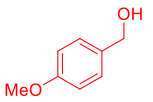	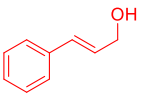	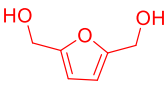
Yield	99%	95%	92%	97%	47%	Traces	52%

[a] Substrate (2 mmol), toluene (2 mL), cat. 3 (0.05 mol%), KO^{t}Bu (1.25 mol%), 80 °C, 10 bar of H_2. [b] Isolated yields. [c] In THF (2 mL).

The aliphatic ketone cyclohexanone (entry 2) was efficiently hydrogenated and the product alcohol isolated with 99% yield. The selective hydrogenation of the carbonyl groups in α,β-unsaturated aldehydes and ketones remains a daunting task.[52,53] Notably, α,β-unsaturated 2-

cyclohexen-1-one (entry 3) and 1-cyclohexene-1-carboxaldehyde (entry 9) were selectively hydrogenated to the allylic alcohols in excellent yield, leaving the C=C double bond untouched. Selective C=O bond reduction was also achieved in the hydrogenation of 3-cyclohexene-1-carboxaldehyde (entry 10). It is worth mentioning that high activity paired to excellent selectivity towards α,β-unsaturated alcohols attained by complex **3** are not achieved by most other ruthenium complexes used for the reduction of ketones and aldehydes. Aromatic substrates with electron-withdrawing groups were also fully hydrogenated to the benzylic alcohols (entries 4 and 11) under the reaction conditions, while the presence of an electron-donating moiety seemed to slow down the reduction of the ketone (entry 5) and even more of the aldehyde (entry 12). Biomass-derived furfural (entry 7) was selectively hydrogenated to furfuryl alcohol. 2,5- Bis(hydroxymethyl)furan,[54,55] an interesting bio-based building block for polyesters (entry 14) was obtained in only 52% isolated yield. Some brown material, presumably humins, also formed in this reaction. The formation of humins has often been observed in reactions of 5-HMF.[55] Moreover, due to the low solubility of 5-HMF in toluene, the reaction was run in THF, which was expected to decrease the catalyst activity based on the results in **Table 5.1**. Finally, α,β-unsaturated cinnamaldehyde (entry 13) and benzalacetone (entry 6) could not be converted to the corresponding alcohols under these conditions. The reasons for this are currently under investigation.

5.2.3 Mechanistic studies

Catalytic homogenous hydrogenation of polar bonds such as ketones and aldehydes are known to proceeds either via an inner-sphere or an outer-sphere mechanism (**Scheme 5.3**).[34][49][51] The inner-sphere mechanism involves the coordination of the substrate to a free site of the metal centre made vacant by displacement of a ligand (**B_{in}I**). Insertion of the C=O bond into the metal hydride leads to the ruthenium alkoxide complex (II) which forms the hydrogen complex (III) from which the alcohol is released to reform the dihydride **B**.

On the other hand, Noyori and co-workers proposed a different mechanism for the Ru-diphosphine-diamine type catalysts. Several mechanistic studies confirmed that the NH group in the ligands are directly involved in the catalytic cycle.[56,57] Coordination of the substrate in step **I′** leads to the formation of complex **B_{out}I**. Concerted migration of hydride and proton to the substrate releases the product (**II′**) forming the coordinative unsaturated amido complex **B_{out}II**. Coordination of dihydrogen (**III′**) and successive heterosplitting regenerate dihydride **B**.

In both cases, activation of the dichloro-complex by KO^{t}Bu under hydrogen atmosphere is expected to afford the corresponding dihydride **B** as active catalyst.[58] Experimental evidence (**Table 5.1**, entry 13) confirms that catalyst **3** is not active in the absence of the base. It has been demonstrated that these types of complexes may form monohydride **A** which still requires base to be active thus meaning these intermediates are just precursors for the dihydride complexes.[59]

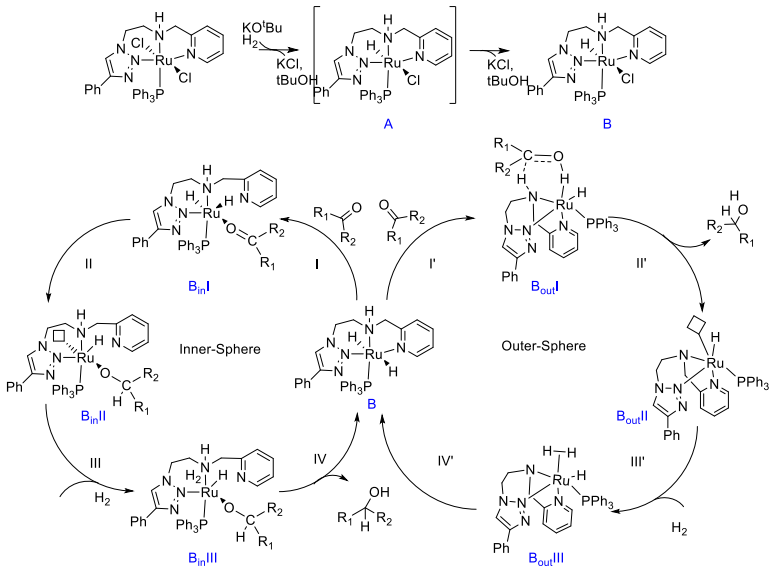

Scheme 5.3. Inner-sphere and outer-sphere proposed mechanisms.

Preliminary DFT calculations carried out using the EDF2 functional allowed to ascertain the most stable isomer of $RuH_2(PPh_3)L3$. The isomers were chosen in order to place the N–H and one M–H bond on the same side, as required in outer-sphere hydrogenation. Five starting geometries were considered, two of them with the N-donor moieties of L mutually in the *mer* position (**is1** and **is2**) and the other three where the tridentate ligand occupies a face of the octahedron (**is3**, **is4** and **is5**). As observable in **Figure 5.2**, the *fac* isomers are in general more stable than the *mer* ones, despite the fact that the ligand occupies three coordination sites in the *mer* position in the dichloro precursor. Among the *fac* isomers, **is4** and **is5** are the most stable, suggesting that triphenylphosphine prefers to be in a *trans* position to the NH moiety or the pyridine heterocycle rather than to the triazole ring, perhaps because this last donor group is less electron rich, as highlighted by population analyses. The interaction of the dihydride with acetophenone was studied starting from the most stable isomer, **is4**.

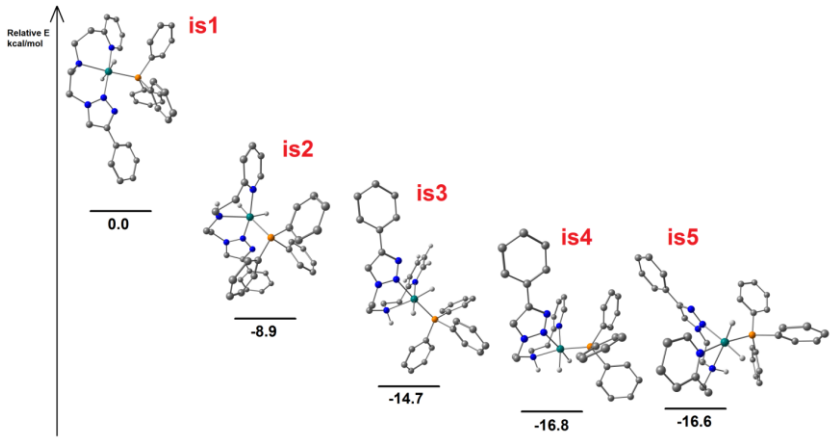

Figure 5.2. DFT EDF2-optimised geometries of the isomers of $RuH_2(PPh_3)L3$ and relative energies (electronic energy plus nuclear repulsion) in kcal mol^{-1}. Hydrogen atoms were omitted for clarity, with the exceptions of N–H and M–H. Colour map: hydrogen, white; carbon, grey; nitrogen, blue; phosphorus, orange; ruthenium, green. Cartesian coordinates of the DFT-optimised structures can be found in the supporting (see section 9.3)

Calculations were carried out at C-PCM/ωB97X/def2-SVP level, considering toluene as continuous medium. The ground-state stationary point is4acetophenoneout, depicted in **Figure 5.3**, shows very weak interactions between the complex and the substrate. In particular, the NH···O distance is 2.199 Å. The coordination of acetophenone to the metal centre was therefore considered by assuming the displacement of the longest Ru–N bond, that with pyridine. In the stationary point thus obtained, indicated as $\mathbf{is4}^{\mathbf{acetophenone}}$ in, the computed Ru···O distance is quite long, 2.274 Å, suggesting weak coordination of acetophenone to the complex. Moreover, $\mathbf{is4}^{\mathbf{acetophenone}}$ in is less stable than $\mathbf{is4}^{\mathbf{acetophenone}}$ out by about 6.3 kcal mol^{-1} (Gibbs free energy), making an inner-sphere hydrogenation mechanism less likely.

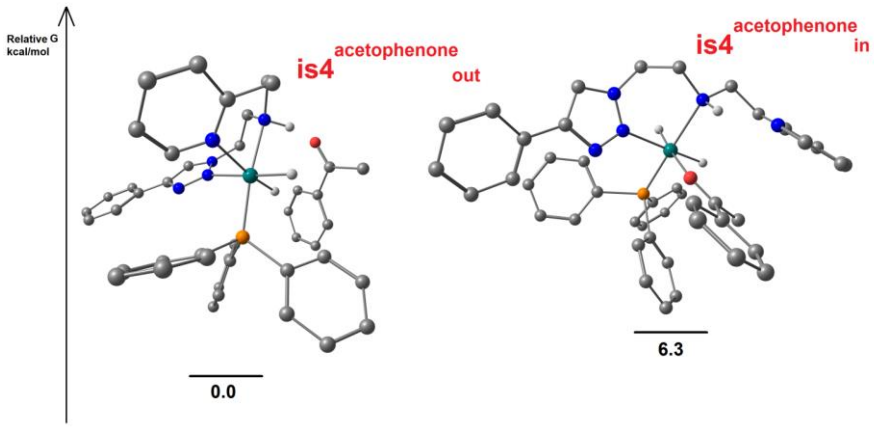

Figure 5.3. DFT C-PCM/ωB97X-optimised geometries of ground-state adducts between $RuH_2(PPh_3)L3$ (**is4**) and acetophenone and relative Gibbs free energies in kcal mol^{-1}. Hydrogen atoms were omitted for clarity, with the exceptions of N–H and M–H. Colour map: hydrogen, white; carbon, grey; nitrogen, blue; oxygen, red; phosphorus, orange; ruthenium, green. Cartesian coordinates of the DFT-optimised structures can be found in the supporting (see section 9.3).

5.3 EXPERIMENTAL

5.3.1 General

Reagents and solvents were purchased from commercial sources and used as received unless noted otherwise. Dry solvents were obtained from a solvent purification system (toluene, CH_2Cl_2, Et_2O, THF). GC analyses were carried out on an Agilent 7890B GC system with a HP-5 normal-phase silica column, using He as a carrier gas and dodecane as standard. NMR spectra were acquired on a Bruker AV400, Bruker AV300 or Bruker Fourier300 NMR spectrometer.

^1H and ^{13}C-NMR spectra were referenced w.r.t. the residual solvent signal. All chemical shifts are in ppm, coupling constants in Hz. HR-MS measurements were recorded on an Agilent 6210 time-of-flight LC/MS (ESI) or Thermo Electron MAT 95-XP (EI, 70 eV). Peaks as listed correspond to the highest abundant peak and are of the expected isotope pattern. X-ray diffraction data were collected on a Bruker Kappa APEX II Duo diffractometer. The structure was solved by direct methods[60] and refined by full- matrix least-squares procedures on F^2.[61] XP (Bruker AXS) was used for graphical representations. CCDC 1912232 contains the supplementary crystallographic data for this paper. The computational geometry optimisations of the complexes were carried out without symmetry constrains, using the hybrid-GGA EDF2 functional[62] in combination with the 6-31G(d,p) basis set and the ECP-based LANL2DZ basis set for ruthenium.[63–65] Further geometry optimisations were performed using the range-separated hybrid functional ωB97X[66–68] and the def2 split-valence polarized basis set of Ahlrichs and Weigend, with 28 core electrons of ruthenium enclosed in pseudopotential.[69,70]

The C-PCM implicit solvation model was added to ωB97X calculations, considering toluene as continuous medium.[71,72] The "restricted" formalism was always applied. The achievement of stationary points was confirmed by IR simulations (harmonic approximation).[73]

Calculations were performed with Spartan'16 (Wavefunction Inc.), build 2.0.3.36 Gaussian'0937 was used for the C-PCM/ωB97X calculations. Cartesian coordinates of the DFT-optimised structures can be found in the supporting (see section 9.3).

5.3.2 Synthesis of the ligands

*5.3.2.1 Synthesis of bis((1-benzyl-1H-1,2,3-triazol-4-yl)methyl)amine(**L1**).*

The ligand was prepared according to a literature report.[48]

Dipropargylamine (0.306 g, 3.28 mmol) and benzylazide (0.875 g, 6.57 mmol) were dissolved in MeOH (25 mL) and H_2O (4 mL) was added. A solution of $CuSO_4 \cdot 5H_2O$ (0.04 g, 0.16 mmol) and sodium ascorbate (0.06 g, 0.32 mmol) in H_2O (1 mL) was added dropwise to the stirred reagent mixture inducing a colour change to yellow-green. The reaction was then stirred for 18 h at room temperature. After this time, MeOH was removed under reduced pressure giving an orange oil that was diluted with CH_2Cl_2 (20 mL) and extracted with a saturated EDTA solution to remove copper salts traces. The organic layer was dried over anhydrous $MgSO_4$, filtered and concentrated under vacuum to afford an orange solid (1.123 g, 95%).

HRMS (ESI) calcd for $C_{20}H_{22}N_7$ [M + H]+: 360.1936; found: 360.1942.

^{1}H NMR (400 MHz, DMSO-d_6) δ (ppm) = 8.01 (s, 2H), 7.40–7.28 (m, 10H), 5.57 (s, 4H), 3.87 (bs, 4H).

^{13}C NMR (400 MHz, DMSO-d_6) δ (ppm) = 136.2, 132.0, 128.7.1, 127.9, 122.9, 52.8.

*Synthesis of 1-(1-benzyl-1H-1,2,3-triazol-4-yl)-N-(pyridin-2- ylmethyl)methanamine (**L2**).*

Ligand L2 was prepared as reported in the literature.[27,48]

Propargylamine (0.55 g, 10 mmol) and 2-pyridinecarboxyaldehyde (1.07 g, 10 mmol) were dissolved in 20 mL of DCM in the presence of 2 equivalents of Na_2SO_4 (3 g, 20 mmol). The reaction mixture was stirred at room temperature overnight. After 18 hours, the reaction was stopped, the solution was filtered and concentrated under reduced pressure. The resulting red oil was then dissolved in MeOH (15 mL), the solution was cooled to 0 °C and 2 equivalents of $NaBH_4$ were added in portions. The solution was then allowed to stir overnight (18 hours) at room temperature. Afterwards, the reaction was quenched with a saturated solution of $NaHCO_3$ (15 mL) and the product extracted with DCM. The combined layers were dried over $MgSO_4$, volatiles were evaporated and the mixture was purified by flash column

chromatography using a mixture of DCM (95%) and MeOH (5%) as an eluent (0.986 g, 6.8 mmol, 68% yield). The dark orange oil obtained was treated with benzylazide (0.758 g, 5.7 mmol), $CuSO_4 \cdot 5H_2O$ (0.07 g, 0.28 mmol) and sodium ascorbate (0.13 g, 0.57 mmol) in MeOH (25 mL) and H_2O (5 mL). The reaction was then stirred for 18 hours at room temperature. Afterwards, the MeOH was removed under reduced pressure giving an orange oil that was diluted with CH_2Cl_2 (20 mL) and extracted with a saturated EDTA solution to remove copper salts traces. The organic layer was dried over anhydrous $MgSO_4$, filtered and concentrated under vacuum to afford a brown oil (66% yield).

HRMS (ESI) calcd for $C_{16}H_{18}N_5$ [M + H]+: 280.1562; found: 280.1564.

^{1}H NMR (300 MHz, $CDCl_3$) δ (ppm) = 8.54 (ddd, *J* = 4.9 Hz, 1.7 Hz, 0.9 Hz, 1H), 7.62 (td, *J* = 7.7, 1.8 Hz 1H), 7.42 (s, 1H), 7.38–7.31 (m, 3H), 7.28 (dm, *J* = 7.8 Hz, 1H), 7.27–7.24 (m, 2H), 7.15 (ddd, *J* = 7.6, 4.9, 1.2 Hz, 1H), 5.49 (s, 2H), 3.94 (s, 4H), 2.51 (bs, 1H).

^{13}C NMR (300 MHz, $CDCl_3$) δ (ppm) = 159.3, 149.4, 147.2, 136.5, 134.7, 129.2, 128.8, 128.2, 122.5, 122.1, 121.8, 54.6, 54.2, 44.5.

*Synthesis of 2-(4-phenyl-1H-1,2,3-triazol-1-yl)-N-(pyridin-2- ylmethyl)ethan-1-amine (**L3**).*

2-Azidoethylamine (0.50 g, 5.80 mmol) and phenylacetylene (0.59 g, 5.80 mmol) were dissolved in MeOH (9 mL) and H_2O (1 mL). $CuSO_4 \cdot 5H_2O$ (0.06 g, 0.25 mmol) was added in portions and the solution was allowed to stir for 1 hour. Afterwards, the reaction mixture was diluted with water (10 mL) and NH_4OH (1 mL) and the product was extracted with CH_2Cl_2 (3 × 10 mL).

The combined organic layers were dried over $MgSO_4$, filtered and concentrated in vacuo to give 4-phenyl-1*H*-1,2,3-triazol-1-amine as a white powder (0.907 mg, 5.21 mmol, 90%). The aminotriazole was then reacted with 2-pyridinecarboxyaldehyde (0.55 g, 5.21 mmol) in the presence of 2 equivalents of Na_2SO_4 (1.42 g, 10 mmol) in DCM (10 mL). After 18 hours, Na_2SO_4 was filtered off and the solution was concentrated under reduced pressure. The resulting oil was dissolved in MeOH (15 mL), the solution was cooled to 0 °C and $NaBH_4$ (0.3 g, 10 mmol) was added in portions. The solution was allowed to stir overnight (18 hours) at room temperature. Afterwards, the reaction was quenched with a saturated solution of $NaHCO_3$ (15 mL) and the product was extracted with DCM. The combined layers were dried over $MgSO_4$, volatiles were evaporated under reduced pressure yielding **L3** as a fine white powder (1.39 g, 4.98 mmol, 85%).

HRMS (ESI) calcd for $C_{16}H_{18}N_5$ [M + H]+: 280.1562; found: 280.1569.

^{1}H NMR (400 MHz, $CDCl_3$) δ (ppm) = 8.52 (ddd, *J* = 4.9 Hz, 1.8 Hz, 0.9 Hz, 1H), 7.36–7.30 (m, 6H), 7.90 (s, 1H), 7.85–7.77 (m, 2H), 7.62 (td, *J* = 7.7, 1.8 Hz 1H), 7.44–7.38 (m, 2H), 7.37–7.30 (m, 1H), 7.24 (ddt, *J* = 7.3, 1.4, 0.8 Hz, 1H), 7.16 (m, 1H), 4.52 (t, *J* = 6 Hz, 2H), 3.92 (s, 2H), 3.18 (t, *J* = 6 Hz, 2H).

^{13}C NMR (400 MHz, $CDCl_3$) δ (ppm) = 159.1, 149.4, 147.8, 136.8, 130.7, 129.1, 128.9, 128.2, 125.8, 122.4, 122.3, 120.5, 54.7, 50.8, 50.7, 48.8.

5.3.3 Synthesis of the complexes

Under inert conditions $Ru(PPh_3)_3Cl_2$ (0.48 g, 0.5 mmol) was suspended in dry toluene (10 mL). After 30 min, the desired ligand (0.5 mmol) was added and the solution was heated under reflux for 2 h. During the reaction the colour of the solution turns from black to orange (**1**), yellow (**2**) or red (**3**). After cooling down the solution to room temperature the complex precipitated. The solid was collected by filtration, washed with Et_2O (2 × 15 mL) and dried under reduced pressure.

*5.3.3.1. Ru(NNNL1)(PPh$_3$)Cl$_2$ (**1**).*

The orange solid was obtained inn82% yield (325 mg).

El. anal. calcd for $C_{38}H_{36}Cl_2N_7PRu$: C, 57.48; H, 4.57; N, 12.36 P, 3.90; Cl, 8.94. Found: C, 57.51; H, 4.55; N, 12.34; P, 3.92; Cl, 8.96.

^{1}H-NMR (400 MHz, DMSO-*d$_6$*, 293 K): δ (ppm) = 8.08 (s, 2H), 7.79–7.63 (m, 6H), 7.40–7.33 (m, 6H), 7.28–7.21 (m, 4H), 7.15 (ddd, *J* = 7.3 Hz, 5.9 Hz, 1.9 Hz, 9H), 5.42–5.21 (q, *J* = 15 Hz, 4H), 4.70–4.59 (m, 2H), 4.56–4.45 (m. 2H).

^{31}P{^{1}H}-NMR (400 MHz, DMSO-*d$_6$*, 293 K), δ (ppm) = 58.5.

HRMS (ESI) calcd for $C_{38}H_{36}N_7PCl_2Ru$ [M]+: 793.1190 found: 793.1189; $C_{38}H_{36}N_7PCl_2RuNa$ [M + Na]+: 816.1088 found: 816.1054.

*Ru(NNNL2)(PPh$_3$)Cl$_2$ (**2**).*

The yellow solid was obtained in 85% yield (305 mg).

El. anal. calcd for $C_{34}H_{32}Cl_2N_5PRu$: C, 57.23; H, 4.52; N, 9.81 P, 4.34; Cl, 9.94. Found: C, 57.18; H, 4.56; N, 9.88; P, 4.36; Cl, 9.96.

^{1}H-NMR (400 MHz, CD_2Cl_2, 293 K): δ (ppm) = 8.18–8.08 (m,1H),7.88–7.69 (m, 6H), 7.52–7.19 (m, 16H), 7.19–7.05 (m,2H),6.78–6.61 (m,2H),6.30(m, 1H), 5.74–5.59 (m, 1H), 4.97 (ddd, *J* = 13.7, 10.9, 1.2 Hz, 1H), 4.62 (dt, *J* = 14.1, 4.6 Hz, 1H), 4.47 (dt, *J* = 13.7, 4.8 Hz, 1H).

^{31}P{^{1}H}-NMR (400 MHz, CD_2Cl_2,293 K), δ (ppm)= 56.5.

HRMS (ESI)calcd for $C_{34}H_{31}Cl_2N_5PRu$ [M]+: 713.0815 found: 713.0807; $C_{34}H_{31}Cl_2N_5PRuNa$ [M + Na]+: 736.0713 found: 736.0688.

*Ru(NNNL3)(PPh_3)Cl_2 (**3**).*

The red solid was obtained in 87% yield (314 mg).

El. anal. calcd for $C_{34}H_{32}Cl_2N_5PRu$: C, 57.23; H, 4.52; N, 9.81 P, 4.34; Cl, 9.94. Found: C, 57.21; H, 4.55; N, 9.83; P, 4.36; Cl, 9.98.

^{1}H-NMR (400 MHz, DMSO-d_6, 293 K): δ (ppm) 8.67 (s, 1H), 8.20 (d, *J* = 5.7 Hz, 1H), 7.78 (ddt, *J* = 8.0, 6.6, 1.8 Hz, 6H), 7.65–7.47 (m, 3H), 7.32–7.11 (m, 16H), 6.85–6.73 (m, 1H), 6.14 (d, *J* = 11.8 Hz, 1H), 5.57 (dd, *J* = 14.2, 8.0 Hz, 1H), 5.34 (t, *J* = 12.9 Hz, 1H), 4.63 (dd, *J* = 14.1, 6.8 Hz, 1H), 4.47 (d, *J* = 13.9 Hz, 1H), 3.75 (s, 1H).

^{31}P{^{1}H}-NMR (400 MHz, DMSO-d_6, 293 K), δ (ppm) = 53.6.

HRMS (ESI) calcd for $C_{34}H_{31}Cl_2N_5PRu$ [M]+: 713.0815 found: 713.0815; $C_{34}H_{31}Cl_2N_5PRuNa$ [M + Na]+: 736.0713 found: 736.0649.

5.3.4 General procedure for hydrogenation reactions

Hydrogenation reactions were performed in 4 mL vials equipped with magnetic stirring bars. Catalyst and solid substrate were weighed in under air and the vials were then closed with PTFE/rubber septa pierced with a needle, and purged with argon. The solvent, a freshly prepared KO^{t}Bu solution in THF (c = 1 [M]), dodecane, when used, and the liquid reagent were then added in this order. The vials were placed in a pre- purged 300 mL stainless steel autoclave which was the sealed. The autoclave was purged with 3 cycles of N_2 followed by 3 cycles of H_2, pressurized with hydrogen to the desired temperature. After the required time, the reactor was cooled to room temperature, depressurized and, for the optimization reactions, a sample was taken, filtered over celite, diluted in acetone and analysed by GC. For the substrates scope, the products were isolated by filtration through silica or by flash column chromatography.

5.3.5 Characterization of hydrogenated products

1-Phenylethanol (Table 2, entry 1).

Colourless liquid.

^{1}H NMR (400 MHz, $CDCl_3$) δ (ppm) = 7.34–7.06 (m, 5H), 4.78 (q, *J* = 6.4 Hz, 1H), 2.13 (s, 1H), 1.40 (d, *J* = 6.5 Hz, 3H).

^{13}C-NMR (400 MHz, $CDCl_3$) δ (ppm) = 145.9, 128.6, 127.5, 125.5, 70.4, 25.2.

Cyclohexanol (Table 2, Entry 2).

Colourless liquid.

^{1}H NMR (400 MHz, $CDCl_3$) δ (ppm) = 3.63-3.48 (m, 1H), 2.11 (s, 1H), 1.94 – 1.79 (m, 2H), 1.75-1.60 (m, 2H), 1.50 (dd, *J*=13.5, 2.5 Hz, 1H), 1.33-1.00 (m, 5H).

^{13}C NMR (400 MHz, $CDCl_3$) δ (ppm) = 70.3, 35.6, 25.5, 24.2.

2-Cyclohexen-1-ol (Table 2, Entry 3).

Colourless liquid.

^{1}H NMR (300 MHz, $CDCl_3$) δ (ppm) = 5.83-5.59 (m, 2H), 4.13 (s, 1H), 2.43 (d, *J*=5.2 Hz, 1H), 2.08-1.42 (m, 6H).

^{13}C NMR (300 MHz, $CDCl_3$) δ (ppm) = 130.2, 130.1, 65.4, 31.9, 31.9, 25.1, 19.1.

4-Chloro-α-methylbenzyl alcohol (Table 2, Entry 4).

Colourless liquid.

^{1}H NMR (400 MHz, $CDCl_3$) δ (ppm) = 7.38- 7.12 (m, 4H), 4.80 (qd, *J*=6.4, 3.1 Hz, 1H), 2.81-2.60 (m, 1H), 1.42 (d, *J*=6.5 Hz, 3H).

^{13}C NMR (400 MHz, $CDCl_3$) (ppm) = 144.3, 130.02, 128.59, 126.9, 69.7, 25.3.

4-Methoxy-α-methylbenzyl alcohol (Table 2, Entry 5).

Colourless liquid.

^{1}H NMR (400 MHz, $CDCl_3$) δ(ppm) = 7.37-7.17 (m, 2H), 6.97-6.75 (m, 2H), 4.80 (q, *J*=6.5 Hz, 1H), 3.79 (s, 3H), 2.91 (bs, 1H), 1.45 (d, *J*=6.5 Hz, 3H).

^{13}C NMR (400 MHz, $CDCl_3$) δ (ppm) = 158.7, 138.1, 126.6, 130.7, 69.7, 55.2, 24.9.

Benzyl alcohol (Table 2, Entry 7).

Colourless liquid.

^{1}H-NMR (400 MHz, $CDCl_3$) δ(ppm) = 7.40-7.07 (m, 5H), 4.55 (s, 2H), 2.23 (s, 1H).

^{13}C-NMR (400 MHz, $CDCl_3$) δ(ppm) = 140.9, 128.6, 127.6, 127.1, 65.3.

1-cyclohexene-1-methanol (Table 2, Entry 8).

Colourless liquid.

^{1}H-NMR (300 MHz, $CDCl_3$) δ (ppm) = 5.70 (bs, 1H), 4.02 (s, 2H), 2.16 (m, 4H), 1.92 (m, 2H), 1.48 (m, 1H), 1.34 (s, 1H).

^{13}C-NMR (300 MHz, $CDCl_3$) δ(ppm) = 137.2, 122.5, 67.3, 30.4, 27.5, 26.1, 20.7.

3-cyclohexene-1-methanol (Table 2, Entry 9).

Colourless liquid.

^{1}H-NMR (400 MHz, $CDCl_3$) δ (ppm) = 5.67(s, 2H), 3.51(d, *J*=5.9 Hz, 2H), 2.07 (m, 4H), 1.77 (m, 3H), 1.25 (m, 1H) .

^{13}C-NMR (300 MHz, $CDCl_3$) δ(ppm) = 127.1, 125.9, 67.7, 36.3, 28.1, 25.2, 24.6.

Furfuryl alcohol (Table 2, Entry 10).

Pale yellow liquid.

^{1}H-NMR (400 MHz, $CDCl_3$) δ (ppm) = 7.36 (m, 1H), 6.31(m, 1H), 6.24 (d, *J*=3.6 Hz, 1H), 4.52 (s, 2H), 3.07 (bs, 1H)

^{13}C-NMR (400 MHz, $CDCl_3$) δ(ppm) = 154.1, 142.4, 110.3, 107.7, 57.1.

2,5-Di(hydroxymethyl)furan (Table 2, Entry 11).

White solid.

^{1}H-NMR (400 MHz, DMSO-d_6) δ (ppm) = 6.19 (s, 2H), 5.19(bs, 2H), 4.36 (s, 1H).

^{13}C-NMR (400 MHz, DMSO-d_6) δ(ppm) = 154.7, 107.5, 55.8.

4-Chloro-benzyl alcohol (Table 2, Entry 12).

White solid.

^{1}H-NMR (400 MHz, $CDCl_3$) δ(ppm) = 7.35-7.17 (m, 4H), 4.61 (s, 2H), 1.92 (bs, 1H).

^{13}C-NMR (400 MHz, $CDCl_3$) δ(ppm) = 139.4, 133.5, 128.8, 128.4, 64.6.

4-Methoxy-benzyl alcohol (Table 2, Entry 13).

White solid.

^{1}H-NMR (400 MHz, $CDCl_3$) δ(ppm) = 7.36-7.17 (m, 2H), 7.00-6.79 (m, 2H), 4.58 (s, 2H), 3.82 (s, 3H), 2.66 (bs, 1H).

^{13}C-NMR (400 MHz, $CDCl_3$) δ(ppm) = 159.1, 133.2, 128.7, 128.6, 113.9, 64.8, 55.3.

5.4 CONCLUSIONS

In conclusion, we have developed new air-stable ruthenium complexes bearing phosphine free, click based NNN-ligands, synthesized from cheap and commercially available reagents, in addition to cheap triphenylphosphine. The complexes have been fully characterized and successfully applied in the catalytic homogenous hydrogenation of ketones and aldehydes.

Most of the substrates were reduced to the corresponding alcohols with high yields using 0.05 mol% of catalyst. In the case of α,β-unsaturated 2-cyclohexenone and cyclohex-1-ene-1-carbaldehyde a high selectivity towards the unsaturated alcohol was observed. Based on DFT calculations, an outer-sphere mechanism seems more favourable than an inner-sphere mechanism.

5.5 REFERENCES

[1] H. C. Kolb, M. G. Finn, K. B. Sharpless, *Angew. Chemie - Int. Ed.* 2001, *40*, 2004–2021.

[2] V. V. Rostovtsev, L. G. Green, V. V. Fokin, K. B. Sharpless, *Angew. Chemie - Int. Ed.* 2002, *41*, 2596–2599.

[3] H. C. Kolb, K. B. Sharpless, *Drug Discov. Today* 2003, *8*, 1128–1137.

[4] V. O. Rodionov, V. V. Fokin, M. G. Finn, *Angew. Chemie - Int. Ed.* 2005, *44*, 2210–2215.

[5] C. Nolte, P. Mayer, B. F. Straub, *Angew. Chemie - Int. Ed.* 2007, *46*, 2101–2103.

[6] B. T. Worrell, J. A. Malik, V. V. Fokin, *Science* 2013, *340*, 457–460.

[7] P. T. Anastas, J. C. Warner, Eds. , *Green Chemistry: Theory and Practice*, Oxford Univ. Pr., 1998.

[8] P. L. Golas, K. Matyjaszewski, *Chem. Soc. Rev.* 2010, *39*, 1338–1354.

[9] D. Fournier, R. Hoogenboom, U. S. Schubert, *Chem. Soc. Rev.* 2007, *36*, 1369–1380.

[10] L. Liang, D. Astruc, *Coord. Chem. Rev.* 2011, *255*, 2933–2945.

[11] H. Struthers, B. Spingler, T. L. Mindt, R. Schibli, *Chem. - A Eur. J.* 2008, *14*, 6173–6183.

[12] M. Meldal, *Macromol. Rapid Commun.* 2008, *29*, 1016–1051.

[13] S. G. Agalave, S. R. Maujan, V. S. Pore, *Chem. - An Asian J.* 2011, *6*, 2696–2718.

[14] D. Schweinfurth, L. Hettmanczyk, L. Suntrup, B. Sarkar, *Zeitschrift fur Anorg. und Allg. Chemie* 2017, *643*, 554–584.

[15] D. Huang, P. Zhao, D. Astruc, *Coord. Chem. Rev.* 2014, *272*, 145–165.

[16] H. Struthers, T. L. Mindt, R. Schibli, *Dalt. Trans.* 2010, *39*, 675–696.

[17] Q. V. C. Van Hilst, N. R. Lagesse, D. Preston, J. D. Crowley, *Dalt. Trans.* 2018, *47*, 997–1002.

[18] S. C. Hockey, G. J. Barbante, P. S. Francis, J. M. Altimari, P. Yoganantharajah, Y. Gibert, L. C. Henderson, *Eur. J. Med. Chem.* 2016, *109*, 305–313.

[19] A. Maisonial, P. Serafin, M. Traïkia, E. Debiton, V. Théry, D. J. Aitken, P. Lemoine, B. Viossat, A. Gautier, *Eur. J. Inorg. Chem.* 2008, 298–305.

[20] J. C. Slootweg, S. Van Der Wal, H. C. Quarles Van Ufford, E. Breukink, R. M. J. Liskamp, D. T. S. Rijkers, *Bioconjugate Chem.* 2013, *24*, 2058.

[21] S. V Kumar, S. Ø. Scottwell, E. Waugh, C. J. Mcadam, L. R. Hanton, H. J. L. Brooks, J. D. Crowley, *Inorg. Chem.* 2016, *55*, 9767.

[22] B. Schulze, A. Winter, C. Friebe, E. Birckner, U. S. Schubert, *ACS Macro Lett.* 2017, *6*, 9.

[23] Y. Li, L. Chen, Y. Ai, E. Yau-Hin Hong, A. Kwun-Wa Chan, V. Wing-Wah Yam, *J. Am. Chem. Soc* 2017, *139*, 50.

[24] B. Colasson, M. Save, P. Milko, J. Roithová, D. Schro, O. Reinaud, *Org. Lett.* 2007, *9*, 30.

[25] E. Amadio, A. Scrivanti, V. Beghetto, M. Bertoldini, M. M. Alam, U. Matteoli, *RSC Adv.* 2013, *3*, 21636–21640.

[26] V. Ervithayasuporn, K. Kwanplod, J. Boonmak, S. Youngme, P. Sangtrirutnugul, *J. Catal.* 2015, *332*, 62–69.

[27] E. M. Schuster, M. Botoshansky, M. Gandelman, *Angew. Chemie - Int. Ed.* 2008, *47*, 4555–4558.

[28] B. M. J. M. Suijkerbuijk, B. N. H. Aerts, H. P. Dijkstra, M. Lutz, A. L. Spek, G. Van Koten, R. J. M. Klein Gebbink, *J. Chem. Soc. Dalt. Trans.* 2007, 1273–1276.

[29] X. C. Cambeiro, M. A. Pericàs, *Adv. Synth. Catal.* 2011, *353*, 113–124.

[30] F. Saleem, G. K. Rao, A. Kumar, G. Mukherjee, A. K. Singh, *Organometallics* 2013, *32*, 16.

[31] S. Hohloch, L. Suntrup, B. Sarkar, *Organometallics* 2013, *32*, 7376–7385.

[32] O. Martínez-Ferraté, C. Werlé, G. Franciò, W. Leitner, *ChemCatChem* 2018, *10*, 4514–4518.

[33] S. Paganelli, M. M. Alam, V. Beghetto, A. Scrivanti, E. Amadio, M. Bertoldini, U. Matteoli, *Appl. Catal. A Gen.* 2015, *503*, 20–25.

[34] J. G. de Vries, C. J. Elsevier, Eds. , *The Handbook of Homogeneous Hydrogenation*, Wiley-

VCH Verlag GmbH & Co. KGaA, Weinheim, Germany, 2006.

[35] S. Gladiali, E. Alberico, *Chem. Soc. Rev.* 2006, *35*, 226–236.

[36] R. Noyori, *Angew. Chemie - Int. Ed.* 2002, *41*, 2008–2022.

[37] J. S. M. Samec, J. E. Bäckvall, P. G. Andersson, P. Brandt, *Chem. Soc. Rev.* 2006, *35*, 237–248.

[38] M. Kitamura, T. Ohkuma, S. Inoue, N. Sayo, H. Kumobayashi, S. Akutagawa, T. Ohta, H. Takaya, R. Noyori, *J. Am. Chem. Soc.* 1988, *110*, 56.

[39] T. Ohkuma, H. Ooka, S. Hashiguchi, T. Ikariya, R. Noyori, *J. Am. Chem. Soc.* 1995, *117*, 2675–2676.

[40] K.-J. Haack, S. Hashiguchi, A. Fujii, T. Ikariya, R. Noyori, *Angew. Chemie - Int. Ed.* 1997, *36*, 285–288.

[41] R. Noyori, T. Ohkuma, *Angew. Chemie - Int. Ed.* 2001, *40*, 40–73.

[42] S. Baldino, S. Facchetti, A. Zanotti-Gerosa, H. G. Nedden, W. Baratta, *ChemCatChem* 2016, *8*, 2279–2288.

[43] S. Giboulot, S. Baldino, M. Ballico, R. Figliolia, A. Pö, S. Zhang, D. Zuccaccia, W. Baratta, 2019, DOI 10.1021/acs.organomet.8b00919.

[44] D. Spasyuk, S. Smith, D. G. Gusev, *Angew. Chemie - Int. Ed.* 2013, *52*, 2538–2542.

[45] B. M. Stadler, P. Puylaert, J. Diekamp, R. van Heck, Y. Fan, A. Spannenberg, S. Hinze, J. G. de Vries, *Adv. Synth. Catal.* 2018, *360*, 1151–1158.

[46] P. Puylaert, R. van Heck, Y. Fan, A. Spannenberg, W. Baumann, M. Beller, J. Medlock, W. Bonrath, L. Lefort, S. Hinze, et al., *Chem. - A Eur. J.* 2017, *23*, 8473–8481.

[47] P. A. Dub, B. L. Scott, J. C. Gordon, *Organometallics* 2015, *34*, 4464–4479.

[48] S. I. Presolski, V. Hong, S. H. Cho, M. G. Finn, *J. Am. Chem. Soc.* 2010, *132*, 14570–14576.

[49] S. Werkmeister, J. Neumann, K. Junge, M. Beller, *Chem. - A Eur. J.* 2015, *21*, 12226–12250.

[50] P. A. Dub, T. Ikariya, *ACS Catal.* 2012, *2*, 1718–1741.

[51] C. Gunanathan, D. Milstein, *Acc. Chem. Res.* 2011, *44*, 588–602.

[52] N. Steinfeldt, K. Junge, in *Sci. Synth.* (Ed.: J.G. de Vries), Georg Thieme Verlag, 2018, pp. 7–45.

[53] R. A. Farrar-Tobar, S. Tin, J. G. de Vries, in *Top. Organomet. Chem.* (Eds.: P.H. Dixneuf, J.-F. Soulè), Springer Nature, 2019, pp. 193–224.

[54] F. A. Kucherov, L. V Romashov, K. I. Galkin, V. P. Ananikov, *ACS Sustain. Chem. Eng.* 2018,

6, 8064–8092.

[55] R.-J. Van Putten, J. C. Van Der Waal, E. De Jong, C. B. Rasrendra, H. J. Heeres, J. G. De Vries, *Chem. Rev.* 2013, *113*, 1499–1597.

[56] P. A. Dub, B. L. Scott, J. C. Gordon, *J. Am. Chem. Soc.* 2017, *139*, 1245–1260.

[57] S. E. Clapham, A. Hadzovic, R. H. Morris, *Coord. Chem. Rev.* 2004, *248*, 2201–2237.

[58] E. P. Cappellani, P. A. Maltby, R. H. Morris, C. T. Schweitzer, M. R. Steele, *Inorg. Chem.* 1989, *28*, 4437–4438.

[59] K. Abdur-Rashid, A. J. Lough, R. H. Morris, *Organometallics* 2000, *19*, 2655–2657.

[60] G. M. Sheldrick, *Acta Crystallogr. Sect. A Found. Crystallogr.* 2008, *64*, 112–122.

[61] G. M. Sheldrick, *Acta Crystallogr. Sect. C Struct. Chem.* 2015, *71*, 3–8.

[62] C. Y. Lin, M. W. George, P. M. W. Gill, *Aust. J. Chem* 2004, *57*, 365–370.

[63] M. Dolg, in *Mod. Methods Algorithms Quantum Chem.* (Ed.: J. Grotendorst), NIC Series, John Neumann Institute For Computing, Julich, 2000, pp. 479–508.

[64] P. J. Hay, W. R. Wadt, *J. Chem. Phys.* 1985, *82*, 270–283.

[65] W. J. Hehre, K. Ditchfield, J. A. Pople, *J. Chem. Phys.* 1972, *56*, 2257–2261.

[66] Y. Minenkov, Å. Singstad, G. Occhipinti, V. R. Jensen, *Dalt. Trans.* 2012, *41*, 5526–5541.

[67] J. Da Chai, M. Head-Gordon, *Phys. Chem. Chem. Phys.* 2008, *10*, 6615–6620.

[68] I. C. Gerber, J. G. Ángyán, *Chem. Phys. Lett.* 2005, *415*, 100–105.

[69] F. Weigend, R. Ahlrichs, *Phys. Chem. Chem. Phys.* 2005, *7*, 3297–3305.

[70] D. Andrae, U. Häußermann, M. Dolg, H. Stoll, H. Preuß, *Theor. Chim. Acta* 1990, *77*, 123–141.

[71] V. Barone, M. Cossi, *J. Phys. Chem. A* 1998, *102*, 1995–2001.

[72] M. Cossi, N. Rega, G. Scalmani, V. Barone, *J. Comput. Chem.* 2003, *24*, 669–681.

[73] C. J. Cramer, Ed. , *Essentials of Computational Chemistry*, Wiley Blackwell, Weinheim, Germany, 2003.

6. NS CLICK BASED LIGANDS FOR IN SITU HYDROGENATION OF CARBONYL COMPOUNDS

6.1 INTRODUCTION

Homogenous catalysts generally provides high activities and selectivities at mild reaction conditions, even if their use in industrial application is rather limited. *Inter alia,* the difficult separation and the challenging recovery and recyclability of the catalysts after the reaction often hamper their upgrade over the laboratory scale.

An attracting way to circumnavigate these deficiencies is the development of water-soluble catalysts, whose separation from reagents and products could allow a prompt recycle of the catalytically active species.[1–5] Due to high polarity of water, most of apolar organic ligands suffer low solubility in this protic solvent. This means that proper routes must be found in order to render organic ligands soluble in water. On the other hand, difference in miscibility makes apolar products easy to separate from a water-soluble active catalyst.

The same is true for hydrogen, which is not very soluble in water (0.81 mM at 20 °C) rather than in other organic solvents.[6]

The use of water as a benign and environmental-friendly solvent not only provides an useful methodology to recover the catalyst, but also avoid the use of toxic solvents, in agreement with the principles of green chemistry.[7]

Nevertheless, first examples of water-soluble complexes for catalysis date back in the 1960s and 1970s, when $[CO(CN)_5]^{3-}$ and $RhCl_3$ were used for the hydrogenation of olefins. Since then, several homogenous catalysts have been developed in the recent years to be used in an aqueous environment or in a water/organic solvent biphasic mixture.

However, in the mid-1970s the well-known OXEA hydroformylation process (ex Ruhrchemie/Rhone-Poulenc) successfully used for the first time water-soluble sulfonated phosphines, such as TPPTS **2** (3,3′,3″-Phosphanetriyltris(benzenesulfonic acid) trisodium salt). This landmark brought to develop a plethora of sulfonated arylphosphines (**Figure 6.1**) which found extensive applications in catalysis in the presence of several different transition metals.

The broad success of sulfonated arylphosphines lies mainly in their stability in water over a broad range of pH.

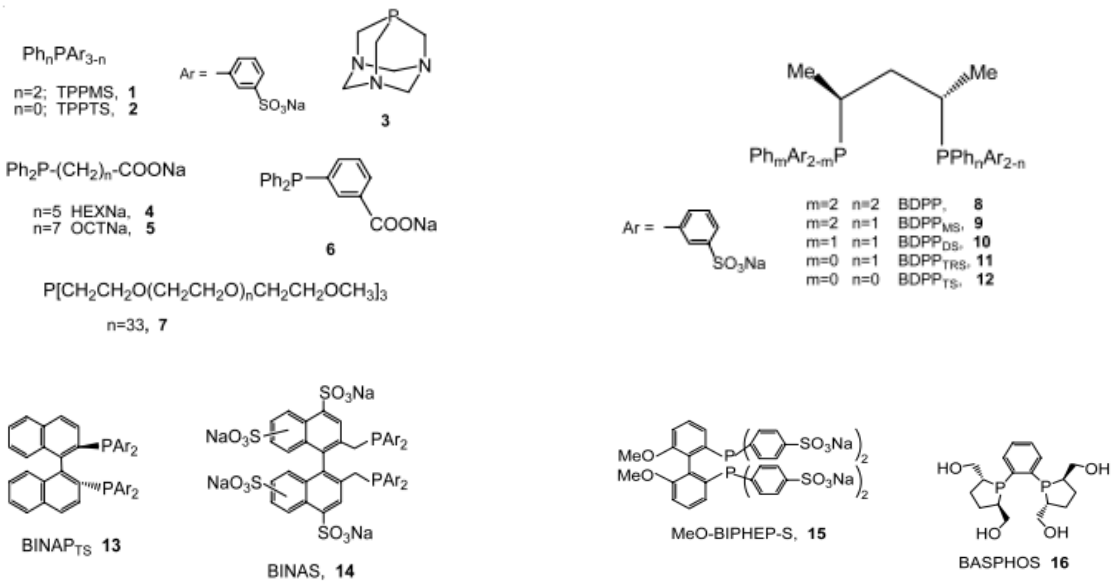

Figure 6.1. Phosphine-based water soluble ligands[5]

Despite the great advantages achieved by using phosphine sulfonated ligands, they often require handling under strictly inert conditions and expensive procedures.

As a response, several further methods have been investigated and published regarding water-soluble ligands derived from natural compounds such as aminoacids, proteins, peptides and carbohydrates. Transition metal complexes bearing these ligand provided water soluble species active in homogenous catalysis.[8–12]

Alternatively, efficient ways to render organic ligand water soluble is by introducing hydrophilic moieties such as -COOH, -NR^{3+}, OH.[1–3]

A greener approach for the synthesis of ligands emerged with the advent of click chemistry, a term coined by Barry Sharpless in 2001. As aforementioned (see section 1.3.1), this synthetic approach allows to synthetize important organic units by using mild reaction conditions, benign solvents, commercially available not hazardous reagents.

Summing up, these high yielding reactions have been used to designed novel ligands incorporating terminal ester or carboxylic groups to induce solubility in aqueous media or in a water/organic biphasic system.

The new ligands have been developed by means of CuAAC [3+2] cycloaddition and thiol-ene addition to synthetize in a facile way a water-soluble ligand (Figure 6.2).

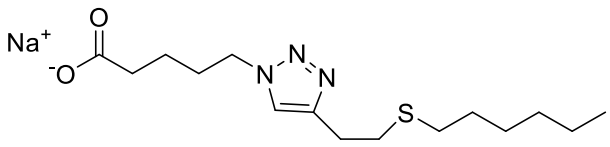

Figure 6.2. NS ligand

Ligands have been tested for the selective hydrogenation of carbonyl compounds, with a particular focus on those derived from natural sources.

As a matter of fact, the conversion of biomass derived furfural, levulinic acid and cinnamaldehyde have been investigated by using $[Ir(COD)Cl]_2$ as metal precursor for preliminary tests.

6.2 RESULTS AND DISCUSSION

6.2.1 Synthesis of ligands and complexes

The ligands have been prepared according to the synthetic pathway reported in **Scheme 6.1**.

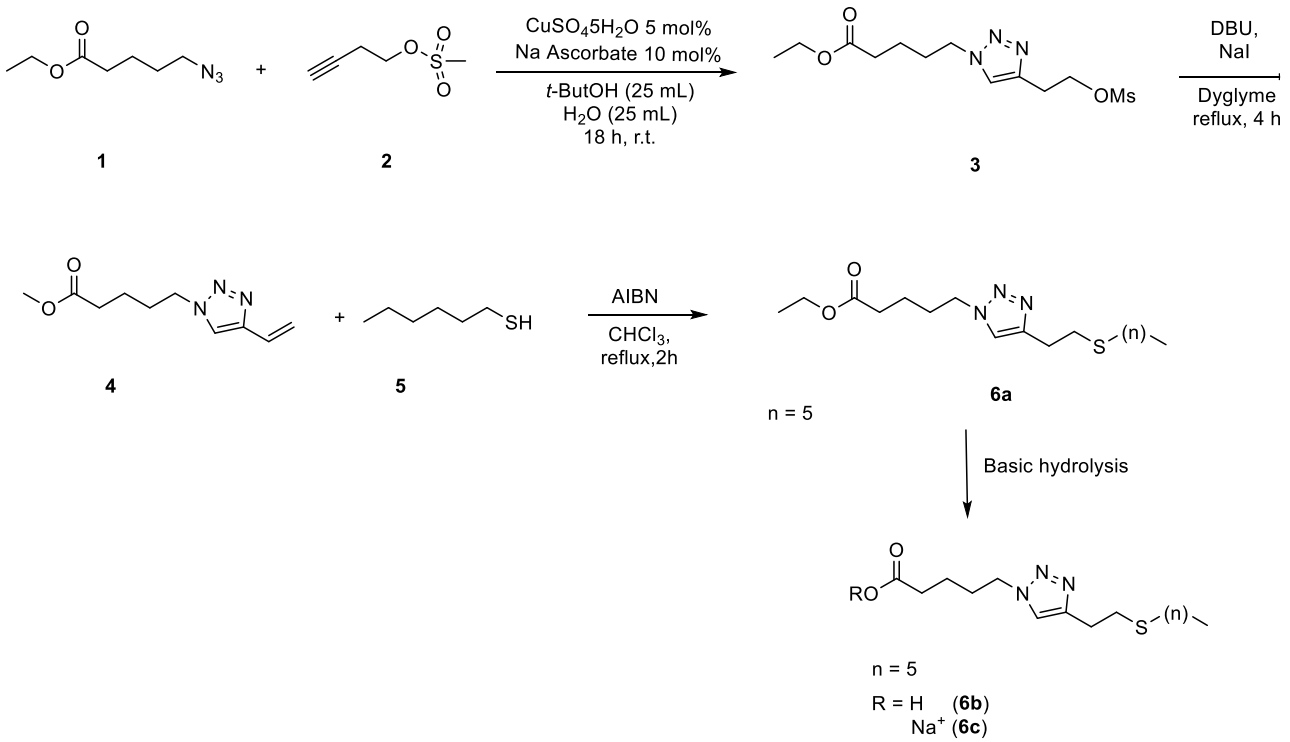

Scheme 6.1. Synthesis of NS ligands (**6a-6c**)

The synthesis of **4** was accomplished by following a literature procedure reported by Takizawa *et al.*[13] Treatment of ethyl-5-azidopentanoate **1** with butyn-3-ynyl methanesulfonate **2** in the presence of a catalytic system consisting of $CuSO_4 \cdot 5H_2O$ and sodium ascorbate, lead to the synthesis of the mesylated triazole **3** which then undergoes elimination of the protecting group *via* NaI/DBU system to afford the desired vinyl triazole. Afterwards, the most efficient procedure to attach sulfur moiety to the triazole core resulted to be the radical addition, by using AIBN as radical initiator, in refluxing chloroform yielding the ligand **6a**. Further basic hydrolysis was carried out by stochiometric addition of NaOH 1M and allowed to obtain the corresponding acid **6b** and the sodium salt **6c**.

All ligands are air stable and have been characterized by means of ^{1}H and ^{13}C NMR spectroscopy. While **6a** and **6b** are soluble only in organic solvents, **6c** is water-soluble.

6.2.2 Catalytic hydrogenations

6.2.2.1 Catalytic hydrogenation of Furfural with the in situ system $[Ir(\eta^4\text{-COD})Cl]_2$/6a-c

With the ligands in hand, *in situ* catalytic hydrogenations of furfural as standard substrate were performed using ligands **6a-c**. Initially the metallic precursor is dissolved in water and then one of the ligand (**6a-c**/Ir = 1:1) is added in water (3 mL) into a glass reactor purged by a stream of N_2. The mixture was then allowed to stir allowing to obtain the catalytically active specie as a bright yellow homogenous solution.

At first, an experiment was run in order to verify the catalytic activity of the iridium precursor (**Table 6.1**, Entry 1). Relatively low conversion and significant formation of black particles was observed at the end of the reaction, thus meaning that the complex is not stable enough, in the reaction conditions tested. Moreover, recyclability of the catalyst is compromised by the decomposition of the precursor. Nonetheless, chemoselectivity is satisfying as only production of FA was observed.

Table 6.1. Optimization of the reaction conditions for the catalytic hydrogenation reactions

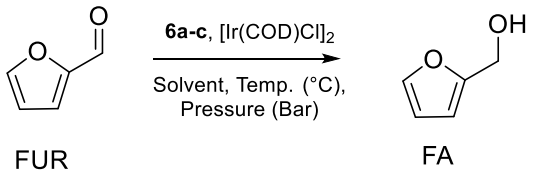

Entry[a]	Ligand	Solvent	Temperature (°C)	Pressure (bar)	Yield (%)[b]
1	/	H_2O/THF	60	40	46
2	**6a**	H_2O/THF	60	40	4
3	**6b**	H_2O/THF	60	40	24
4	**6c**	H_2O/THF	60	40	83
5	**6a**	THF	80	60	3
6	**6b**	THF	80	60	11
7	**6a**	*i*-PrOH	80	60	5
8	**6b**	*i*-PrOH	80	60	6
9	**6c**	H_2O/THF	80	10	41
10	**6c**	H_2O/THF	80	20	90
11	**6c**	H_2O/THF	80	40	99
12[c]	**6c**	H_2O/THF	80	40	66
13[d]	**6c**	H_2O/THF	80	40	32
14	**6c**	H_2O/Me-THF	80	40	54
15	**6c**	H_2O/CPME	80	40	68
16	**6c**	H_2O	80	40	62
17[e]	**6c**	H_2O/THF	80	40	83
18[f]	**6c**	H_2O/THF	80	40	n.d.

[a] Reaction conditions: Furfural = 5.3 mmol, 40 bar of H_2, Temp. = 80 °C, THF = 3.0 mL, H_2O = 3.0 mL, Time = 18 hours
[b] GC yields using dodecane as internal standard
[c] 8 hours
[d] 2 hours
[e] catalyst loading 0.05 mol%
[f] no $[Ir(COD)Cl]_2$

Afterwards, ligands **6a-6c** were tested in different solvents. The use of **6a** and **6b** showed very low activities in a mixture of H_2O/THF (Entries 2-3), but also when other solvent such as pure THF and *i*-PrOH were used (Entries 5-8).

On the other hand, ligand **6c** showed good activity starting from 60 °C and 40 bar of hydrogen pressure (Entry 4). Encouraged by these preliminary results, we screened different parameters to evaluate the activity of the *in situ* system $[Ir(\eta^4\text{-COD})Cl]_2$/**6c** (Entries 9-13), wherein the selectivity is always observed towards FA.

Pressure plays a crucial role on conversion with the drastic decreased observed at 10 bar (Entry 9) even if temperature was increased to 80 °C. The best conditions were found to be 80°C and 40 bar (Entry 11), with complete conversion of FUR to FA.

Reaction time of 18 hours were necessary to reach these results, as shorter times (Entries 12-13) led to lower conversions.

Aiming to develop a biphasic system for the easier separation of the catalyst, water immiscible and green solvents such as Me-THF and cyclopentyl methyl ether (CPME) were also tested (Entries 14-15) but their use did not lead to satisfying results. Surprisingly, the use of only water as solvent provides lower conversions compared to the H_2O/THF mixture (1/1 vol/vol) (Entries 11,16). Even at a low catalyst loading such as 0.05 mol% (Entry 17) the catalyst is active reaching 83% conversion of FUR to FA.

Importantly, the crude mixture recovered after the hydrogenation doesn't present dark precipitates thus suggesting that the ligand may preserve the metal from deactivation and degradation (**Figure 6.3**).

Figure 6.3. Glass reactor containing the reaction mixture of furfural hydrogenation by the in situ system ligand $[Ir(\eta^4\text{-COD})Cl]_2$/**6c.** Reaction depicted: **Table 6.1** Entry 11

One of the main tasks of this project regards the recyclability of the catalyst. The solubility in water allows to separate the aqueous phase containing the active catalyst solution from the organic products by liquid/liquid extraction.

Different solvents have been used as extracting solvents. *Inter alia,* diethyl ether resulted to be the most efficient. Addition of diethyl ether to the glass reactor containing the reaction mixture allowed to separate the aqueous phase from the organic one, which was then dried over $MgSO_4$ anhydrous, filtered and analysed by GC.

Noteworthy, the catalyst aqueous phase recovered from the experiment which gave the most promising activity (**Table 6.1,** Entry 11) showed no loss in activity even after 4 recycling experiments. Just at the fifth experiment, conversion slightly decreased to 97%.

The confinement of the active specie into the aqueous phase is a crucial parameter to evaluate the robustness of the catalyst. Leaching of the metal in the organic phase may decrease the activity of the catalyst over the recycling tests.

Inductively coupled plasma mass spectrometry (ICP-MS) analysis revealed that between 0.5-1 mol% of the metal is present in the organic phases recovered at the end of the 1st recycling test, meaning that the metal-**6c** system is well confined into the aqueous phase.

6.2.2.2 Catalytic hydrogenation of levulinic acid with the in situ system [Ir(η⁴-COD)Cl]₂/6c

Stimulated by the results showed above achieved with ligand **6c**, we considered other substrates to explore the activity of the catalytic system [Ir(η⁴-COD)Cl]₂/**6c**.

Levulinic acid (LA) is a biomass derived platform chemical directly obtained by sugars. The valorisation of this C-5 molecule opened-up a library of major and fine chemicals which find extensive application over a broad range of fields (see section 1.1.1.3).

Among the variety of products which can be derived from LA, we focused on its selective hydrogenation to yield γ-valerolactone (GVL), a potentially major chemical used as a solvent or to produce biofuels and food additives.

The generally accepted mechanism for the hydrogenation of LA to GVL relies on the formation of the intermediate 4-hydroxyvaleric acid (4-HVA), a not stable compound which easily converts to GVL (Scheme 6.2).

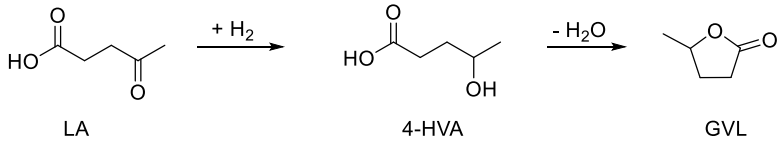

Scheme 6.2. Hydrogenation of LA to GVL *via* 4-HVA

Despite several iridium and ruthenium complexes have been developed over the time for the homogenous hydrogenation in organic media of LA to GVL (see section 1.2.3.1),[14–17] the use of recyclable water-soluble complexes is still challenging.[18]

In 2011 Herees and co-workers reported good activity of an *in situ* hydrogenation of LA to GVL by using $RuCl_3 \cdot 3H_2O$ at 1.0 mol% and Na_3TPPTS in a biphasic system CH_2Cl_2/water.[19] However, catalyst separation was not very efficient as after one run a significant loss of activity was observed.

Deng *et al.* reported the use of reusable half-sandwich iridium complex in acidic aqueous media at low catalyst loading (0.01 mol%) reaching high TON (10.000). High temperatures (120 °C) and 10 bar of H_2 were required Only 5% activity loss was observed after catalyst recycle. [20]

Summing up, in Table 6.2 are summarized the explorative experiments carried out with ligand **6c** and $[Ir(\eta^4\text{-COD})Cl]_2$ regarding the selective hydrogenation of LA to GVL. It is worth to mention that the formation of other products has never been observed, thus meaning that the system is selective towards GVL.

Table 6.2. Optimization of the reaction conditions for the catalytic hydrogenation reactions

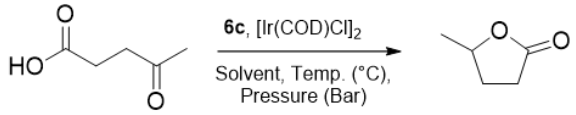

LA GVL

Entry[a]	Temperature (°C)	Pressure (bar)	Yield (%)[b]
1	60	60	70
2	70	40	64
3	80	60	80
4	80	80	81
5	100	40	69
6	100	60	89
7	100	80	83
8[c]	100	60	85

[a] Reaction conditions: LA = 5.2 mmol, cat.loading = 0.1%, THF = 3.0 mL, H_2O = 3.0 mL, Time = 18 hours
[b] GC yields using dodecane as internal standard
[c] No THF

From data reported above, it is possible to demonstrate that the catalytic system $[Ir(\eta^4\text{-COD})Cl]_2$/**6c** requires less milder condition to give appreciable conversion. Best operating conditions were found to be 100 °C and 60 bar in a THF/water mixture (Entry 6). Notably, the use of only water also proceeds in a similar way (Entry 8), as 85% yield was detected. Nevertheless, these conditions are not far from data present in literature.[18]

Recycle of the catalysts lead to a loss activity of 3% after three runs, meaning that the catalytic system is robust enough to enhance recyclability of the catalyst.

6.2.2.3 Catalytic hydrogenation of cinnamaldehyde with the in situ system [Ir(η^4-COD)Cl]$_2$/6c

Cinnamaldehyde (CIN) is an α,β-unsaturated aldehyde which can be obtained by direct extraction or steam distillation of the oil derived from cinnamon bark.

Due to the presence of both C=O and aliphatic C=C bonds it is often choosen as a model substrate to verify the efficiency, in terms of selectivity, of a novel catalytic system.

Hydrogenation of CIN can lead to the formation of different products (Scheme 6.3). Selective hydrogenation of the carbonyl moiety affords cinnamyl alcohol (CA), a precious chemical used as flagrance by food industry or in the field of cosmetic and personal care. On the other hand, catalyst can be selective towards the saturated 3-phenylpropionaldehyde (PA) due to the hydrogenation of only C=C bond. When selectivity is lacking, fully reduced 3-phenylpropanol (PP) is obtained.

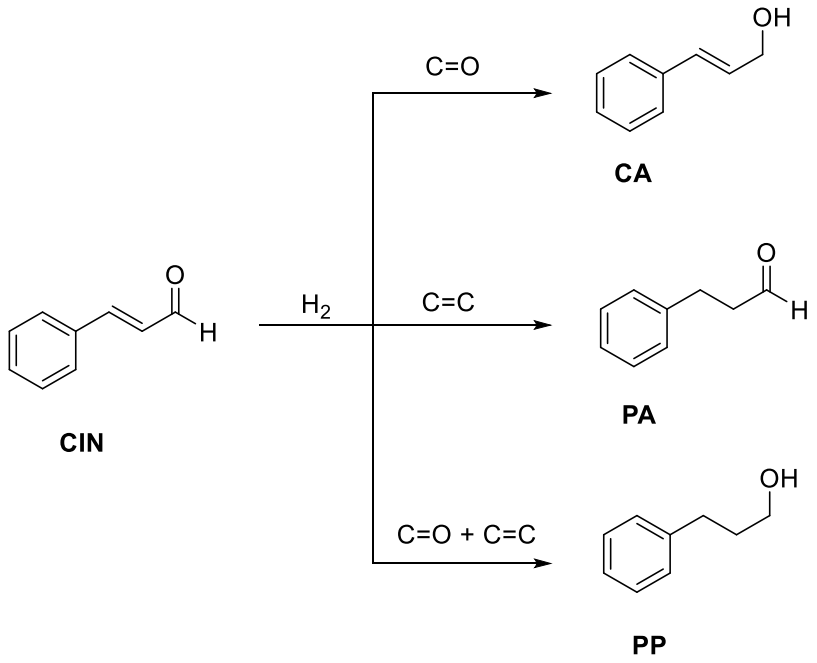

Scheme 6.3. Potential products derived from hydrogenation of cinnamaldehyde

In the examples aforementioned, the combination of the metal precursor [Ir(η^4-COD)Cl]$_2$ and ligand 6c showed good performances in the selective conversion of FUR and LA to the corresponding hydrogenated products. Good results from the recycling experiments have been also achieved.

Data showing the influence of solvents, temperature and pressure in the reduction of CIN are listed in Table 6.3.

Table 6.3. Optimization of reaction conditions for conversion of CIN

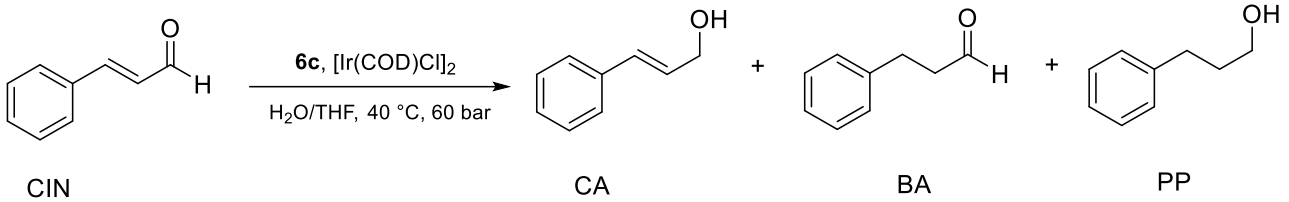

CIN CA BA PP

Entry[a]	Temperature (°C)	Pressure (bar)	Conversion (%)	Yield CA (%)[b]	Yield BA (%)[b]	Yield PP (%)[b]
1	40	20	13	8	5	n.d.
2	60	20	99	56	n.d.	43
3	80	20	99	20	n.d.	79
4	40	40	98	80	n.d.	18
5	40	60	99	86	n.d.	13
6	60	40	99	68	n.d.	31
7	60	60	99	58	n.d.	41
8	80	40	99	33	n.d.	66
9	100	40	99	18	10	71
10[c]	40	20	97	83	n.d	13
11[c]	40	60	99	85	n.d	14

[a] Reaction conditions: CIN= 5.2 mmol, cat.loading = 0.1%, THF = 3.0 mL, H_2O = 3.0 mL, Time = 18 hours

[b] GC yields using dodecane as internal standard

[c] No THF

The selectivity of the reaction resulted to be strongly dependent both from temperature and pressure. At very mild conditions (Entry 1) low conversion of CIN towards CA is achieved together with a comparable amount of BA. However, a significant increasing in conversion is observed once the temperature is increased of 20°C (Entry 2), even if a mixture of CA and PP is obtained with no selectivity. At 80°C, selectivity is shifted to PP (Entry 3), while maintaining full conversion of the substrate. At this point the effect of pressure at 40°C was took in account. At 40 bar, almost full conversion of the substrate led to a good selectivity towards CA (Entry 4), which slightly increased at 60 bar (Entry 5). These were found to be the best operating conditions to achieve appreciable selectivities. In fact, at 60°C and 40 bar selectivity towards CA started to decrease (Entry 6). A similar result, confirming the change in selectivity when the temperature is increased over 40 °C, was achieved at 60°C-60 bar (Entry 7), 80°C-40 bar (Entry 8) and 100°C-40 bar (Entry 9). This lead to the expected conclusion that pushing the reaction conditions promotes the formation of the fully hydrogenated product.

Surprisingly, running the reaction on only water as solvent allowed to achieve similar results, meaning that hydrogenation can be run in water for an easier separation of the catalyst phase.

Table 6.3. Influence of time on the hydrogenation of CIN

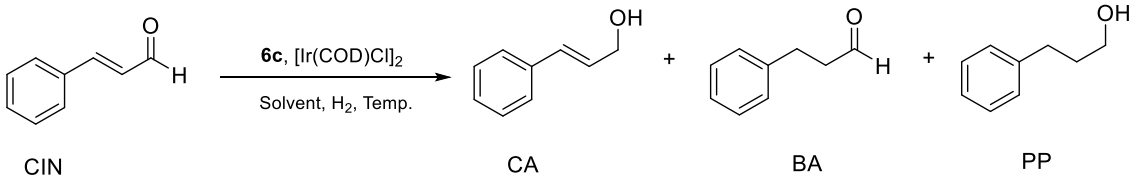

CIN CA BA PP

Entry[a]	Time (h)	Conversion (%)	Yield CA (%)[b]	Yield BA (%)[b]	Yield PP (%)[b]
1	2	18	8	65	21
2	4	36	7	26	2
3	8	99	30	4	65
4	18	99	86	n.d.	13
5	24	99	87	1	12

[a] Reaction conditions: CIN= 5.2 mmol, cat.loading = 0.1%, THF = 3.0 mL, H_2O = 3.0 mL, $P_{(H2)}$=60 bar, Temp. = 40°C

[b] GC yields using dodecane as internal standard

After having optimized the best reaction conditions for a good selectivity towards CIN, reaction time were screened in **Table 6.3.** At 2 hours, only 18% conversion was obtained (Entry 1). Similarly, at 4 hours conversion was still too low (Entry 2). Full conversion was achieved after 8 hours, even if selectivity was shifted to PP (Entry 3). 18 hours were necessary to reach the desired selectivity to CA. Increasing the time to 24 did not allow to increase the selectivity, thus meaning that the catalyst is deactivated after 18 hours.

These findings confirms that the formation of BA requires mild reaction conditions thus leading to the conclusion that the catalytic system $[Ir(\eta^4\text{-COD})Cl]_2$/**6c** is active in C=C hydrogenation at the reported conditions.

Recycling tests gave no appreciable results. The reason of this peculiar catalyst deactivation is still under investigation.

6.3 EXPERIMENTAL

6.3.1 Materials and instrumentation

Commercial solvents (Aldrich) were purified as described in the literature.[21] Ethyl 5-Bromovalerate, 3-butyn-1-ol and 1-hexanthiol were purchased from Aldrich. Azobisisobutyronitrile (AIBN) was purchased from Acros organics.

Ethyl-5-azidopentanoate and 5-(4-vinyl-1*H*-1,2,3-triazol-1-yl)pentanoate were prepared according to procedures reported in the literature. [13,22]

All syntheses were carried out under inert atmosphere (nitrogen) using standard Schlenk techniques. ^{1}H and ^{13}C $\{^{1}H\}$ NMR spectra were recorded on a Bruker AVANCE 300 spectrometer operating at 300.21 and 75.44 MHz, respectively. The chemical shift values of the spectra are reported in δ units with reference to the residual solvent signal. The proton assignments were performed by standard chemical shift correlations as well as by ^{1}H 2D COSY experiments.

ESI-MS analyses were performed using a Finnigan LCQ-Duo ion-trap instrument, operating in positive ion mode (sheath gas N_2, source voltage 4.0 KV, capillary voltage 21 V, capillary temperature 200 °C). All mass spectra were recorded on freshly prepared solutions.

Elemental analyses (C, H, N) were carried out at the University of Padua using a Fison EA1108 microanalyzer. IR spectra were collected in the range 4000 – 400 cm^{-1} using a Perkin-Elmer Spectrum One spectrophotometer. Melting points were determined using a Büchi B-535 apparatus.

6.3.2 Ligands synthesis

*6.3.2.1 Synthesis of Ethyl-5-azidopentanoate (**1**)*

In a mixture of acetone (50 mL) and H_2O (30 mL) were dissolved ethyl 5-bromovalerate (3.71 mL, 23.38 mmol) and sodium azide (4.56 g, 70.14 mmol). The colourless solution was allowed to stir for 18 hours under reflux. Afterwards, no changing in the colour of the solution was observed. Acetone was removed under reduced pressure and aqueous residues were extracted with CH_2Cl_2 (15 mL x 3).

Organic layers were dried over MgSO4, filtered and concentrated under vacuo to yield **1** as a colourless oil (92% yield).

EA calcd for for $C_7H_{13}N_2O_3$: C (49.11) H(7.65) N(24.54); found: C(49.78) H(7.71) N(24.6).

^{1}H NMR (300 MHz, $CDCl_3$) δ (ppm) = 4.12 (q, *J*=7.1 Hz, 2H), 3.28 (t, *J*=6.5 Hz, 2H), 2.32 (t, *J*=7.1 Hz, 2H), 1.83 – 1.50 (m, 4H), 1.24 (td, *J* = 7.2, 0.7 Hz, 3H).

^{13}C NMR (300 MHz, $CDCl_3$) δ (ppm) = 173.2, 60.4, 51.2, 33.8, 28.4, 22.2, 14.3.

HRMS (ESI) calcd for $C_7H_{13}N_2O_3$ $[M+H]^+$: 173.09264 found: 173.09301

*6.3.2.2. Synthesis of But-3-ynyl methanesulfonate (**2**)*

3-butyn-1-ol (1.62 mL, 21.40 mmol) and triethylamine (8.94 mL, 64.30 mmol) were dissolved in 100 mL of CH_2Cl_2 and vigorously stirred. Afterwards, an ice bath was placed under the round bottom

flask and methanesulfonic acid chloride (2.16 mL, 27.76 mmol) was dropwise added to the stirring solution over 20 minutes. At the end of the addition, the ice bath was removed and the orange solution was allowed to stir overnight at room temperature. After 18 hours, a solution of HCl 1M was added at the solution and the organic layer was extracted and washed three times with CH_2Cl_2 (15 mL x 3), dried over $MgSO_4$, filtered. Volatiles were removed under reduced pressure and **2** was obtained as an orange oil (98% yield).

EA calcd for for $C_5H_8O_3S$: C (40.53) H(5.44) S(21.64); found: C(40.66) H(5.34) S(22.01).

^{1}H NMR (300 MHz, $CDCl_3$) δ (ppm) = 4.29 (t, J = 6.7 Hz, 2H), 3.04 (s, 3H), 2.64 (td, J = 6.7, 2.7 Hz, 2H), 2.07 (t, J = 2.7 Hz, 1H).

^{13}C NMR (300 MHz, $CDCl_3$) δ(ppm) = 78.7, 71.0, 67.2, 37.6, 19.7.

HRMS (ESI) calcd for $C_5H_8O_3N_3S$ $[M+H]^+$: 148.01943 found:148.01923

*6.3.2.3. Synthesis of ethyl 5-(4-(2-((methylsulfonyl)oxy)ethyl)-1H-1,2,3-triazol-1-yl)pentanoate (**3**)*

1 (3.21 g, 18.77 mmol) and **2** (2.78 g, 18.77 mmol) were dissolved in *t*-ButOH (25 mL) and H_2O (20 mL). In a separate vial $CuSO_4 \cdot 5H_2O$ (0.23 g, 0.94 mmol) and Na Ascorbate (0.37 g, 1.87 mmol) were dissolved in 5 mL of H_2O and vigorously mixed trough a Pasteur pipette until a light brown emulsion was obtained. The mixture was then transferred dropwise to the reaction flask which after addition turned into a brown solution. The reaction was then allowed to stir at room temperature for 24 hours. A yellow solution was obtained and *t*-ButOH was eliminated under reduced pressure. The aqueous residues were then diluted with 10 mL of a saturated solution of EDTA and extracted with CH_2Cl_2 (15 mL x 3) in order to remove copper salts traces. The organic layers were collected and dried over $MgSO_4$, filtered and volatiles eliminated under vacuo to yield **3** as a yellow oil (88% yield).

EA calcd for for $C_{12}H_{21}N_3O_5S$: C (45.13) H(6.63) N(13.16) S(10.04); found: C(44.98) H(6.55) N(13.55) S(10.32)

^{1}H NMR (300 MHz, $CDCl_3$) δ(ppm) = 7.46 (s, 1H), 4.48 (t, J = 6.4 Hz, 2H), 4.32 (t, J = 7.1 Hz, 2H), 4.08 (q, J = 7.1 Hz, 2H), 3.14 (t, J = 7.2 Hz, 2H), 2.95 (s, 3H), 2.31 (t, J = 7.3 Hz, 2H), 2.04 – 1.81 (m, 2H), 1.72 – 1.49 (m, 2H), 1.21 (t, J = 7.1 Hz, 4H).

^{13}C NMR (300 MHz, $CDCl_3$) δ (ppm) = 172.8, 122.1, 68.7, 60.4, 49.9, 37.3, 33.3, 29.5, 26.0, 21.7, 14.2.

HRMS (ESI) calcd for $C_{12}H_{21}O_5N_3S$ $[M+H]^+$: 319.12022 found:319.12088

*6.3.2.4. Synthesis of ethyl 5-(4-vinyl-1H-1,2,3-triazol-1-yl)pentanoate (**4**)*

3 (5.27 g, 16.50 mmol) and NaI (7.42 g, 49.50 mmol) were dissolved in glyme (80 mL) and stirred at room temperature for 1 hour until an intense orange solution was obtained. DBU (4.93 mL, 33.00 mmol) was then added and the solution was refluxed for 3 hours while the solution turned into a white emulsion. Afterwards, solids formed during reaction were filtered and washed with EtOAc. Organic layers were dried over $MgSO_4$, filtered and concentrated to yield **4** as a yellow oil (85% yield).
EA calcd for for $C_{11}H_{17}O_2N_3$: C (59.17) H(7.67) N(18.82); found: C(59.21) H(7.83) N(18.12)
^{1}H NMR (300 MHz, $CDCl_3$) δ(ppm) = 7.53 (s, 1H), 6.73 (dd, *J*=17.8, 11.2 Hz, 1H), 5.89 (dd, *J*=17.7, 1.3 Hz, 1H), 5.35 (dd, *J*=11.2, 1.3 Hz, 1H), 4.37 (t, *J* = 7.1 Hz, 2H), 4.13 (d, *J* = 7.2 Hz, 2H), 2.36 (t, *J*= 7.2 Hz, 2H), 2.13 – 1.85 (m, 2H), 1.80 – 1.59 (m, 2H), 1.26 (dd, *J*=8.2, 6.1 Hz, 3H).
^{13}C NMR (300 MHz, $CDCl_3$) δ (ppm) = 172.9, 146.4, 125.7, 120.0, 115.9, 60.5, 49.8, 33.4, 29.6, 21.8, 14.2.
HRMS (ESI) calcd for $C_{11}H_{17}O_2N_3$ $[M+H]^+$: 223.13209 found: 223.13232

*6.3.2.5. Synthesis of ethyl 5-(4-(2-(hexylthio)ethyl)-1H-1,2,3-triazol-1-yl)pentanoate (**6a**)*

4 (1.82 g, 8.14 mmol),1-hexanthiol (1.38 mL, 9.76 mmol) and AIBN (0.67 g, 4.07 mmol) were dissolved in choroform (25 mL) and refluxed. The reaction was monitored by ^{1}H NMR. After 2 hours, complete conversion of **4** was observed and the reaction was stopped. The crude mixture was then purified by flash chromatography (Hexan/EtOAc 7:3) to yield **5** as a yellow oil (75% yield).
EA calcd for for $C_{17}H_{31}O_2N_3S$: C (59.79) H(9.15) N(12.30) S(9.39); found: C(59.21) H(9.54) N(12.66) S(9.57)
^{1}H NMR (300 MHz, $CDCl_3$) δ (ppm) = 7.40 (s, 1H), 4.36 (t, J = 7.1 Hz, 2H), 4.15 (q, J = 7.1 Hz, 2H), 3.02 (t, J = 7.4 Hz, 2H), 2.86 (t, J = 7.4 Hz, 2H), 2.55 (t, J = 7.4 Hz, 2H), 2.36 (t, J = 7.2 Hz, 2H), 1.96 (m, 2H), 1.77 – 1.50 (m, 4H), 1.48 – 1.05 (m, 11H), 0.91 (t, J = 6.6 Hz, 3H).
^{13}C NMR (300 MHz, $CDCl_3$) δ (ppm) = 172.9, 146.4, 121.1, 60.5, 49.8, 33.4, 32.2, 31.7, 31.4, 29.6, 28.6, 26.3, 22.5, 22.5, 21.8, 14.2, 14.0.
HRMS (ESI) calcd for $C_{17}H_{31}O_2N_3S$ $[M+H]^+$: 341.21371 found: 341.21354

*6.3.2.6. Synthesis of 5-(4-(2-(hexylthio)ethyl)-1H-1,2,3-triazol-1-yl)pentanoic acid (**6b**) and sodium 5-(4-(2-(hexylthio)ethyl)-1H-1,2,3-triazol-1-yl)pentanoate (**6c**)*

Ethyl ester **6a** (0.90 g, 2.67 mmol) was dissolved in EtOH (6 mL) and a solution of NaOH (0.20 g, 5 mmol) and H_2O (4 mL) was added and the reaction was allowed to gently stir for 16 hours at room

temperature. At the end of this period, EtOH was removed under vacuo and aqueous layer was diluted with HCl 1 M (25 mL) and extracted with CH_2Cl_2 (15 mL x 3). Organic solutions were dried over $MgSO_4$, filtered and concentrated to yield **6b** as a white solid (99% yield).

EA calcd for for $C_{15}H_{26}O_2N_3S$: C (57.66) H(8.39) N(13.45) S(10.26); found: C(57.11) H(8.54) N(13.54) S(10.56)

^{1}H NMR (300 MHz, $CDCl_3$) δ (ppm) 10.51 (bs, 1H), 7.43 (s, 1H), 4.34 (t, *J* = 7.0 Hz, 2H), 2.99 (t, *J* = 7.2 Hz, 2H), 2.81 (s, 2H), 2.50 (t, *J* = 7.4 Hz, 2H), 2.38 (t, *J* = 7.2 Hz, 2H), 2.05 – 1.87 (m, 2H), 1.60 (m, 4H), 1.43 – 1.18 (m, 9H), 0.85 (t, *J* = 6.7 Hz, 3H).

^{13}C NMR (300 MHz, $CDCl_3$) δ (ppm) = 178.4, 130.7, 121.9, 52.1, 33.4, 32.2, 31.7, 31.4, 29.6, 28.6, 26.3, 22.5, 22.5, 21.8, 14.2.

HRMS (ESI) calcd for $C_{15}H_{26}O_2N_3S$ $[M+H]^+$: 312.17458 found: **312.17323**

An aqueous solution of NaOH 1M (10 mL) was added to a round bottom flask containing carboxyl ligand **6b** (**6b**/NaOH=1:1) The heterogenous mixture was allowed to vigorously stir for 2 hours until an homogenous colourless solution was obtained. Evaporating water under vacuo allowed to obtained **6c** as a white solid with quantitative yield.

EA calcd for for $C_{15}H_{25}O_2N_3SNa$: C (53.87) H(7.53) N(12.56) S(9.59); found: C(54.11) H(7.34) N(13.12) S(9.78)

(300 MHz, $CDCl_3$) δ (ppm) 10.51 (bs, 1H), 7.43 (s, 1H), 4.34 (t, *J* = 7.0 Hz, 2H), 2.99 (t, *J* = 7.2 Hz, 2H), 2.81 (s, 2H), 2.50 (t, *J* = 7.4 Hz, 2H), 2.38 (t, *J* = 7.2 Hz, 2H), 2.05 – 1.87 (m, 2H), 1.60 (m, 4H), 1.43 – 1.18 (m, 9H), 0.85 (t, *J* = 6.7 Hz, 3H).

^{13}C NMR (300 MHz, $CDCl_3$) δ (ppm) = 178.4, 130.7, 121.9, 52.1, 33.4, 32.2, 31.7, 31.4, 29.6, 28.6, 26.3, 22.5, 22.5, 21.8, 14.2,

HRMS (ESI) calcd for $C_{15}H_{26}O_2N_3S$ $[M+H]^+$: 312.17458 found: **312.17323**

6.3.3 Generic procedure for catalytic hydrogenations

Hydrogenation reactions were performed in 50 mL glass reactor equipped with magnetic a stirring bar and a pierced septum purged with N_2. $[Ir(\eta^4\text{-COD})Cl]_2$, the ligand, solvents, dodecane and substrates were added in this order in the glass reactor under a stream of N_2. The glass reactor was then transferred in a pre- purged 150 mL stainless steel autoclave which was the sealed. The autoclave was purged with 3 cycles of N_2 followed by 3 cycles of H_2, pressurized with hydrogen to the desired pressure and then heated to the desired temperature. After the required time, the autoclave was cooled to room temperature, depressurized and the glass reactor was carefully took out.

Afterwards, the extracting solvent was added and the organics were removed, dried over anhydrous $MgSO_4$ and filtered. A sample was taken and analysed by GC.

6.4 CONCLUSIONS

In conclusion, this work presents preliminary results concerning the use of an efficient catalytic system for the selective hydrogenation of carbonyl compounds. $[Ir(\eta^4\text{-COD})Cl]_2$ in combination with a *click* based triazole-thioether ligand **6a-c** showed to be active for the reduction of biomass derived platform chemicals. As a matter of fact, FUR has been hydrogenated to FA at 80°C and 40 bar. Remarkable recyclability of the catalyst was achieved since no loss in activity was observed even after 4 recycles with ligand **6c**. The solvent mixture water/THF (1/1 vol/vol) gave the best results.

Reduction of LA to GVL required harsher condition to reach good conversions, as 86% GVL yield were achieved at 100 °C and 60 bar. However, also in this case the catalytic system showed good performances when recycled. Notably, when run in only water as reaction solvent activity did not decrease.

Finally, CIN was choose as target substrate to verify the performances of the catalytic system for the reduction of αβ-unsaturated aldehyde. Quantitative conversions were achieved at mild reaction conditions (40 °C and 60 bar) matching a good selectivity towards cinnamyl alcohol (86%). Also in this case, the use of water did not slowed the reaction, affording similar yields.

6.5 REFERENCES

[1] P. H. Dixneuf, V. Cadierno, Eds. , *Metal-Catalyzed Reactions in Water*, Wiley-VCH Verlag, Weinheim, Germany, 2013.

[2] B. Cornils, W. A. Herrmann, *Aqueous-Phase Organometallic Catalysis Edited By*, Wiley-VCH Verlag, Weinheim, Germany, 2004.

[3] D. J. Cole-Hamilton, *Science (80-.).* 2003, *299*, 1702–1706.

[4] B. Cornils, *J. Mol. Catal. A Chem.* 1999, *143*, 1–10.

[5] B. Cornils, W. A. Herrmann, J. Horvat, W. Leitner, S. Mecking, H. Olivier-Bourbigou, D. Vogt, Eds. , *Multiphase Homogenous Catalysis*, Wiley-VCH Verlag GmbH & Co. KGaA, Weinheim, Germany, 2005.

[6] C. L. Young, Ed. , *Hydrogen and Deuterium: Solubility Data Series*, Pergamon Press, 1983.

[7] P. T. Anastas, J. C. Warner, Eds. , *Green Chemistry: Theory and Practice*, Oxford Univ Pr, 1998.

[8] N. Zhang, F. Li, Q. jia Fu, S. C. Tsang, *React. Kinet. Catal. Lett.* 2000, *71*, 393–404.

[9] J. Steinreiber, T. R. Ward, *Coord. Chem. Rev.* 2008, *252*, 751–766.

[10] M. Marchetti, F. Minello, S. Paganelli, O. Piccolo, *Appl. Catal. A Gen.* 2010, *373*, 76–80.

[11] C. Bertucci, C. Botteghi, D. Giunta, M. Marchetti, S. Paganelli, *Adv. Synth. Catal.* 2002, *344*, 556–562.

[12] S. Di Dio, M. Marchetti, S. Paganelli, O. Piccolo, *Appl. Catal. A Gen.* 2011, *399*, 205–210.

[13] K. Takizawa, H. Nulwala, R. J. Thibault, P. Lowenhielm, K. Yoshinaga, K. L. Wooley, C. J. Hawker, *J. Polym. Sci. Part A Polym. Chem.* 2008, *46*, 2897–2912.

[14] G. Amenuvor, B. C. E. Makhubela, J. Darkwa, *ACS Sustain. Chem. Eng.* 2016, *4*, 6010–6018.

[15] F. D. Pileidis, M. M. Titirici, *ChemSusChem* 2016, *9*, 562–582.

[16] Z. Zhang, *ChemSusChem* 2016, *9*, 156–171.

[17] K. Yan, Y. Yang, J. Chai, Y. Lu, *Appl. Catal. B Environ.* 2015, *179*, 292–304.

[18] F. Liguori, C. Moreno-Marrodan, P. Barbaro, *ACS Catal.* 2015, *5*, 1882–1894.

[19] M. Chalid, A. A. Broekhuis, H. J. Heeres, *J. Mol. Catal. A Chem.* 2011, *341*, 14–21.

[20] J. Deng, Y. Wang, T. Pan, Q. Xu, Q. X. Guo, Y. Fu, *ChemSusChem* 2013, *6*, 1163–1167.

[21] W. L. F. Armarego, Ed. , *Purification of Laboratory Chemicals*, 1996.

[22] R. Kolb, N. C. Bach, S. A. Sieber, *Chem. Commun.* 2014, *50*, 427–429.

7. CONCLUSIONS AND FINAL REMARKS

In this thesis work, novel solutions for the valorisation of biomass have been proposed.

In the first part, animal proteins recovered from the industrial tanning process have been selected as target biomass to be exploited. It has been shown that an enzymatic hydrolytic process allowed to obtain water soluble hydrolysed proteins (Bio-A) in the form of a fine yellowish powder, deeply characterized by means of GPC, FTIR and NMR analysis. Reaction of Bio-A with glycerol and maleic anhydride afforded the product Bio-IA *via* intermediate I1. The study highlights the crucial role of the reactants ratio in wt%, as glycerol/MA between 10/90 and 45/55 wt/wt%, gave very viscous mixtures. Thus, for all further tests a glycerol/MA ratio ≥50/50 wt/wt% was employed. With optimized conditions parameters in hand, a co-polymerization with acrylic acid led to the synthesis of Bio-Ac, with a molecular weight of 42.400 Da (Scheme 7.1). This biomass derived biopolymer showed interesting activities when used as retanning agent instead of common recipes making use of petrochemicals derived retanning agents, thus representing an eco-friendly product for the leather industry market.

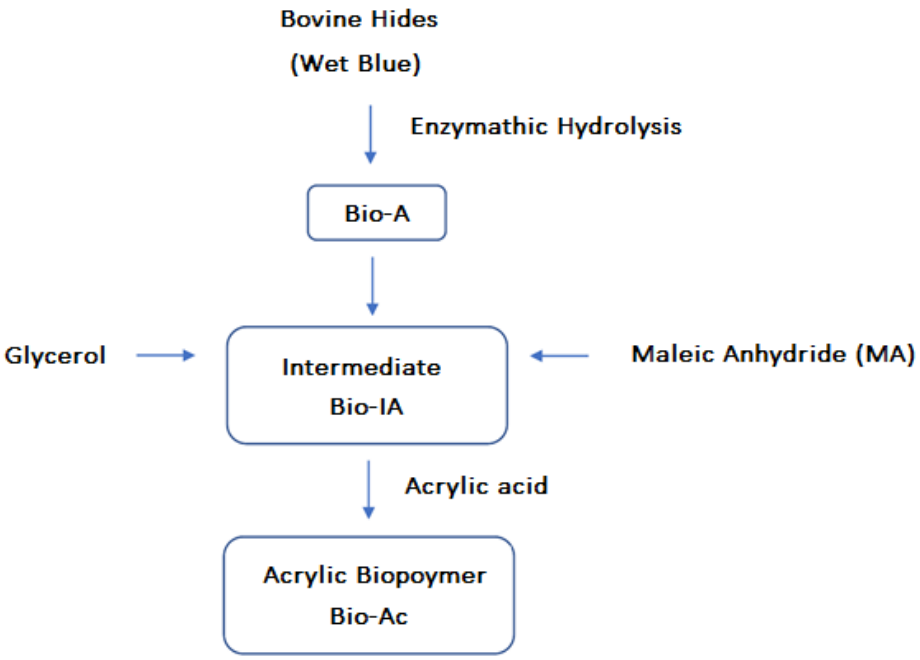

Scheme 7.1. Synthetic process for the synthesis of Bio-Ac

The second part of this thesis dealt with the valorisation of biomass derived platform chemicals. FUR, LA, 5-HMF and CIN have been considered as target reagents.

Initially, the synthesis of a novel class of palladium complexes bearing novel click based TryOX ligands was investigated (Scheme 7.2). While the synthesis of palladium allyl complexes Pd1a-c has been accomplished straightforwardly, with the ligand acting as NN bidentate ligands, few experiments were necessary to understand the coordination behaviour of the ligands when trying to obtain Pd(TryOx)Cl_2 bidentate species. In fact, only in one case the formation of bidentate Pd2d complex was confirmed by X-ray analysis. Otherwise, dimeric or mononunclear palladium complexes were obtained, with the ligands behaving as monodentate. Stimulated by the lack in literature of palladium complexes used for the hydro sults, especially when the allyl complexes wer

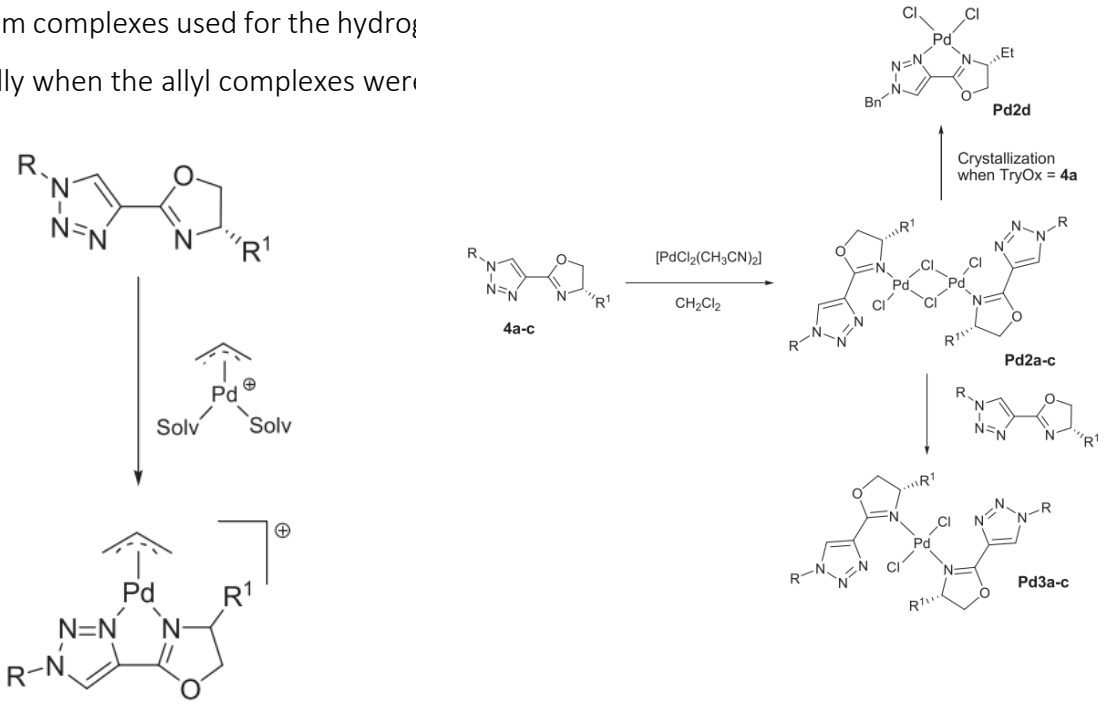

Scheme 7.2. Synthesis of complexes Pd1a-c, Pd2a-c, Pd3a-c, Pd4a

The hydrogenation of FUR and 5-HMF has been taken into account when a novel class of ruthenium complexes bearing NNN click based ligands have been synthetized (Scheme 7.3). While FA was obtained with 97% yield, 5-HMF was converted into BHMF with moderate yield (52%). The reason of this low activity must be sought in the easy formation of humins when HMF is heated. Complexes synthetized showed a remarkable activity for aldehydes and ketones hydrogenation.

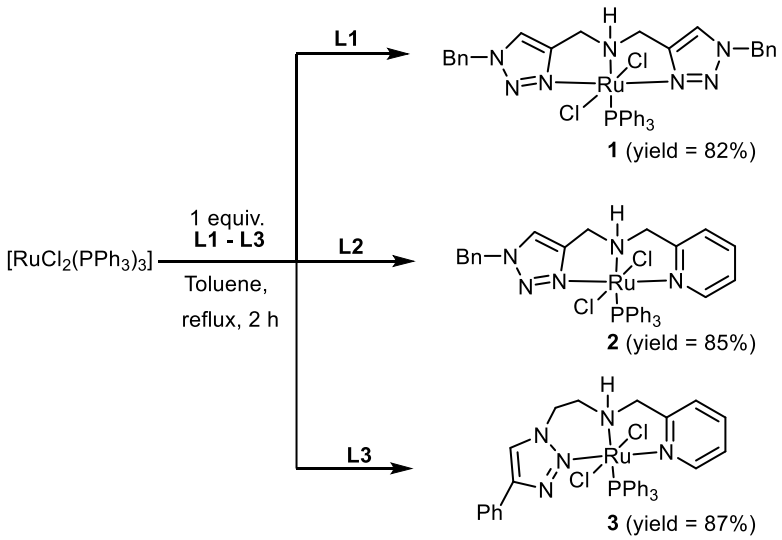

Scheme 7.3. Synthesis of $[RuCl_2(NNN)(PPh_3)]$ complexes **1–3**.

Finally, a catalytic system obtained by $[Ir(COD)Cl]_2$/NS ligands (**Figure 7.1**) were used for the hydrogenation in aqueous media of FUR, LA and CIN. Hydrogenation of FUR to FA showed interesting activity of the catalytic system, as FUR was hydrogenated to FA at 80°C and 40 bar. Remarkable recyclability of the catalyst was achieved since no loss in activity was observed after 5 runs. The solvent mixture water/THF (1/1 vol/vol) revealed to be the most efficient. Reduction of LA to GVL required harsher condition to reach good conversions, as 86% GVL yield were achieved at 100 °C and 60 bar. However, also in this case the catalytic system showed good performances when recycled. Notably, when the reaction is run only in water as solvent, activity didn't decrease. Finally, CIN was choose as target substrate to verify the performances of the catalytic system for the reduction of α,β-unsaturated aldehyde. Quantitative conversions were achieved at mild reaction conditions (40 °C and 60 bar) matching a good selectivity towards cinnamyl alcohol (86%). Also in this case, the use of water didn't slow the reaction, affording similar yields.

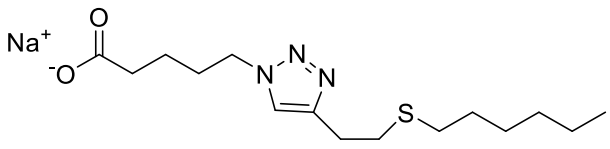

Figure 7.1. NS ligand

Summing up, we believe that this thesis describes a spectrum of innovative solutions for the valorisation of biomass derived compounds. Further studies will implement the quality of the data reported.

8.1. BIOMASS DERIVED BIOPOLYMERS FOR ECOFRIENDLY LEATHER

8.1.1. ^{1}H NMR

Bio-A

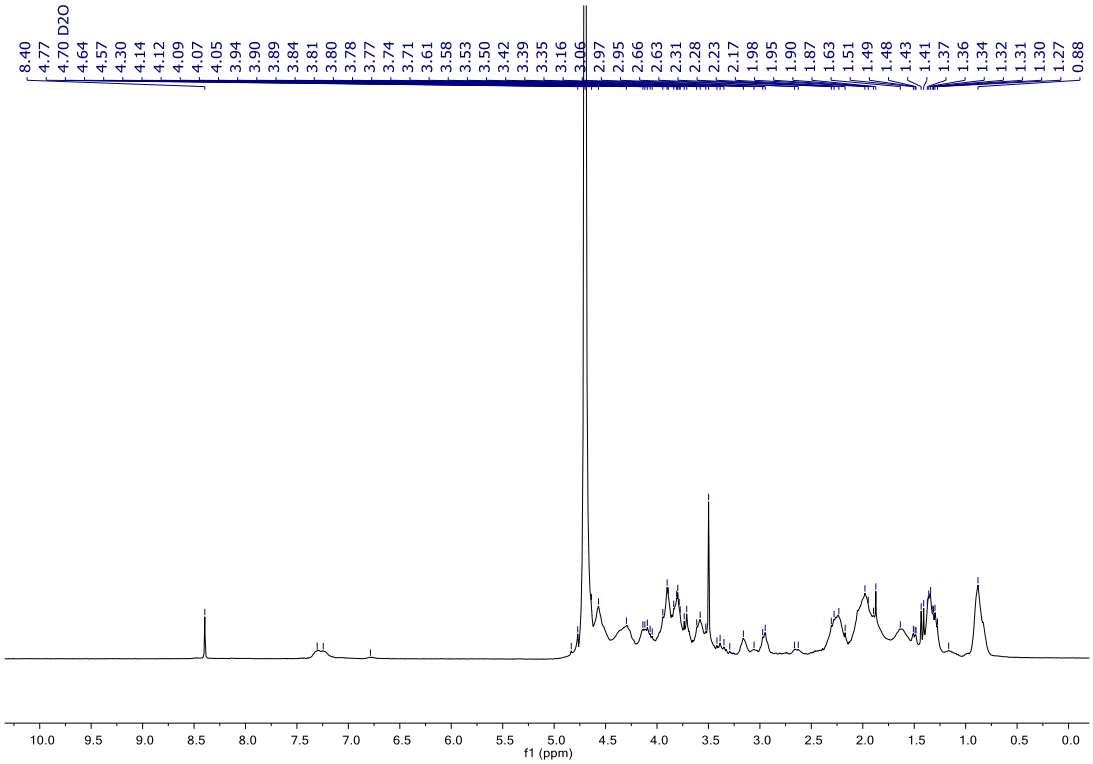

BIO-IA

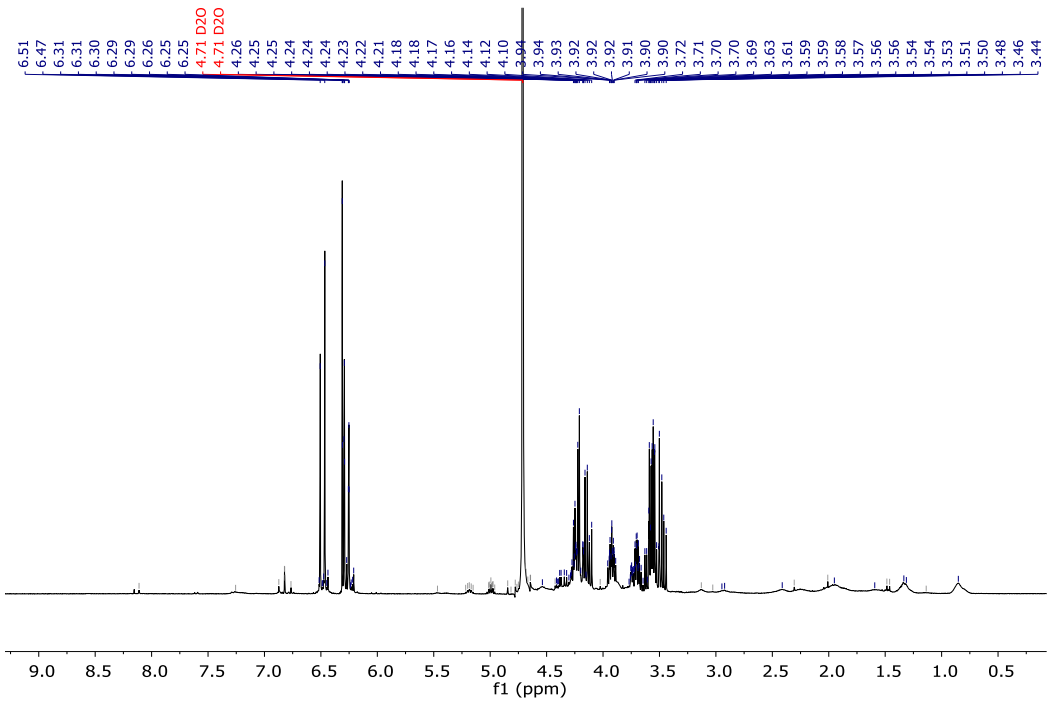

BIO-Ac

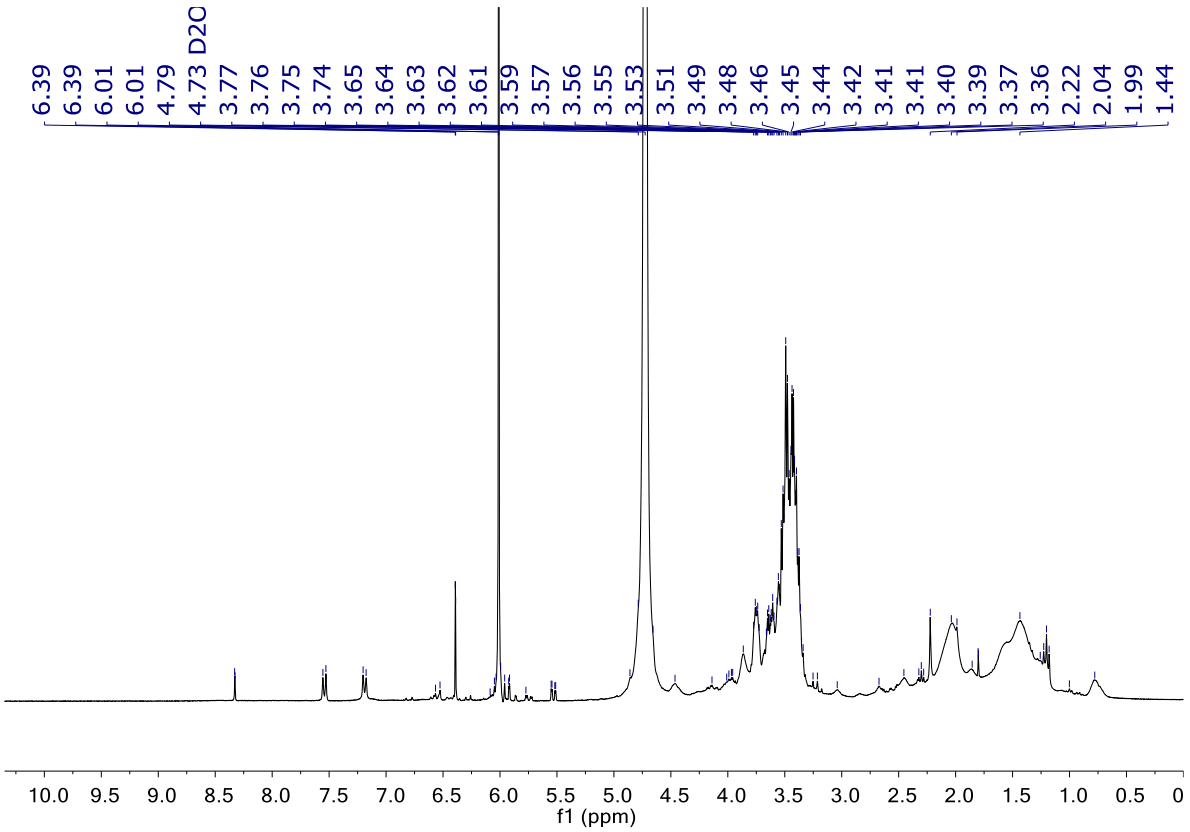

8.1.2 GPC

BIO-A

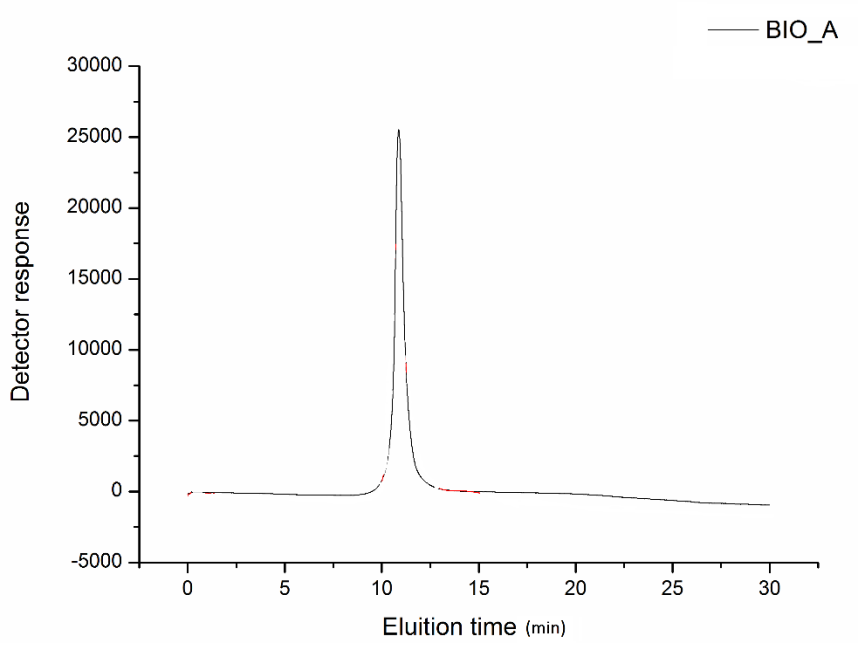

BIO-Ac

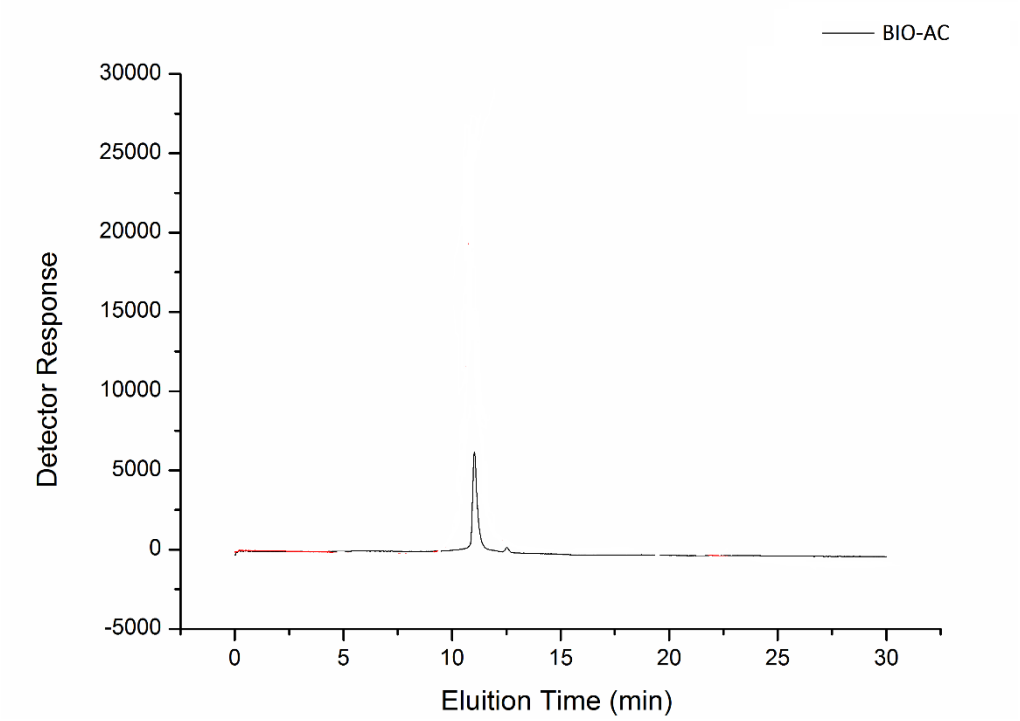
BIO-AC
Detector Response
30000
25000
20000
15000
10000
5000
0
-5000
0
5
10
15
20
25
30
Eluition Time (min)

8.2 SYNTHESIS, CHARACTERIZATION AND CATALYTIC ACTIVITY OF NEW TRIAZOLYL-OXAZOLINE CHIRAL LIGANDS COORDINATED TO PD(II) METAL CENTERS

8.2.1 NMR Characterization of ligands (4a-c)

*1-Benzyl-((S)-4-ethyl-4,5-dihydrooxazol-2-yl)-1H-[1,2,3]-triazole(**4a**)*

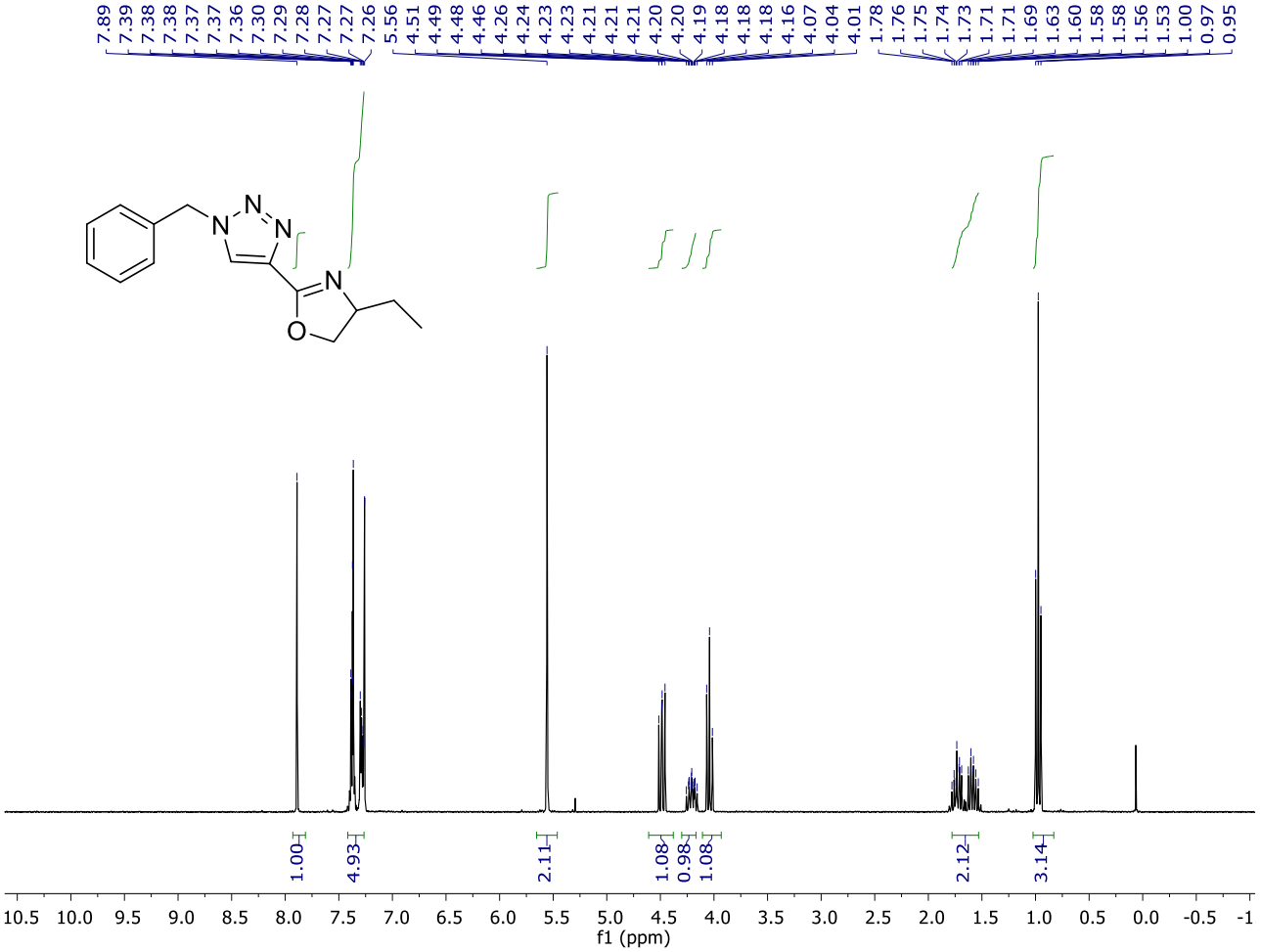

^{1}H NMR ($CDCl_3$, 298 K) δ: 7.89 (s, 1H, C***H***$_{triaz.}$), 7.40–7.25 (m, 5H, ***H***$_{arom.}$), 5.55 (s, 2H, C***H*****$_{2benz.}$**). 4.49 (dd, 1H, $^{2}J_{HH}$ = 9.3,$^{3}J_{HH}$ = 8.1 Hz, C***H***$_{2oxaz.}$), 4.16–4.26 (m, 1H, C***H***$_{oxaz.}$), 4.02–4.07(m, 1H, C***H***$_{2oxaz.}$), 1.51–1.58 (m, 2H, C***H*****$_{2Ethyl}$**), 0.98 (t, 3H, $^{2}J_{HH}$ = 7.4 Hz, C***H*****$_{3Ethyl}$**).

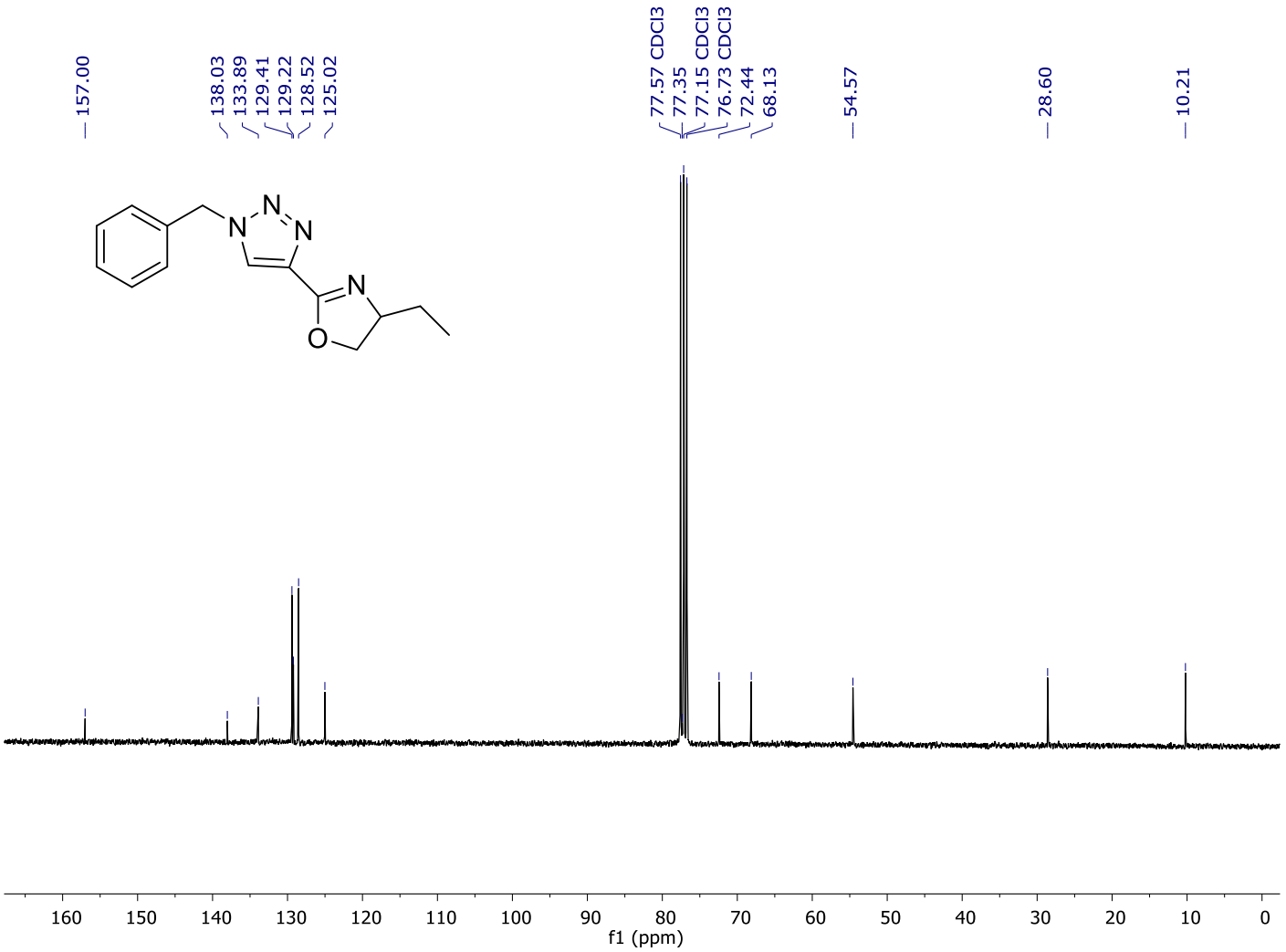

^{13}C NMR ($CDCl_3$, 298 K) δ: 157.0 (***C***=N), 138.0 ($\boldsymbol{C}_{(IV)Triaz.}$), 133.92 ($\boldsymbol{C}_{(IV)Ph}$), 128.5-129.2-129.2 (5$\boldsymbol{C}_{arom.}$)m, 124.9 ($\boldsymbol{C}_{Triaz.}$) 72.5 ($\boldsymbol{C}H_{2\ Oxaz.}$), 68.1 ($\boldsymbol{C}H_{\ Oxaz.}$), 54.7 ($\boldsymbol{C}H_{2\ Benz.}$), 28.6 ($\boldsymbol{C}H_{2Ethyl}$), 10.2 ($\boldsymbol{C}H_{3Ethyl}$).

*1- tert-Butyl-4-((S)-1-4-isobutyl-4,5-dihydrooxazol-2-yl)-1H-1,2,3- triazole (**4b**)*

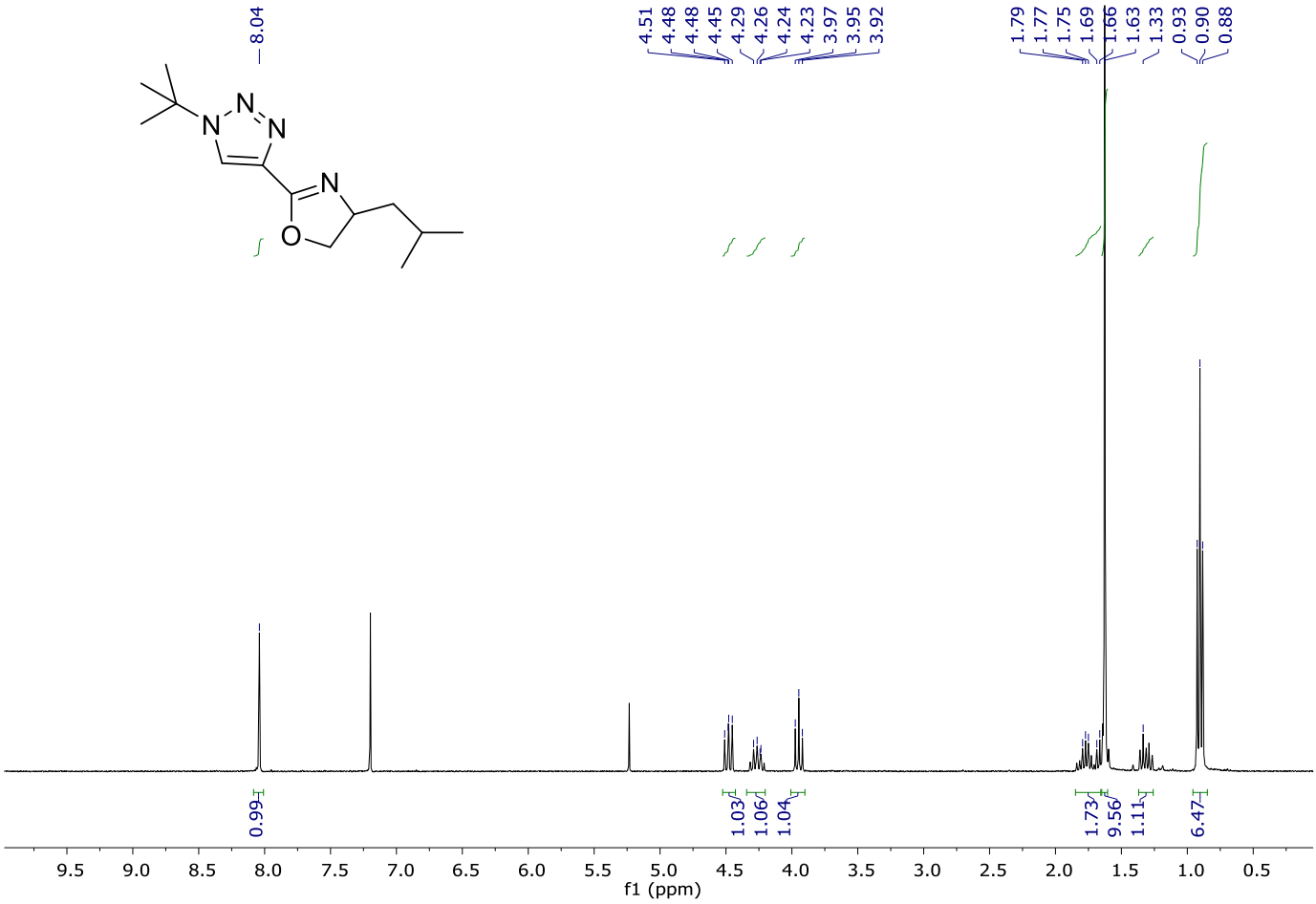

^{1}H NMR ($CDCl_3$, 298 K) δ: 8.04 (s, 1H, C***H***$_{Triaz}$), 4.47 (t, 1H, ^{2}J = 8.1 Hz, C***H***$_{2\ Oxaz.}$), 4.25 (m, 1H, C***H***$_{Oxaz.}$), 3.97 (t, 1H, ^{2}J =8.1 Hz, C***H***$_{2\ Oxaz.}$), 1.75 -1.62(m, 2H, C***H***$_{2\ Isobut.}$) 1.61 (s, 9H, (C***H***$_3$)$_{3\ t\text{-}buthyl.}$), 1.38 (m, 1H, C***H***$_{Isobut.}$), 0.89 (t, 6H, J =6.5 Hz, (C***H***$_3$)$_{2\ Isobuthyl}$).

*2-tert-butyl-4-((S)-4-tert-butyl-4,5-dihydrooxazol-2-yl) –1H- 1,2,3-triazole (**4c**)*

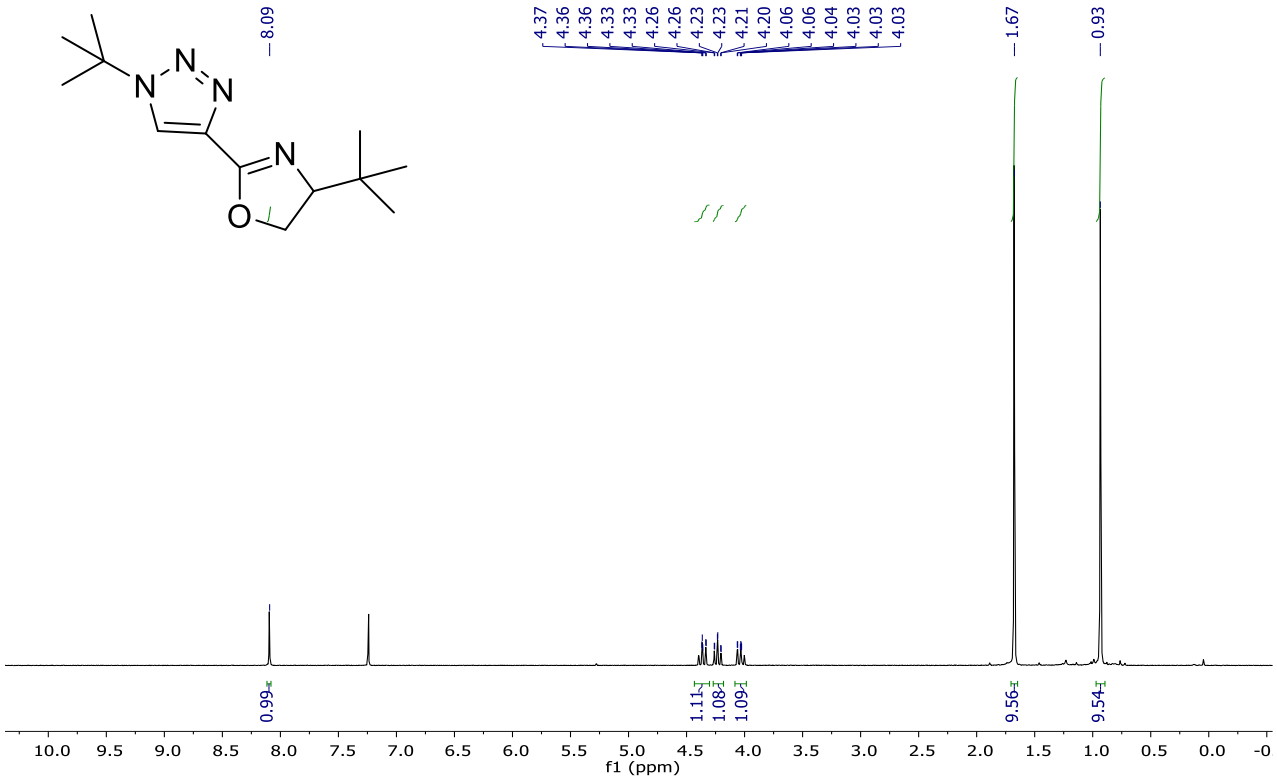

^{1}H NMR ($CDCl_3$, 298 K) δ: 8.09 (s, 1H, C***H***$_{triaz}$), 4.35 (t, 1H, $^{2}J_{HH}$ = 8.7 Hz), 4.22 (t, 1H, $^{2}J_{HH}$ = 8.4 Hz), 4.02 (t, 1H, $^{2}J_{HH}$ = 8.1 Hz), 1.67 (s, 9H), 0.93 (s, 9H).

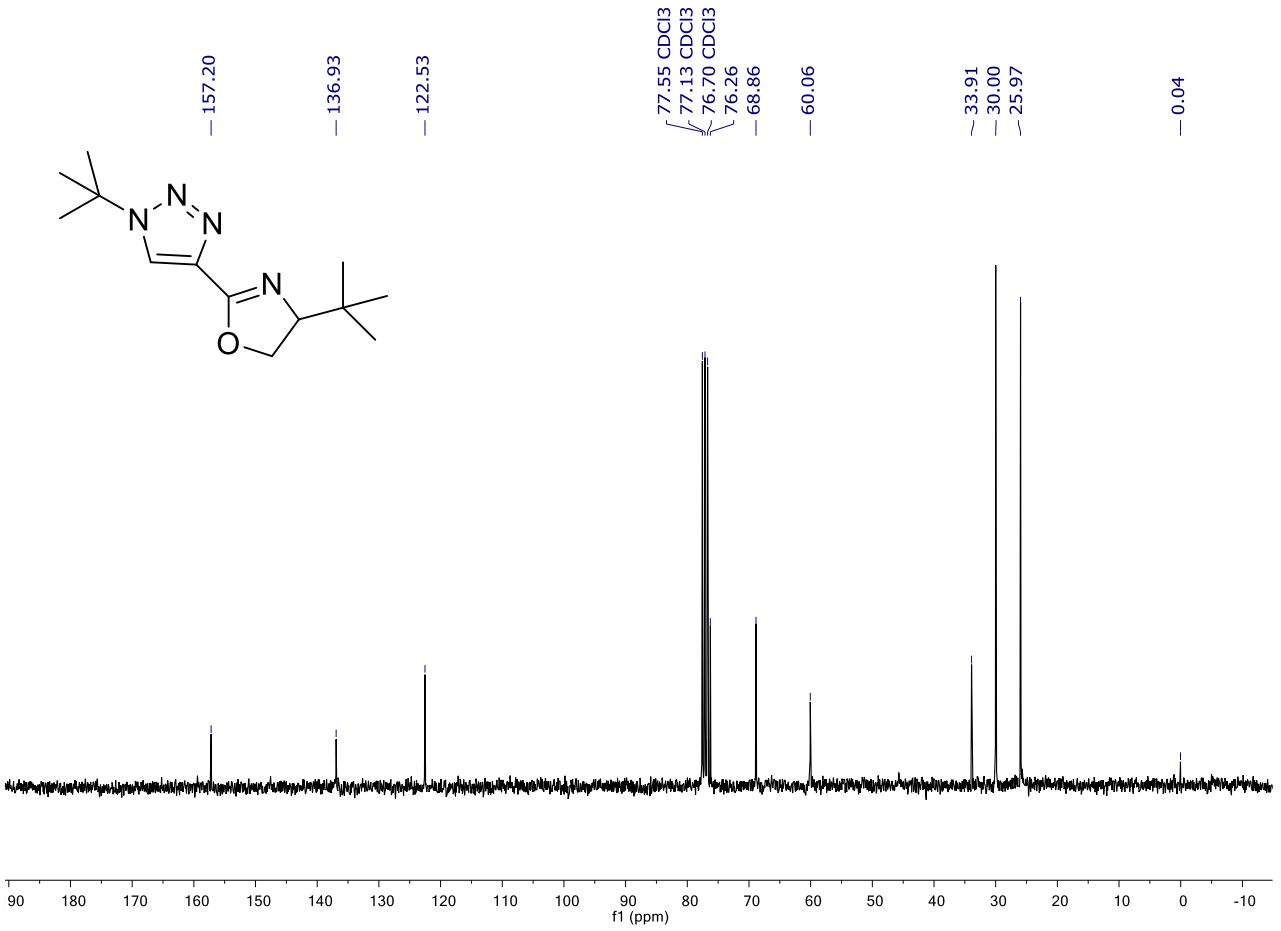

^{13}C NMR ($CDCl_3$, 298 K) δ: 157.2 (***C***=N), 137.0 ($\boldsymbol{C}_{(IV)Triaz.}$), 122.5 ($\boldsymbol{C}_{Triaz.}$), 76.3 ($\boldsymbol{C}H_{2\ Oxaz.}$), 68.9 ($\boldsymbol{C}H_{\ Oxaz.}$), 60.1 ($\boldsymbol{C}H_{\ Oxaz.}$), 34.0 ($\boldsymbol{C}_{(IV)}$), 30.1 ($\boldsymbol{C}H_3)_3$, 26.0 ($\boldsymbol{C}H_3)_3$.

8.2.2 NMR Characterization of allyl complexes (Pd1 a-c)

*[Pd(η³-C₃H₅)(4a)](ClO₄) (**Pd1a**)*

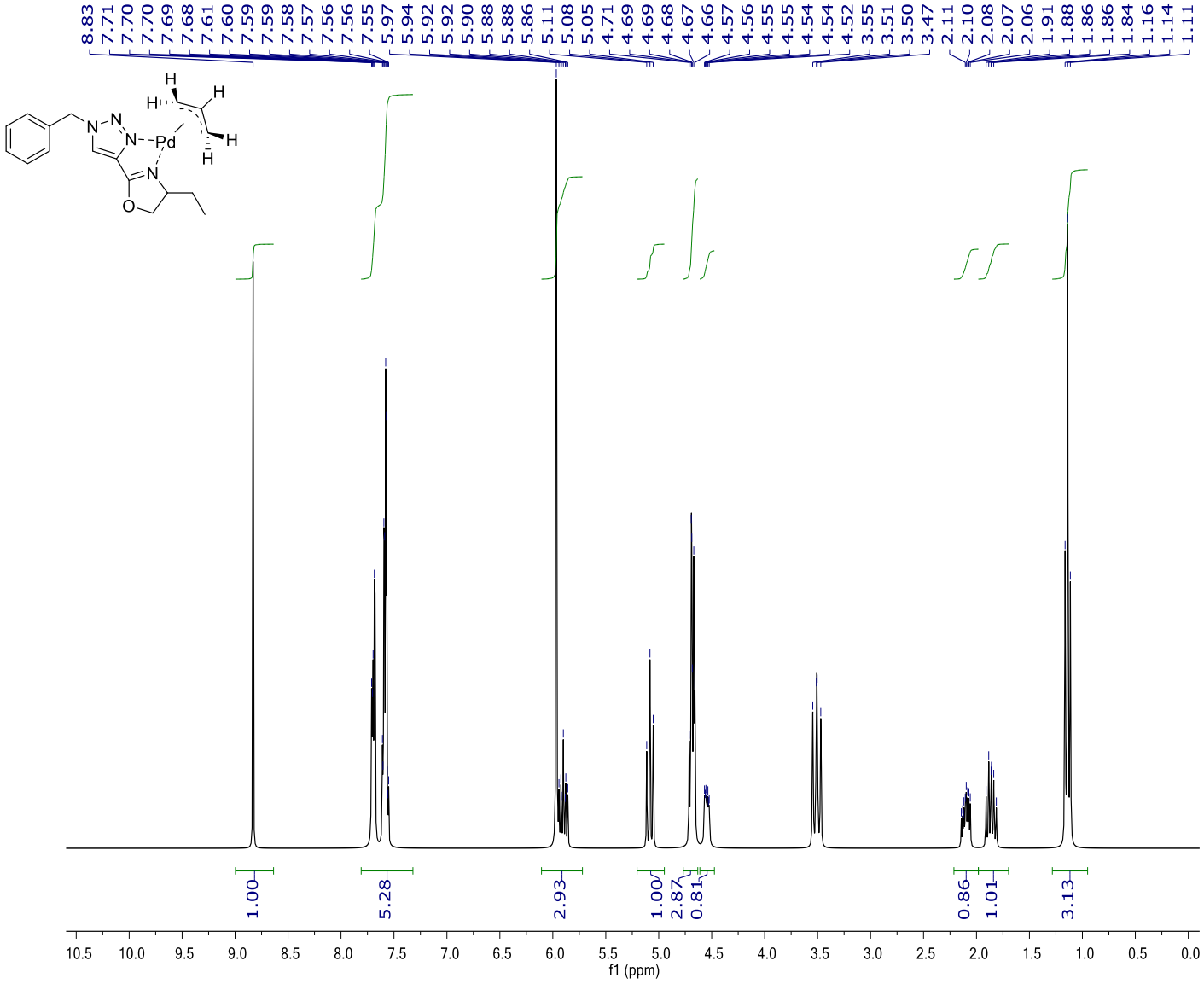

^{1}H NMR ($CDCl_3$, 298 K) δ: 8.83 (s, 1H, C***H***$_{triaz.}$), 7.42–7.36 (m, 5H, ***H*** arom.), 5.68 (s, 2H, C***H***$_2$), 5.66 (quintet, 1H, ^{3}J = 11.7 Hz, **allyl central**), 4.91–4.85 (t, 1H, C***H₂*** oxaz.), 4.61–4.47 (overlapping broad m, 3H, **allyl- syn** and C***H*** oxazoline), 3.38–3.16 (br m, 2H, **allyl-anti**), 1.82–1.64 (m, 2H), 0.93 (t, $^{2}J_{HH}$ =7.0 Hz, 3H).

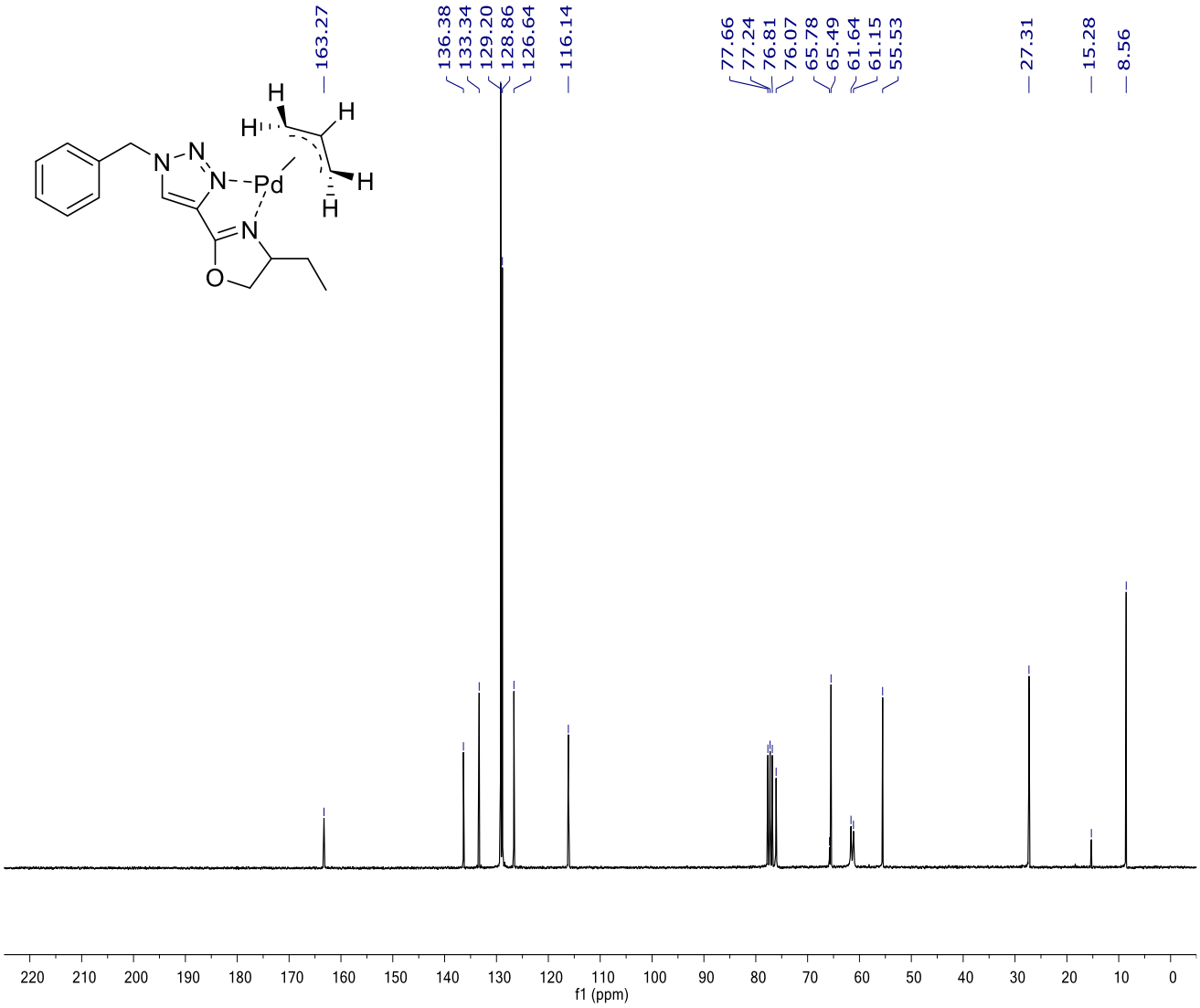

^{13}C NMR ($CDCl_3$, 298 K) δ: 163.2 (***C***=N), 136.4 (***C***$_{(IV)Triaz.}$), 133.4 (***C***$_{(IV)Ph}$), 129.4-129.2-128.4 (5***C***$_{arom.}$)126.7 (***C***$_{Triaz}$), 116.1 (1C, H***C***$_{allyl}$), 75.9 (***C***$H_{2\ Oxaz.}$), 65.5 (***C***$H_{\ Oxaz.}$), 62.5 (1C, H_2***C***$_{allyl\text{-}syn}$), 60.5 (1C, $H_2C_{allyl\text{-}anti}$), 55.5 (***C***$H_{2Benz.}$), 27.6 (***C***H_{2Ethyl}), 8.5 (***C***H_{3Ethyl}).

[Pd(η³-C₃H₅)(4c)](PF₆) (**Pd1c**)

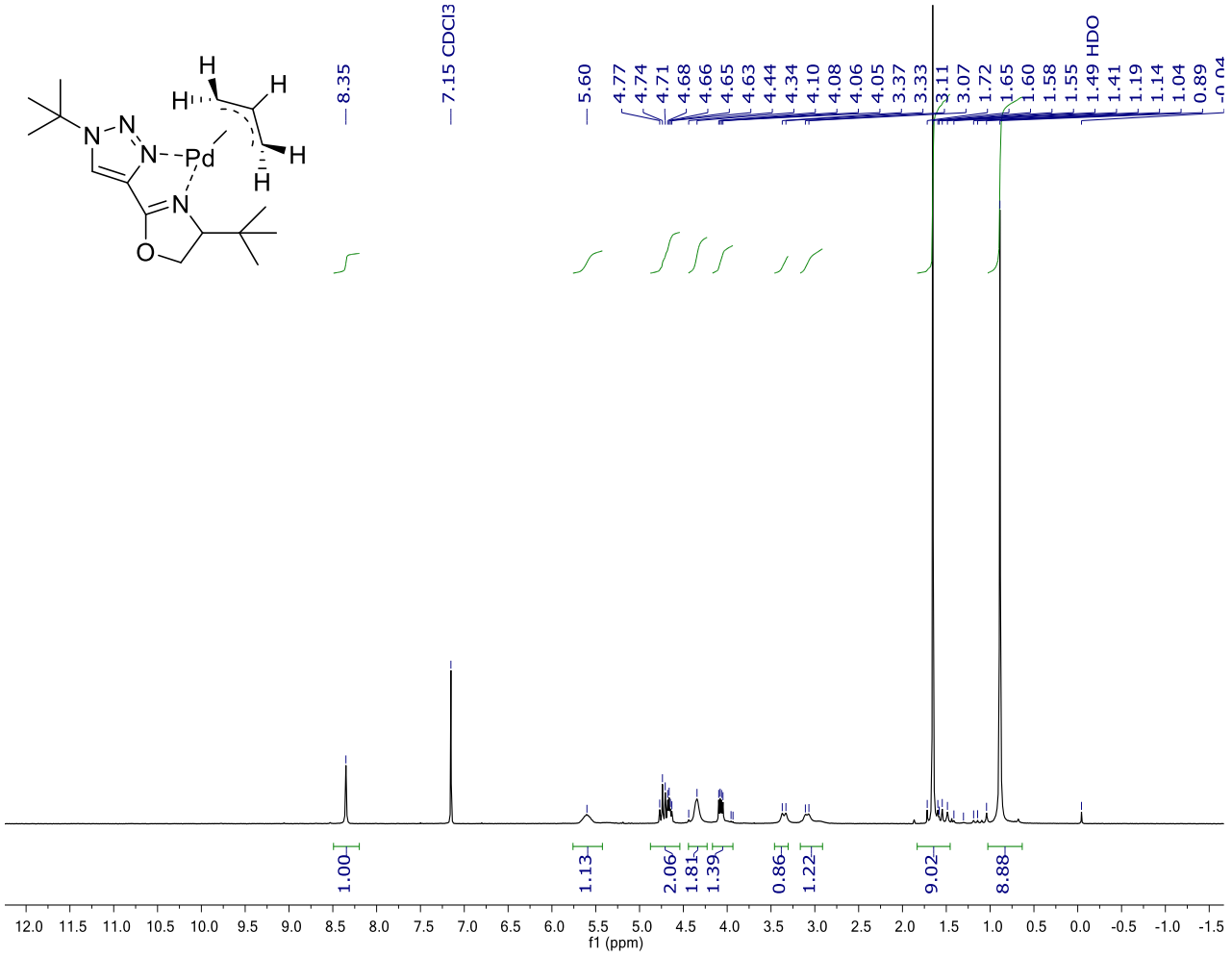

^{1}H NMR ($CDCl_3$, 298 K) δ: 8.35 (s, 1H, C***H***$_{triaz.}$), 5.66 (quintet, 1H, *J* = 6.5 Hz, **allyl central**), 4.92 (t, 1H, *J* =9.0 Hz), 4.44 (t, 1H, *J* =7.2 Hz), 4.40–4.25 (br overlapping m, 3H, **allyl-syn** and C***H***$_{Oxaz}$), 3.27 (br m, 2H, **allyl-anti**), 1.85–1.60 (m, 2H), 1.74 (s, 9H), 1.54–1.41(m, 1H), 0.96 (dd, 6H, *J* =10.6, 5.6 Hz).

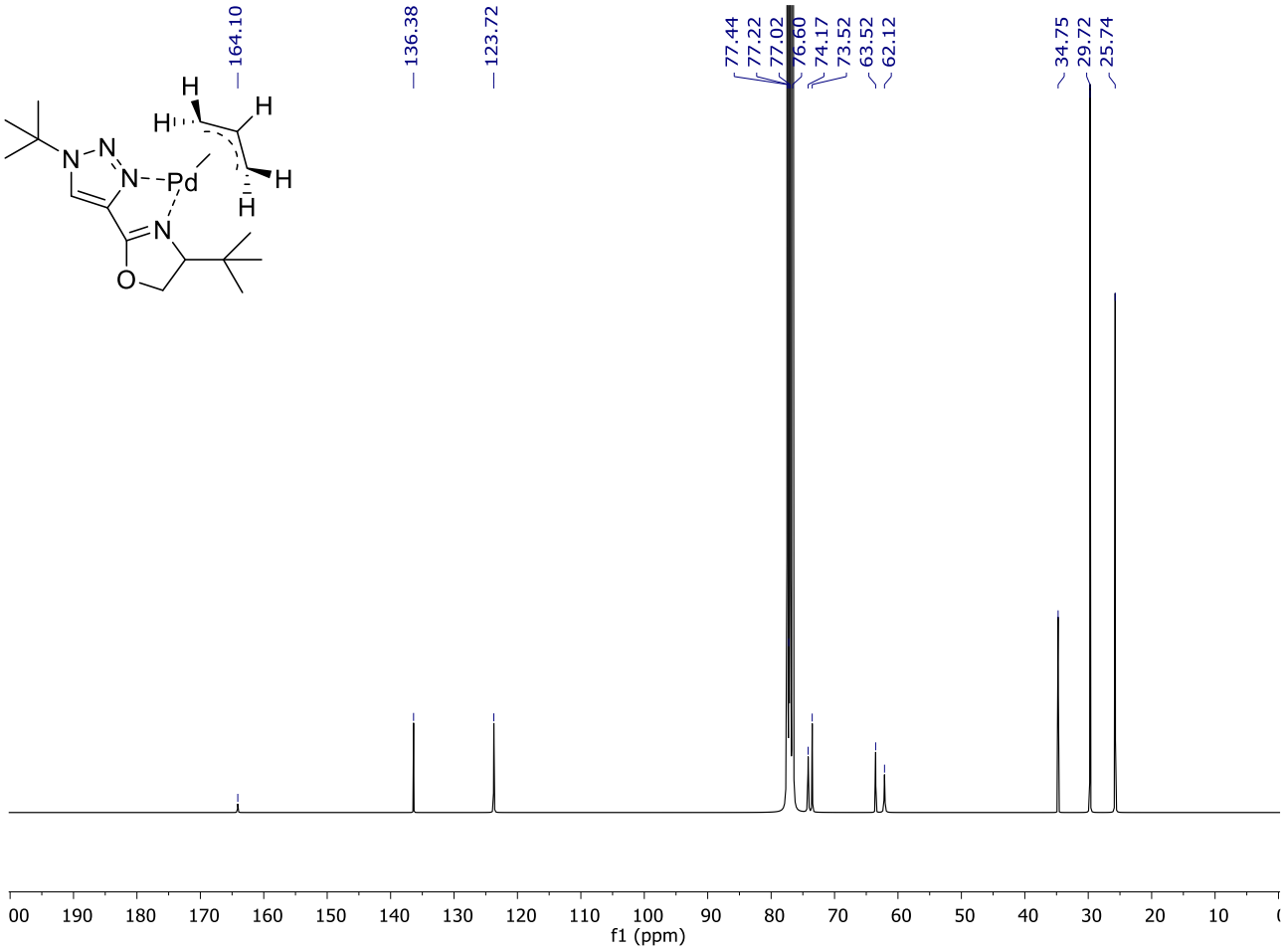

^{13}C NMR ($CDCl_3$, 298 K) δ: 164.0 (***C***=N), 136.3 (***C***$_{(IV)Triaz.}$), 123.8 (***C***$_{Triaz.}$), 115.7 (H***C***$_{allyl}$), 74.1 (), 73.5(), 63.5 (br, H_2***C***$_{allyl\text{-}syn}$), 62.1 (br, H_2***C***$_{allyl\text{-}anti}$), 34.7 (***C***$_{(IV)}$), 29.7 (***C***$H_3)_3$, 25.7, (***C***$H_3)_3$.

8.2.3 NMR Characterization of dimeric complexes (Pd2 a-c)

*[PdCl(μ-Cl)(4a)]$_2$ (**Pd2a**)*

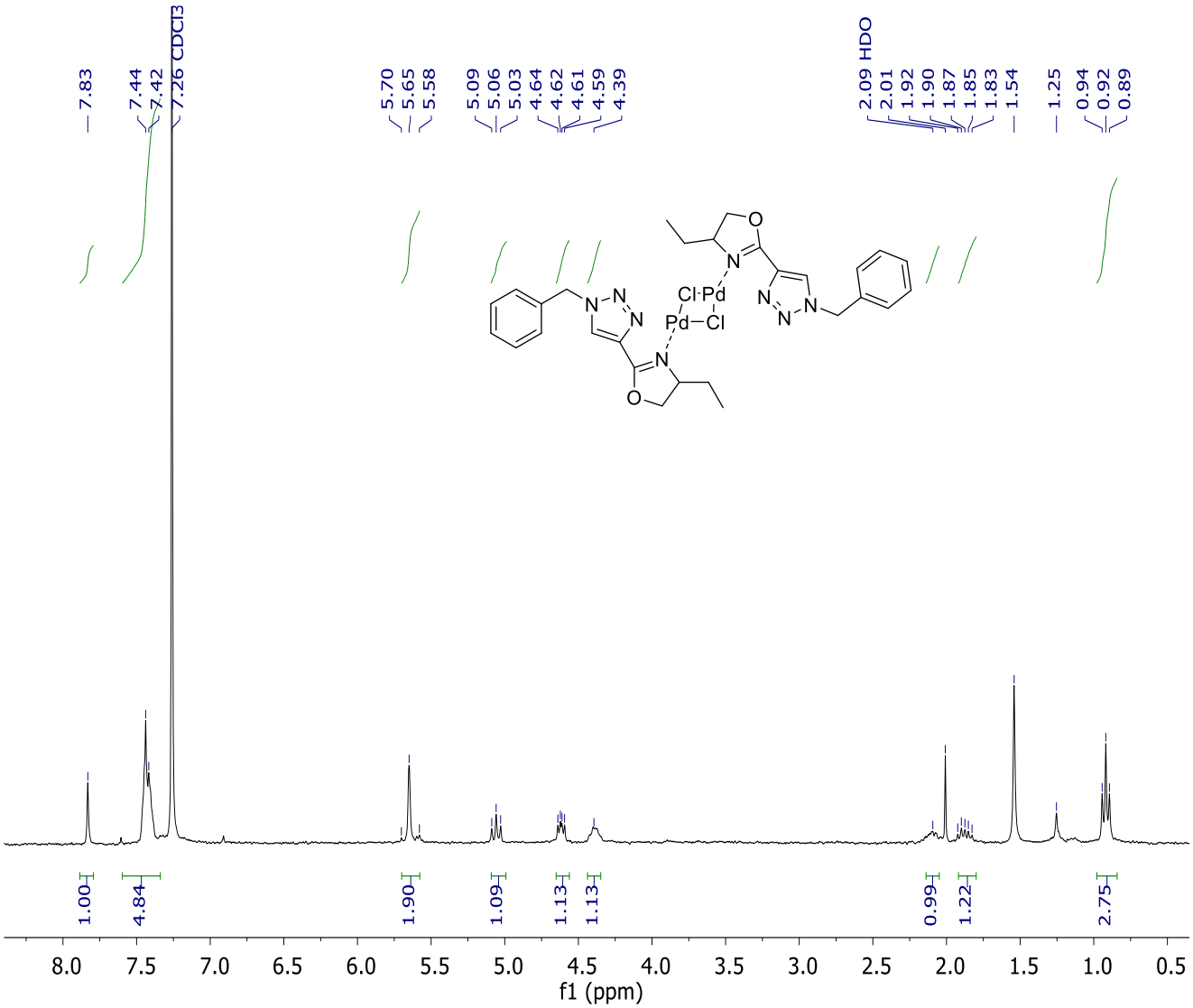

^{1}H NMR ($CDCl_3$, 298 K) δ: 7.84 (s, 1H, C***H***$_{triaz.}$), 7.48–7.37 (m, 5H, **H arom.**), 5.65 (d, 1H, *J* =15.0 Hz, ***HH***C), 5.62 (d, 1H, *J* =15.0 Hz, ***HH***C), 5.10 (t, 1H, *J* =9.1 Hz), 4.62 (dd, 1H, *J* =5.1, 8.3 Hz), 4.45–4.34 (br m, 1H), 2.17–2.00 (br m, 1H), 1.97–1.80 (m, 1H), 0.92 (t, 1H, *J* =7.2 Hz).

*[PdCl(μ-Cl)(4b)]$_2$ (**Pd2b**)*

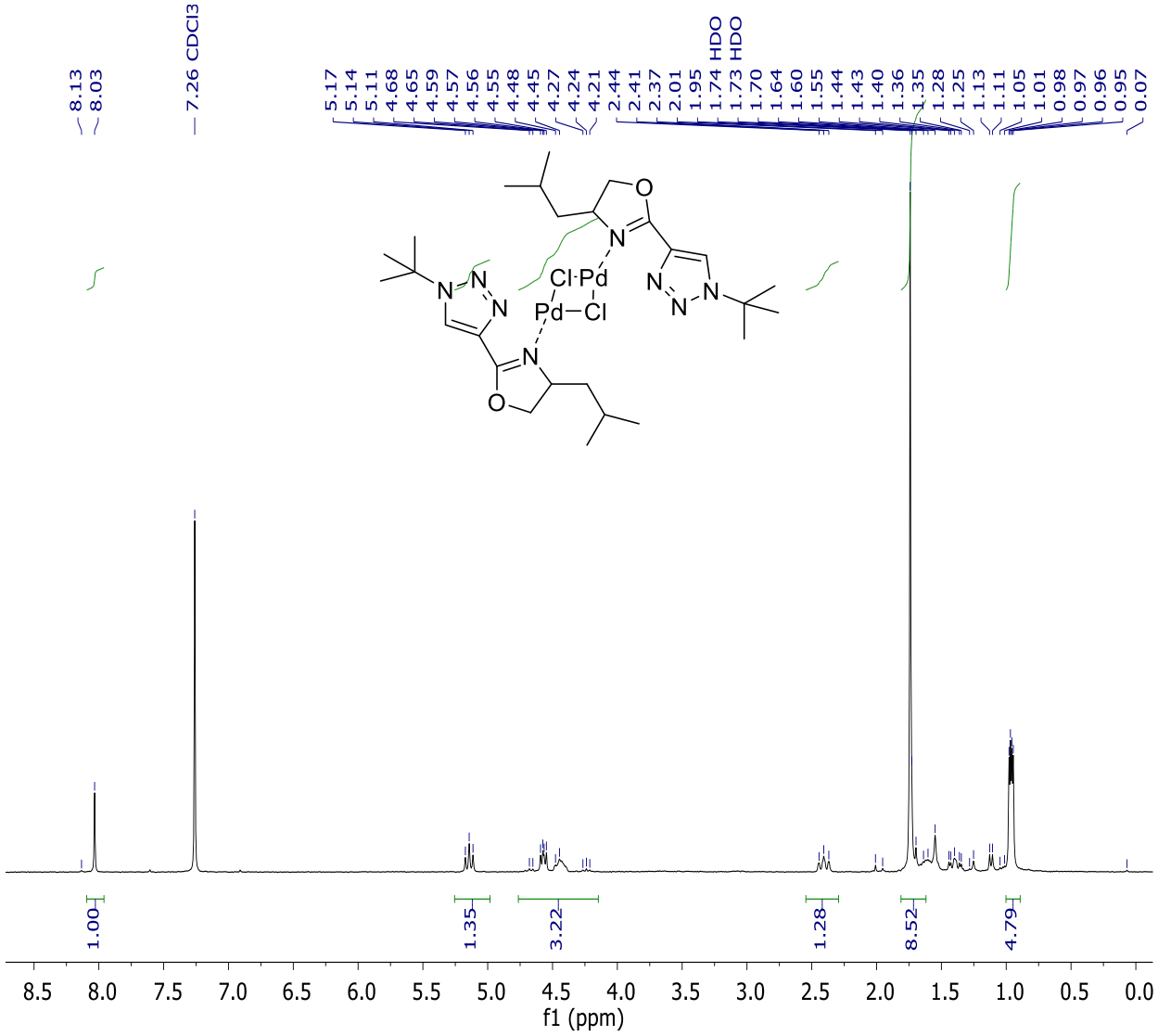

^{1}H NMR ($CDCl_3$, 298 K) δ: 8.08 (s, 1H, C***H***$_{Triaz.}$), 5.18 (t, 1H, *J* =8.8 Hz, C***H***$_{Oxazo.}$), 4.55 (t, 1H, *J* =8.4) 4.49–4.39 (m, 1H), 2.38 (t, 2H, *J* =13.0 Hz) 1.73 (s, 9H), 1.64–1.41 (m, 2H) 1.00–0.90 (m, 6H) .

*[PdCl(μ-Cl)(4c)]$_2$ (**Pd2c**)*

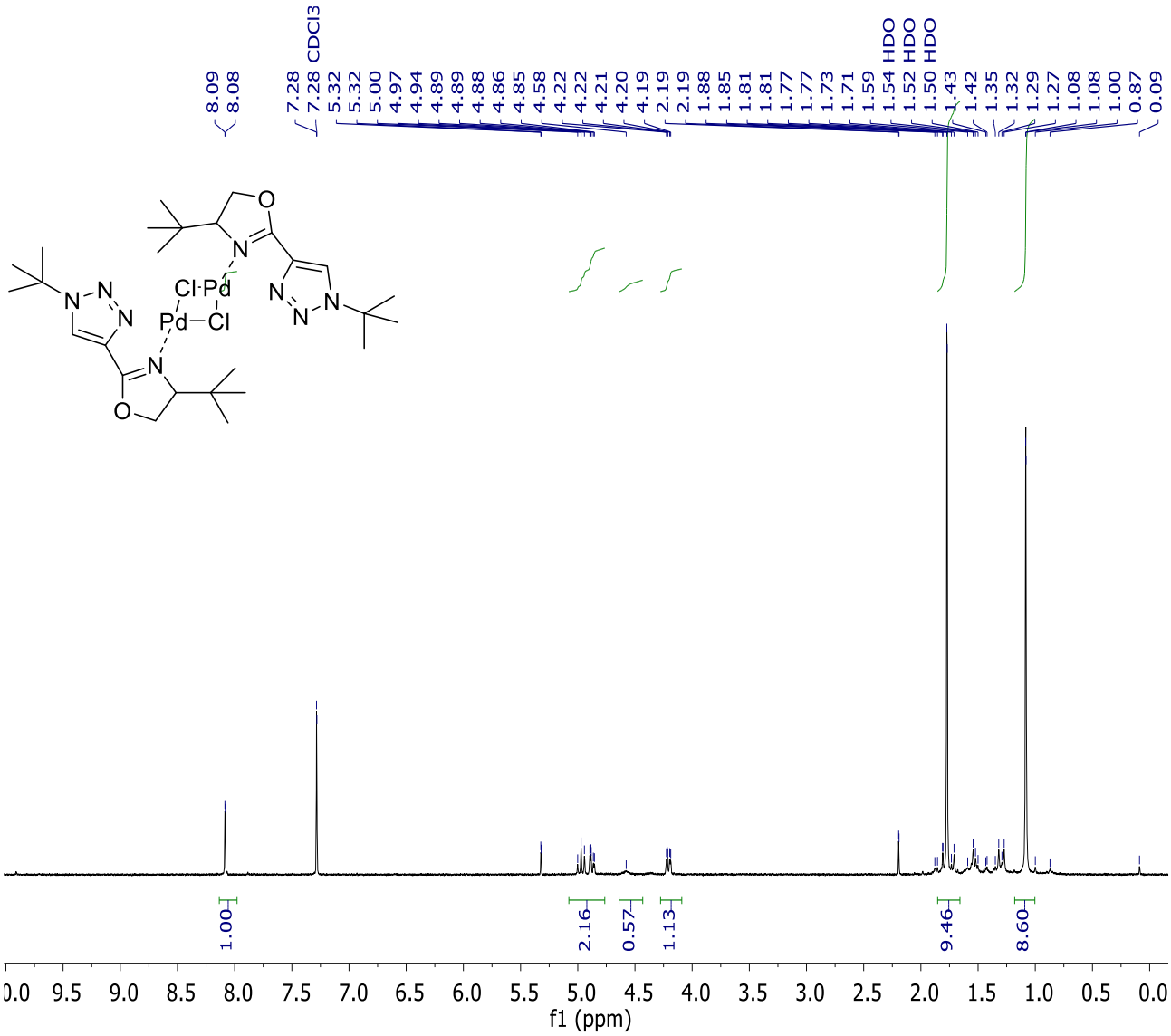

^{1}H NMR ($CDCl_3$, 298 K) δ: 9.85 (s, 1H), 4.63–4.47 (2 overlapping m, 2H), 4.34 (dd, J=9.7 and 5.8 Hz), 1.51 (s, 9H), 1.26 (s, 9H).

8.2.4 NMR Characterization of mononuclear complexes (Pd3 a-c)

*$[PdCl(\mu\text{-}Cl)(4a)]_2$ (**Pd3a**)*

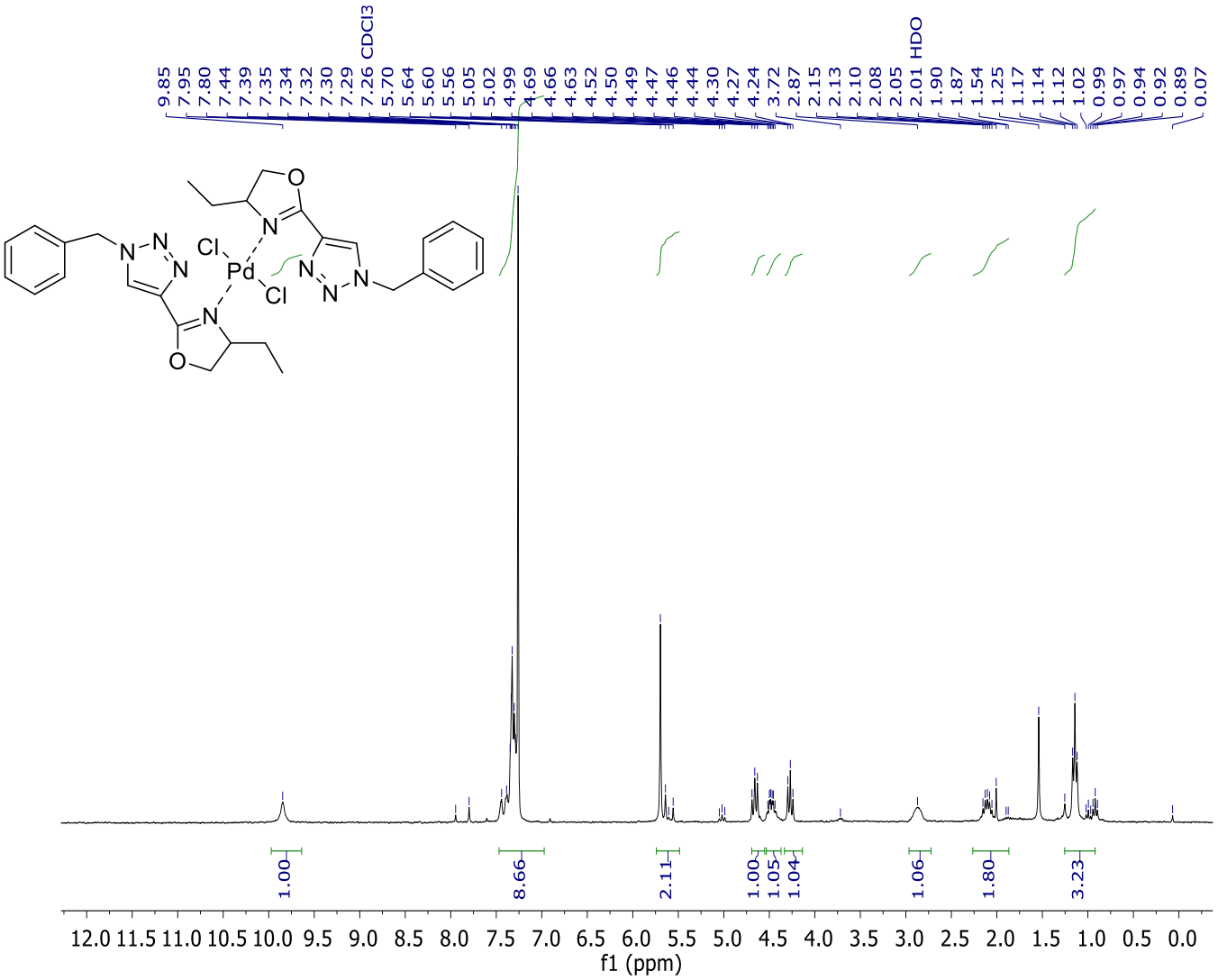

^{1}H NMR ($CDCl_3$, 298 K) δ: 9.85 (s, 1H, CH try), 7.51–7.27 (m, 5H,arom.), 5.70 (s, 1H, HHC), 4.65 (t, 1H, *J* =9.1 Hz), 4.48 (dd, 1H, *J* =3.8 and 9.1 Hz), 4.27(t, 1H, *J* =8.5 Hz), 2.87 (br m, 1H), 2.09 (m,1H), 1.14 (t, 1H, *J* =7.2 Hz).

*[PdCl(μ-Cl)(4b)]$_2$(**Pd3b**)*

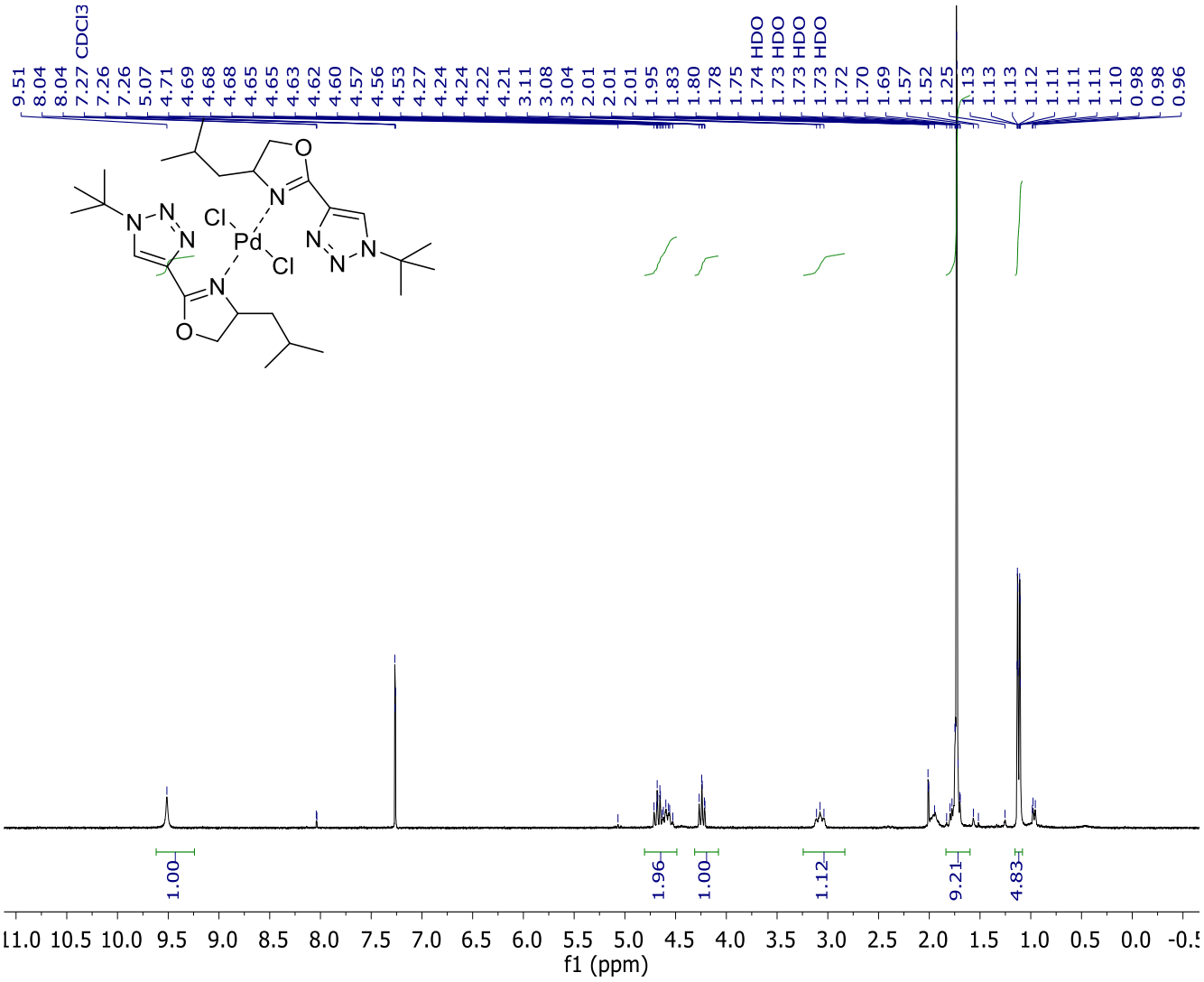

[PdCl(μ-Cl)(4c)]$_2$ (***Pd3c***)

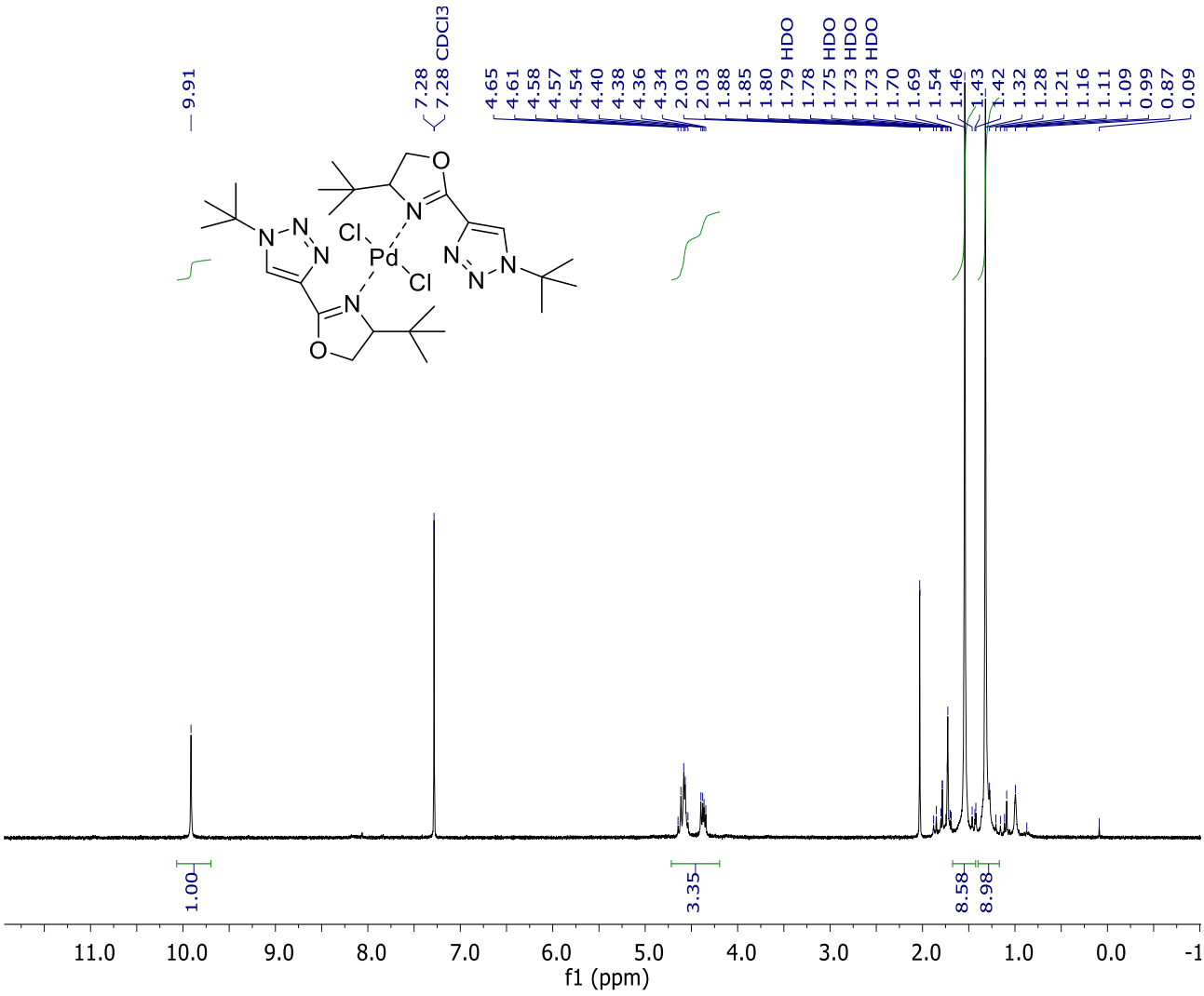

8.3 Synthesis, characterization and catalytic activity of novel ruthenium complexes bearing NNN click based ligands

8.3.1 Characterization of ligands and complexes

bis((1-benzyl-1*H*-1,2,3-triazol-4-yl)methyl)amine (L1)

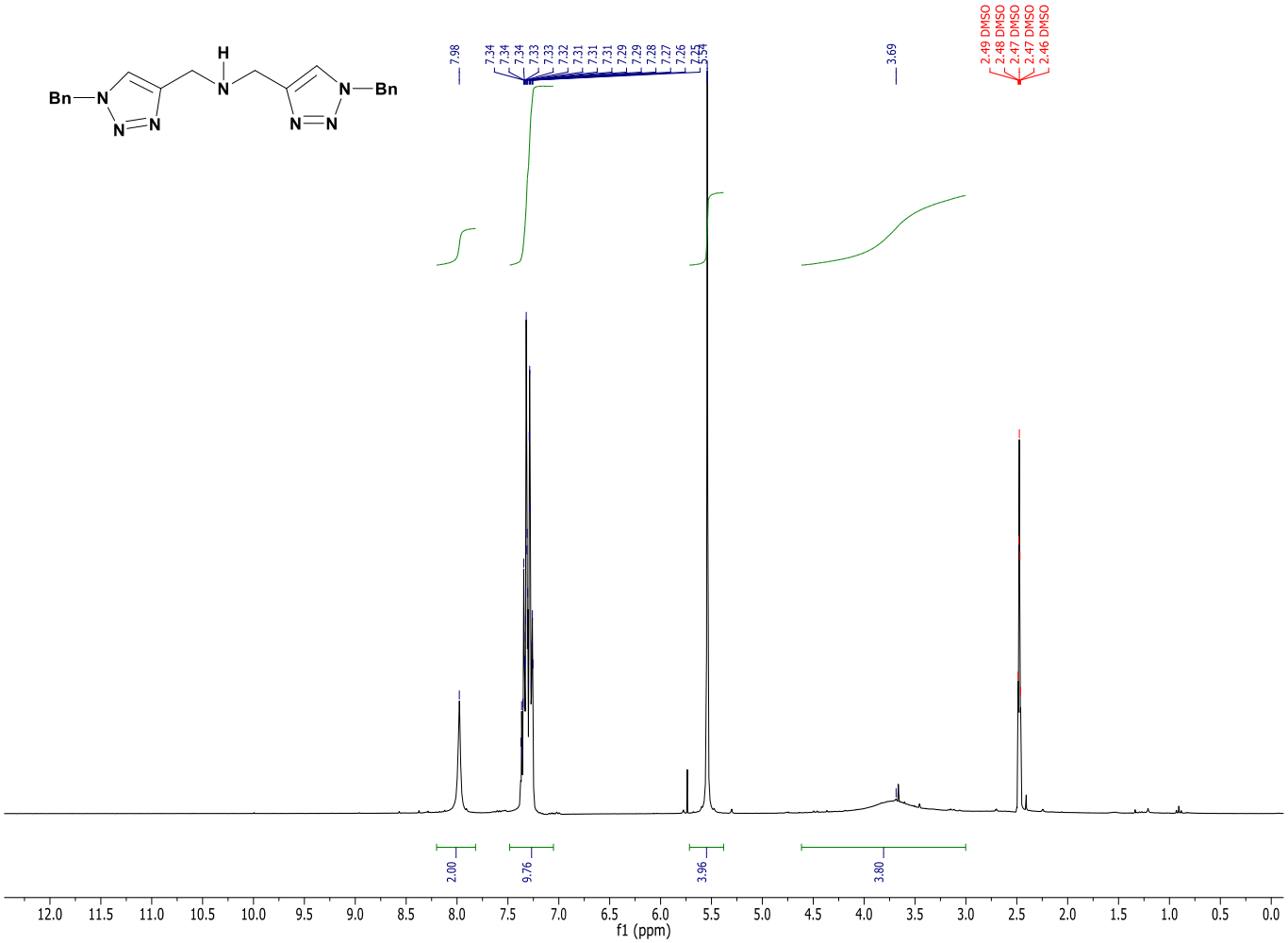

^{1}H NMR (400 MHz, DMSO-d_6) δ (ppm) = 8.01 (s, 2H), 7.40–7.28 (m, 10H), 5.57 (s, 4H), 3.87 (bs, 4H).

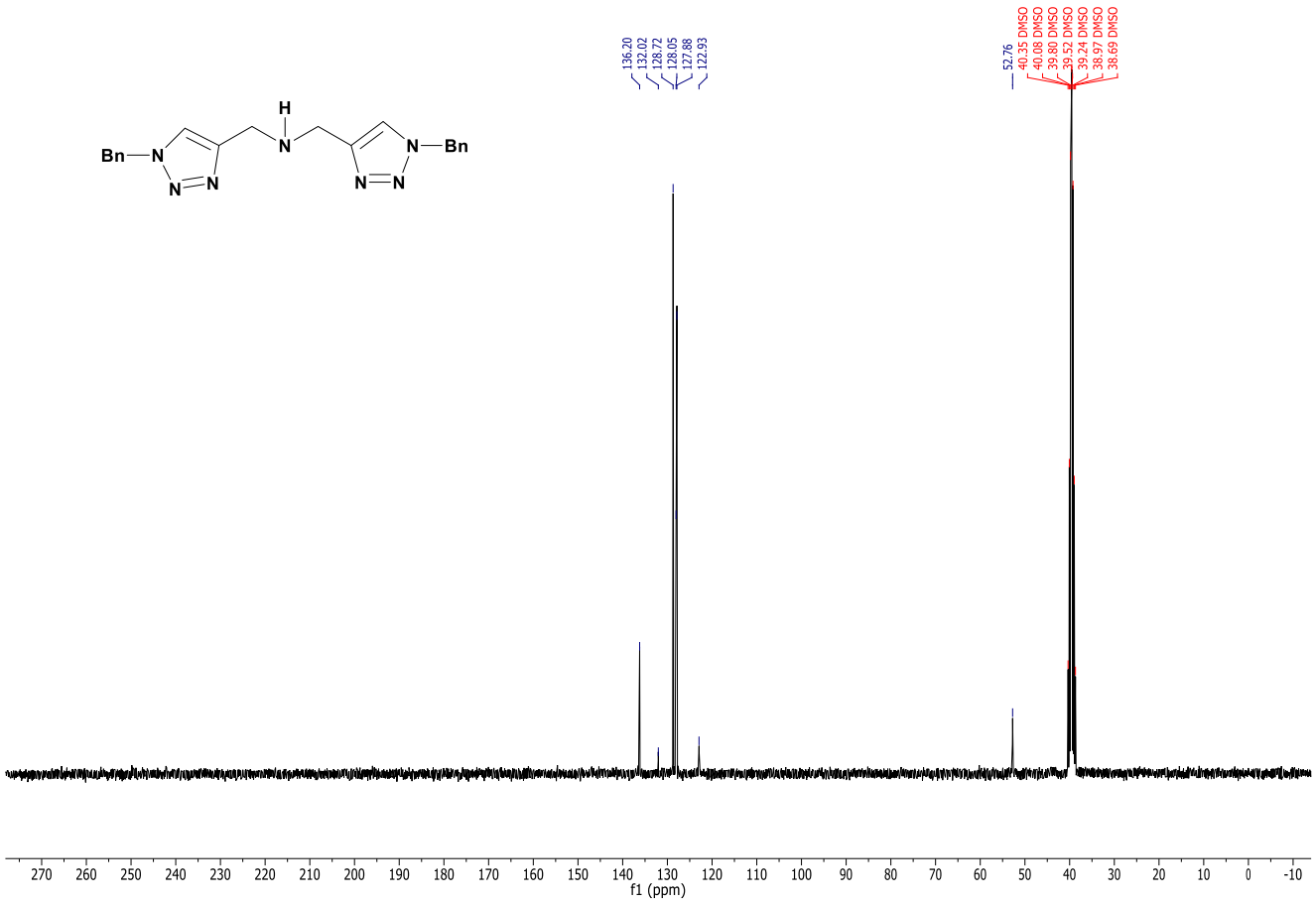

^{13}C NMR (400 MHz, DMSO-d_6) δ (ppm) = 136.2, 132.0, 128.7.1, 127.9, 122.9, 52.8.

1-(1-benzyl-1*H*-1,2,3-triazol-4-yl)-N-(pyridin-2-ylmethyl)methanamine (L2)

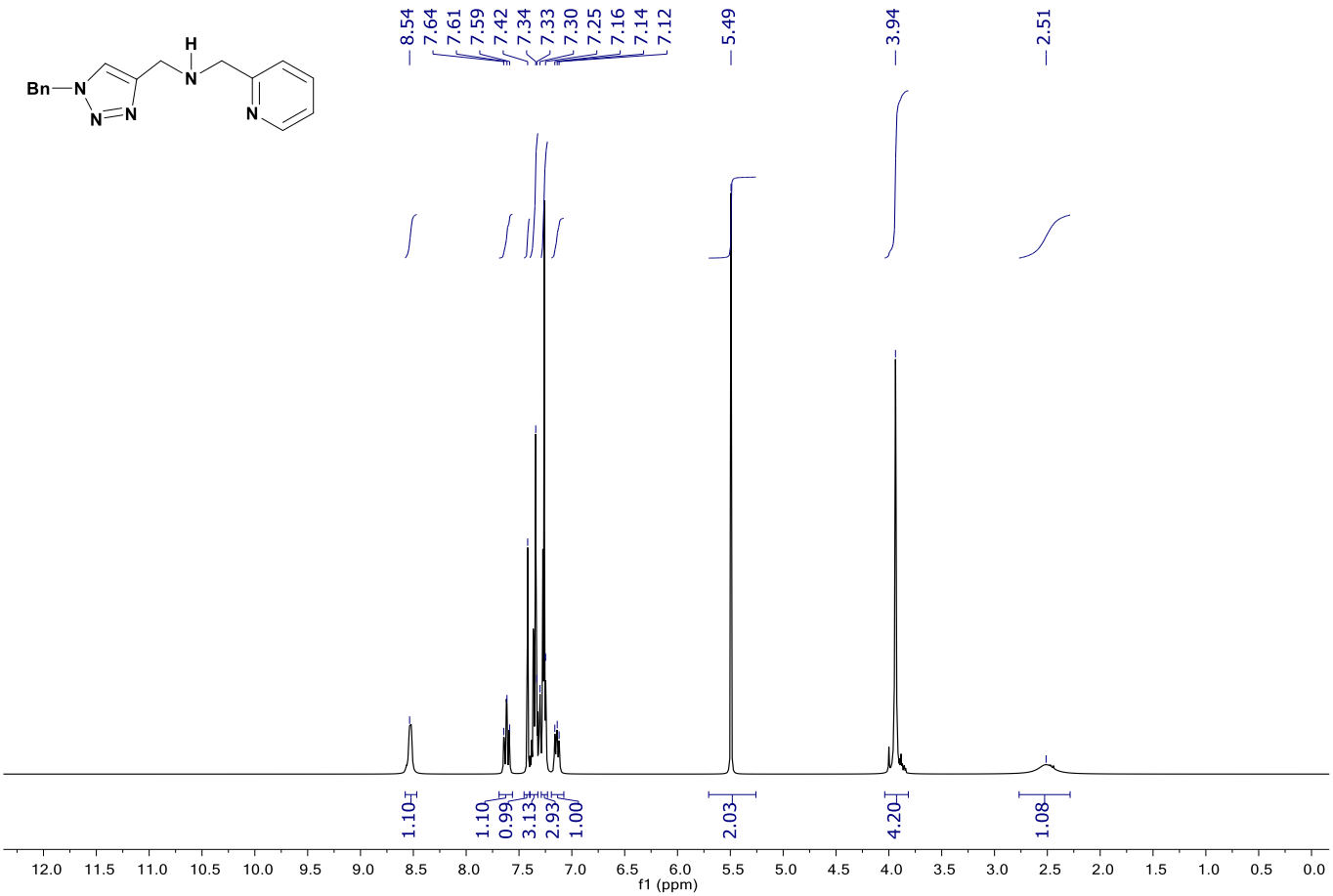

^{1}H NMR (300 MHz, $CDCl_3$) δ (ppm) = 8.54 (ddd, *J* = 4.9 Hz, 1.7 Hz, 0.9 Hz, 1H), 7.62 (td, *J* = 7.7, 1.8 Hz 1H), 7.42 (s, 1H), 7.38–7.31 (m, 3H), 7.28 (dm, *J* = 7.8 Hz, 1H), 7.27–7.24 (m, 2H), 7.15 (ddd, *J* = 7.6, 4.9, 1.2 Hz, 1H), 5.49 (s, 2H), 3.94 (s, 4H), 2.51 (bs, 1H).

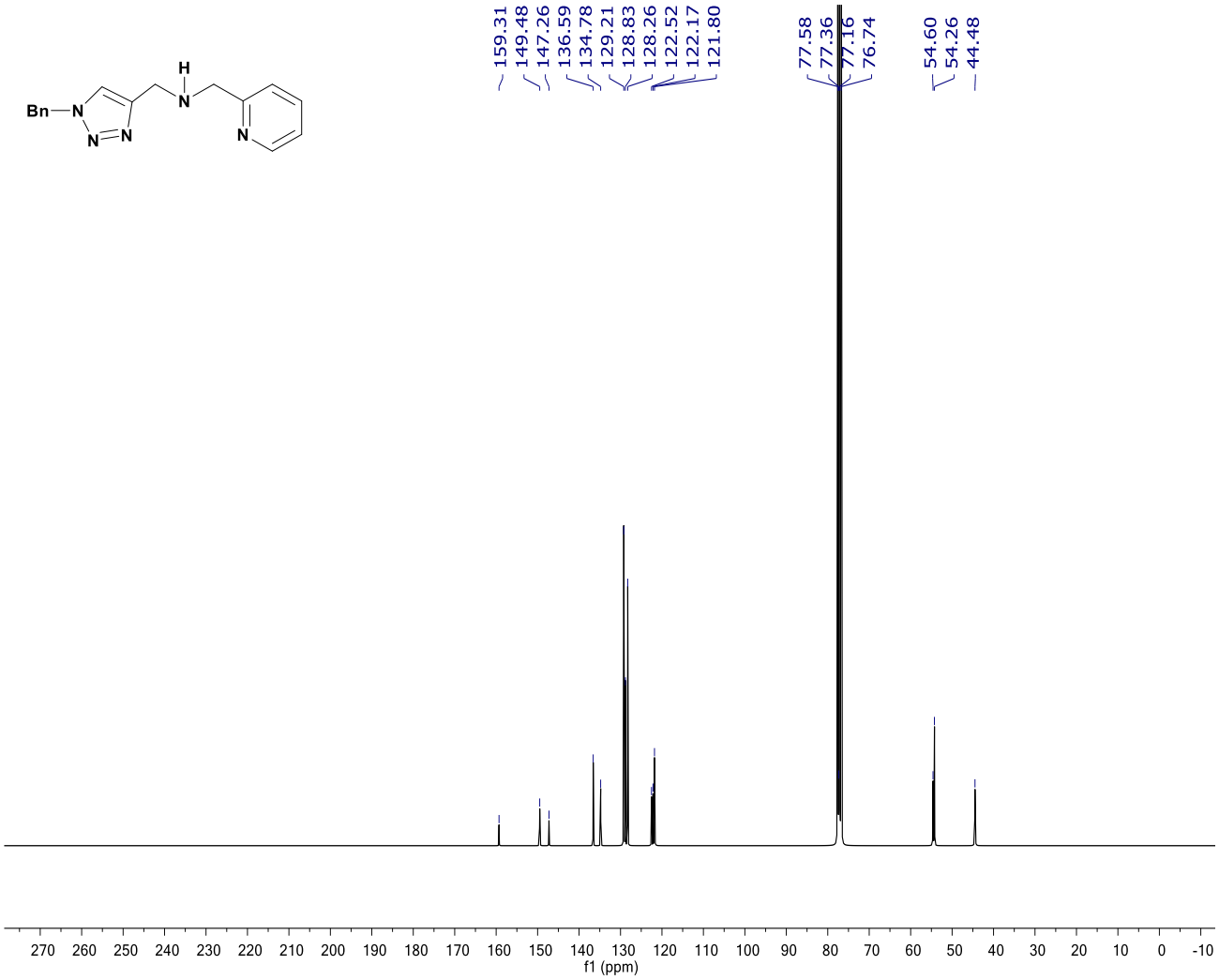

^{13}C NMR (300 MHz, $CDCl_3$) δ (ppm) = 159.3, 149.4, 147.2, 136.5, 134.7, 129.2, 128.8, 128.2, 122.5, 122.1, 121.8, 54.6, 54.2, 44.5.

2-(4-phenyl-1*H*-1,2,3-triazol-1-yl)-N-(pyridin-2-ylmethyl)ethan-1-amine (L3)

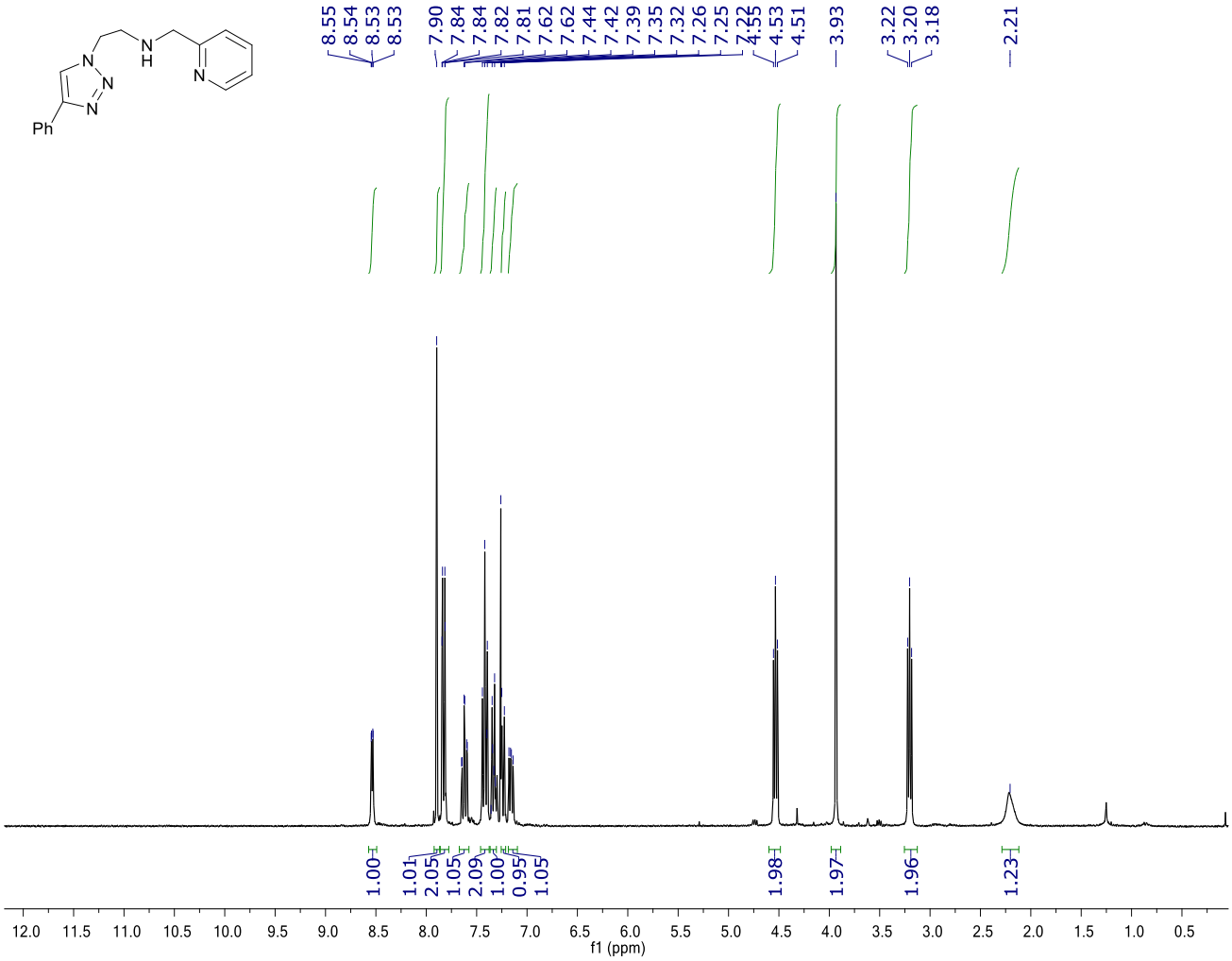

^{1}H NMR (400 MHz, $CDCl_3$) δ (ppm) = 8.52 (ddd, *J* = 4.9 Hz, 1.8 Hz, 0.9 Hz, 1H), 7.36–7.30 (m, 6H), 7.90 (s, 1H), 7.85–7.77 (m, 2H), 7.62 (td, *J* = 7.7, 1.8 Hz 1H), 7.44–7.38 (m, 2H), 7.37–7.30 (m, 1H), 7.24 (ddt, *J* = 7.3, 1.4, 0.8 Hz, 1H), 7.16 (m, 1H), 4.52 (t, *J* = 6 Hz, 2H), 3.92 (s, 2H), 3.18 (t, *J* = 6 Hz, 2H).

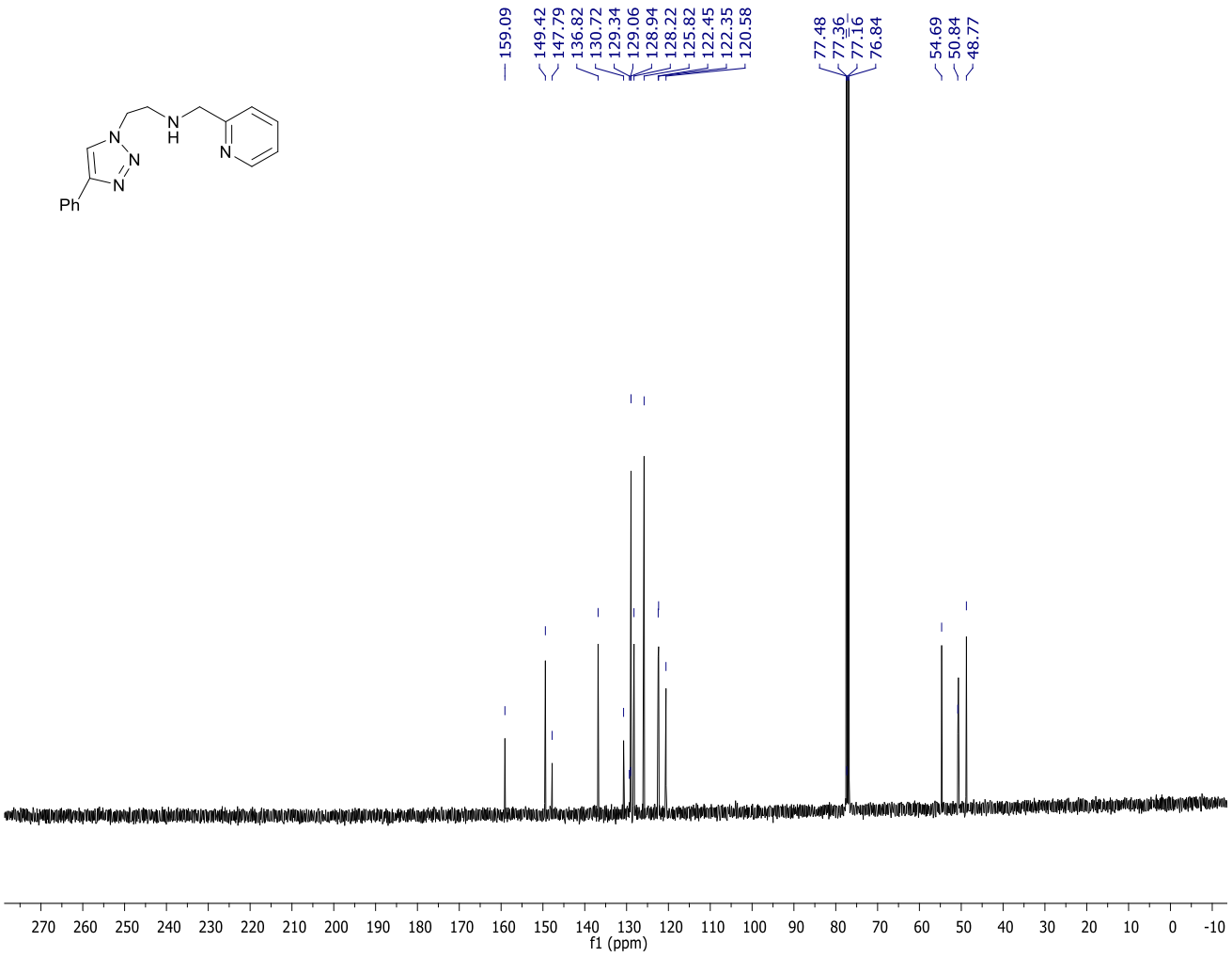

^{13}C NMR (400 MHz, $CDCl_3$) δ (ppm) = 159.1, 149.4, 147.8, 136.8, 130.7, 129.1, 128.9, 128.2, 125.8, 122.4, 122.3, 120.5, 54.7, 50.8, 50.7, 48.8.

Ru(NNN$_{L1}$)(PPh$_3$)Cl$_2$ (1)

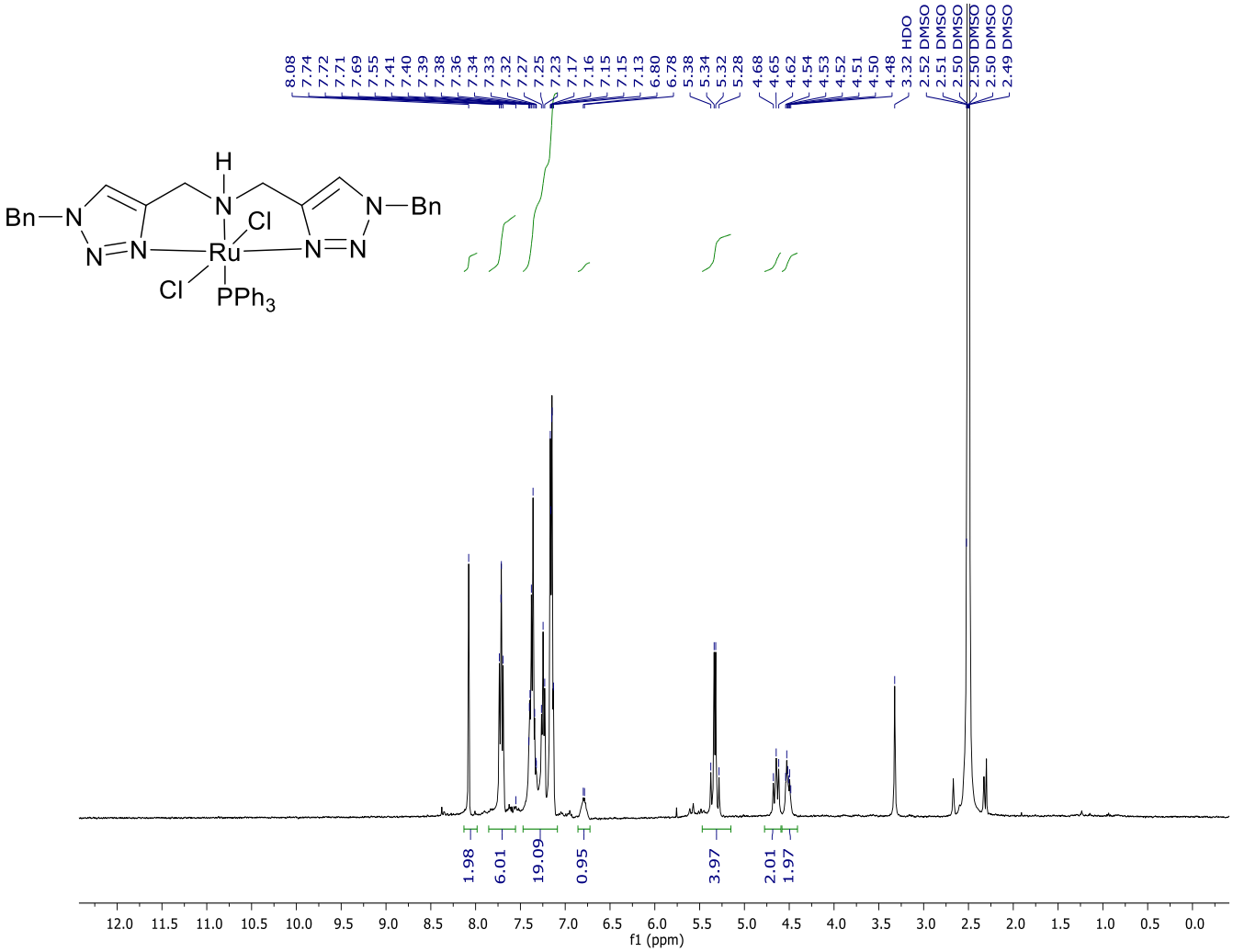

^{1}H-NMR (400 MHz, DMSO-d_6, 293 K): δ (ppm) = 8.08 (s, 2H), 7.79–7.63 (m, 6H), 7.40–7.33 (m, 6H), 7.28–7.21 (m, 4H), 7.15 (ddd, *J* = 7.3 Hz, 5.9 Hz, 1.9 Hz, 9H), 5.42–5.21 (q, *J* = 15 Hz, 4H), 4.70–4.59 (m, 2H), 4.56–4.45 (m. 2H)

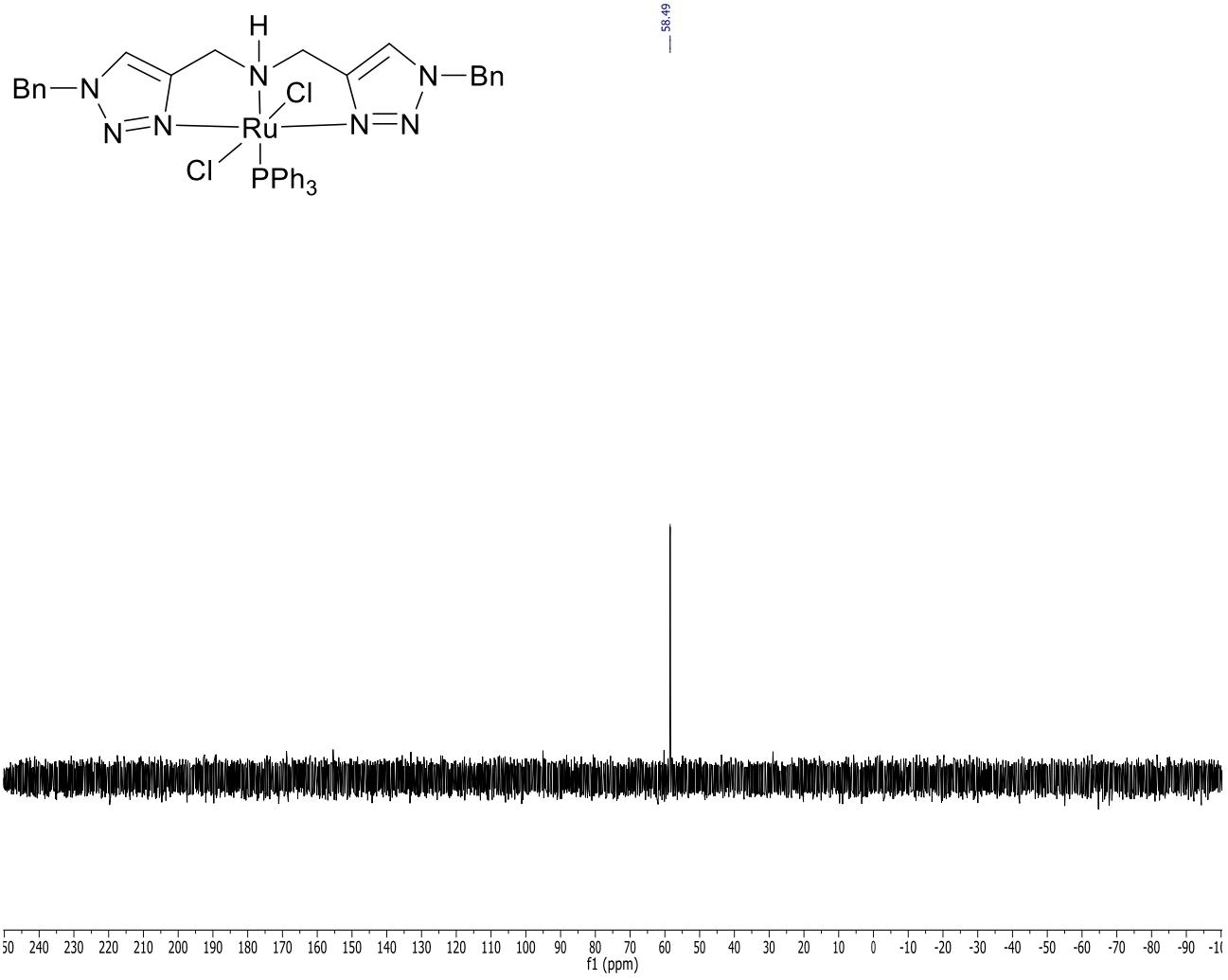

$^{31}P\{^{1}H\}$-NMR (400 MHz, DMSO-d_6, 293 K), δ (ppm) = 58.5.

$Ru(NNN_{L2})(PPh_3)Cl_2$ (2)

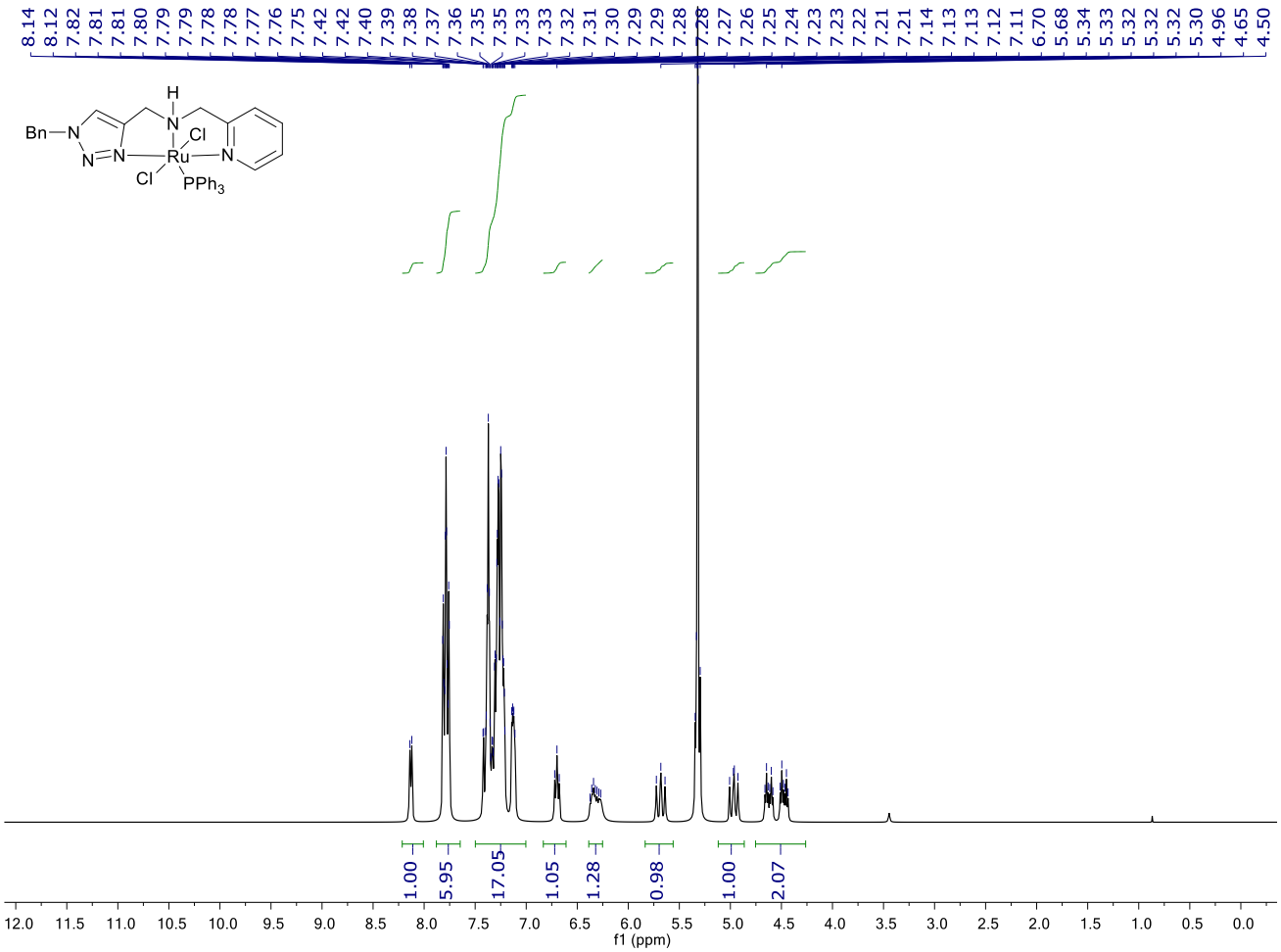

^{1}H-NMR (400 MHz, CD_2Cl_2, 293 K): δ (ppm) = 8.18–8.08 (m,1H),7.88–7.69 (m, 6H), 7.52–7.19 (m, 16H), 7.19–7.05 (m,2H),6.78–6.61 (m,2H),6.30(m, 1H), 5.74–5.59 (m, 1H), 4.97 (ddd, *J* = 13.7, 10.9, 1.2 Hz, 1H), 4.62 (dt, *J* = 14.1, 4.6 Hz, 1H), 4.47 (dt, *J* = 13.7, 4.8 Hz, 1H).

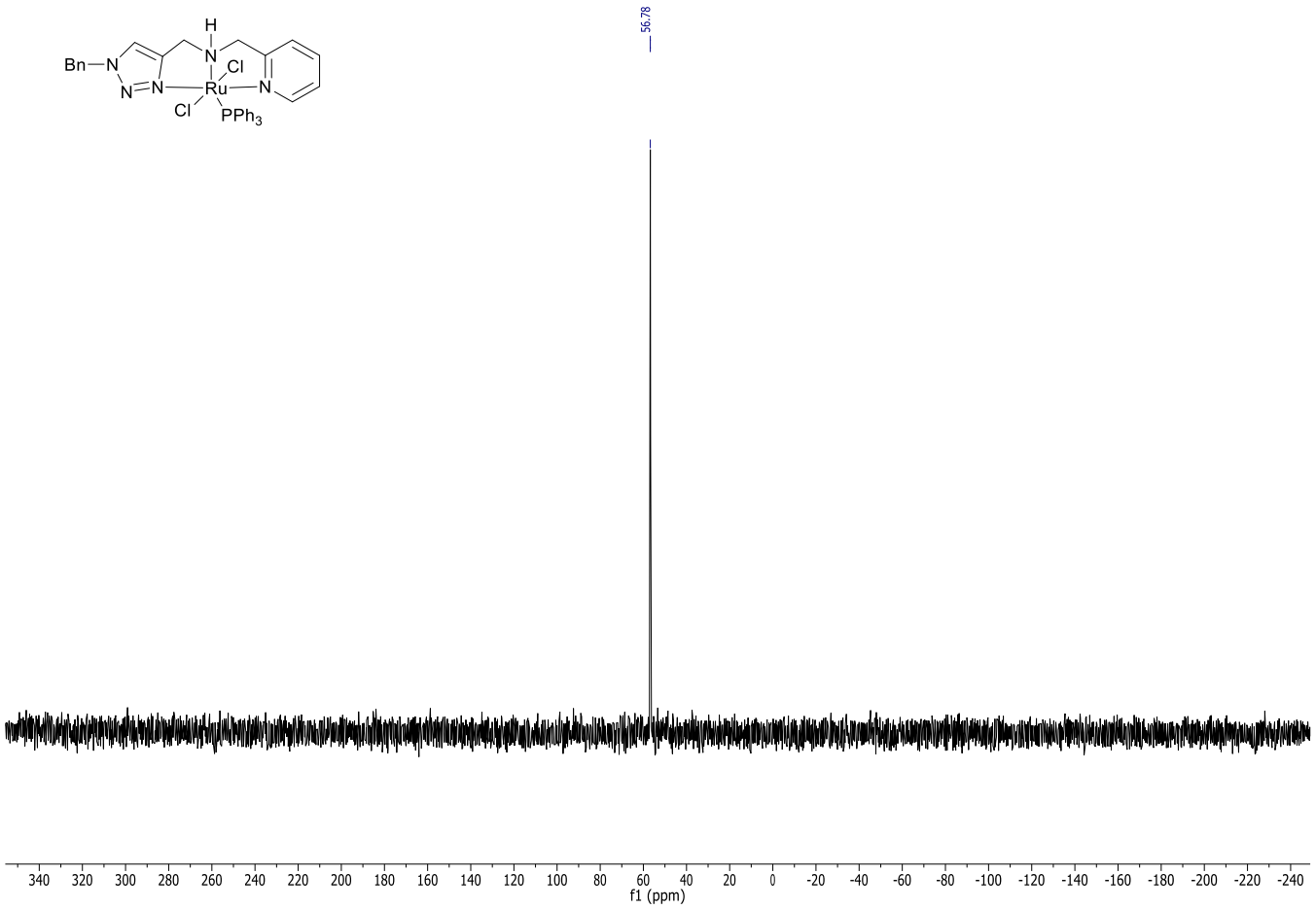

$^{31}P\{^{1}H\}$-NMR (400 MHz, CD_2Cl_2,293 K), δ (ppm)= 56.5.

Ru(NNN$_{L3}$)(PPh$_3$)Cl$_2$ (3)

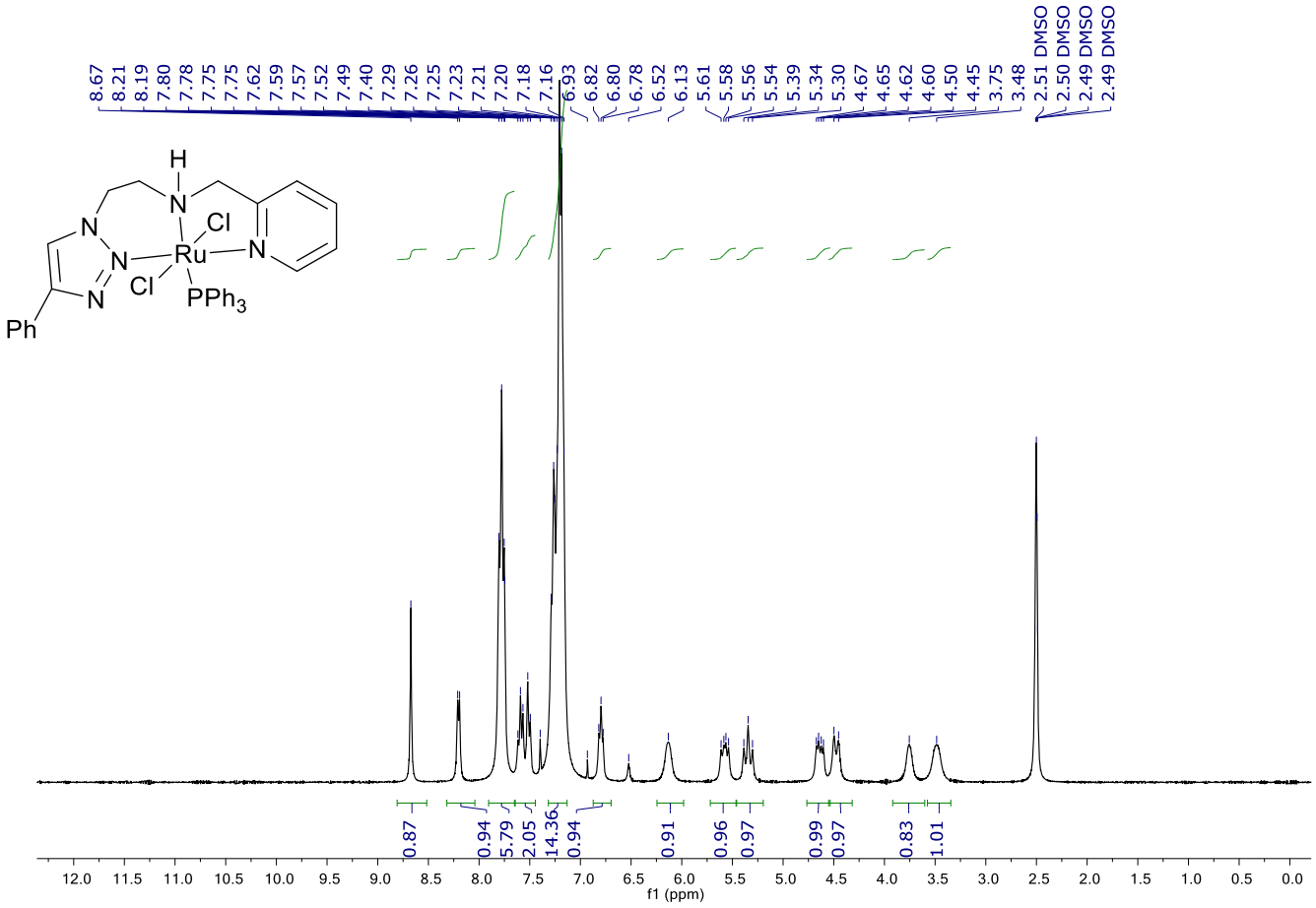

^{1}H-NMR (400 MHz, DMSO-d_6, 293 K): δ (ppm) 8.67 (s, 1H), 8.20 (d, J = 5.7 Hz, 1H), 7.78 (ddt, J = 8.0, 6.6, 1.8 Hz, 6H), 7.65–7.47 (m, 3H), 7.32–7.11 (m, 16H), 6.85–6.73 (m, 1H), 6.14 (d, J = 11.8 Hz, 1H), 5.57 (dd, J = 14.2, 8.0 Hz, 1H), 5.34 (t, J = 12.9 Hz, 1H), 4.63 (dd, J = 14.1, 6.8 Hz, 1H), 4.47 (d, J = 13.9 Hz, 1H), 3.75 (s, 1H).

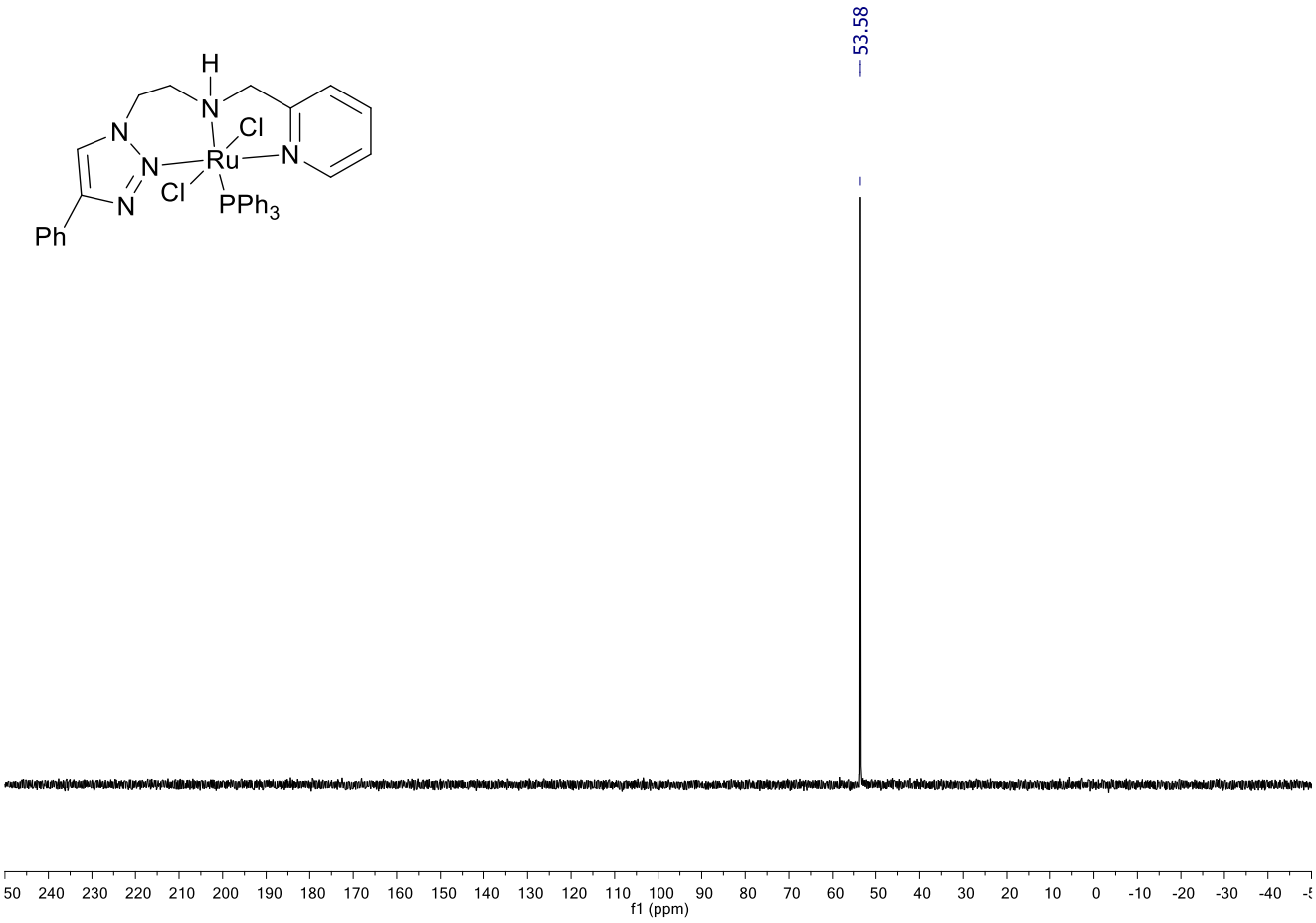

$^{31}P\{^{1}H\}$-NMR (400 MHz, DMSO-d_6, 293 K), δ (ppm) = 53.6.

8.3.1.2. ATR-IR spectra complexes

bis((1-benzyl-1H-1,2,3-triazol-4-yl)methyl)amine (L1)

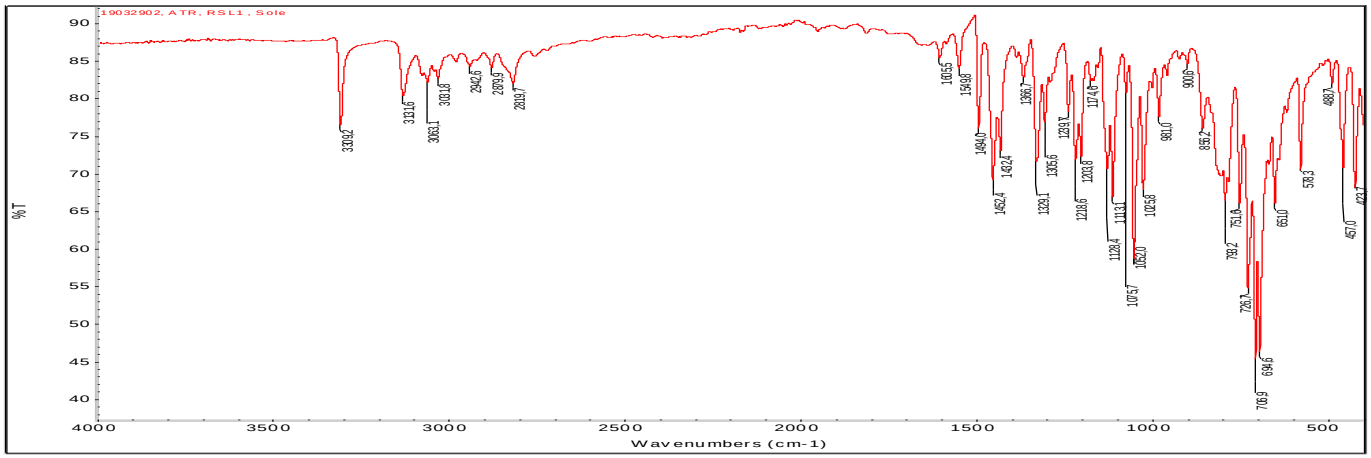

1-(1-benzyl-1H-1,2,3-triazol-4-yl)-N-(pyridin-2-ylmethyl)methanamine (L2)

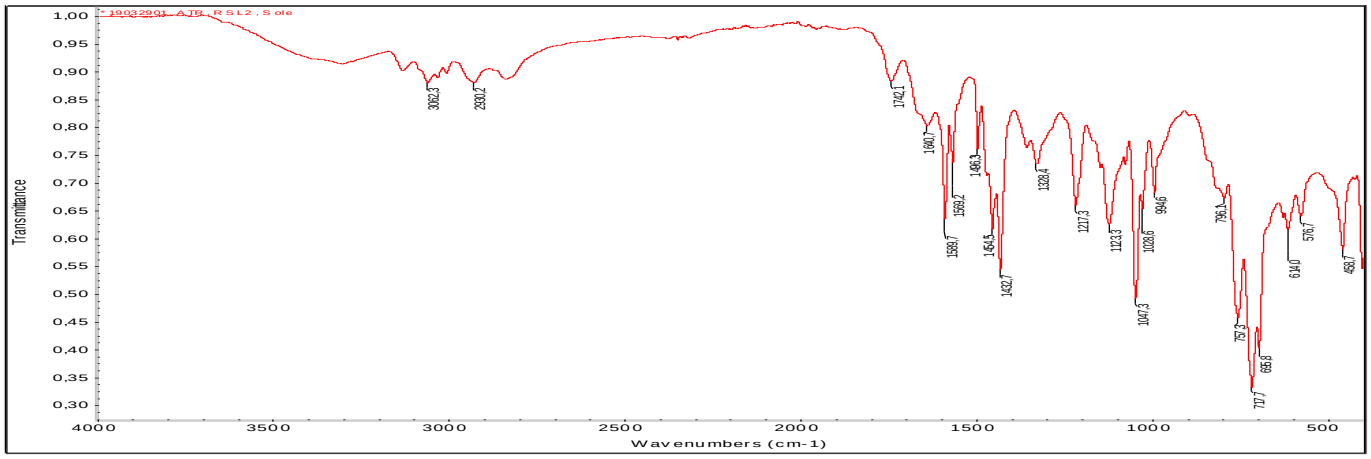

2-(4-phenyl-1*H*-1,2,3-triazol-1-yl)-N-(pyridin-2-ylmethyl)ethan-1-amine (L3)

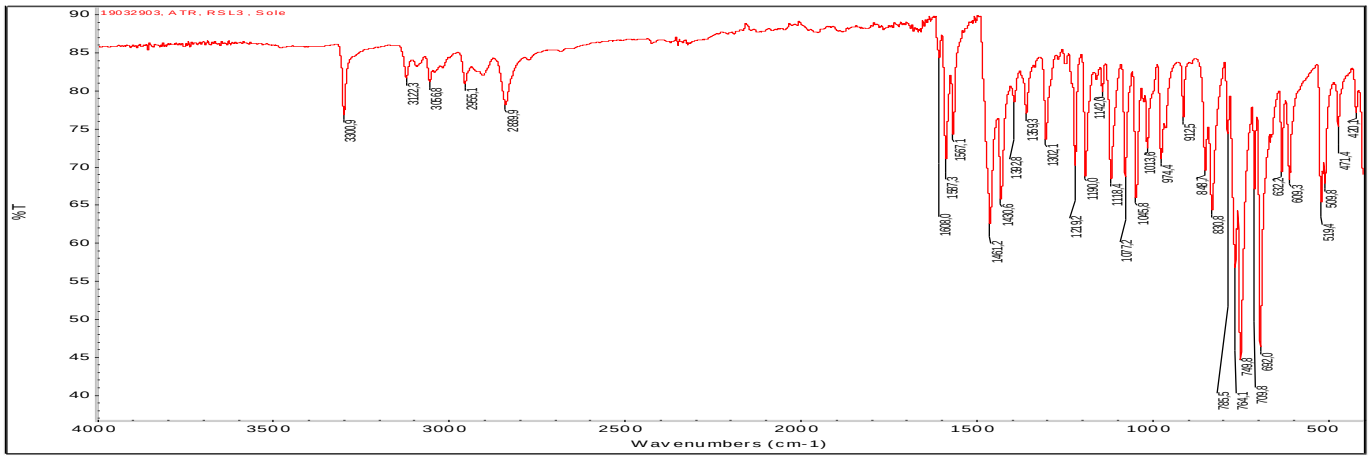

$Ru(NNN_{L1})(PPh_3)Cl_2$ (1)

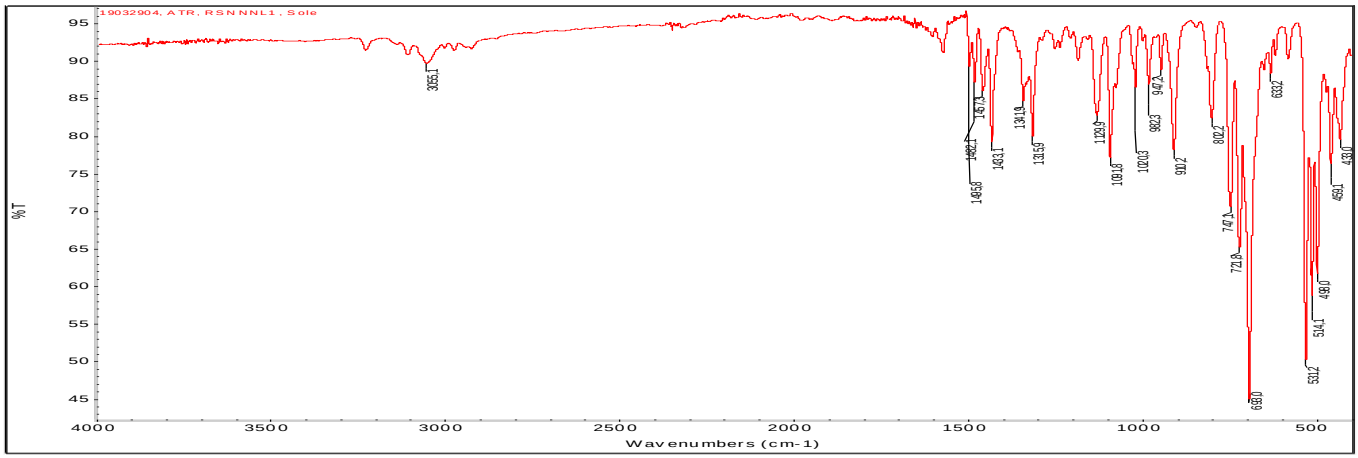

$Ru(NNN_{L2})(PPh_3)Cl_2$ (2)

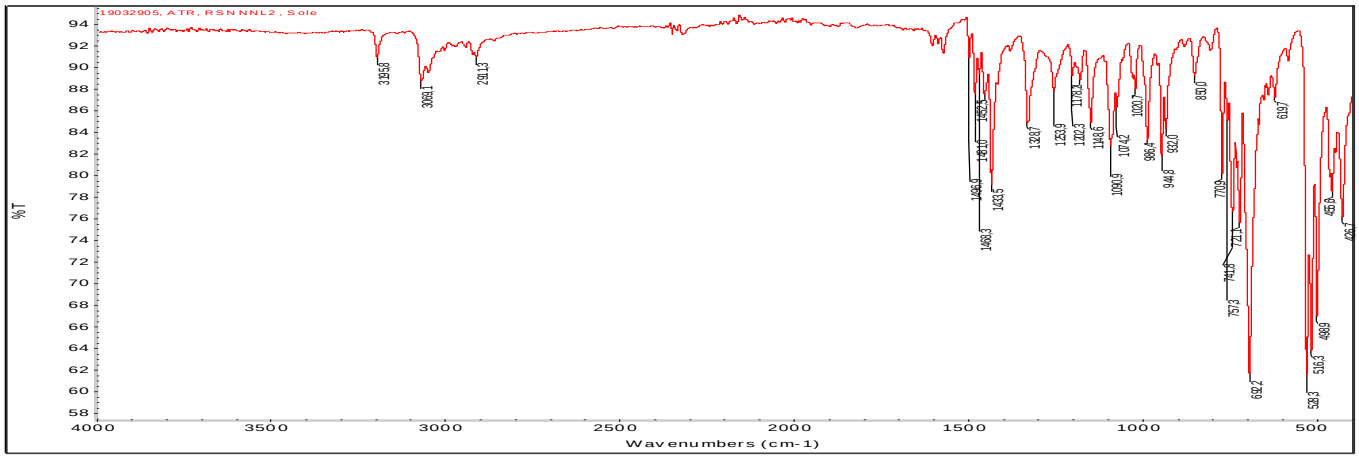

$Ru(NNN_{L3})(PPh_3)Cl_2$ (3)

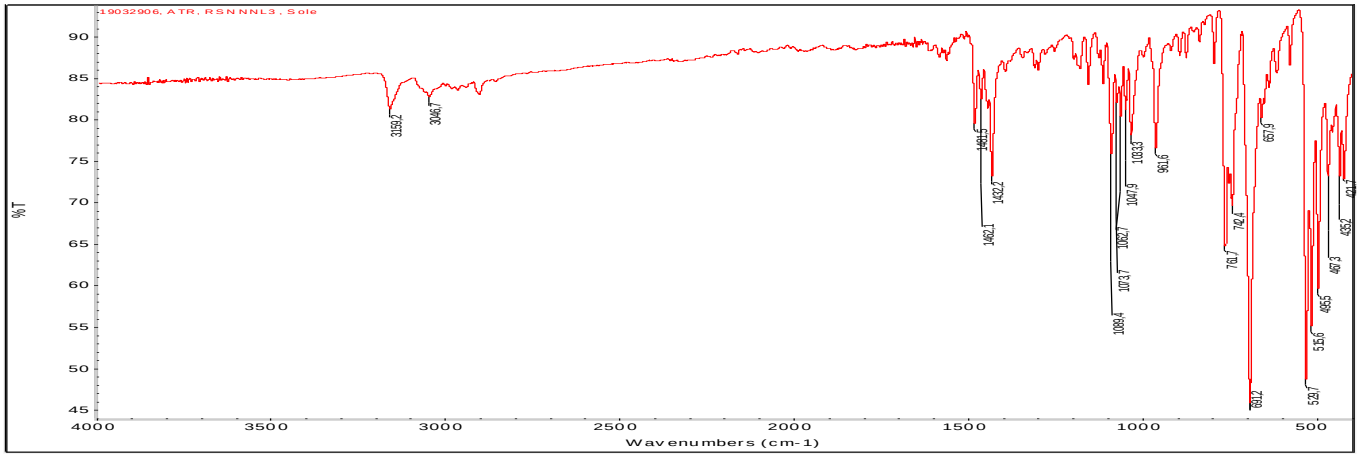

8..3.1.3 ESI-HRMS spectra complexes

bis((1-benzyl-1*H*-1,2,3-triazol-4-yl)methyl)amine (L1)

ESI-TOF Accurate Mass Report Page 2
File:19031323 Sample Name:RS NNN UserName:R. Sole
Vial:1:E,2 Date:13-Mar-2019 Time:15:46:15
Description:MeOH/0.1%HCOOH in H2O 9:1

Sample Report:

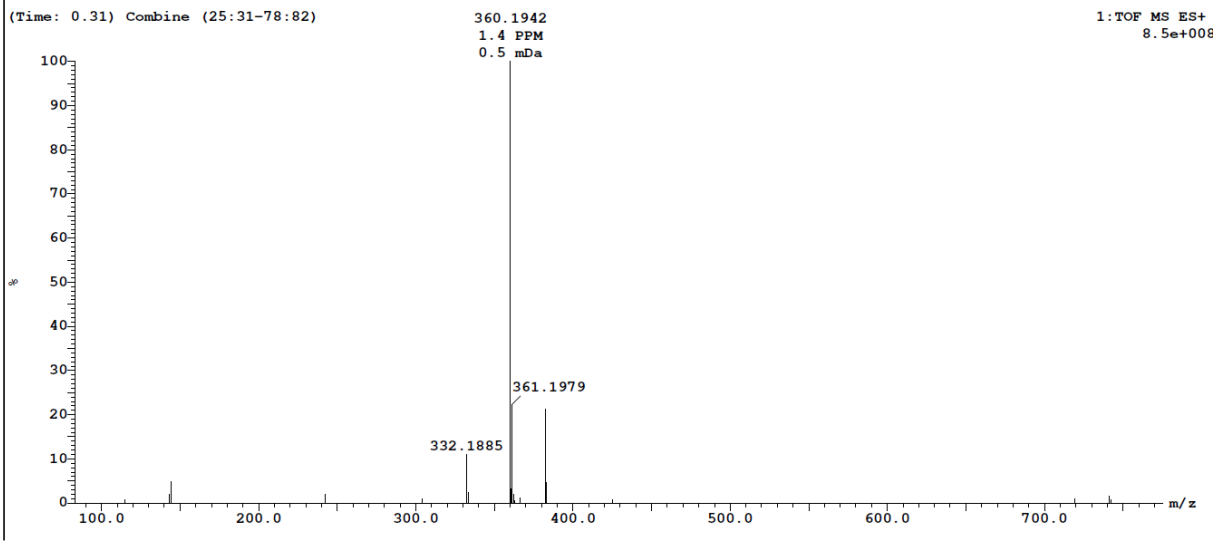

1-(1-benzyl-1*H*-1,2,3-triazol-4-yl)-N-(pyridin-2-ylmethyl)methanamine (L2)

ESI-TOF Accurate Mass Report Page 2
File:19041113 Sample Name:RS NNNL3 UserName:R. Sole
Vial:1:E,2 Date:11-Apr-2019 Time:16:12:56
Description:MeOH/0.1%HCOOH in H2O 90:10

Sample Report:

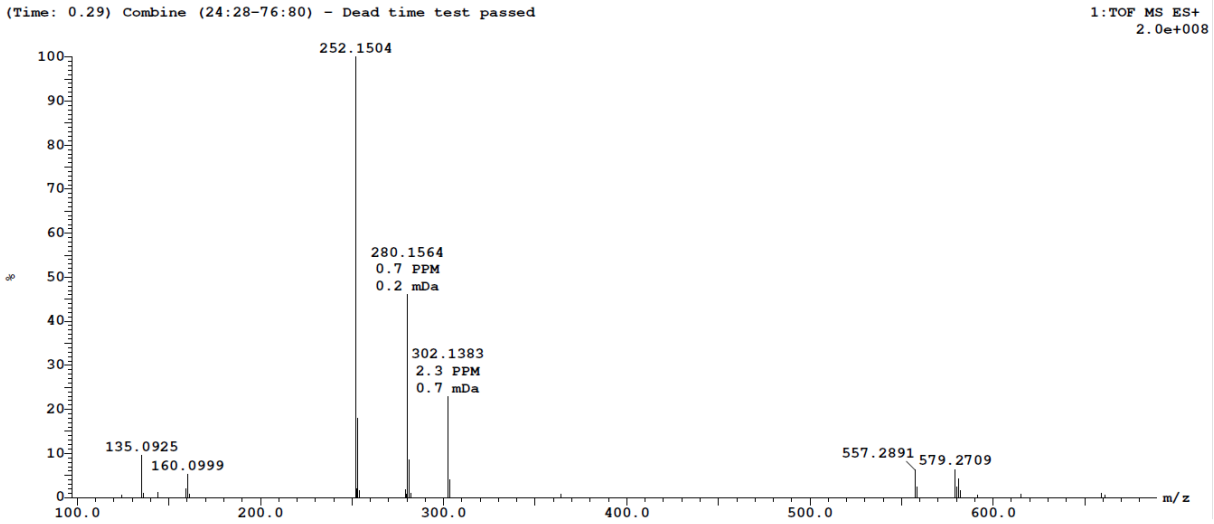

2-(4-phenyl-1*H*-1,2,3-triazol-1-yl)-N-(pyridin-2-ylmethyl)ethan-1-amine (L3)

ESI-TOF Accurate Mass Report Page 2

File:19041114 Sample Name:RS ? UserName:R. Sole
Vial:1:E,3 Date:11-Apr-2019 Time:16:15:32
Description:MeOH/0.1%HCOOH in H2O 90:10

Sample Report:

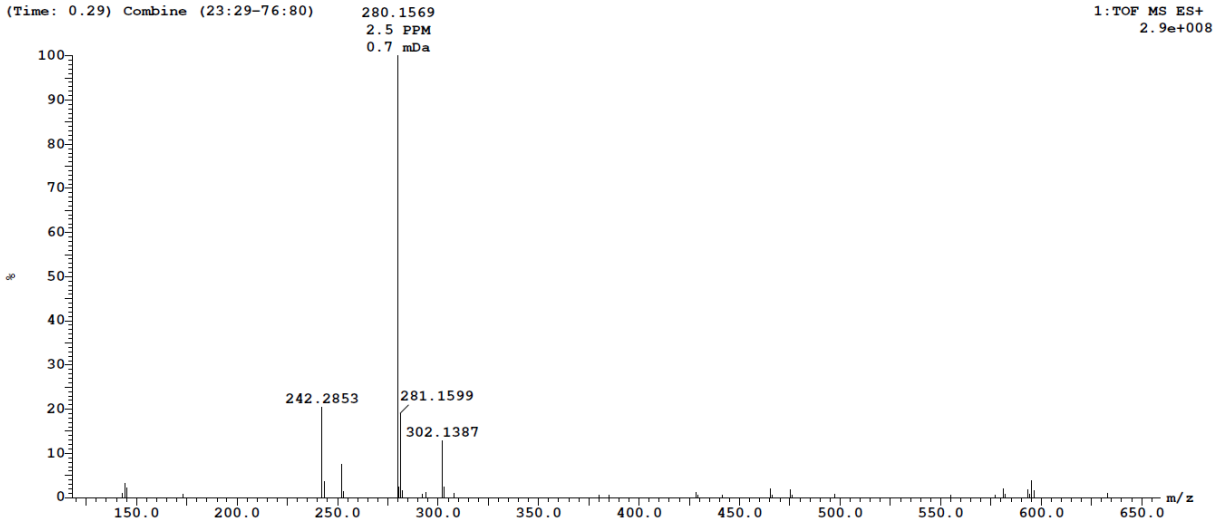

$Ru(NNN_{L1})(PPh_3)Cl_2$ (1)

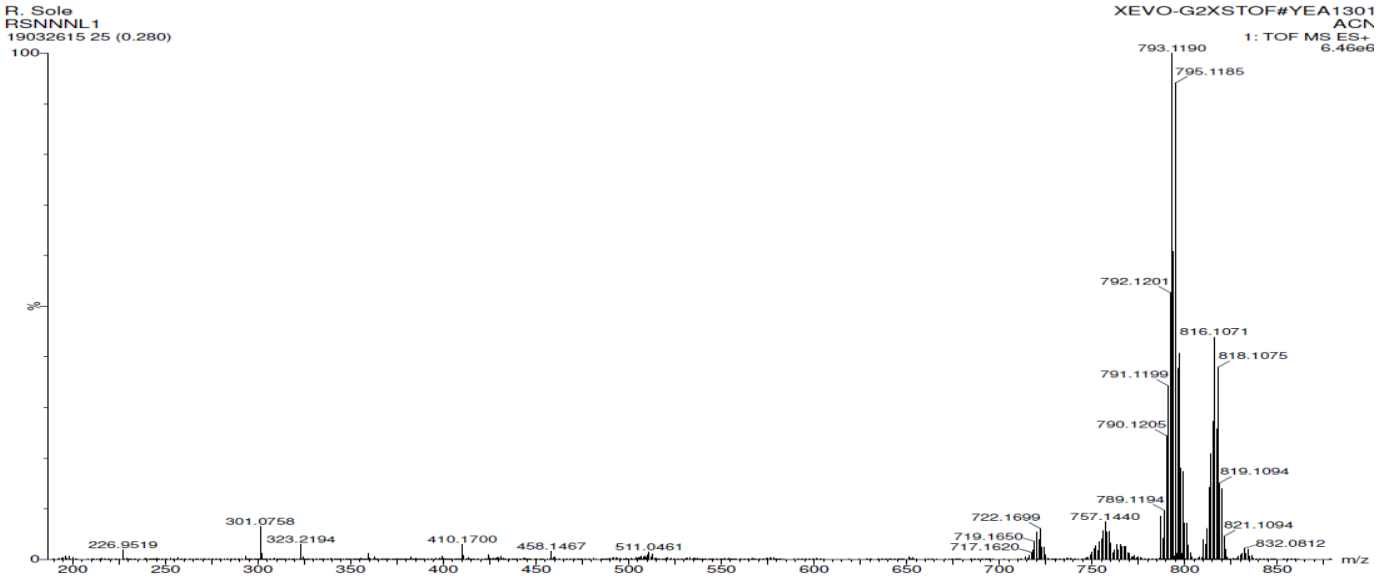

$Ru(NNN_{L2})(PPh_3)Cl_2$ (2)

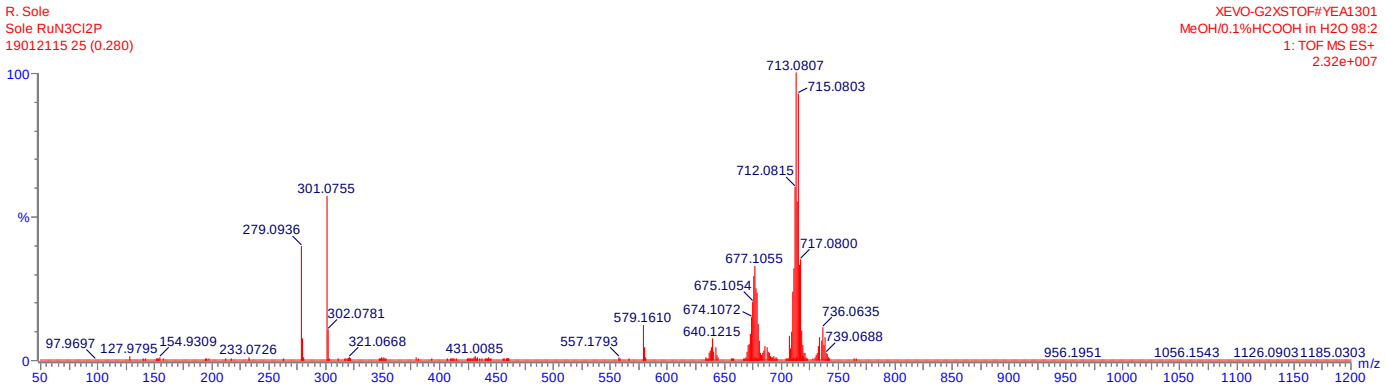

$Ru(NNN_{L3})(PPh_3)Cl_2$ (3)

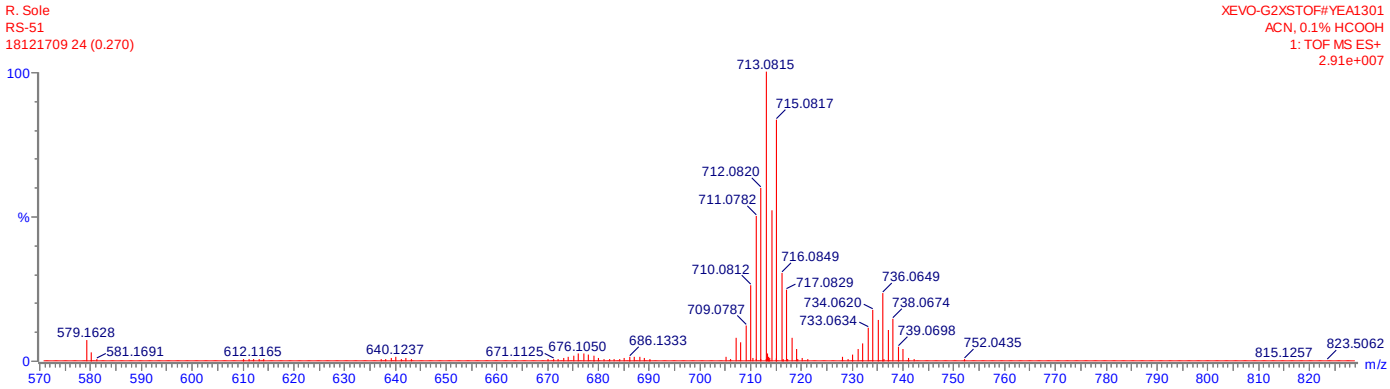

8.3.2 ^{1}H-^{13}C NMR spectra hydrogenation products

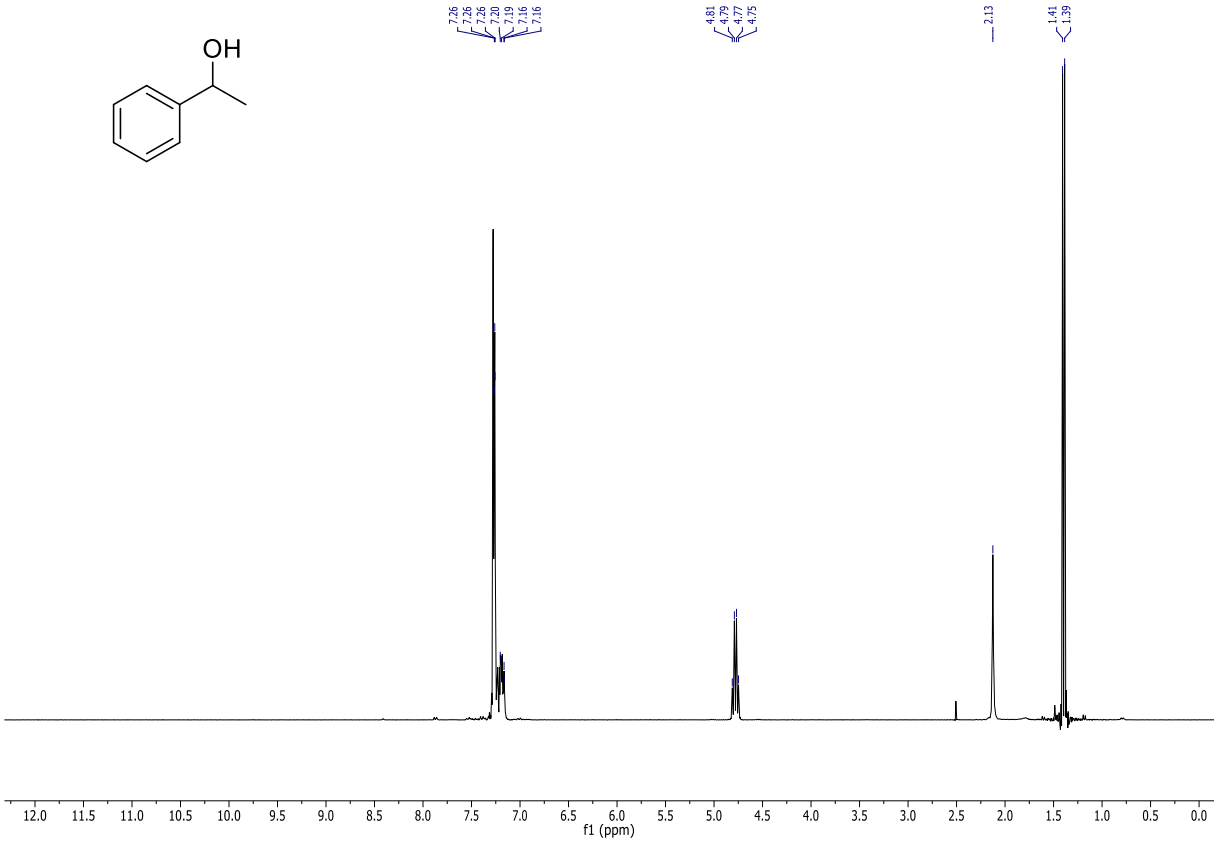

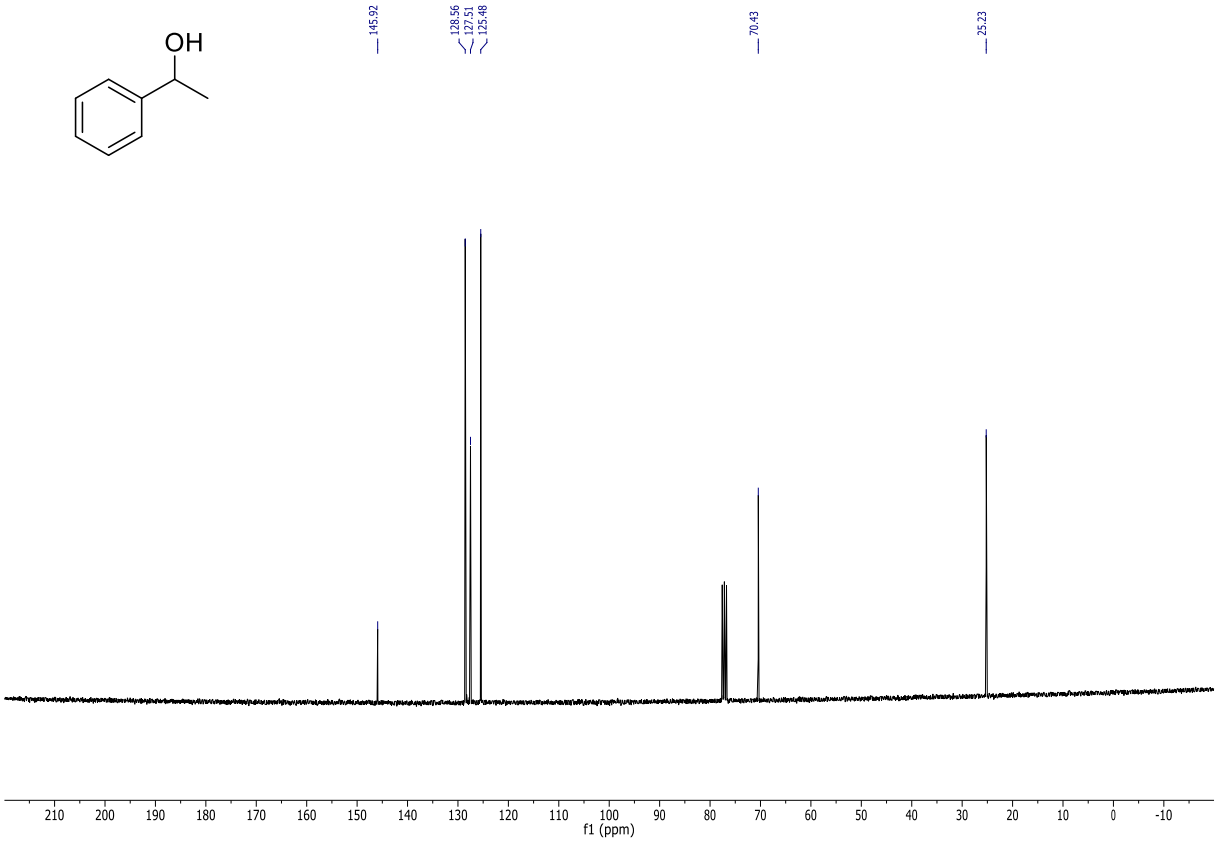

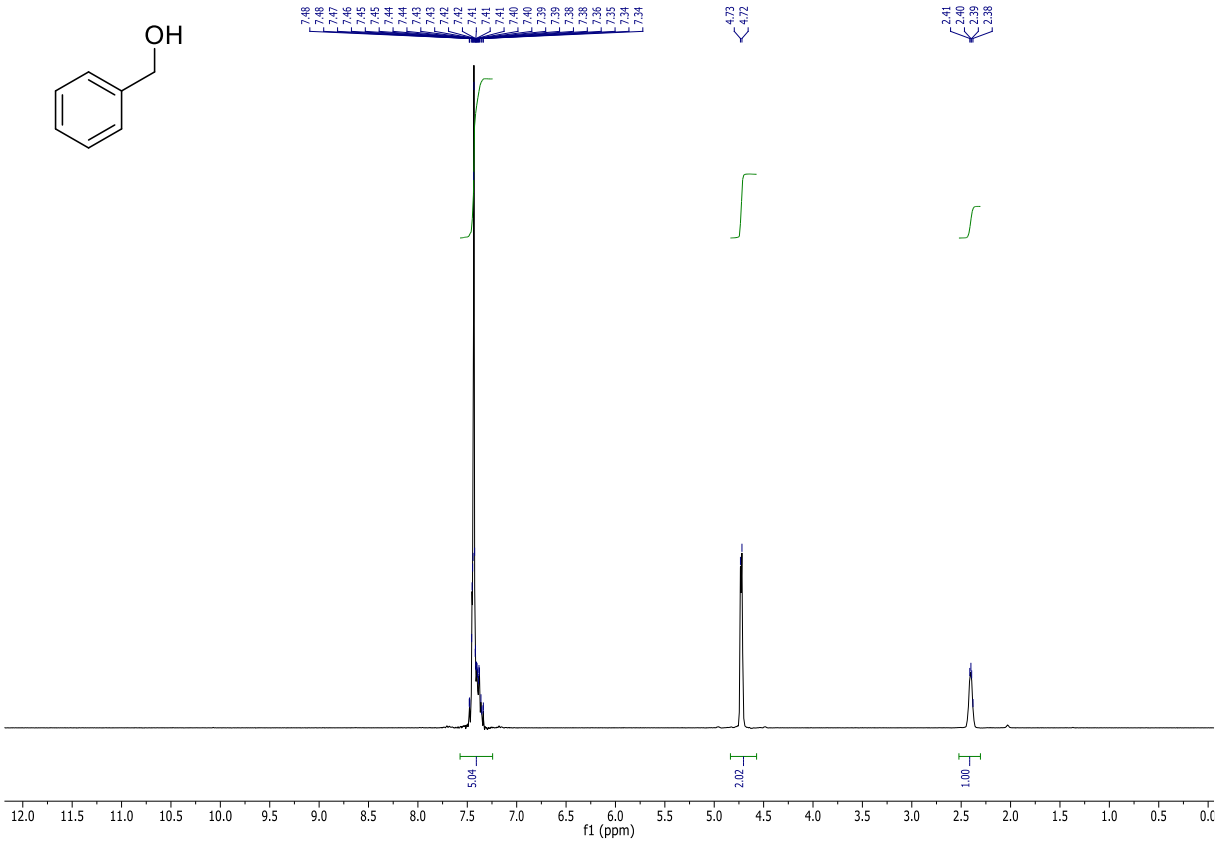
OH
7.48
7.48
7.47
7.46
7.45
7.45
7.44
7.44
7.43
7.43
7.42
7.42
7.41
7.41
7.41
7.40
7.40
7.39
7.39
7.38
7.38
7.36
7.35
7.34
7.34
4.73
4.72
2.41
2.40
2.39
2.38
5.04
2.02
1.00
f1 (ppm)

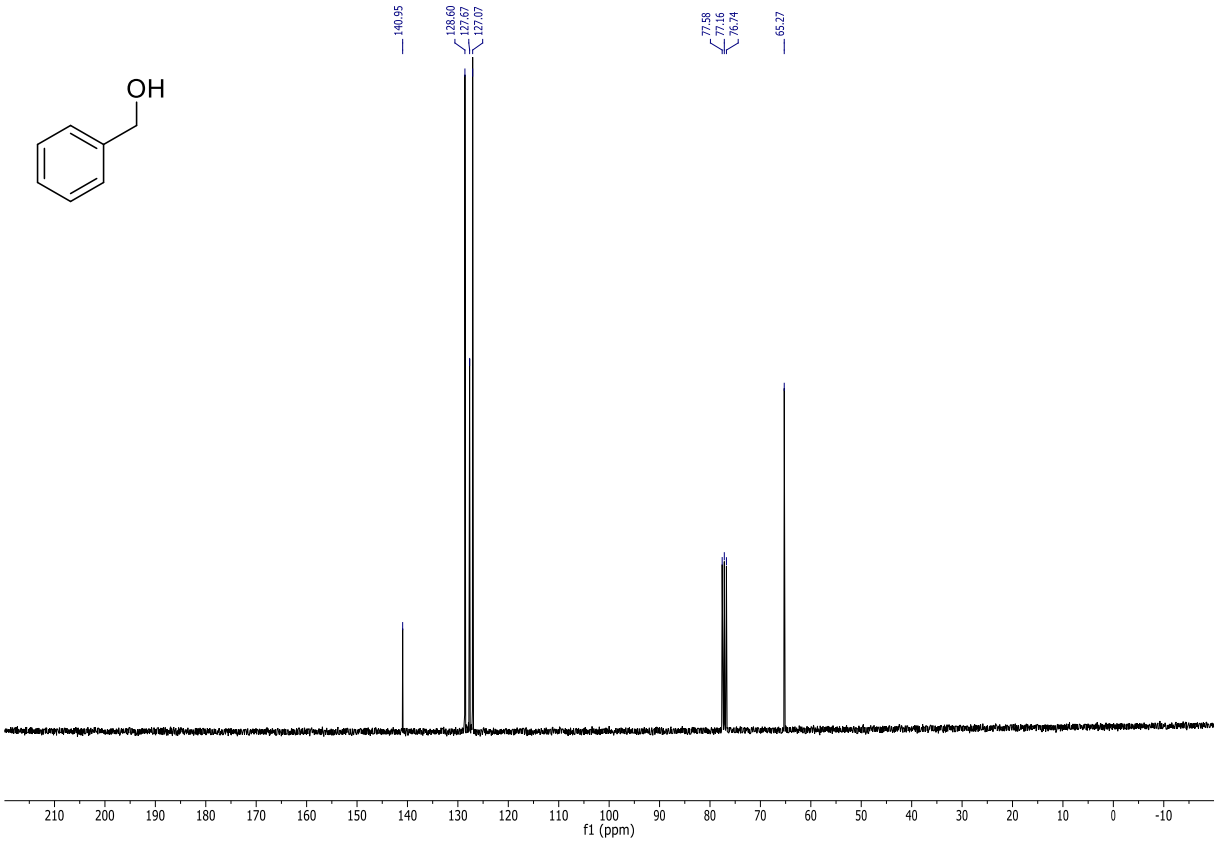
OH
140.95
128.60
127.67
127.07
77.58
77.16
76.74
65.27
f1 (ppm)

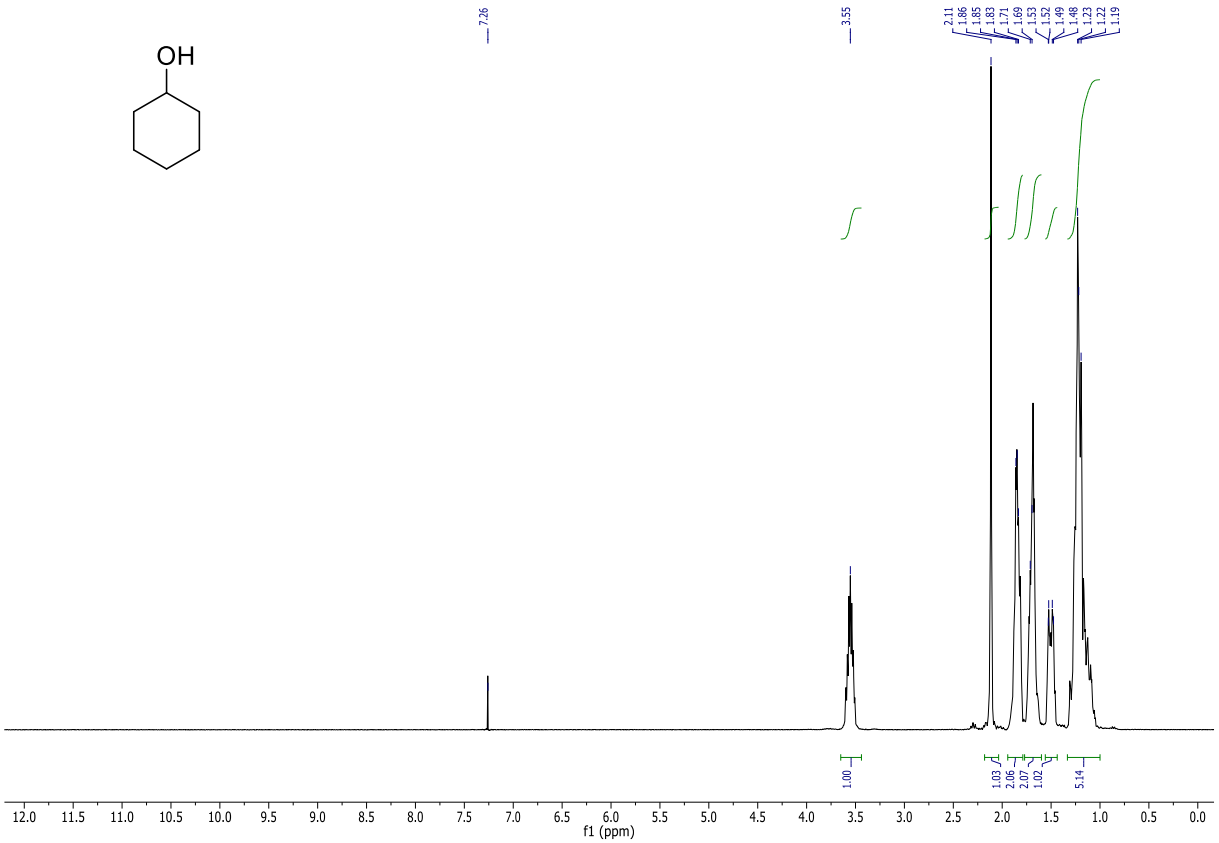
OH
7.26
3.55
2.11
2.06
1.85
1.83
1.71
1.69
1.53
1.52
1.49
1.48
1.23
1.22
1.19
1.00
1.03
2.06
2.07
1.02
5.14
f1 (ppm)

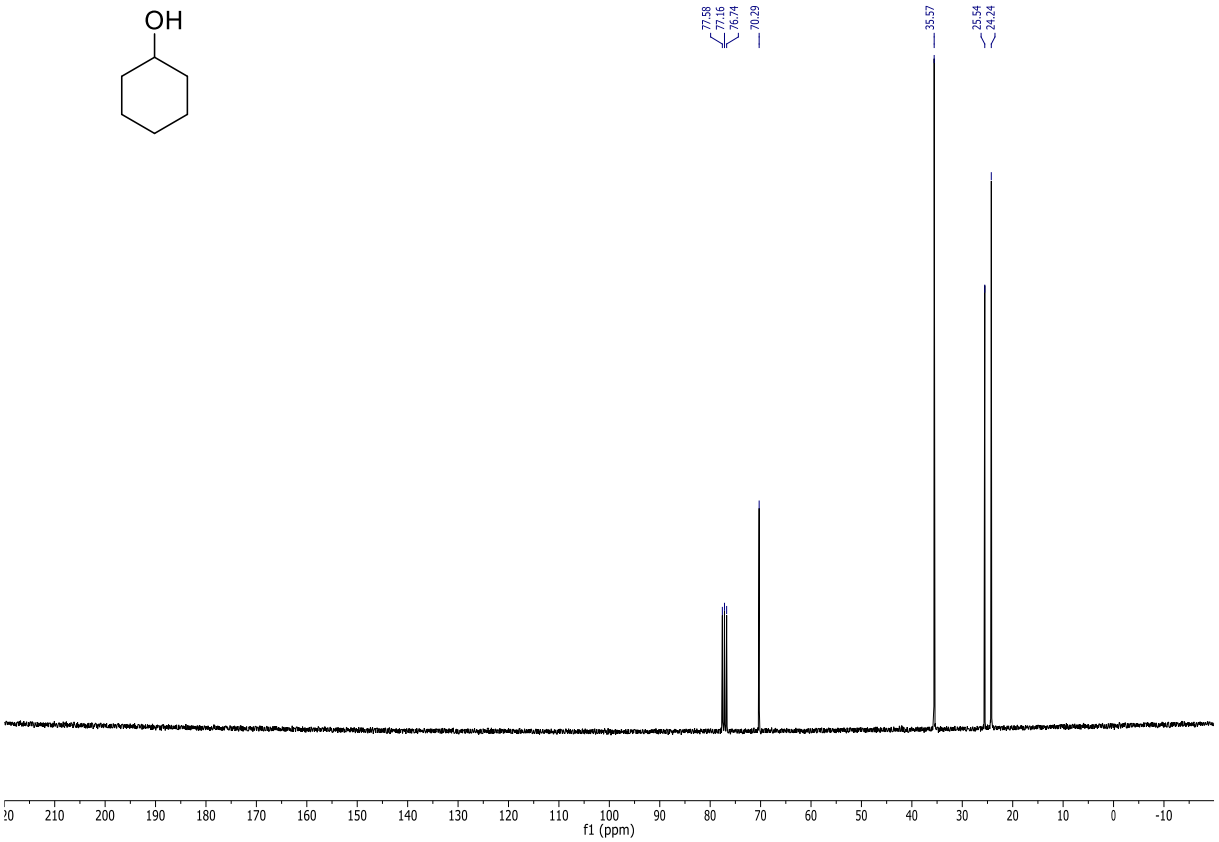
OH
77.58
77.16
76.74
70.29
35.57
25.54
24.24
f1 (ppm)

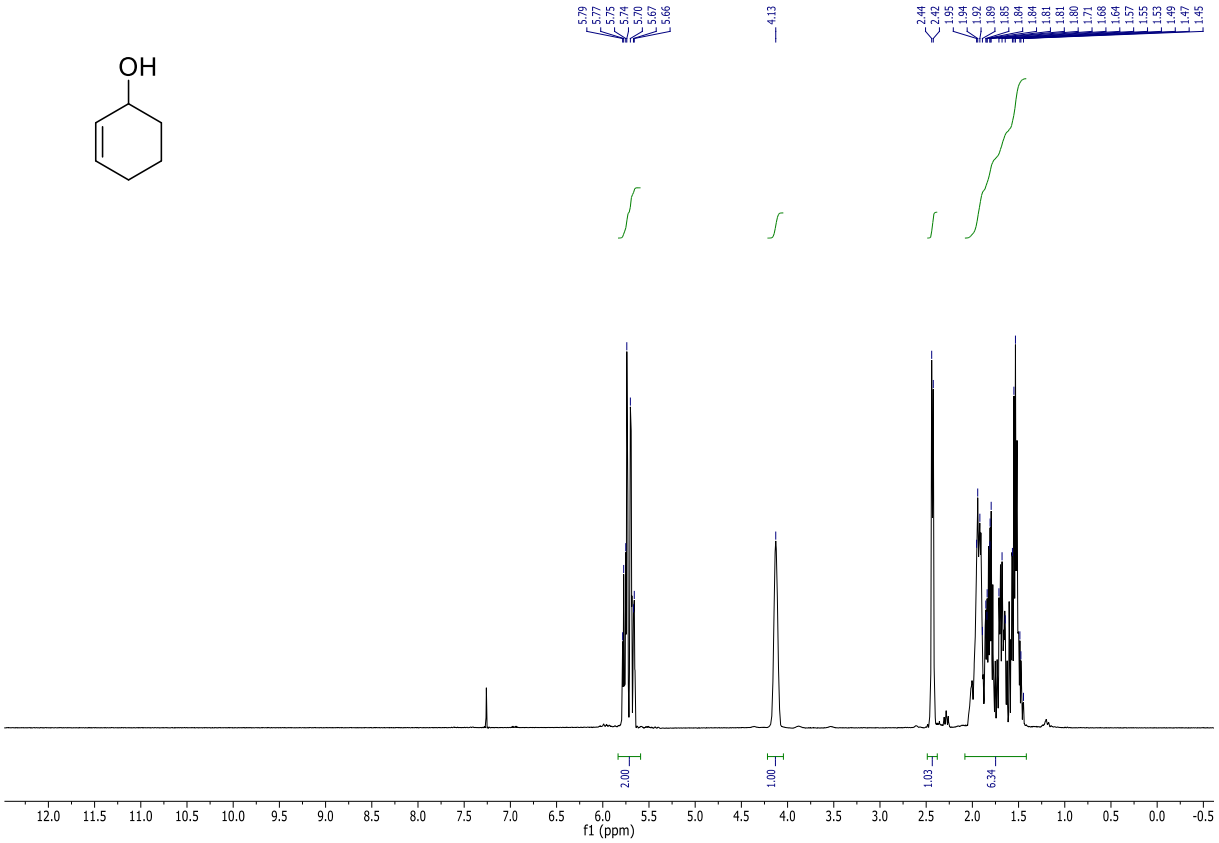
OH
5.79
5.77
5.75
5.74
5.70
5.67
5.66
4.13
2.44
2.42
1.95
1.94
1.92
1.89
1.85
1.84
1.84
1.81
1.81
1.80
1.71
1.68
1.64
1.57
1.55
1.53
1.49
1.47
1.45
2.00
1.00
1.03
6.34
f1 (ppm)

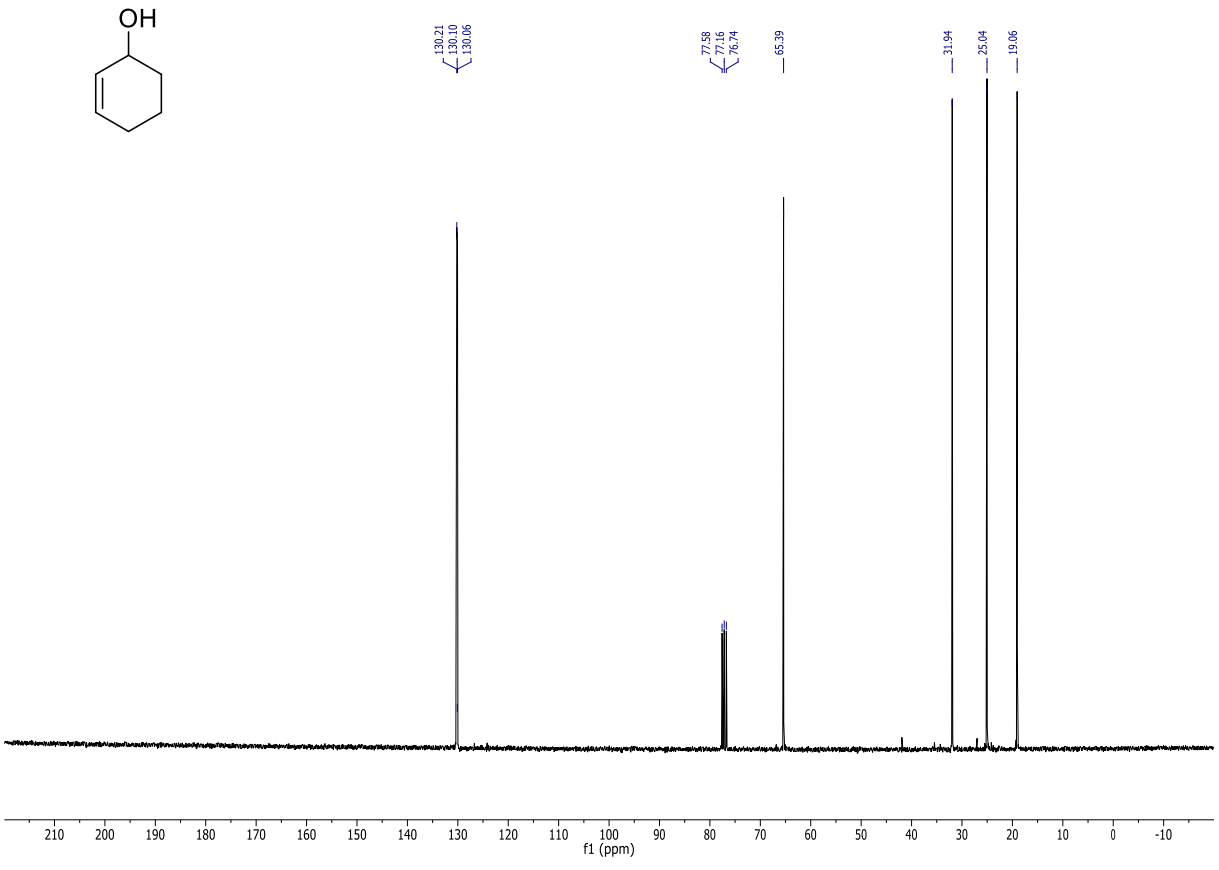
OH
130.21
130.10
130.06
77.58
77.16
76.74
65.39
31.94
25.04
19.06
f1 (ppm)

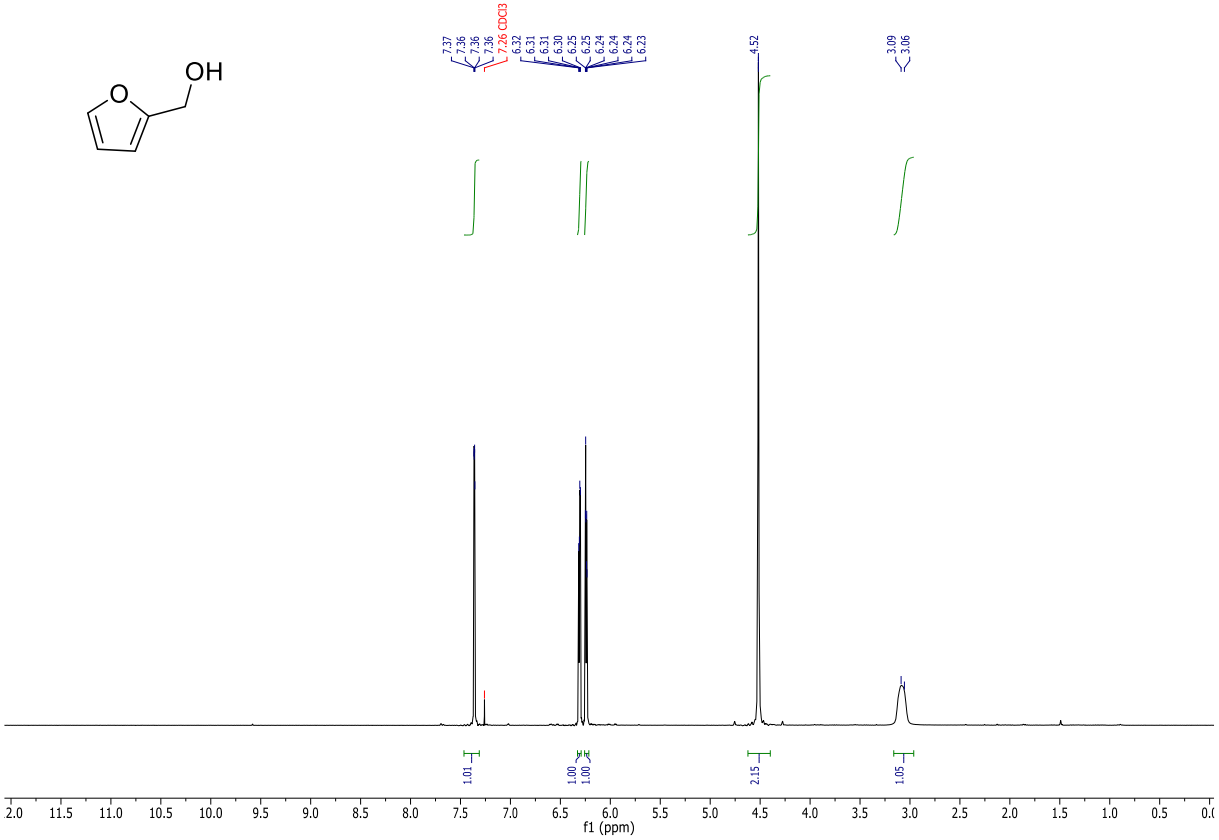
OH
O
7.37
7.36
7.36
7.36
7.26 CDCl3
6.32
6.31
6.31
6.30
6.25
6.25
6.24
6.24
6.24
6.23
4.52
3.09
3.06
1.01
1.00
1.00
2.15
1.05
f1 (ppm)

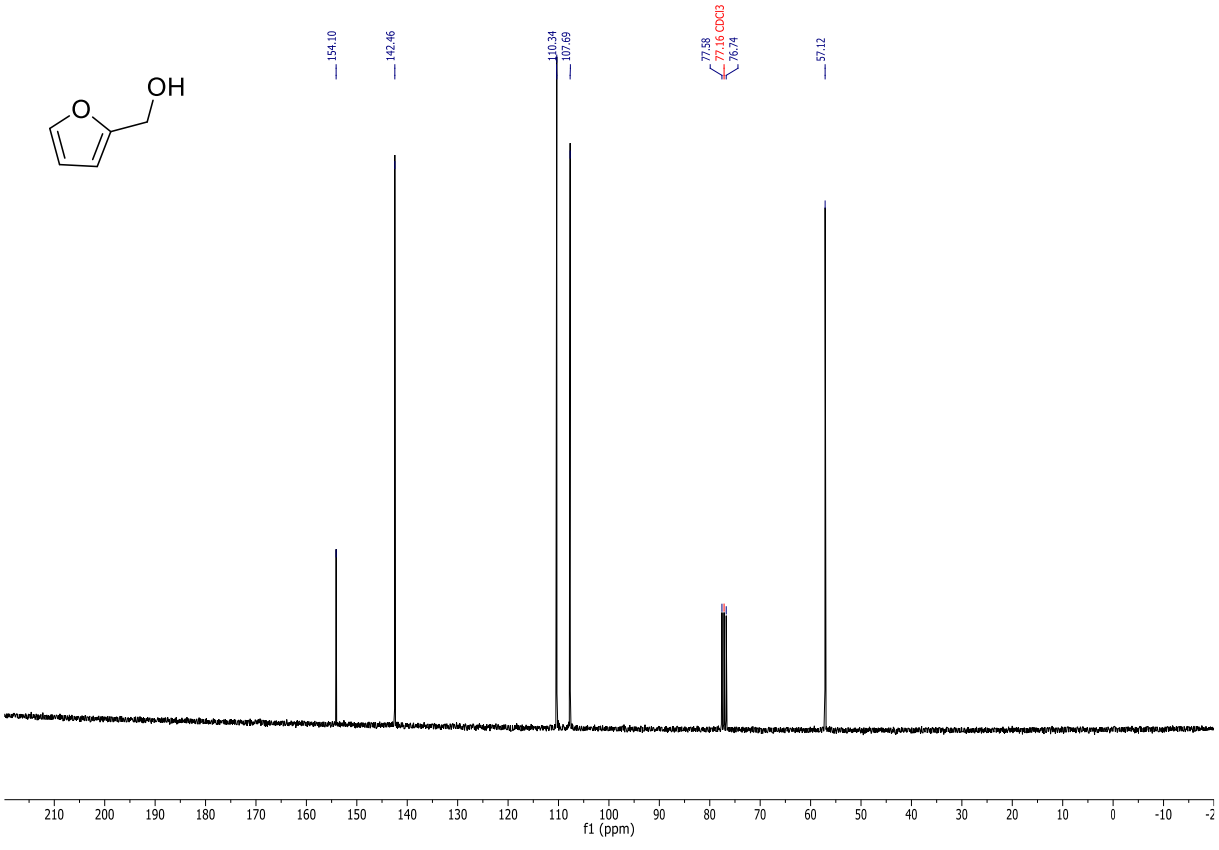
OH
O
154.10
142.46
110.34
107.69
77.58
77.16 CDCl3
76.74
57.12
f1 (ppm)

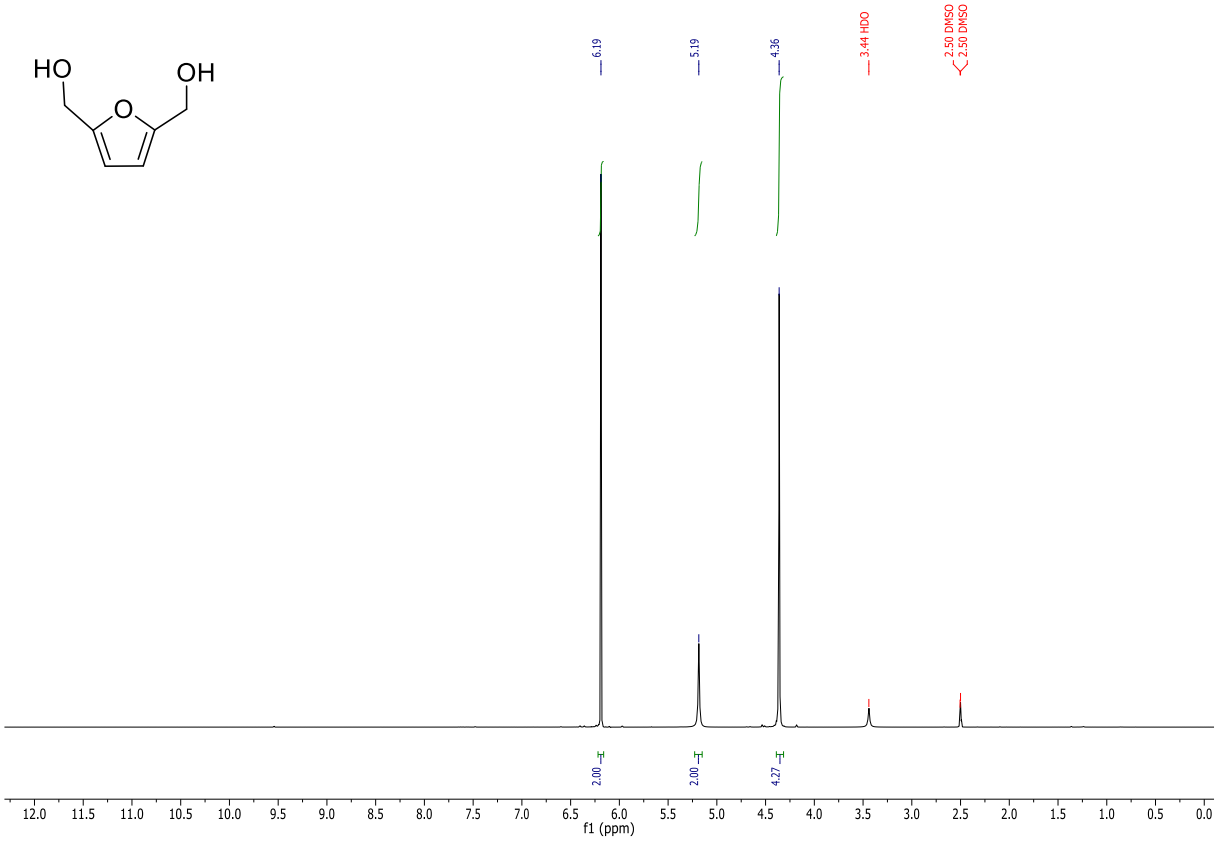
HO
OH
O
6.19
5.19
4.36
3.44 HDO
2.50 DMSO
2.50 DMSO
2.00
2.00
4.27
f1 (ppm)

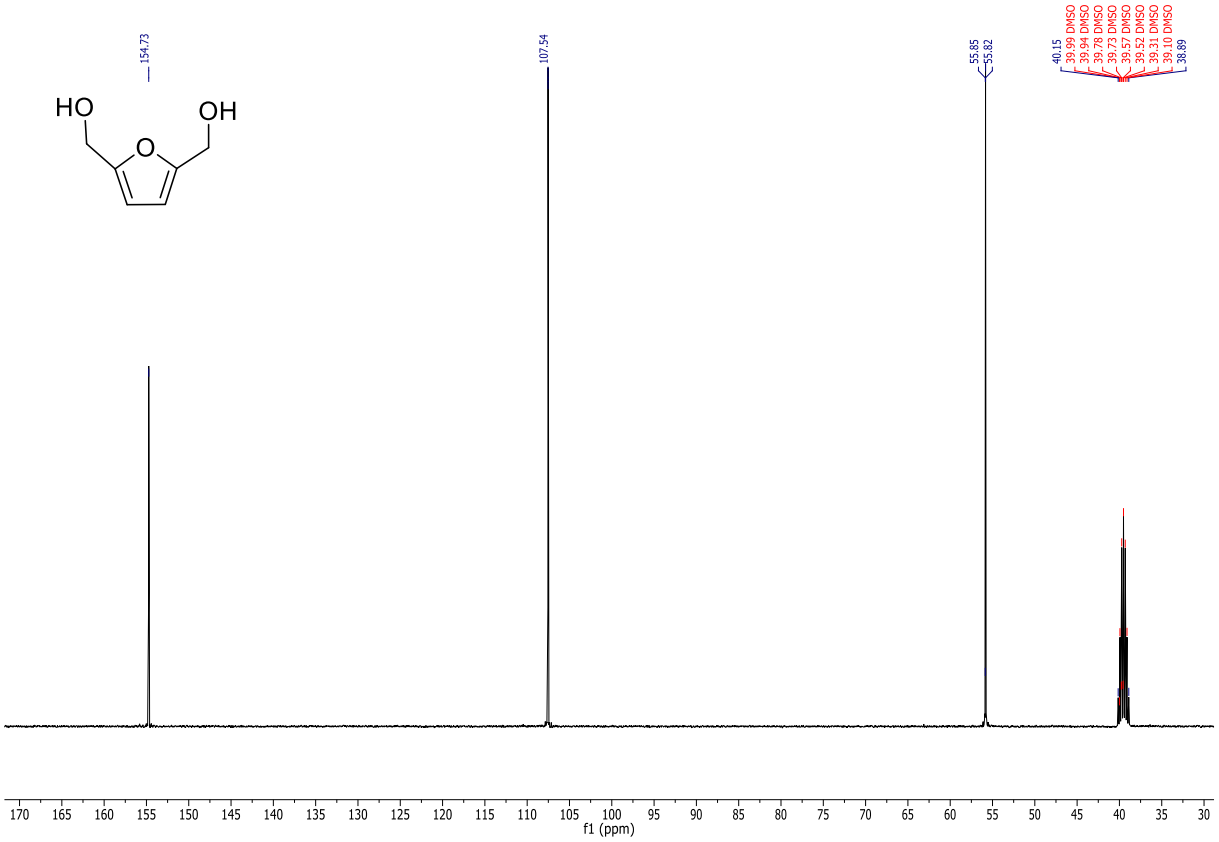
HO
OH
O
154.73
107.54
55.85
55.82
40.15
39.99 DMSO
39.94 DMSO
39.78 DMSO
39.73 DMSO
39.57 DMSO
39.52 DMSO
39.31 DMSO
39.10 DMSO
38.89
f1 (ppm)

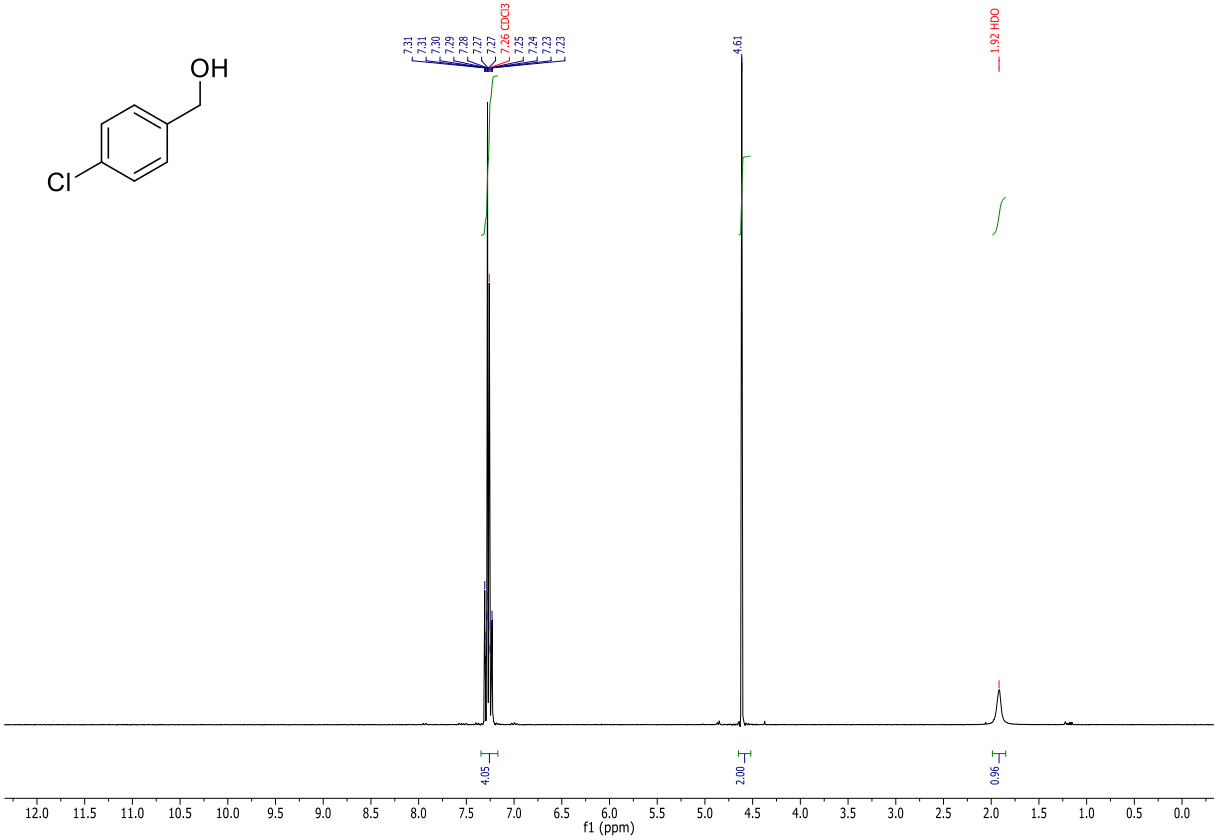
OH
Cl
7.31
7.31
7.30
7.29
7.28
7.27
7.27
7.26 CDCl3
7.25
7.24
7.23
7.23
4.61
1.92 HDO
4.05
2.00
0.96
f1 (ppm)

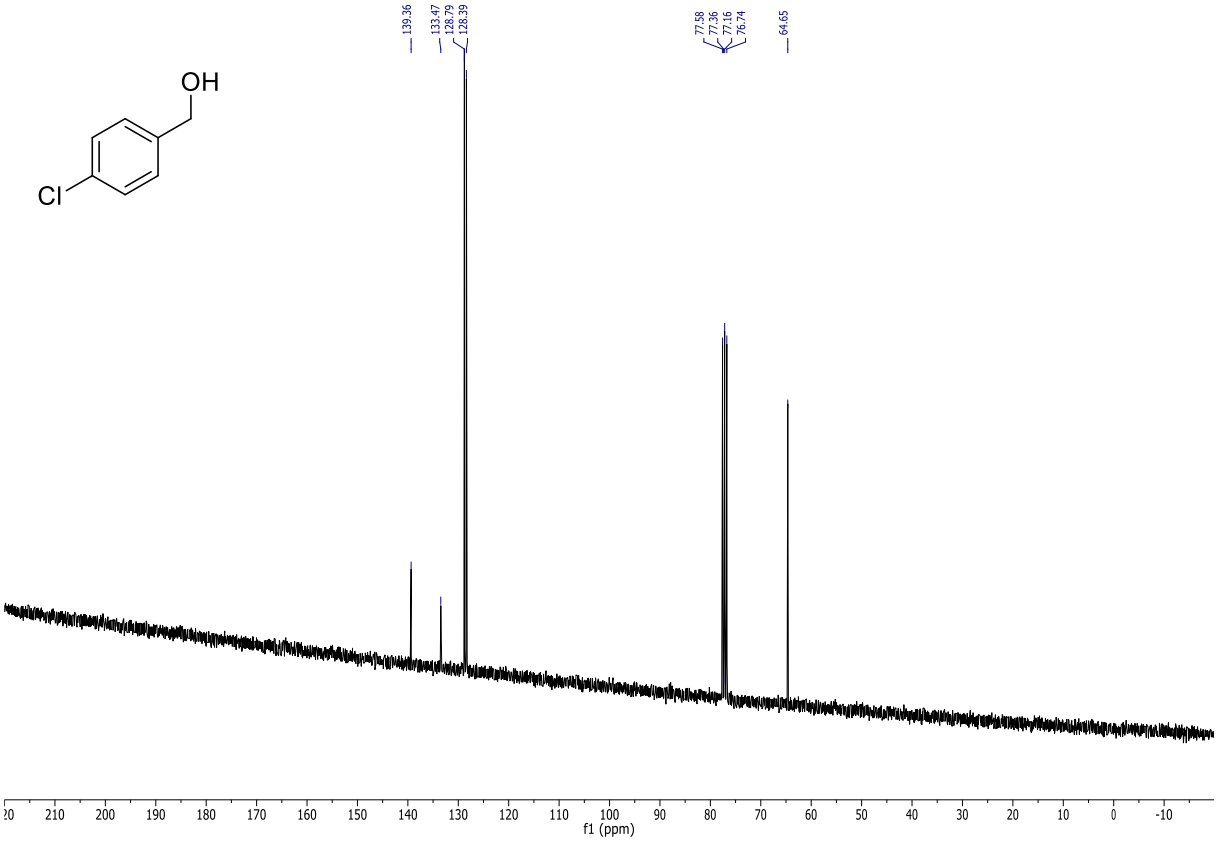
OH
Cl
139.36
133.47
128.79
128.39
77.58
77.36
77.16
76.74
64.65
f1 (ppm)

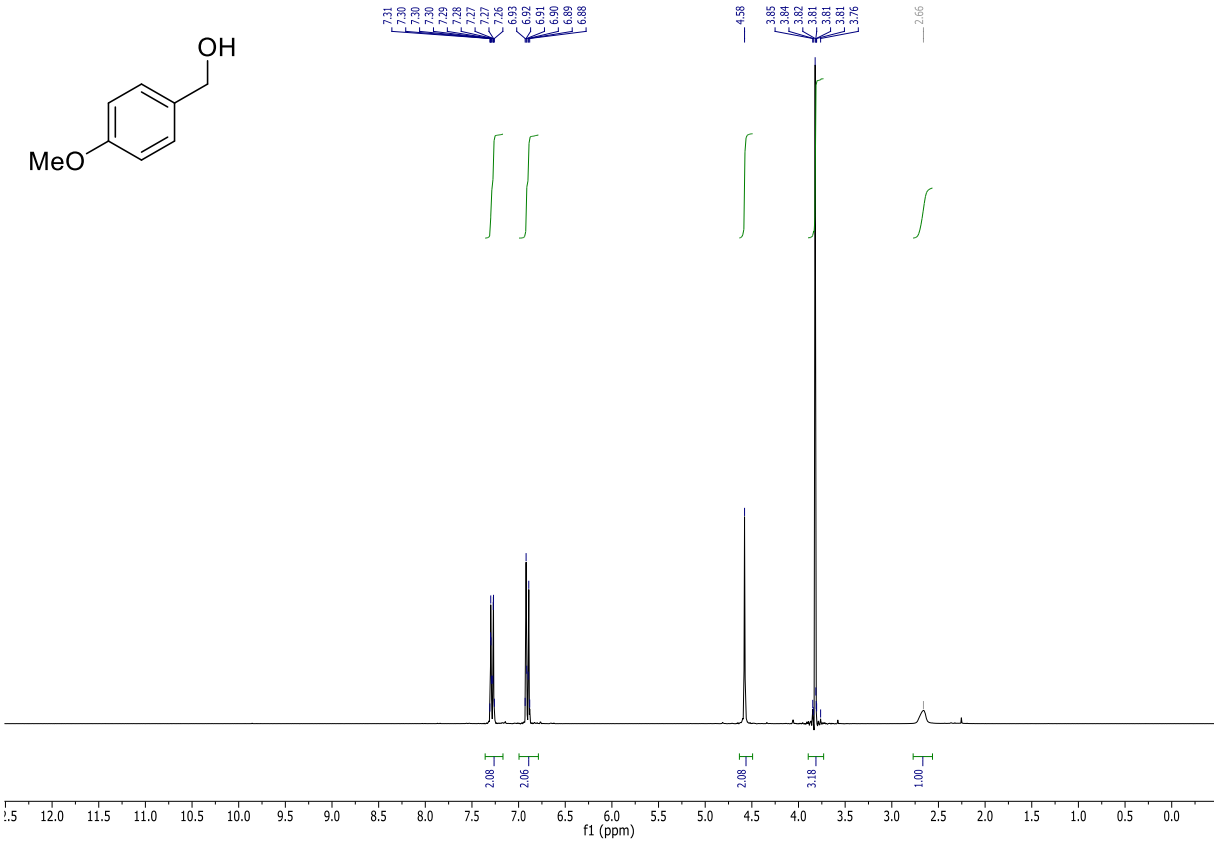
OH
MeO
7.31
7.30
7.30
7.30
7.29
7.28
7.27
7.27
7.26
6.93
6.92
6.91
6.90
6.89
6.88
4.58
3.85
3.84
3.82
3.81
3.81
3.81
3.76
2.66
2.08
2.06
2.08
3.18
1.00
f1 (ppm)

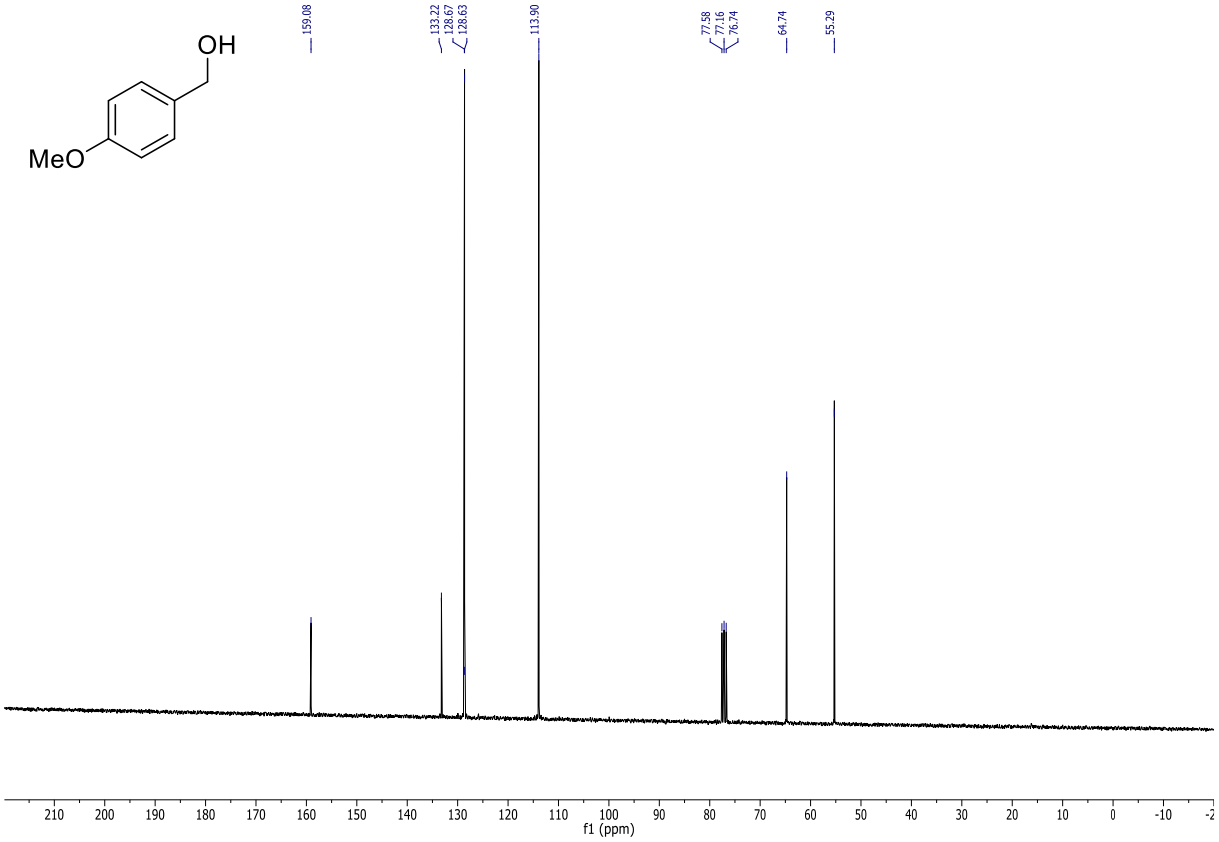
OH
MeO
159.08
133.22
128.67
128.63
113.90
77.58
77.16
76.74
64.74
55.29
f1 (ppm)

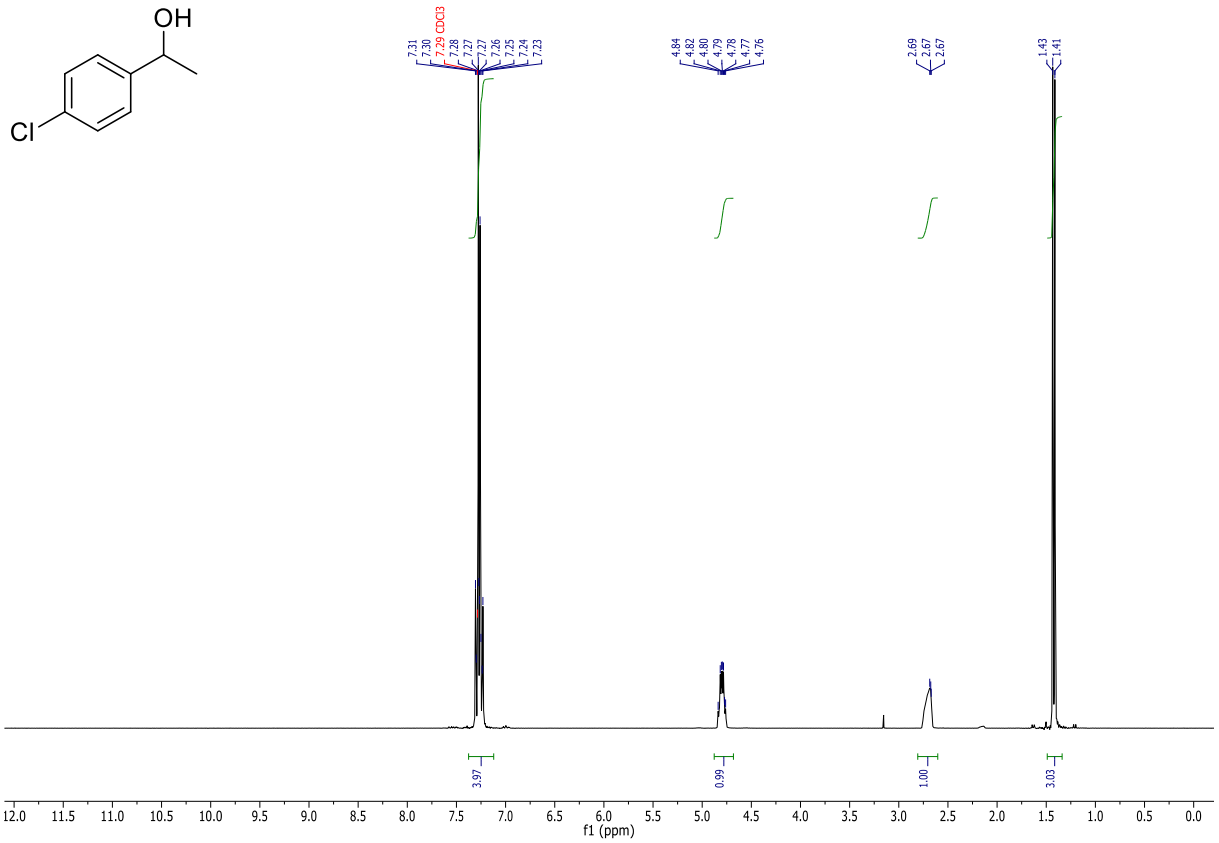
OH
Cl
7.31
7.30
7.29 CDCl3
7.28
7.27
7.27
7.26
7.25
7.24
7.23
4.84
4.82
4.80
4.79
4.78
4.77
4.76
2.69
2.67
2.67
1.43
1.41
3.97
0.99
1.00
3.03
f1 (ppm)

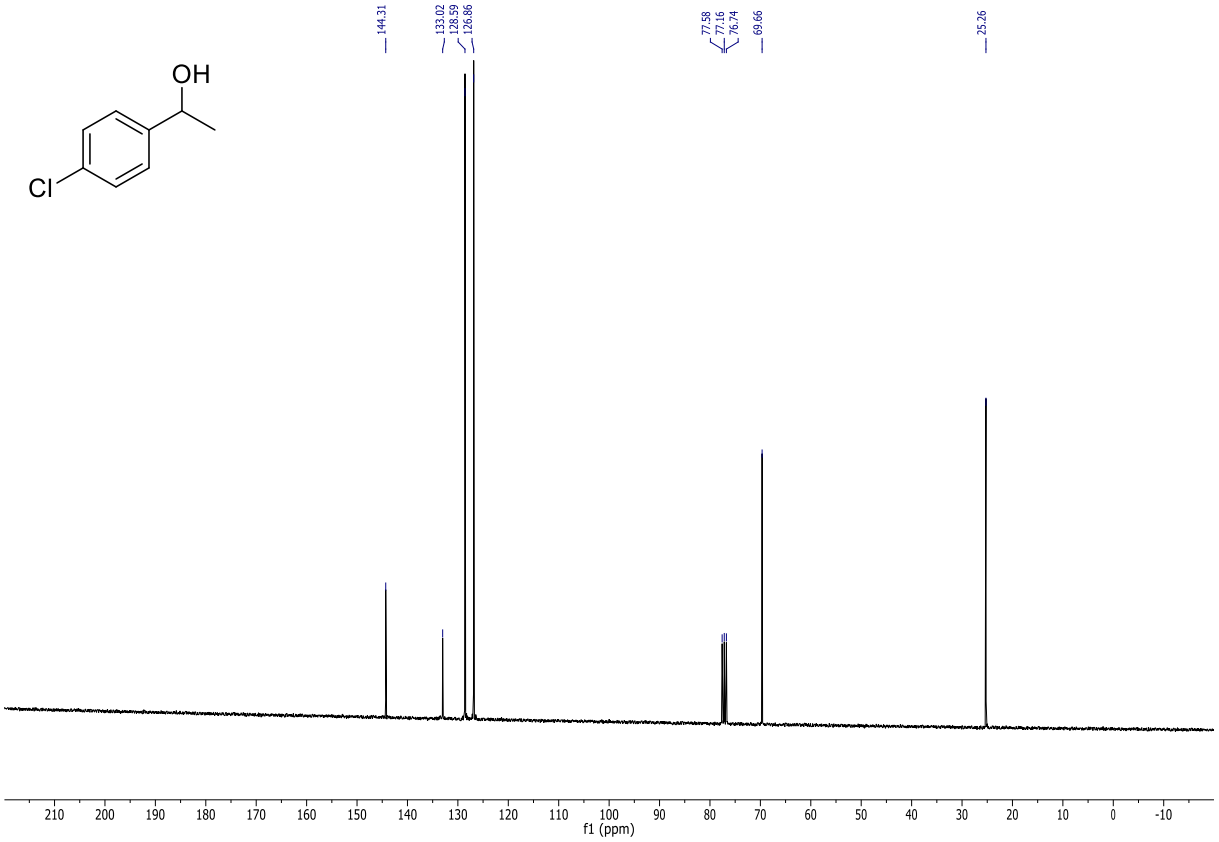
OH
Cl
144.31
133.02
128.59
126.86
77.58
77.16
76.74
69.66
25.26
f1 (ppm)

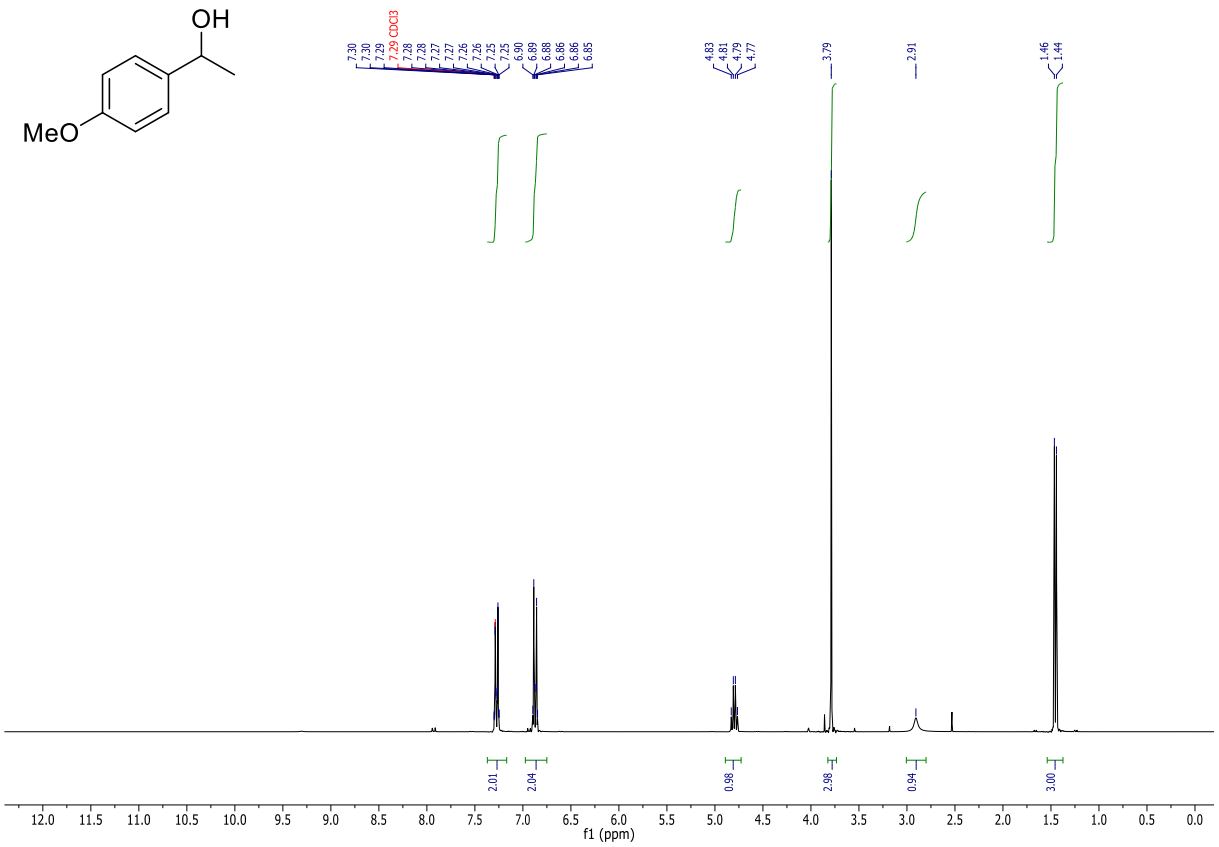
OH
MeO
7.30
7.30
7.29
7.29 CDCl3
7.28
7.28
7.27
7.27
7.26
7.26
7.25
7.25
6.90
6.89
6.88
6.86
6.86
6.85
4.83
4.81
4.79
4.77
3.79
2.91
1.46
1.44
2.01
2.04
0.98
2.98
0.94
3.00
f1 (ppm)

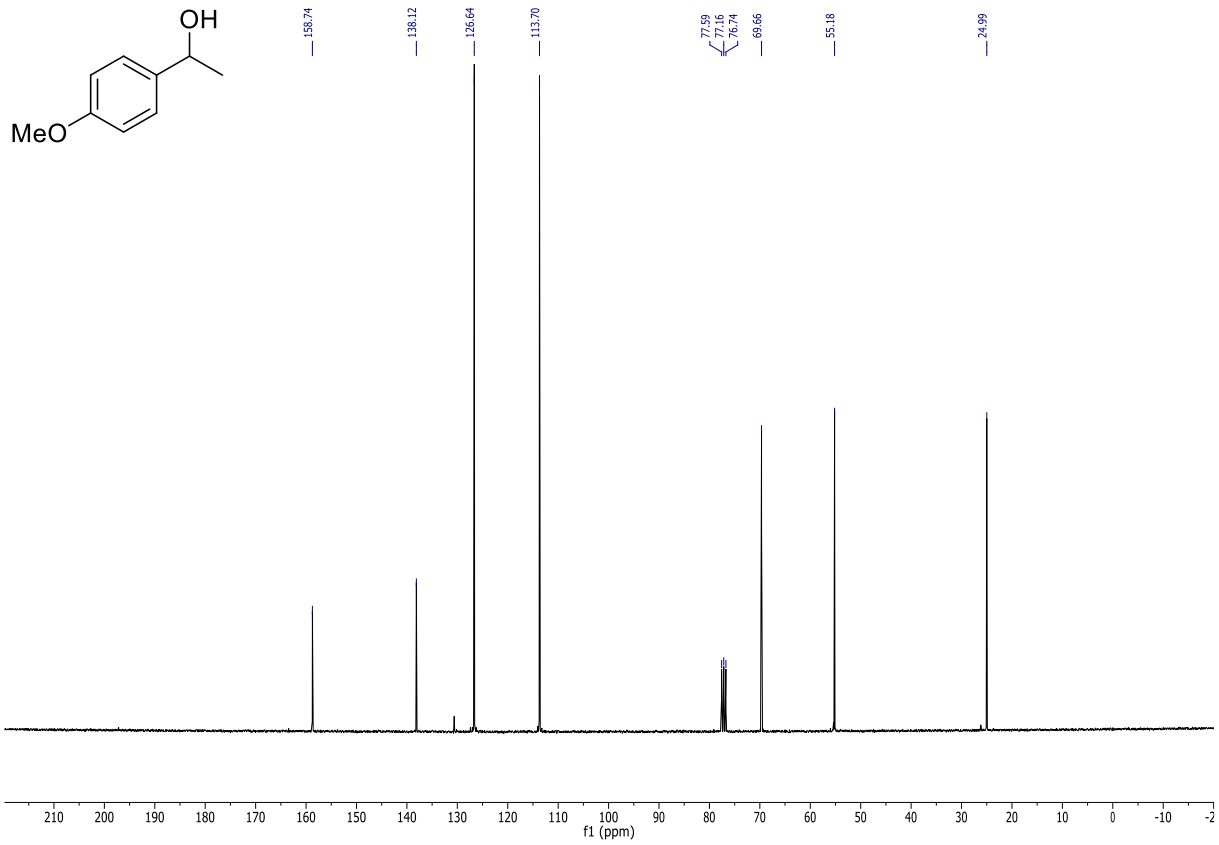
OH
MeO
158.74
138.12
126.64
113.70
77.59
77.16
76.74
69.66
55.18
24.99
f1 (ppm)

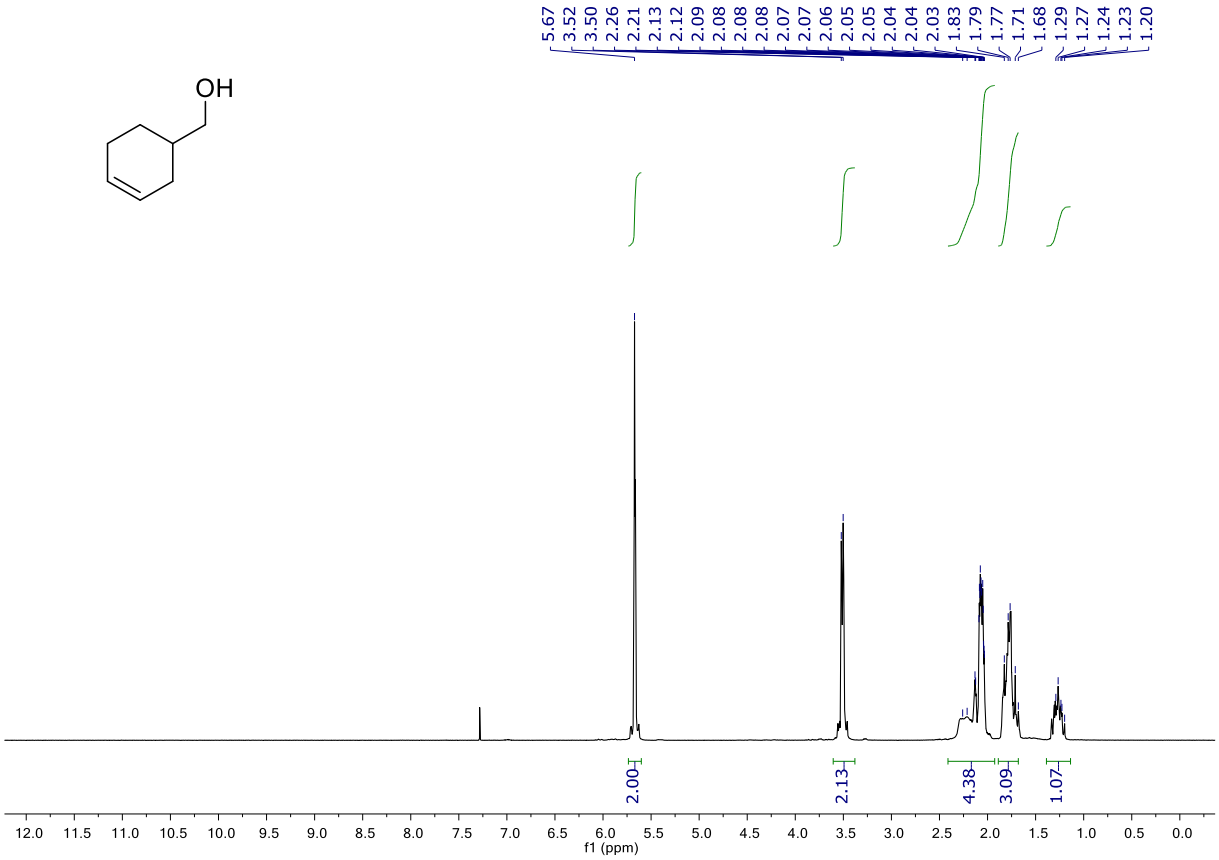
OH
5.67
3.52
3.50
2.26
2.21
2.13
2.12
2.09
2.08
2.08
2.08
2.07
2.07
2.06
2.05
2.05
2.04
2.04
2.03
1.83
1.79
1.77
1.71
1.68
1.29
1.27
1.24
1.23
1.20
2.00
2.13
4.38
3.09
1.07
f1 (ppm)

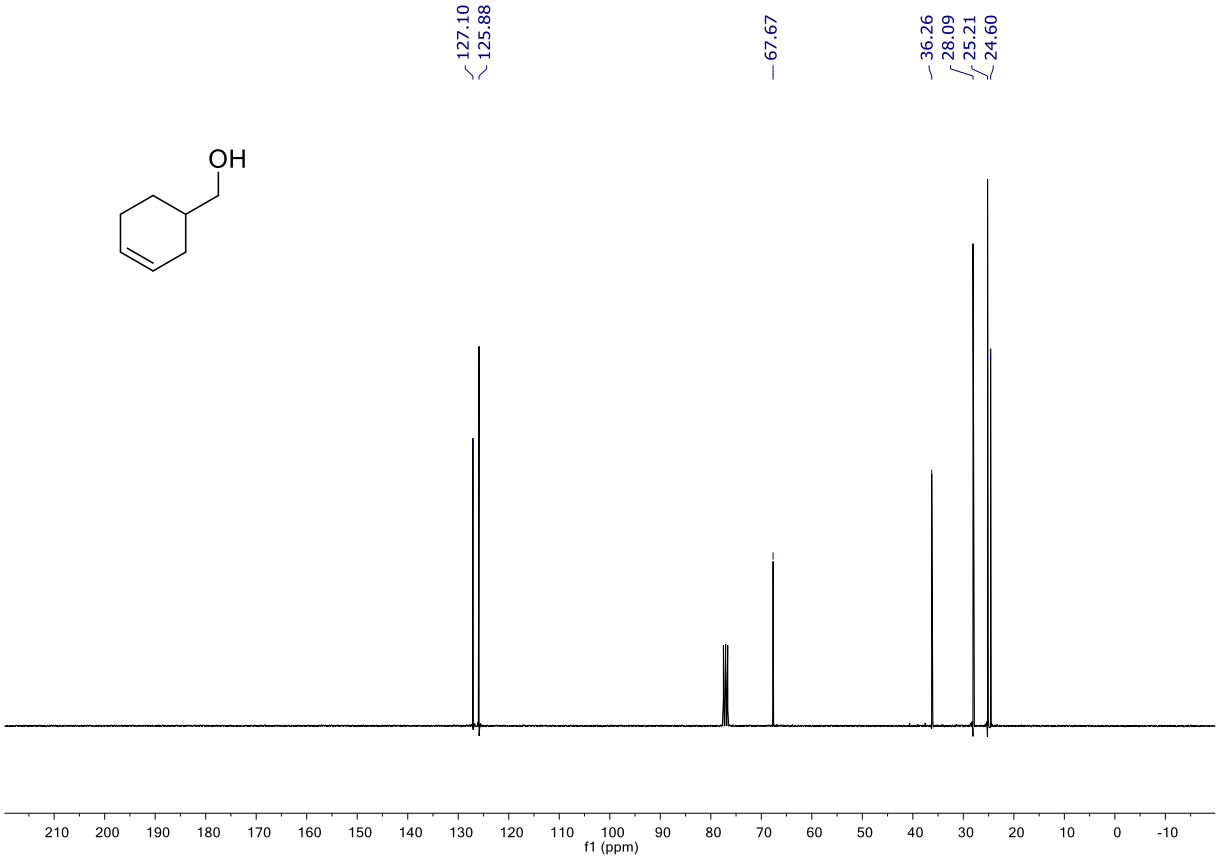
OH
127.10
125.88
67.67
36.26
28.09
25.21
24.60
f1 (ppm)

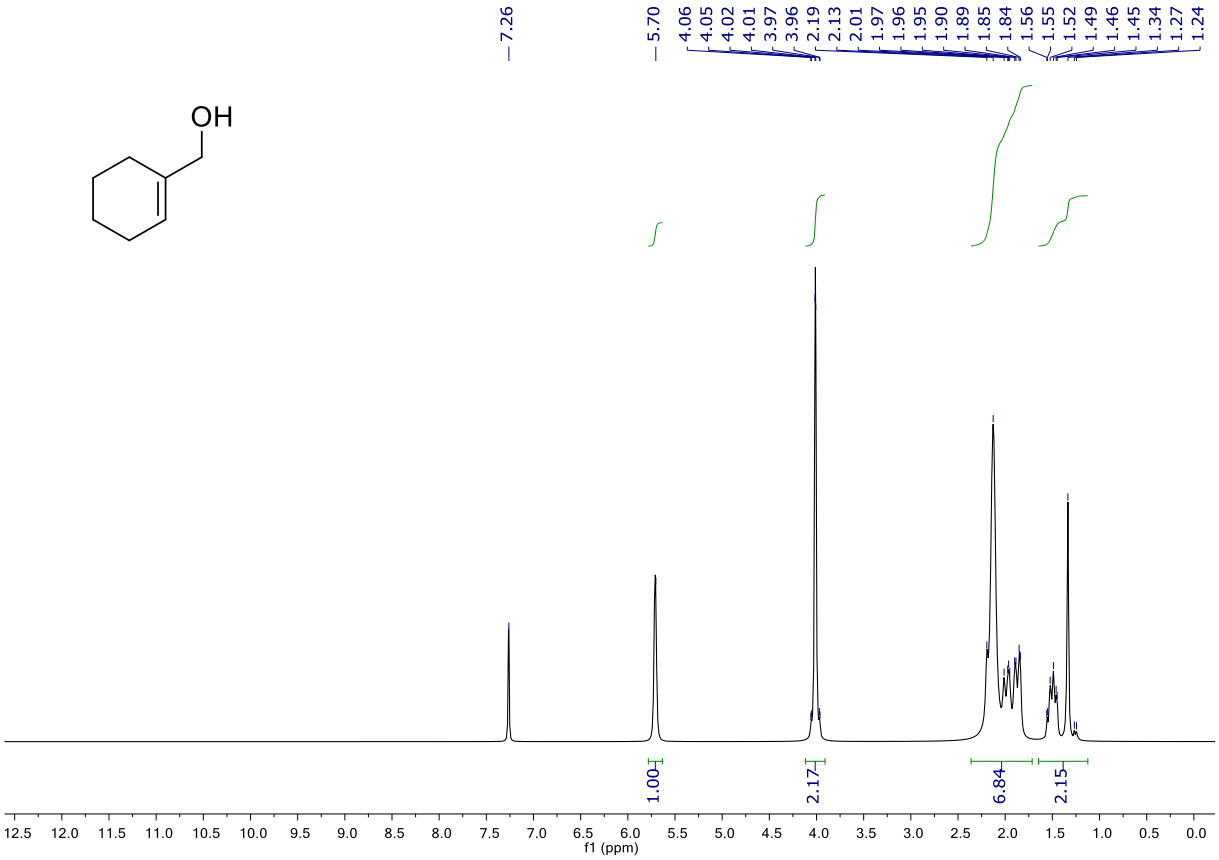
OH
7.26
5.70
4.06
4.05
4.02
4.01
3.97
3.96
2.19
2.13
2.01
1.97
1.96
1.95
1.90
1.89
1.85
1.84
1.56
1.55
1.52
1.49
1.46
1.45
1.34
1.27
1.24
1.00
2.17
6.84
2.15
f1 (ppm)

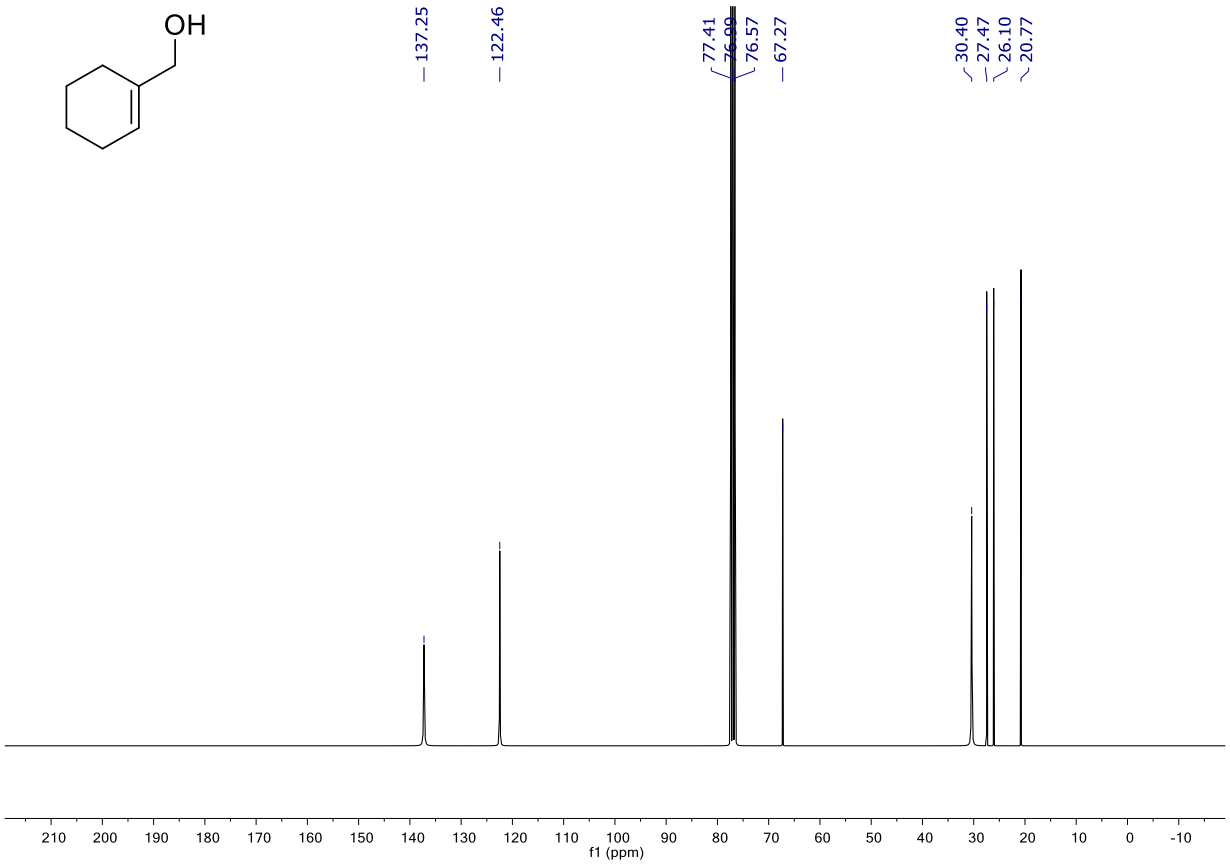
OH
137.25
122.46
77.41
76.99
76.57
67.27
30.40
27.47
26.10
20.77
f1 (ppm)

8.3.3 Crystallographic data

$Ru(NNN_{L3})(PPh_3)Cl_2$ (3)

Chemical formula	$C_{34}H_{32}Cl_2N_5PRu$
Formula weight	713.58
Crystal color & shape	brown needle
Crystal size	0.16 x 0.05 x 0.03
Crystal system	triclinic
Space group	*P*1
a (Å)	9.8760(3)
b (Å)	10.6624(4)
c (Å)	15.3841(5)
a(°)	78.8256(14)
β (°)	80.6086(13)
γ(°)	81.4425(14)
V (Å^3)	1556.43(9)
Z	2
T (K)	150(2)
D_c (g·cm^{-3})	1.523
μ (mm^{-1})	6.400
Reflections collected	21508
Independent reflections	5494 [R_{int} = 0.03]
Reflections observed [I>2σ(I)]	5124
Parameters	392
Final *R* indices [$I>2\sigma(I)$]	R_1 = 0.0237
	wR_2 = 0.0588
R indices (all data)	R_1 = 0.0262
	wR_2 = 0.0604
Goodness-of-fit on F^2	1.042
Largest diff. peak and hole (e·Å^{-3})	0.50 and -0.34

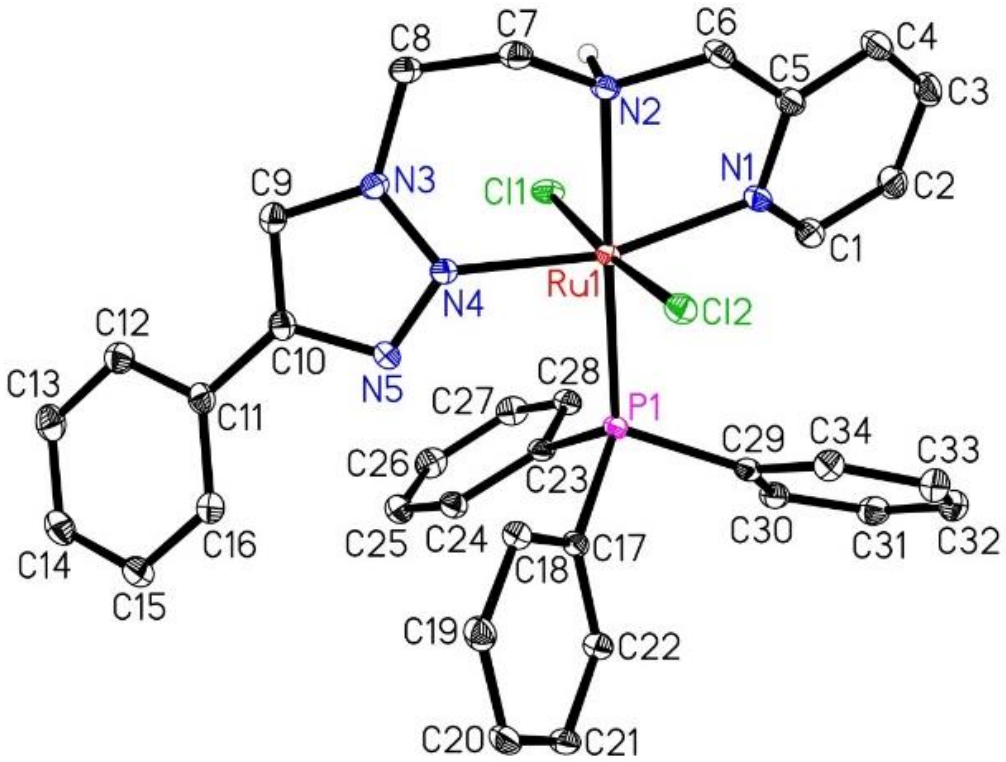

Fig. 1. Molecular structure of **$Ru(NNNL_3)(PPh_3)Cl_2$ (3)** with atom labelling and displacement ellipsoids drawn at the 30% probability level. Hydrogen atoms except the N-bound are omitted for clarity. Selected bond lengths (Å) and angles (°):Cl1-Ru1 2.3958(5), Cl2-Ru1 2.4340(5), N1-Ru1 2.0972(17), N2-Ru1 2.1296(16), N4-Ru1 2.0759(16), P1-Ru1 2.3099(5); N4-Ru1-N1 165.11(7), N4-Ru1-N2 90.39(6), N1-Ru1-N2 77.24(7), N4-Ru1-P1 90.80(5), N1-Ru1-P1 101.69(5), N2-Ru1-P1 178.58(5), N4-Ru1-Cl1 84.18(5), N1-Ru1-Cl1 86.63(5), N2-Ru1-Cl1 85.73(5), P1-Ru1-Cl1 95.165(17), N4-Ru1-Cl2 96.35(5), N1-Ru1-Cl2 91.63(5), N2-Ru1-Cl2 88.44(5), P1-Ru1-Cl2 90.657(17), Cl1-Ru1-Cl2 174.149(16).

9.3.4 DFT cartesian coordinates

Dihydride-is1-EDF2

C	-3.431000000	-2.983000000	0.339000000
H	-4.328000000	-3.512000000	0.674000000
C	-2.554000000	-3.939000000	-0.474000000
H	-2.617000000	-4.952000000	-0.053000000
H	-2.929000000	-3.993000000	-1.499000000
N	-1.143000000	-3.511000000	-0.533000000
C	-0.307000000	-4.160000000	0.479000000
H	-0.493000000	-3.672000000	1.439000000
H	-0.559000000	-5.230000000	0.566000000
C	1.161000000	-4.104000000	0.114000000
H	1.291000000	-4.478000000	-0.912000000
H	1.712000000	-4.776000000	0.776000000
N	1.806000000	-2.810000000	0.219000000
N	1.204000000	-1.627000000	-0.071000000
N	2.133000000	-0.716000000	-0.141000000
C	3.347000000	-1.285000000	0.090000000
C	3.149000000	-2.626000000	0.311000000
H	3.823000000	-3.446000000	0.491000000
C	4.584000000	-0.510000000	0.057000000
C	6.952000000	0.982000000	-0.037000000
C	4.617000000	0.730000000	-0.590000000
C	5.752000000	-0.990000000	0.658000000
C	6.927000000	-0.252000000	0.608000000
C	5.792000000	1.469000000	-0.633000000
H	3.714000000	1.096000000	-1.065000000
H	5.735000000	-1.939000000	1.186000000
H	7.824000000	-0.636000000	1.082000000
H	5.802000000	2.427000000	-1.141000000
H	7.869000000	1.560000000	-0.072000000
H	-0.780000000	-3.731000000	-1.456000000
Ru	-0.806000000	-1.298000000	-0.388000000
H	-0.457000000	-1.295000000	-2.062000000
P	-0.518000000	0.921000000	0.102000000
C	0.195000000	2.082000000	-1.159000000
C	1.294000000	3.713000000	-3.159000000
C	0.513000000	1.554000000	-2.412000000
C	0.446000000	3.440000000	-0.918000000
C	0.987000000	4.250000000	-1.911000000
C	1.058000000	2.365000000	-3.406000000
H	0.328000000	0.494000000	-2.580000000
H	0.229000000	3.866000000	0.056000000
H	1.174000000	5.299000000	-1.708000000
H	1.301000000	1.938000000	-4.374000000
H	1.719000000	4.345000000	-3.932000000
C	-2.116000000	1.761000000	0.582000000
C	-4.566000000	2.895000000	1.387000000
C	-2.560000000	2.974000000	0.047000000
C	-2.946000000	1.111000000	1.506000000
C	-4.149000000	1.675000000	1.912000000
C	-3.770000000	3.535000000	0.446000000
H	-1.967000000	3.490000000	-0.698000000
H	-2.652000000	0.134000000	1.877000000
H	-4.768000000	1.152000000	2.634000000
H	-4.089000000	4.479000000	0.014000000
H	-5.507000000	3.334000000	1.701000000
C	0.533000000	1.283000000	1.600000000
C	2.092000000	1.719000000	3.901000000
C	1.758000000	1.950000000	1.524000000
C	0.117000000	0.817000000	2.852000000
C	0.883000000	1.038000000	3.990000000
C	2.530000000	2.167000000	2.661000000
H	2.127000000	2.292000000	0.567000000
H	-0.803000000	0.253000000	2.933000000
H	0.532000000	0.670000000	4.950000000
H	3.481000000	2.681000000	2.570000000
H	2.693000000	1.889000000	4.789000000
H	-1.205000000	-1.441000000	1.278000000
N	-2.824000000	-1.010000000	-0.944000000
C	-5.487000000	-0.536000000	-1.685000000
C	-3.157000000	-0.024000000	-1.804000000
C	-3.823000000	-1.800000000	-0.484000000
C	-5.153000000	-1.575000000	-0.832000000
C	-4.456000000	0.247000000	-2.192000000
H	-2.324000000	0.549000000	-2.187000000
H	-5.917000000	-2.230000000	-0.428000000
H	-4.646000000	1.063000000	-2.878000000
H	-6.520000000	-0.349000000	-1.957000000
H	-2.851000000	-2.643000000	1.207000000

Dihydride-is2-EDF2

C	2.839000000	-0.935000000	-2.482000000
H	3.754000000	-0.702000000	-3.035000000
C	1.652000000	-0.781000000	-3.438000000
H	1.503000000	0.286000000	-3.626000000
H	1.875000000	-1.254000000	-4.407000000
N	0.420000000	-1.321000000	-2.868000000
C	-0.798000000	-0.845000000	-3.507000000
H	-0.860000000	0.241000000	-3.385000000
H	-0.806000000	-1.058000000	-4.589000000
C	-2.023000000	-1.513000000	-2.888000000
H	-1.815000000	-2.573000000	-2.709000000
H	-2.873000000	-1.425000000	-3.567000000
N	-2.450000000	-0.927000000	-1.633000000
N	-1.656000000	-0.886000000	-0.534000000
N	-2.339000000	-0.337000000	0.431000000
C	-3.583000000	-0.018000000	-0.020000000
C	-3.662000000	-0.397000000	-1.341000000
H	-4.447000000	-0.338000000	-2.076000000
C	-4.563000000	0.634000000	0.846000000
C	-6.407000000	1.912000000	2.525000000
C	-4.210000000	0.981000000	2.155000000
C	-5.851000000	0.936000000	0.391000000
C	-6.764000000	1.569000000	1.224000000
C	-5.127000000	1.614000000	2.984000000
H	-3.213000000	0.749000000	2.511000000
H	-6.146000000	0.672000000	-0.620000000
H	-7.760000000	1.795000000	0.855000000
H	-4.836000000	1.878000000	3.996000000
H	-7.121000000	2.406000000	3.175000000
H	0.442000000	-2.334000000	-2.945000000
Ru	0.282000000	-1.585000000	-0.551000000
H	-0.373000000	-3.051000000	-0.961000000
P	1.011000000	0.483000000	0.415000000
C	0.312000000	0.959000000	2.073000000
C	-0.634000000	1.596000000	4.633000000
C	-0.303000000	-0.013000000	2.863000000
C	0.450000000	2.254000000	2.584000000
C	-0.024000000	2.573000000	3.851000000
C	-0.769000000	0.304000000	4.137000000
H	-0.423000000	-1.011000000	2.455000000
H	0.928000000	3.025000000	1.989000000
H	0.089000000	3.584000000	4.230000000
H	-1.243000000	-0.465000000	4.739000000
H	-1.000000000	1.842000000	5.625000000
C	2.805000000	0.759000000	0.811000000
C	5.499000000	0.988000000	1.565000000
C	3.525000000	-0.358000000	1.249000000
C	3.458000000	1.996000000	0.766000000
C	4.795000000	2.108000000	1.134000000
C	4.858000000	-0.245000000	1.627000000
H	3.023000000	-1.318000000	1.294000000
H	2.921000000	2.880000000	0.440000000
H	5.285000000	3.075000000	1.090000000
H	5.397000000	-1.123000000	1.969000000
H	6.542000000	1.078000000	1.853000000
C	0.562000000	1.961000000	-0.611000000
C	-0.324000000	3.932000000	-2.421000000
C	-0.709000000	2.538000000	-0.487000000
C	1.378000000	2.399000000	-1.663000000
C	0.945000000	3.375000000	-2.554000000
C	-1.147000000	3.509000000	-1.382000000
H	-1.364000000	2.222000000	0.317000000
H	2.373000000	1.984000000	-1.782000000
H	1.605000000	3.707000000	-3.350000000
H	-2.135000000	3.940000000	-1.260000000
H	-0.663000000	4.694000000	-3.115000000
H	0.140000000	-2.152000000	0.936000000
N	2.109000000	-2.601000000	-0.835000000
C	4.272000000	-4.283000000	-1.436000000
C	2.319000000	-3.755000000	-0.162000000
C	3.001000000	-2.264000000	-1.804000000
C	4.075000000	-3.096000000	-2.121000000
C	3.374000000	-4.609000000	-0.424000000
H	1.580000000	-3.969000000	0.597000000
H	4.761000000	-2.787000000	-2.902000000
H	3.478000000	-5.517000000	0.157000000
H	5.108000000	-4.932000000	-1.675000000
H	2.733000000	-0.189000000	-1.690000000

Dihydride-is3-EDF2

C	1.782000000	-2.063000000	1.398000000
H	2.546000000	-2.779000000	1.715000000
C	0.625000000	-2.106000000	2.397000000
H	-0.083000000	-2.887000000	2.104000000
H	1.012000000	-2.380000000	3.391000000
N	-0.103000000	-0.834000000	2.443000000
C	-1.310000000	-0.903000000	3.279000000
H	-1.613000000	-1.951000000	3.371000000
H	-1.118000000	-0.540000000	4.298000000
C	-2.480000000	-0.109000000	2.707000000
H	-2.159000000	0.910000000	2.470000000
H	-3.307000000	-0.094000000	3.420000000
N	-2.984000000	-0.683000000	1.476000000
N	-2.244000000	-0.646000000	0.348000000
N	-2.925000000	-1.214000000	-0.606000000
C	-4.126000000	-1.623000000	-0.110000000
C	-4.168000000	-1.286000000	1.227000000
H	-4.921000000	-1.401000000	1.989000000
C	-5.125000000	-2.281000000	-0.949000000
C	-7.033000000	-3.521000000	-2.583000000
C	-4.921000000	-2.382000000	-2.329000000
C	-6.297000000	-2.813000000	-0.400000000
C	-7.243000000	-3.425000000	-1.211000000
C	-5.867000000	-2.998000000	-3.137000000
H	-4.013000000	-1.968000000	-2.752000000
H	-6.469000000	-2.753000000	0.670000000
H	-8.146000000	-3.832000000	-0.769000000
H	-5.696000000	-3.066000000	-4.206000000
H	-7.772000000	-3.999000000	-3.216000000
H	0.520000000	-0.120000000	2.810000000
Ru	-0.342000000	0.253000000	0.306000000
H	-1.019000000	1.582000000	0.980000000
H	-0.701000000	0.875000000	-1.116000000
N	0.503000000	-1.562000000	-0.629000000
C	1.514000000	-3.804000000	-1.955000000
C	0.118000000	-1.868000000	-1.880000000
C	1.385000000	-2.379000000	-0.017000000
C	1.906000000	-3.502000000	-0.658000000
C	0.594000000	-2.968000000	-2.575000000
H	-0.604000000	-1.188000000	-2.313000000
H	2.617000000	-4.130000000	-0.134000000
H	0.247000000	-3.156000000	-3.584000000
H	1.916000000	-4.672000000	-2.466000000
H	2.230000000	-1.064000000	1.445000000
P	1.443000000	1.628000000	0.135000000
C	2.398000000	1.954000000	1.704000000
C	3.621000000	2.425000000	4.195000000
C	3.789000000	2.040000000	1.815000000
C	1.632000000	2.128000000	2.866000000
C	2.234000000	2.363000000	4.097000000
C	4.394000000	2.267000000	3.050000000
H	4.410000000	1.932000000	0.933000000
H	0.548000000	2.099000000	2.775000000
H	1.619000000	2.506000000	4.981000000
H	5.476000000	2.327000000	3.114000000
H	4.095000000	2.602000000	5.154000000
C	1.114000000	3.383000000	-0.380000000
C	0.607000000	6.018000000	-1.179000000
C	2.122000000	4.351000000	-0.325000000
C	-0.152000000	3.752000000	-0.837000000
C	-0.401000000	5.063000000	-1.237000000
C	1.872000000	5.659000000	-0.721000000
H	3.110000000	4.081000000	0.035000000
H	-0.927000000	2.995000000	-0.865000000
H	-1.391000000	5.336000000	-1.591000000
H	2.664000000	6.400000000	-0.670000000
H	0.410000000	7.040000000	-1.487000000
C	2.760000000	1.166000000	-1.087000000
C	4.555000000	0.270000000	-3.062000000
C	3.704000000	0.170000000	-0.809000000
C	2.728000000	1.693000000	-2.383000000
C	3.614000000	1.250000000	-3.360000000
C	4.597000000	-0.268000000	-1.781000000
H	3.759000000	-0.264000000	0.183000000
H	2.002000000	2.458000000	-2.631000000
H	3.569000000	1.677000000	-4.356000000
H	5.327000000	-1.033000000	-1.535000000
H	5.250000000	-0.072000000	-3.823000000

Dihydride-is4-EDF2

C	-2.874000000	3.378000000	-0.287000000
H	-3.541000000	4.167000000	-0.648000000
C	-2.139000000	3.905000000	0.950000000
H	-1.356000000	4.600000000	0.630000000
H	-2.838000000	4.481000000	1.573000000
N	-1.500000000	2.839000000	1.741000000
C	-0.431000000	3.347000000	2.607000000
H	0.164000000	4.062000000	2.032000000
H	-0.834000000	3.889000000	3.476000000
C	0.494000000	2.243000000	3.114000000
H	-0.100000000	1.387000000	3.449000000
H	1.105000000	2.619000000	3.937000000
N	1.405000000	1.770000000	2.091000000
N	0.940000000	1.095000000	1.020000000
N	1.955000000	0.810000000	0.251000000
C	3.095000000	1.301000000	0.815000000
C	2.748000000	1.924000000	1.995000000
H	3.320000000	2.432000000	2.753000000
C	4.401000000	1.139000000	0.180000000
C	6.889000000	0.817000000	-1.069000000
C	4.513000000	0.407000000	-1.008000000
C	5.555000000	1.706000000	0.731000000
C	6.787000000	1.546000000	0.112000000
C	5.746000000	0.249000000	-1.625000000
H	3.619000000	-0.033000000	-1.433000000
H	5.490000000	2.282000000	1.649000000
H	7.672000000	1.993000000	0.554000000
H	5.815000000	-0.322000000	-2.545000000
H	7.852000000	0.693000000	-1.553000000
H	-2.205000000	2.381000000	2.313000000
Ru	-1.178000000	0.807000000	0.749000000
H	-1.395000000	0.150000000	2.230000000
N	-1.092000000	1.951000000	-1.163000000
C	-1.025000000	3.332000000	-3.593000000
C	-0.193000000	1.652000000	-2.114000000
C	-1.941000000	2.977000000	-1.391000000
C	-1.929000000	3.676000000	-2.597000000
C	-0.129000000	2.303000000	-3.336000000
H	0.505000000	0.864000000	-1.868000000
H	-2.634000000	4.487000000	-2.744000000
H	0.610000000	1.996000000	-4.066000000
H	-1.015000000	3.862000000	-4.539000000
H	-3.479000000	2.513000000	0.006000000
P	-1.153000000	-1.333000000	0.068000000
H	-2.796000000	0.711000000	0.647000000
C	-2.636000000	-2.386000000	0.463000000
C	-4.821000000	-3.988000000	1.183000000
C	-2.843000000	-3.628000000	-0.146000000
C	-3.538000000	-1.960000000	1.439000000
C	-4.621000000	-2.758000000	1.799000000
C	-3.928000000	-4.422000000	0.207000000
H	-2.156000000	-3.979000000	-0.909000000
H	-3.374000000	-0.992000000	1.897000000
H	-5.313000000	-2.412000000	2.560000000
H	-4.076000000	-5.380000000	-0.281000000
H	-5.668000000	-4.607000000	1.460000000
C	0.173000000	-2.436000000	0.773000000
C	2.098000000	-4.071000000	2.003000000
C	0.710000000	-2.100000000	2.018000000
C	0.612000000	-3.614000000	0.159000000
C	1.569000000	-4.422000000	0.765000000
C	1.662000000	-2.910000000	2.629000000
H	0.359000000	-1.194000000	2.499000000
H	0.216000000	-3.902000000	-0.808000000
H	1.900000000	-5.328000000	0.268000000
H	2.065000000	-2.630000000	3.598000000
H	2.845000000	-4.701000000	2.476000000
C	-0.975000000	-1.616000000	-1.753000000
C	-0.718000000	-1.738000000	-4.552000000
C	-2.102000000	-1.563000000	-2.582000000
C	0.285000000	-1.710000000	-2.357000000
C	0.412000000	-1.778000000	-3.742000000
C	-1.975000000	-1.624000000	-3.965000000
H	-3.090000000	-1.485000000	-2.141000000
H	1.175000000	-1.735000000	-1.738000000
H	1.398000000	-1.866000000	-4.187000000
H	-2.865000000	-1.589000000	-4.587000000
H	-0.621000000	-1.794000000	-5.631000000

Dihydride-is5-EDF2

C	0.724000000	-0.160000000	2.588000000
H	1.162000000	0.180000000	3.529000000
C	0.134000000	-1.554000000	2.772000000
H	0.958000000	-2.271000000	2.834000000
H	-0.388000000	-1.580000000	3.740000000
N	-0.737000000	-1.953000000	1.664000000
C	-0.919000000	-3.409000000	1.589000000
H	0.034000000	-3.881000000	1.846000000
H	-1.651000000	-3.755000000	2.334000000
C	-1.346000000	-3.890000000	0.199000000
H	-2.142000000	-3.235000000	-0.170000000
H	-1.743000000	-4.906000000	0.294000000
H	-1.648000000	-1.513000000	1.785000000
Ru	-0.445000000	-0.838000000	-0.431000000
H	-0.056000000	0.544000000	2.290000000
C	-0.228000000	-3.894000000	-0.801000000
C	1.848000000	-3.866000000	-2.599000000
C	0.221000000	-5.090000000	-1.360000000
N	0.336000000	-2.712000000	-1.133000000
C	1.358000000	-2.712000000	-2.008000000
C	1.266000000	-5.084000000	-2.273000000
H	-0.258000000	-6.018000000	-1.072000000
H	1.783000000	-1.740000000	-2.219000000
H	1.617000000	-6.009000000	-2.718000000
H	2.671000000	-3.799000000	-3.301000000
N	1.782000000	-0.116000000	1.597000000
N	1.521000000	-0.293000000	0.283000000
N	2.652000000	-0.202000000	-0.364000000
C	3.660000000	0.036000000	0.523000000
C	3.106000000	0.091000000	1.784000000
H	3.522000000	0.275000000	2.760000000
C	5.046000000	0.206000000	0.093000000
C	7.694000000	0.542000000	-0.758000000
C	5.352000000	0.270000000	-1.271000000
C	6.086000000	0.311000000	1.023000000
C	7.398000000	0.479000000	0.601000000
C	6.665000000	0.436000000	-1.690000000
H	4.545000000	0.193000000	-1.990000000
H	5.871000000	0.252000000	2.085000000
H	8.192000000	0.558000000	1.336000000
H	6.886000000	0.486000000	-2.751000000
H	8.719000000	0.673000000	-1.087000000
H	-0.179000000	-0.230000000	-1.881000000
H	-1.875000000	-1.353000000	-1.003000000
P	-1.689000000	1.012000000	-0.114000000
C	-3.035000000	1.326000000	-1.353000000
C	-4.975000000	1.850000000	-3.308000000
C	-4.244000000	1.941000000	-1.013000000
C	-2.816000000	0.969000000	-2.686000000
C	-3.775000000	1.236000000	-3.656000000
C	-5.209000000	2.197000000	-1.983000000
H	-4.447000000	2.206000000	0.019000000
H	-1.893000000	0.460000000	-2.941000000
H	-3.588000000	0.953000000	-4.687000000
H	-6.146000000	2.667000000	-1.699000000
H	-5.726000000	2.049000000	-4.066000000
C	-0.908000000	2.700000000	-0.073000000
C	0.374000000	5.194000000	-0.113000000
C	0.450000000	2.798000000	-0.384000000
C	-1.620000000	3.875000000	0.199000000
C	-0.983000000	5.111000000	0.186000000
C	1.087000000	4.036000000	-0.404000000
H	0.996000000	1.894000000	-0.628000000
H	-2.682000000	3.828000000	0.412000000
H	-1.550000000	6.012000000	0.401000000
H	2.142000000	4.094000000	-0.653000000
H	0.870000000	6.159000000	-0.128000000
C	-2.673000000	0.966000000	1.463000000
C	-4.008000000	0.524000000	3.905000000
C	-3.611000000	-0.071000000	1.599000000
C	-2.422000000	1.773000000	2.578000000
C	-3.082000000	1.553000000	3.786000000
C	-4.273000000	-0.287000000	2.803000000
H	-3.821000000	-0.707000000	0.744000000
H	-1.711000000	2.589000000	2.503000000
H	-2.872000000	2.196000000	4.635000000
H	-5.003000000	-1.087000000	2.879000000
H	-4.525000000	0.356000000	4.844000000

Dihydride-is4-acetophenone-out-wB97X

C	-0.475997000	-3.021383000	-3.362720000
H	-0.548760000	-3.825695000	-4.110381000
C	-0.623168000	-1.680955000	-4.083934000
H	0.304969000	-1.482291000	-4.645233000
H	-1.429670000	-1.755723000	-4.835759000
N	-0.870966000	-0.538062000	-3.187701000
C	-0.416451000	0.717700000	-3.796132000
H	0.597229000	0.566061000	-4.202184000
H	-1.068797000	0.999548000	-4.642291000
C	-0.379457000	1.884286000	-2.819819000
H	-1.286341000	1.887072000	-2.198701000
H	-0.314725000	2.832821000	-3.369927000
N	0.781692000	1.832960000	-1.943990000
N	0.974375000	0.803082000	-1.127649000
N	2.084403000	0.982873000	-0.487139000
C	2.636035000	2.160280000	-0.879386000
C	1.798710000	2.715953000	-1.827053000
H	1.839449000	3.632427000	-2.410685000
C	3.910916000	2.654821000	-0.327262000
C	6.341479000	3.578314000	0.727357000
C	4.633542000	1.871975000	0.582406000
C	4.420122000	3.904926000	-0.700556000
C	5.626825000	4.363242000	-0.177508000
C	5.839740000	2.332654000	1.105109000
H	4.235810000	0.896240000	0.873764000
H	3.867276000	4.533178000	-1.405133000
H	6.011204000	5.341837000	-0.478086000
H	6.394333000	1.711696000	1.814145000
H	7.288079000	3.938556000	1.139418000
H	-1.879982000	-0.444778000	-3.065331000
Ru	-0.463942000	-0.805864000	-0.959248000
H	-1.679394000	0.230027000	-0.663702000
N	1.101870000	-2.275598000	-1.643876000
C	3.016839000	-4.160822000	-2.405837000
C	2.310185000	-2.313531000	-1.064589000
C	0.839508000	-3.143393000	-2.640342000
C	1.778597000	-4.101410000	-3.036166000
C	3.293765000	-3.235443000	-1.404886000
H	2.493647000	-1.559253000	-0.295681000
H	1.527214000	-4.796063000	-3.841493000
H	4.253769000	-3.219071000	-0.884336000
H	3.756376000	-4.910083000	-2.701427000
H	-1.298862000	-3.135540000	-2.640771000
P	-0.351513000	-0.919604000	1.260687000
H	-1.601419000	-1.982769000	-0.913865000
C	-1.789582000	-1.632144000	2.205249000
C	-4.070448000	-2.523746000	3.592330000
C	-1.673010000	-2.226362000	3.468356000
C	-3.066538000	-1.495131000	1.649749000
C	-4.199117000	-1.930670000	2.336362000
C	-2.803259000	-2.672832000	4.154598000
H	-0.688609000	-2.356337000	3.927547000
H	-3.141208000	-1.046216000	0.656047000
H	-5.189147000	-1.816373000	1.882993000
H	-2.690303000	-3.141606000	5.136478000
H	-4.955979000	-2.874215000	4.130440000
C	-0.223842000	0.688395000	2.203409000
C	-0.172253000	3.137081000	3.596359000
C	-0.536740000	1.889306000	1.557248000
C	0.103536000	0.735932000	3.566730000
C	0.134162000	1.946053000	4.256724000
C	-0.511431000	3.103776000	2.245775000
H	-0.819122000	1.857250000	0.501597000
H	0.342470000	-0.186071000	4.105148000
H	0.395062000	1.958558000	5.319001000
H	-0.765010000	4.028746000	1.718631000
H	-0.149403000	4.087652000	4.137258000
C	1.064956000	-1.887669000	1.963058000
C	3.315152000	-3.446410000	2.627448000
C	1.007992000	-3.288300000	1.924021000
C	2.273440000	-1.282499000	2.330597000
C	3.389057000	-2.054540000	2.660601000
C	2.118230000	-4.061537000	2.257812000
H	0.079787000	-3.783912000	1.619683000
H	2.352526000	-0.191580000	2.342506000
H	4.323200000	-1.561082000	2.945624000
H	2.049181000	-5.152690000	2.223538000
H	4.188372000	-4.051378000	2.888300000
C	-4.119177000	0.894898000	-2.057100000
O	-3.493260000	1.049316000	-3.091655000
C	-4.116868000	1.964701000	-1.005875000
C	-3.972163000	3.979600000	0.928662000
C	-4.560694000	1.723736000	0.299661000
C	-3.614498000	3.229230000	-1.336844000
C	-3.545850000	4.234102000	-0.376522000
C	-4.478908000	2.724799000	1.265358000
H	-4.950300000	0.741863000	0.580188000
H	-3.282686000	3.407455000	-2.363073000
H	-3.157134000	5.220743000	-0.643392000
H	-4.807879000	2.521550000	2.287663000
H	-3.910051000	4.764294000	1.687876000
C	-4.892973000	-0.372452000	-1.806291000
H	-4.354698000	-0.983586000	-1.064335000
H	-4.960691000	-0.940859000	-2.742272000
H	-5.899331000	-0.166832000	-1.414389000

Dihydride-is4-acetophenone-in-wB97X

C	-3.737019000	0.984940000	-2.646466000
H	-4.377881000	1.584267000	-3.313053000
C	-2.706151000	0.257260000	-3.494310000
H	-3.229751000	-0.452922000	-4.164702000
H	-2.191527000	0.992281000	-4.133672000
N	-1.690855000	-0.474098000	-2.713969000
C	-0.912854000	-1.375283000	-3.579106000
H	-0.877393000	-2.377331000	-3.121618000
H	-1.416097000	-1.495624000	-4.554126000
C	0.519833000	-0.926040000	-3.845334000
H	0.561505000	0.160266000	-4.012501000
H	0.929402000	-1.448738000	-4.720436000
N	1.385271000	-1.251819000	-2.724184000
N	1.115947000	-0.776324000	-1.515011000
N	1.950836000	-1.290084000	-0.671076000
C	2.801945000	-2.111458000	-1.337853000
C	2.437291000	-2.098898000	-2.670204000
H	2.836782000	-2.589250000	-3.554772000
C	3.912573000	-2.807482000	-0.662583000
C	6.049341000	-4.087407000	0.623655000
C	4.411709000	-2.309032000	0.547868000
C	4.492397000	-3.954112000	-1.219151000
C	5.556164000	-4.588739000	-0.580989000
C	5.472822000	-2.947557000	1.185359000
H	3.968160000	-1.404326000	0.972999000
H	4.100326000	-4.363153000	-2.155414000
H	5.999356000	-5.484307000	-1.025255000
H	5.858337000	-2.545900000	2.126762000
H	6.884241000	-4.585255000	1.124643000
H	-2.238472000	-1.062888000	-2.081418000
Ru	-0.427911000	0.716677000	-1.176779000
H	0.171990000	1.697800000	-2.306723000
N	-4.239663000	-1.133100000	-1.513341000
C	-6.568174000	-0.129350000	-0.379135000
C	-4.990445000	-1.889112000	-0.707181000
C	-4.617650000	0.121996000	-1.773388000
C	-5.791625000	0.656835000	-1.218786000
C	-6.161454000	-1.438130000	-0.110732000
H	-4.630779000	-2.908678000	-0.523306000
H	-6.079015000	1.686050000	-1.449779000
H	-6.739289000	-2.094731000	0.543579000
H	-7.484319000	0.271598000	0.063772000
H	-3.198397000	1.689513000	-1.990071000
P	0.749020000	1.894232000	0.290120000
H	-1.599245000	1.823472000	-0.952088000
C	0.644740000	3.750189000	0.321103000
C	0.448175000	6.555723000	0.367023000
C	1.532103000	4.520270000	1.088263000
C	-0.335332000	4.409202000	-0.426915000
C	-0.433607000	5.802367000	-0.404348000
C	1.434327000	5.909609000	1.115019000
H	2.314799000	4.029656000	1.674904000
H	-1.018809000	3.805170000	-1.029310000
H	-1.205583000	6.300908000	-0.997957000
H	2.134159000	6.492380000	1.720940000
H	0.371768000	7.646926000	0.384553000
C	2.600711000	1.708539000	0.246298000
C	5.390485000	1.419959000	0.001214000
C	3.215255000	1.709434000	-1.013544000
C	3.408195000	1.565215000	1.380284000
C	4.792633000	1.421490000	1.259540000
C	4.595787000	1.568589000	-1.136969000
H	2.588434000	1.803443000	-1.906387000
H	2.957206000	1.557902000	2.376869000
H	5.405299000	1.307306000	2.158825000
H	5.056022000	1.568864000	-2.129445000
H	6.473573000	1.301218000	-0.094629000
C	0.372427000	1.471691000	2.057696000
C	-0.409380000	0.592368000	4.614172000
C	-0.234410000	2.350737000	2.960474000
C	0.581039000	0.140172000	2.454732000
C	0.199012000	-0.294419000	3.721455000
C	-0.623726000	1.914158000	4.230229000
H	-0.414928000	3.390752000	2.674464000
H	1.032967000	-0.563185000	1.745258000
H	0.368435000	-1.335739000	4.011867000
H	-1.098018000	2.616678000	4.921910000
H	-0.713928000	0.250469000	5.607668000
O	-1.315785000	-0.842986000	0.219848000
C	-2.163169000	-0.877841000	1.100987000
C	-2.408206000	-2.176169000	1.808217000
C	-2.798393000	-4.634582000	3.084909000
C	-3.407449000	-2.317308000	2.779072000
C	-1.602551000	-3.276860000	1.487442000
C	-1.796019000	-4.499582000	2.121915000
C	-3.602301000	-3.543292000	3.413045000
H	-4.041762000	-1.468390000	3.046199000
H	-0.818799000	-3.148485000	0.736488000
H	-1.161274000	-5.352840000	1.868099000
H	-4.384709000	-3.646017000	4.169685000
H	-2.951191000	-5.595424000	3.584391000
C	-2.946494000	0.337629000	1.494122000
H	-2.715505000	0.602136000	2.539565000
H	-4.028375000	0.140277000	1.423250000
H	-2.664731000	1.164145000	0.828161000

8.4 NS click based ligands for *in situ* hydrogenation of carbonyl compounds

8.4.1 Characterization of ligands

*Ethyl 5-(4-vinyl-1H-1,2,3-triazol-1-yl)pentanoate (**4**)*

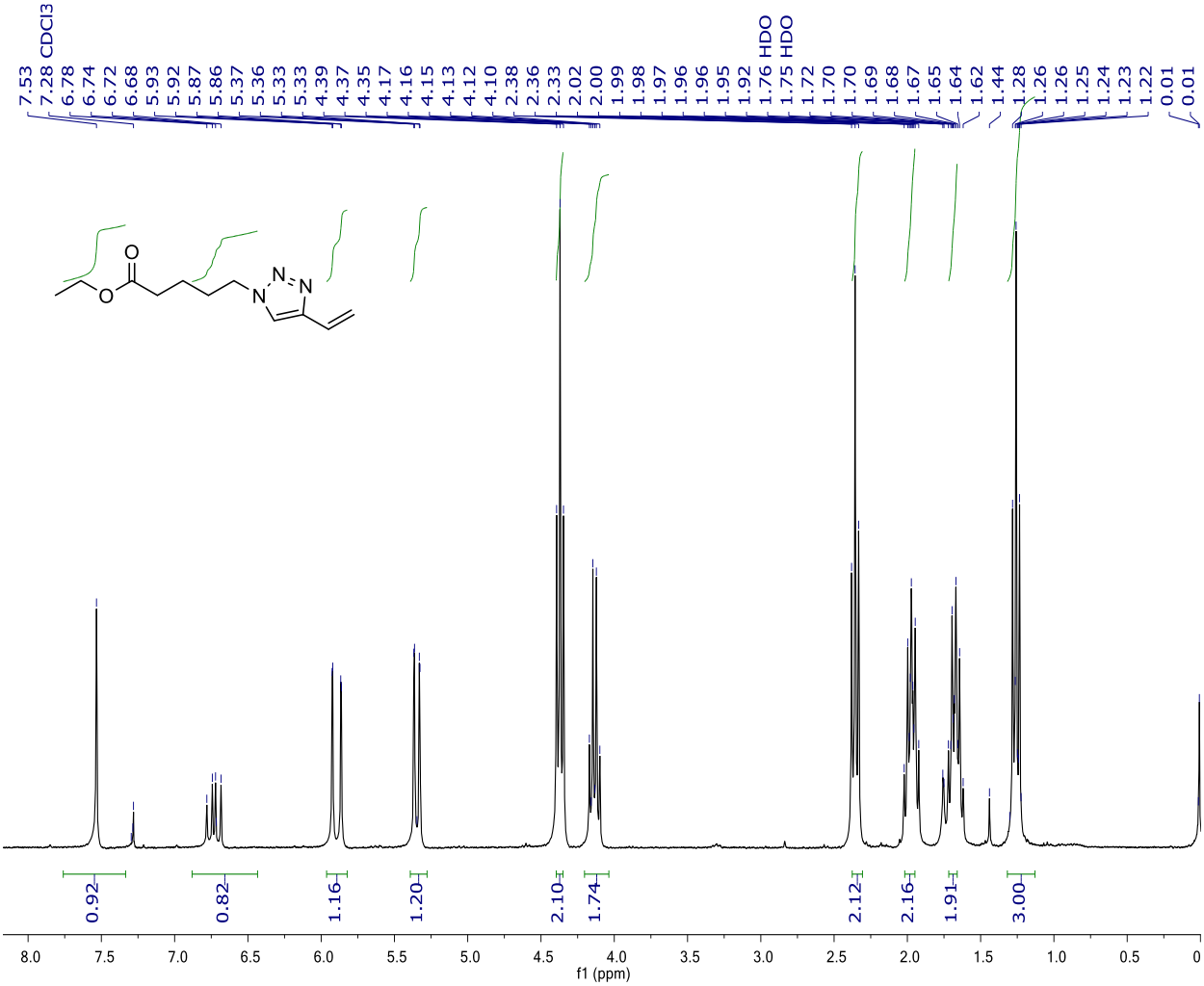

^{1}H NMR (300 MHz, $CDCl_3$) δ(ppm) = 7.53 (s, 1H), 6.73 (dd, *J*=17.8, 11.2 Hz, 1H), 5.89 (dd, *J*=17.7, 1.3 Hz, 1H), 5.35 (dd, *J*=11.2, 1.3 Hz, 1H), 4.37 (t, *J* = 7.1 Hz, 2H), 4.13 (d, *J* = 7.2 Hz, 2H), 2.36 (t, *J*= 7.2 Hz, 2H), 2.13 – 1.85 (m, 2H), 1.80 – 1.59 (m, 2H), 1.26 (dd, *J*=8.2, 6.1 Hz, 3H).

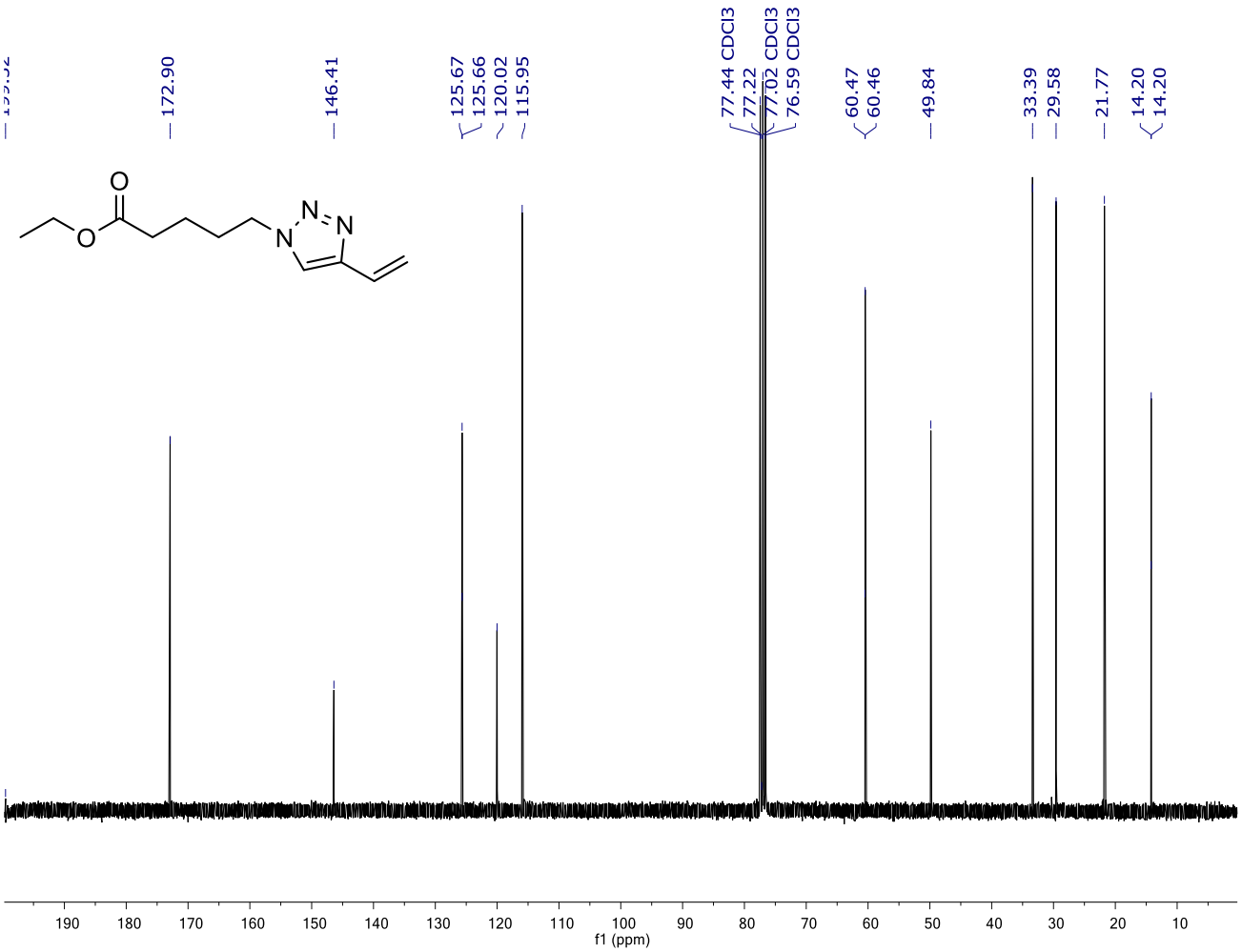

^{13}C NMR (300 MHz, $CDCl_3$) δ (ppm) = 172.9, 146.4, 125.7, 120.0, 115.9, 60.5, 49.8, 33.4, 29.6, 21.8, 14.2.

*Ethyl 5-(4-(2-(hexylthio)ethyl)-1H-1,2,3-triazol-1-yl)pentanoate (**6a**)*

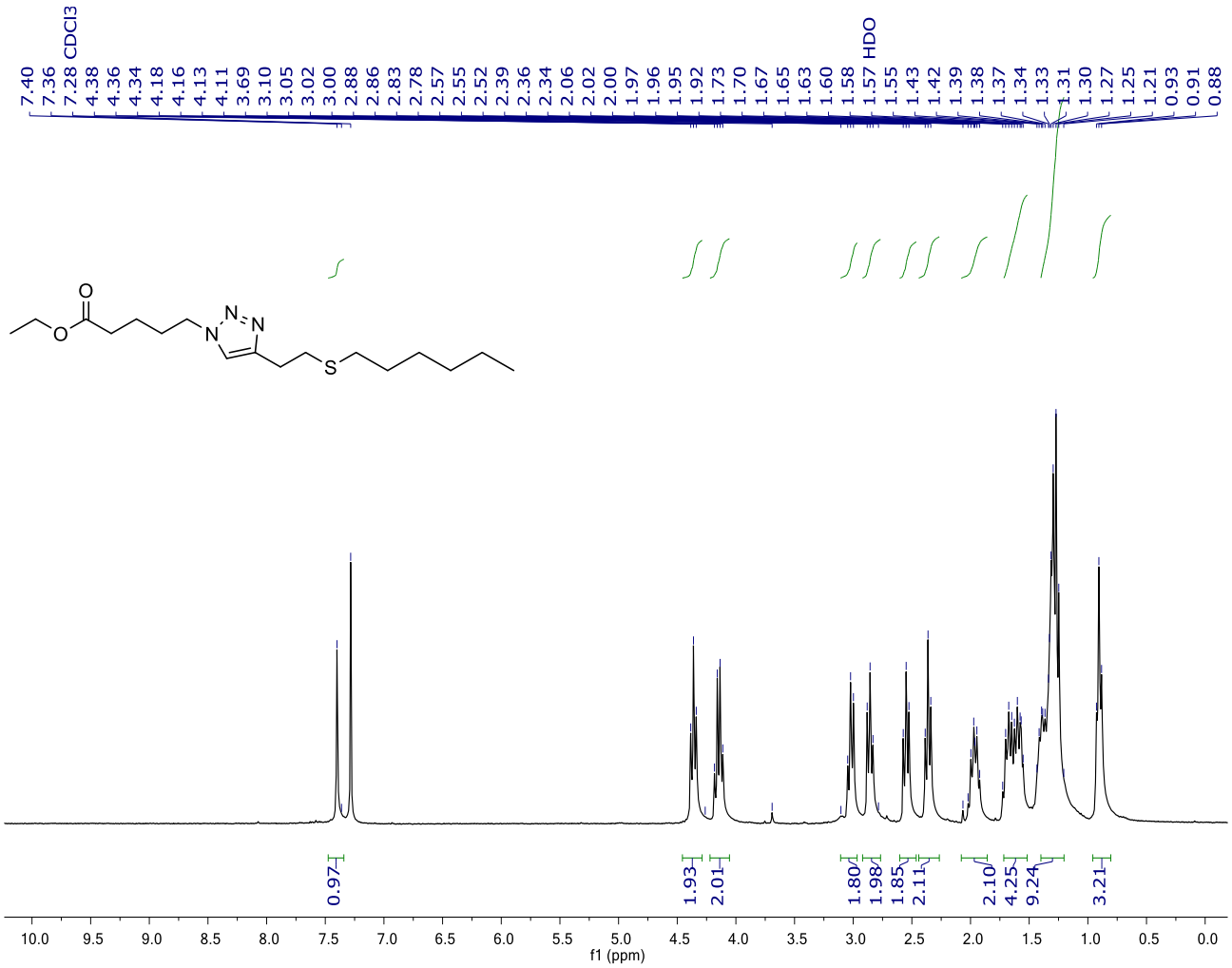

^{1}H NMR (300 MHz, $CDCl_3$) δ (ppm) = 7.40 (s, 1H), 4.36 (t, J = 7.1 Hz, 2H), 4.15 (q, J = 7.1 Hz, 2H), 3.02 (t, J = 7.4 Hz, 2H), 2.86 (t, J = 7.4 Hz, 2H), 2.55 (t, J = 7.4 Hz, 2H), 2.36 (t, J = 7.2 Hz, 2H), 1.96 (m, 2H), 1.77 – 1.50 (m, 4H), 1.48 – 1.05 (m, 11H), 0.91 (t, J = 6.6 Hz, 3H).

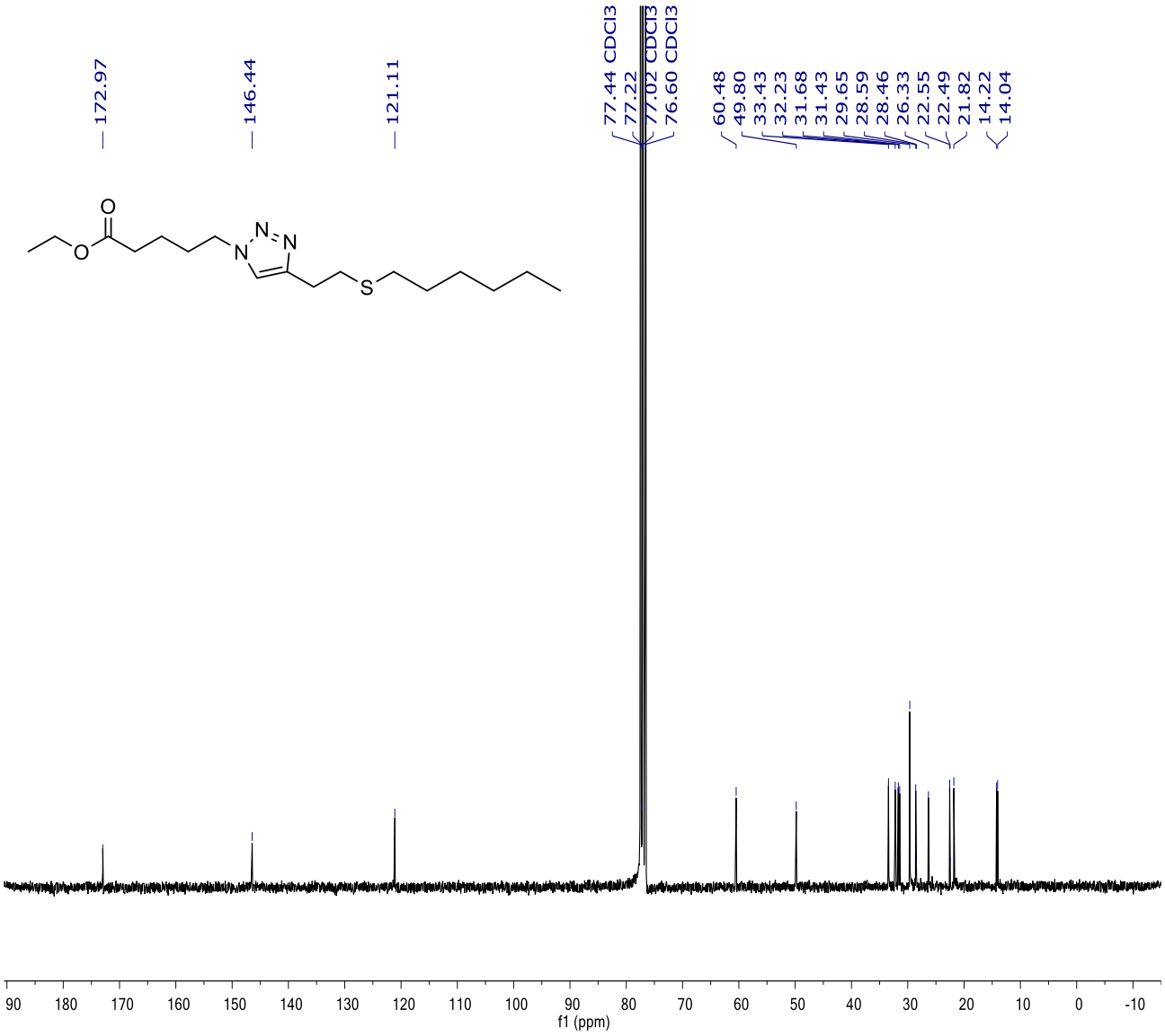

^{13}C NMR (300 MHz, $CDCl_3$) δ (ppm) = 172.9, 146.4, 121.1, 60.5, 49.8, 33.4, 32.2, 31.7, 31.4, 29.6, 28.6, 26.3, 22.5, 22.5, 21.8, 14.2, 14.0.

*5-(4-(2-(hexylthio)ethyl)-1H-1,2,3-triazol-1-yl)pentanoic acid (**6b**)*

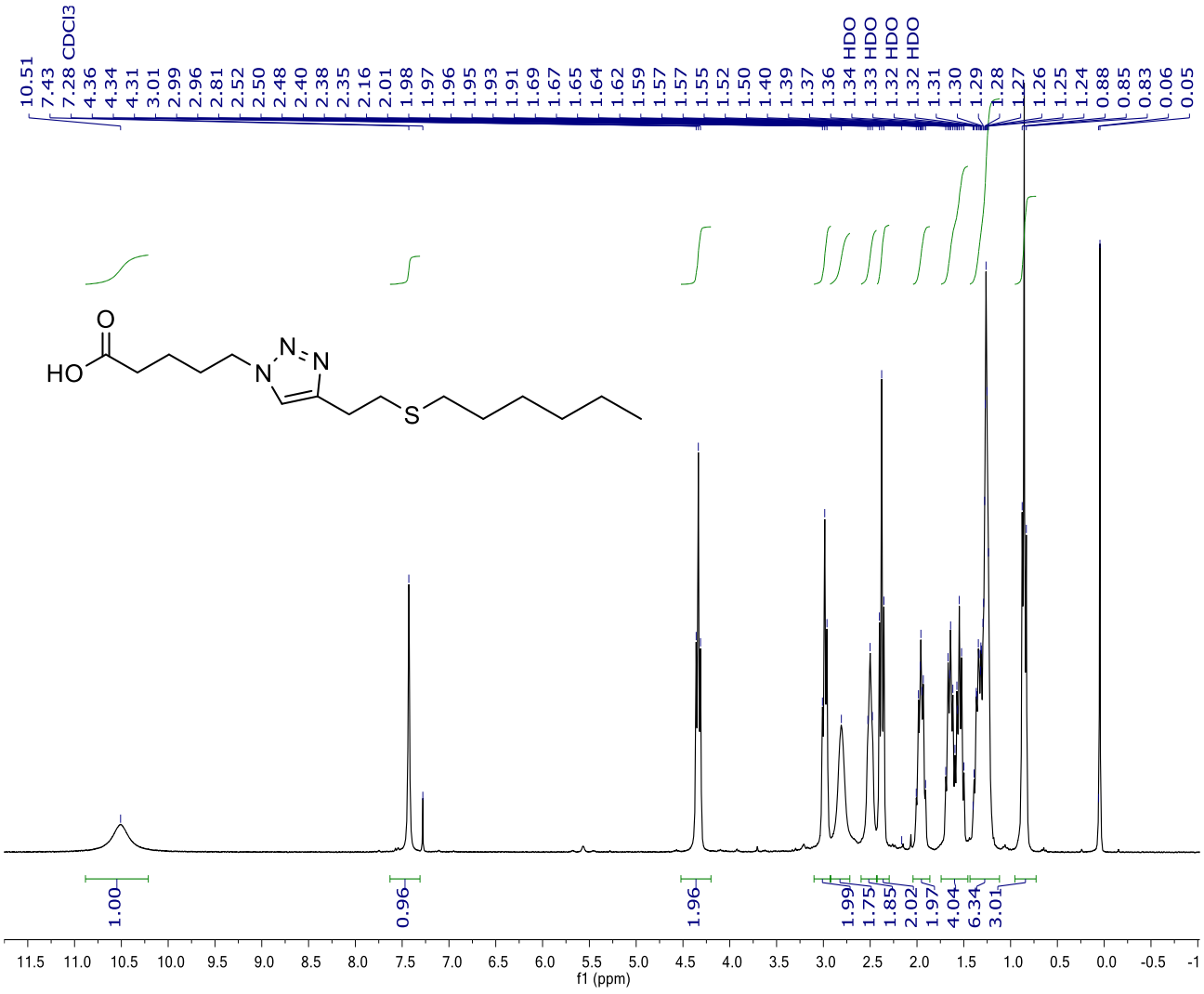

^{1}H NMR (300 MHz, $CDCl_3$) δ (ppm) 10.51 (bs, 1H), 7.43 (s, 1H), 4.34 (t, *J* = 7.0 Hz, 2H), 2.99 (t, *J* = 7.2 Hz, 2H), 2.81 (s, 2H), 2.50 (t, *J* = 7.4 Hz, 2H), 2.38 (t, *J* = 7.2 Hz, 2H), 2.05 – 1.87 (m, 2H), 1.60 (m, 4H), 1.43 – 1.18 (m, 9H), 0.85 (t, *J* = 6.7 Hz, 3H).

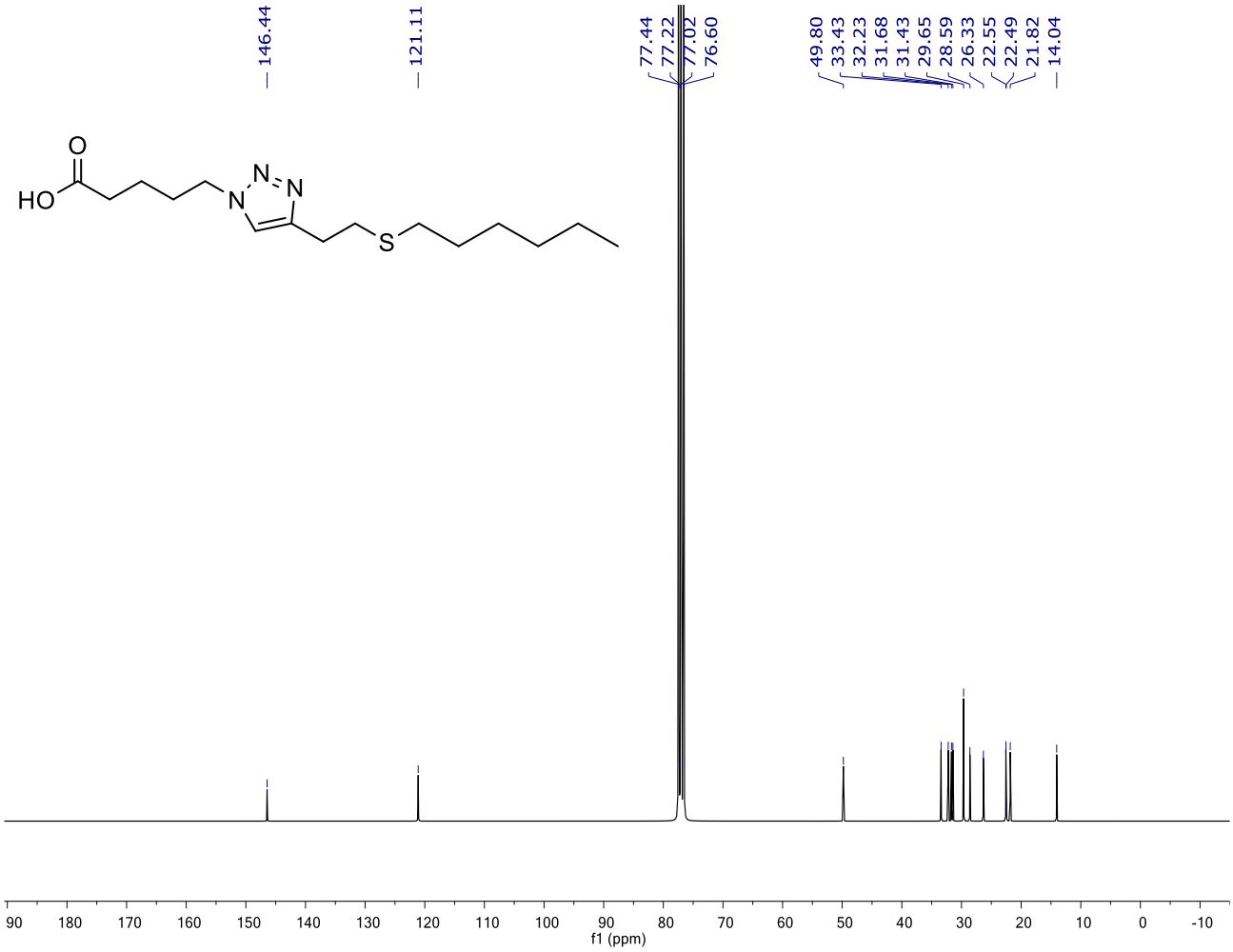

^{13}C NMR (300 MHz, $CDCl_3$) δ (ppm) = 178.4, 130.7, 121.9, 52.1, 33.4, 32.2, 31.7, 31.4, 29.6, 28.6, 26.3, 22.5, 22.5, 21.8, 14.2.

*Sodium 5-(4-(2-(hexylthio)ethyl)-1H-1,2,3-triazol-1-yl)pentanoate (**6c**)*

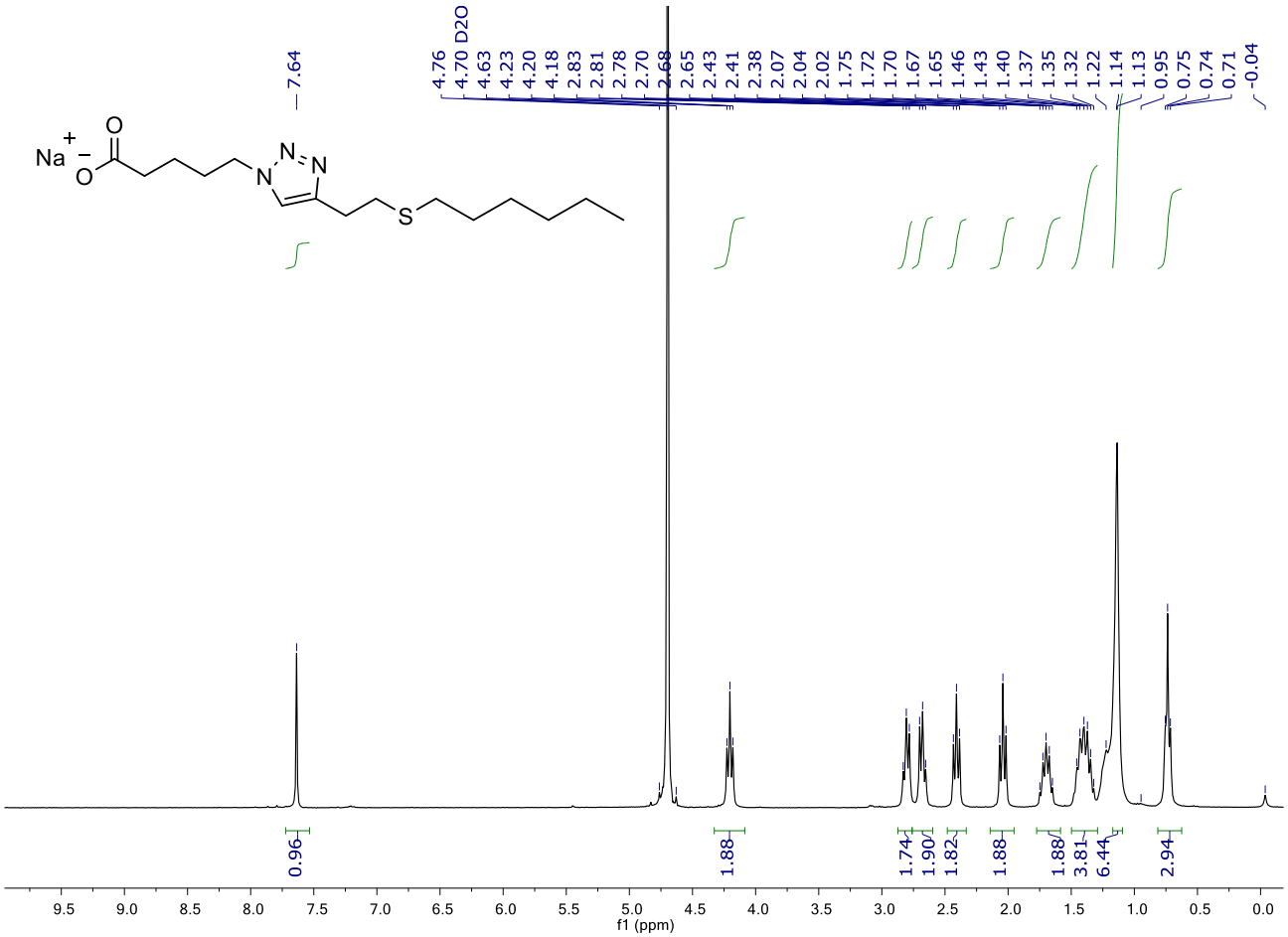

^{1}H NMR (300 MHz, $CDCl_3$) δ (ppm) 7.64 (s, 1H, C***H***$_{Triaz.}$), 4.30 (t, J_{HH} = 7.0 Hz, 2H), 2.83(dt, J_{HH} = 39.0 Hz, J_{HH} = 7.2 Hz, 4H), 2.50 (t, J_{HH} = 7.3 Hz, 2H), 2.13 (t, J_{HH} = 7.5 Hz, 2H), 1.79 (p, J_{HH} = 7.3 Hz, 2H), 1.49 (m, 4H), 1.23 (m, 6H), 0.83 (m, 3H).